FUNCTIONAL INVESTIGATIONS OF CYTOCHROME P450 3A4

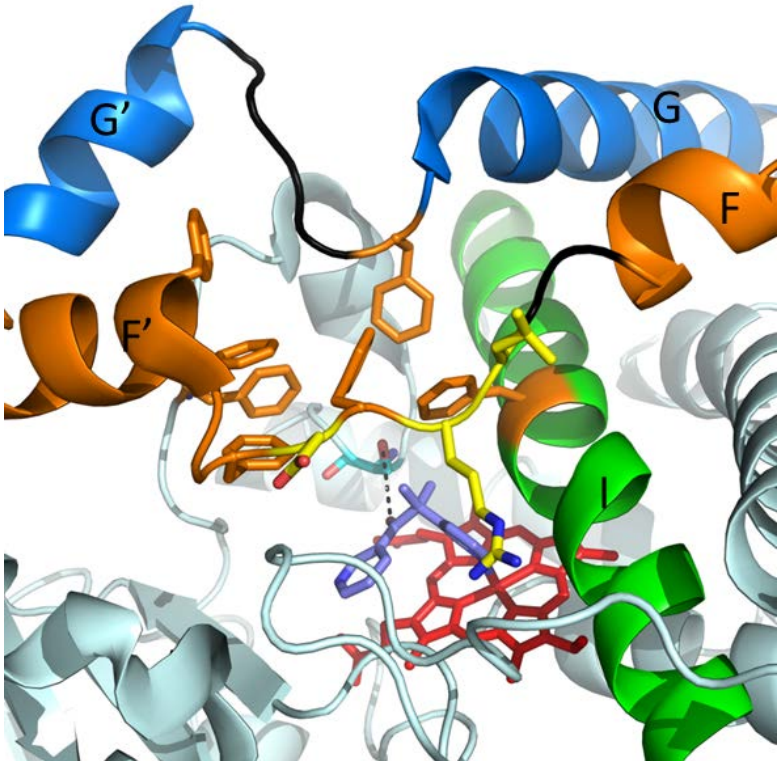

Christian S. Müller
Diss. ETH Nr. 22234
Zürich 2014

DISS. ETH NO 22234

FUNCTIONAL INVESTIGATIONS OF CYTOCHROME P450 3A4

A thesis submitted to attain the degree of

DOCTOR OF SCIENCES of ETH ZURICH

(Dr. sc. ETH Zurich)

presented by

CHRISTIAN SAMUEL MÜLLER

Dipl. Natw. ETH Zurich

born on *01.07.1981*

citizen of Zofingen (AG)

accepted on the recommendation of

Prof. Dr. Willem H. Koppenol, ETH Zurich
Prof. Dr. Peter Kast, ETH Zurich
Prof. Dr. Ursula von Mandach, University of Zurich
Prof. Dr. Amedeo Caflisch, University of Zurich

2014

Do not go where the path may lead, go instead where there is no path and leave a trail.

Ralph Waldo Emerson (1803 – 1882)

ACKNOWLEDGMENTS

My sincere thanks go to **Prof. Willem H. Koppenol** for allowing me to perform my PhD thesis in his lab, for his financial support, and for giving me the freedom to choose the topics of my studies most independently. I wish to thank **Prof. Ursula von Mandach** for offering me the opportunity to elaborate my PhD thesis in her team.

I would like to thank **Prof. Amedeo Caflisch** and **Tim Knehans** from the University of Zürich for the very fruitful collaboration, without which this thesis would not have been complete; and in particular for their brilliant intuition in choosing suitable targets for mutagenesis in the enzyme CYP3A4, which elucidated new features of this intriguing enzyme.

I owe special thanks to **Dr. Dmitri R. Davydov** for his exceptionally instrumental thoughts, for the supervision during my internship in his group at the University of California at San Diego, USA, for his help on the writing of manuscripts, and his copious and indispensable discussions that ultimately made the writing of this thesis possible. **Prof. James Halpert** is acknowledged for his very generous offer to let me work for two months in his lab under the supervision of Dr. Davydov.

I would like to thank **Dr. Patricia L. Bounds** for her support in the establishment of HPLC methods, for fruitful discussions and editing of manuscripts and other pieces of scientific writing. I wish to acknowledge **Dr. Reinhard Kissner** for his help with the measurements on the stopped-flow apparatus and for numerous tips and insightful discussions. I owe special thanks to **Alexandra Dolder** who was a charming company during the time of my thesis and who assisted me in countless experiments. **Dr. Linda Thöny** and **Dr. Michael Fairhead** are acknowledged for their help with the molecular biology and protein purification techniques. I am grateful to **Dr. Manale Maalouf** and **Dr. Thomas Nauser** for the proof-reading of the thesis. I sincerely thank my parents for their ceaseless encouragement to accomplish my PhD.

Christian S. Müller Zurich, August 20, 2014

TABLE OF CONTENTS

Abstract 1

Kurzfassung 2

Abbreviations 3

Foreword 5

1 Introduction and Background Summary 7

1.1 Cytochrome P450 8

1.2 The Catalytic Cycle of Cytochrome P450 9

1.3 NADPH Cytochrome P450 Oxidoreductase 11

1.4 Cytochrome P450 3A4 (CYP3A4) 12

1.5 Ligand Binding to CYP3A4 and Regulation 16

1.6 Cooperativity and Atypical Kinetics in CYP3A4 19

1.6.1 Cooperativity and Allostery 19

1.6.2 Mathematical Frameworks for Allostery in Cytochromes P450 23

1.7 Reconstitution of the Activity of Purified Cytochrome P450 29

1.8 Coupling of Cytochrome P450 to Electrodes 30

1.9 Scope of this Thesis 31

2 Materials and Methods 33

2.1 Reagents 34

2.2 Experimental Methods 36

2.2.1 Recombinant DNA Manipulations 36

2.2.2 Expression and Purification of Rat NADPH-P450 Reductase and Human Cytochrome P450 3A4 42

2.2.3 Functional Reconstitution of Purified CYP3A4 and CPR 51

2.2.4 Formation of Carbamazepine-10,11-epoxide (Chapter 4) 53

2.2.5 Derivation of an Equation that Combines an Allowance for Partial Substrate Inhibition with an Approximation of Cooperative Interactions in Terms of the Hill Equation* 54

2.2.6 Spectral Binding Titrations (Chapters 5-7) 56

2.2.7 Principal Component Analysis (PCA) 58

2.2.8 CO Binding to Iron (II) CYP3A4 (Chapter 6) 59

2.2.9 Kinetics of Dithionite-Dependent Reduction of CYP3A4 (Chapter 7) 59

2.3 Computational Methods (Chapter 4)* 61

3 Cytochrome P450 3A4 and NADPH-P450 Reductase: Molecular Biology and Biochemistry **63**
3.1 Sequencing Result of the Expression Product 64
3.2 Recombinant DNA Manipulations 66
3.3 Spectral Characterisations of Recombinant Enzymes 69
3.4 SDS-PAGE of Recombinant Enzymes 72
3.5 Kinetic Chraracterization of Recombinant CYP3A4 and CPR 74
3.6 Illustration of the Principal Component Analysis Method 76
3.7 Effect of Solvents on the CYP3A4 S119A Spin Equilibrium 79
3.8 Discussion 80

4 Concurrent Cooperativity and Substrate Inhibition in the Epoxidation of Carbamazepine by Cytochrome P450 3A4* **81**
4.1 Abstract 82
4.2 Introduction 83
4.3 Results 84
4.3.1 CBZ Epoxidation by CYP3A4-Containing Bactosomes 84
4.3.2 Probing the CBZ Binding Mode to CYP3A4 with MD Simulations 86
4.3.3 Selection and Suggestion of Mutants 88
4.3.4 Enzyme Production, Purification, and Reconstitution 90
4.3.5 Effect of Mutations on CYP3A4-Dependent Epoxidation of CBZ 91
4.3.6 MD Simulations of 2-4 CBZ Molecules in CYP3A4 Binding Pocket 97
4.4 Discussion 100

5 Bromocriptine and Erythromycin Reveal Inverse Type-I Transition in CYP3A4 S119A **109**
5.1 Abstract 110
5.2 Introduction 110
5.3 Results 112
5.3.1 Bromocriptine Titrations 112
5.3.2 Erythromcycin Titrations 115
5.4 Discussion 117

6 Evidence for Spectrally Silent Allosteric Ligand Binding in CYP3A4 **125**
6.1 Abstract 126
6.2 Introduction 126
6.3 Results 128
6.3.1 Effect of Solvents on Spin Equilibrium 128

6.3.2 Titrations of CYP3A4 Wild Type and S119A with Allosteric Substrates 131
6.3.3 Formation of Cytochrome P420 upon Binding of 7BQ 139
6.4 Discussion 141

7 Additional Studies 145
7.1 CYP3A4 I369F - Affinity and Activity Studies 146
7.1.1 Introduction 146
7.1.2 Results 148
7.1.3 Discussion 154
7.2 Kinetics of Dithionite-Dependent Reduction of CYP3A4 Point Mutants 157
7.2.1 Introduction 157
7.2.2 Results 158
7.2.3 Discussion 160

8 Conclusion 163

References 167

Curriculum Vitae 179

ABSTRACT

Cytochrome P450 3A4 (CYP3A4) is the most abundant cytochrome P450 in humans. It metabolizes a broad range of substrates that are of pharmaceutical and toxicological interest and exhibits complex atypical substrate interactions. To reduce and eventually avoid harmful drug-drug interactions and adverse drug effects in pharmacotherapies, it is important to discern the variety and complexity of the kinetics of CYP3A4. Commonly, atypical kinetics of cytochromes P450 are explored *via* enzyme catalysis studies *in vitro*, and, in the case of homotropic cooperativity, *via* studies of the substrate dependence of the spin transition in the heme iron.

CYP3A4 is responsible for the metabolism of the anticonvulsive drug carbamazepine (CBZ). To explore the mechanism of interaction between CYP3A4 and CBZ, we generated several active site mutants. These were generated based on a model of a putative productive binding mode of the CBZ-CYP3A4 complex and screened for their CBZ epoxidation activity. The results elucidate the existence of concurrent cooperativity and substrate inhibition in the epoxidation of CBZ. Whereas wild-type CYP3A4 exhibits predominant substrate inhibition, the cloned mutants reveal either more pronounced substrate inhibition kinetics (the I369F and I369L mutants) or S-shaped profiles indicative of homotropic cooperativity (the S119A, A370V, and A370L mutants). Analysis of the kinetic profiles of CBZ metabolism with a novel model combining the formalism of the Hill equation with an allowance for substrate inhibition demonstrates a mechanism of CYP3A4-CBZ interactions that encompasses the association of multiple substrate molecules.

The produced enzyme variants were also applied to binding studies with further CYP3A4 ligands. The S119A mutant shows novel types of inverse and bidirectional spin transitions upon ligand association. CYP3A4 I369F exhibits on average a 2-fold higher affinity and a several-fold increase in turnover at low substrate concentration ($<< S_{50}$) towards a group of structurally diverse substrates. The I369F mutant therefore constitutes an optimized enzyme variant with the intriguing possibility to be employed in cytochrome P450-based biosensors for the detection of drugs and their prospective applications in personalized medicine. This comprehensive study introduces novel enzyme mutants whose study allows an improved understanding of the complexity and functional diversity of CYP3A4.

KURZFASSUNG

Cytochrom P450 3A4 (CYP3A4) ist das häufigste Cytochrom P450 im Menschen. Es metabolisiert ein breites Spektrum an Substraten, die von pharmazeutischem und toxikologischem Interesse sind, und weist komplexe atypische Substrat-Wechselwirkungen auf. Die Vermeidung ungünstiger Wechselwirkungen zwischen Medikamenten und deren gesundheitsschädlicher Effekte in Pharmakotherapieen erfordert ein Verständnis der Vielfalt und Komplexität der CYP3A4-Kinetiken. Atypische Kinetiken werden üblicherweise mithilfe von enzymkatalytischen Studien *in vitro* und, im Falle von homotroper Kooperativität, mithilfe von Studien der Substratabhängigkeit des Spin-Übergangs im Häm-Eisen erforscht.

CYP3A4 ist verantwortlich für den Metabolismus des Antiepileptikums Carbamazepin (CBZ). Um die Wechselwirkungen zwischen CYP3A4 und CBZ zu untersuchen, wurden mehrere Mutanten basierend auf dem Modell eines mutmasslich produktiven CBZ-CYP3A4-Bindungsmodus generiert und die Mutanten hinsichtlich ihrer CBZ-Epoxidierungs-Aktivität untersucht. Die Resultate verdeutlichen, dass die komplexen Kinetiken der CBZ-Epoxidierung sowohl Kooperativität als auch Substratinhibition beinhalten. Während im Wildtyp Substratinhibition vorherrscht, enthüllen die Mutanten entweder verstärkte Substratinhibition (Mutanten I369F und I369L) oder S-förmige Profile, welche auf homotrope Kooperativität schliessen lassen (Mutanten A370V, A370L und S119A). Die Analyse der Kinetiken des CBZ-Metabolismus mit einem neuen Modell, welches den Formalismus der Hill-Gleichung unter Berücksichtigung von Substratinhibition anwendet, demonstriert einen Mechanismus für die Wechselwirkung zwischen CBZ und CYP3A4, welcher die Assoziation mehrerer Substratmoleküle beinhaltet.

Die produzierten Enzymvarianten wurden ebenfalls hinsichtlich ihrer Interaktion mit weiteren CYP3A4-Liganden untersucht. Die S119A-Mutante zeigt neuartige Typen inverser und bidirektionaler Spin-Übergänge unter Assoziation von Liganden. Die I369F-Mutante weist (gegenüber dem Wildtyp) eine im Mittel verdoppelte Affinität und eine um ein Mehrfaches gesteigerte Enzym-Aktivität bei geringer Substratkonzentration ($<< S_{50}$) gegenüber einer Gruppe von strukturell verschiedenen Substraten auf. Die I369F-Mutante stellt deshalb eine optimierte Enzymvariante dar für die Verwendung in Cytochrom-P450-basierten Biosensoren mit deren prospektiven Anwendungen in der Detektion von Medikamenten und in der personalisierten Medizin. Diese umfassende Studie präsentiert neuartige CYP3A4-Mutanten, deren Studium ein besseres Verständnis der funktionellen Komplexität und Vielfalt von CYP3A4 ermöglichen.

ABBREVIATIONS

7BQ	7-benzyloxyquinoline
ALA	5-amino-4-oxo-pentanoic acid (δ-aminolevulinic acid, δ-ALA)
AMP	adenosine monophosphate
BCT	bromocriptine
CHAPS	3-[(3-cholamidopropyl)-dimethylammonio]-1-propanesulfonate
CYP3A4	cytochrome P450 3A4
CPR	NADPH-cytochrome P450 oxidoreductase
DMSO	dimethyl sulfoxide
DTT	dithiothreitol
EDTA	ethylenediaminetetraacetic acid
ERY	erythromycin
EST	estradiol
FAD	flavin adenine dinucleotide
FMN	flavin mononucleotide
HEPES	2-[4-(2-hydroxyethyl)piperazin-1-yl]ethanesulfonic acid
IPTG	isopropyl β-D-1-thiogalactopyranoside
NADPH	nicotinamide adenine dinucleotide phosphate
PC	principal component
PCA	principal component analysis
PCR	polymerase chain reaction
PMSF	phenylmethanesulfonyl fluoride
SDS	sodium dodecyl sulfate
SDS-PAGE	sodium dodecyl sulfate (SDS) polyacrylamide gel-electrophoresis
TRIS	tris(hydroxymethyl)aminomethane hydrochloride
TST	testosterone

FOREWORD

This PhD thesis deals with functional aspects of the 3A4 isozyme of the cytochrome P450 superfamily, which has been stated to undoubtedly be the most popular research topic in biochemistry and molecular biology over the 2nd half of the 20th century due to its importance for the pharmaceutical industry (*1*). It has been more than fifty years since Garfinkel (*2*) and Klingenberg (*3*) first reported the existence of an unusual cytochrome with a characteristic Soret absorption maximum of its carbon monoxide adduct (*4*) at 450 nm. Hence, it was later named cytochrome P450. Cytochromes P450 comprise a vast family of heme-thiolate enzyme proteins that are able to activate molecular dioxygen into highly oxidizing forms of oxygen. The activated oxygen is subsequently inserted into a non-activated substrate; hence the other name, mono-oxygenases, for cytochromes P450. The popularity of cytochrome P450 in research may also partially stem from their ubiquitous nature. Even though they are represented in all five biological kingdoms and are found in most organisms, they seem to have diversified from a single ancestral protein during the course of biological evolution (*5*). Cytochromes P450 share a common protein fold but vastly differ in substrate selectivity. Processes catalysed by cytochromes P450 range from drug metabolism to the biosynthesis and metabolism of fatty acids, steroids, prostanoids, vitamins D and bile acids, alkaloids, terpenes, the detoxication of carcinogens, pesticides, and other xenobiotics, the metabolic activation of procarcinogens, and the generation of potentially harmful oxidizing agents (*1*).

Cytochrome P450 families metabolize more than 200,000 chemicals and catalyse many different types of reactions including oxidations, epoxidation, *N*- and *O*-demethylations, and reductions, including dehalogenations. Some 1200 cytochromes P450 had been isolated up to 2001, and the number is expected to have greatly increased by today due to significant advances in sequencing technologies and the radical transformation of the field in the age of next-generation sequencing (*6-10*).

In the 21st century, cytochromes P450 continue to attract a high level of interest; 2013 has been a particularly active year in the field. A survey into the number of publications per year that contain the keyword '*P-450'* or '*CYP3A4'* on PubMed reveals that the number of publications comprising any of the two keywords is still increasing[1] (Figure 1). In 2013 alone, there were more than 2000 citations of *'P-450'* per year. CYP3A4, the most abundant cytochrome P450 in human liver, has seen a remarkable boost in attention in the last year, which is reflected in a jump by

[1] data retrieved on April 28, 2014 from http://www.ncbi.nlm.nih.gov/pubmed

almost 200 hits. Due to its unique importance for the pharmaceutical industry, such as its relevant role in drug-drug interactions and adverse drug reactions, CYP3A4 has become the most considered cytochrome P450. The list of approved drug products of the U.S. Food and Drug Administration (FDA) from December 2012, that starts with abacavir and ends with zyvox, encompasses 60 pages with ca. 60 drug products per page (→ totally ≈ 3600 drugs). As CYP3A4 is estimated to metabolize ~ 50% of all currently marketed drugs, we may conclude that a vast number of at least 1800 substrates and these are just the pharmaceuticals (!) - is metabolized by this isoform. Moreover, such transformations may result in an incredible number of potential drug-drug interactions, i.e. situations where the activity of a drug is affected in the presence of another drug: $\frac{1800 \cdot 1799}{2} = 1'530'000$. From such astronomic numbers, it is easily understood why CYP3A4 has maintained its role as an extensively studied enzyme. Given the steady increase in the number of available pharmaceuticals, the interest in CYP3A4 is likely to increase even more.

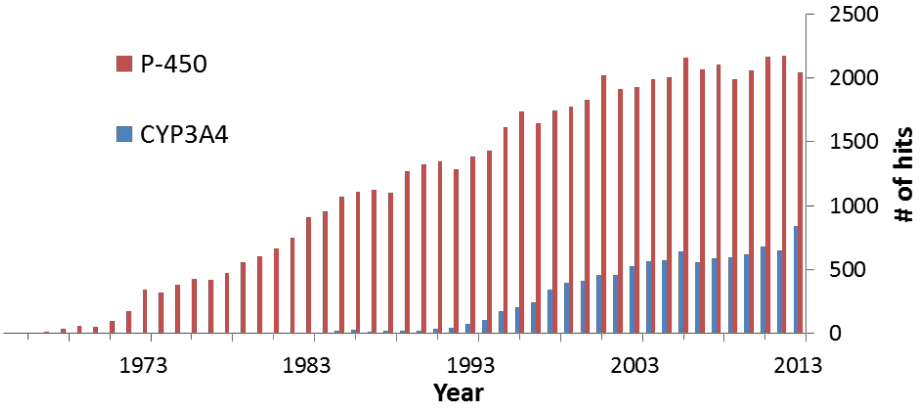

Figure 1: Increase of the hits for the search terms *"P-450"* and *"CYP3A4"* over time. While the first papers on CYP3A4 have appeared in 1975, the share of the total number of publications that deal with CYP3A4 in some form has risen over the past decades. Note that cytochrome P450 was mostly referred to as 'P-450' before the mid-1980s.

1 INTRODUCTION AND BACKGROUND SUMMARY

1.1 CYTOCHROME P450

Cytochromes P450 (P450s, CYPs) are a diverse group of heme-thiolate enzymes found in almost all organisms across all kingdoms of life (*1*). Members of the enzyme superfamily catalyse a wide variety of mono-oxygenation reactions. Cytochromes P450 are arranged into families (> 40% sequence identity) and subfamilies (> 55% sequence identity) based on their amino acid sequence similarity (*11*). The first purification of a cytochrome P450 was achieved in 1970 for a soluble enzyme from *Pseudomonas putida*, P450cam (*12*). It was the first to be characterized *via* x-ray crystallography (*13*) and is one of the most extensively investigated of all cytochromes P450. Membrane-bound cytochromes P450 from animal and plant sources were more difficult to purify in the beginning due to their instability towards solubilization with detergents that converted the enzyme to its inactivated P420 form. A breakthrough in the purification of membrane-bound P450s was the discovery that high concentrations of glycerol stabilize the enzyme (*14*), which marked the beginning of an era of successful purifications of various forms that started in the 2nd half of the 1970s.

The term “cytochrome P450” stems from the characteristic spectrophotometric property of the enzymes to absorb at 450 nm when bound to CO in the iron (II) form of the heme cofactor (*4*). Most cytochromes P450 rely on a protein partner that delivers one or more electrons to the heme iron to be transferred subsequently to molecular oxygen. Based on the type of the electron transfer protein, cytochromes P450 can be classified into several groups (*15*) (Table 1).

Table 1: Cytochrome P450 systems and their electron sources.

Cytochrome P450 System	Source of Electrons
Bacterial P450	Ferredoxin reductase and ferredoxin
CYB5R/cyb5/P450	Cytochrome b_5 (both electrons)
FMN/Fd/P450	FMN-domain-containing reductase (fused to P450)
Mitochondrial P450	Adrenodoxin reductase, adrenodoxin
Microsomal P450	NADPH (*via* cytochrome P450 reductase, CPR)
P450-only	No external reducer

The major families of cytochromes P450 are CYP1A, 2A, 2B, 2C, 2D, 2E, 3, 4, 5, 7, 11 (animals), 51-66 (fungi), 71-100 (plants), 101-120 (bacteria) (*1*). While mitochondrial and the bulk of bacterial cytochromes P450 are highly selective in their choice of substrates and the specificity of their reactions, the mammalian microsomal enzymes exhibit a high level of promiscuity in substrates and reactions. The latter have important roles in the oxidative detoxification of drugs and

environmental chemicals as well as in pathways of endogenous metabolism, including steroid biogenesis and the metabolism of retinol and retinoic acid.

In humans, 57 genes coding for cytochromes P450 have been identified. The human forms are primarily membrane-associated enzymes that are either located in the inner membrane of mitochondria or in the endoplasmatic reticulum of cells. The liver exhibits the highest content of cytochromes P450, although they are found in most tissues including kidney, breast, prostate, skin and nasal epithelium, gonads, placenta, brain, lung, spleen, pancreas, and gastro-intestinal tract (*1*). 12-15 % of the endoplasmatic reticulum is composed of cytochromes P450, accounting for about 1-2 weight % of an individual hepatocyte (*1*). The major human forms are CYP1A1, CYP1A2, CYP2C9, CYP2D6, CYP2E1, and CYP3A4 (*16*).

1.2 THE CATALYTIC CYCLE OF CYTOCHROME P450

Cytochromes P450 catalyse the incorporation of one atom of molecular O_2 into a substrate RH, while the second atom is reduced to H_2O obeying the stoichiometry:

$$RH + O_2 + NAD(P)H + H^+ \rightarrow ROH + H_2O + NAD(P)^+$$

In microsomal P450s such as CYP3A4, electrons are transferred via a route involving the co-factors nicotinamide adenine dinucleotide phosphate (NADPH), flavin adenine dinucleotide (FAD), and flavin mononucleotide (FMN) from cytochrome P450 oxidoreductase (CPR) via P450 onto the substrate (*15*):

$$NADPH \rightarrow FAD \rightarrow FMN \rightarrow P450 \rightarrow O_2/\ RH$$

Some microsomal forms may obtain the second electron from NADH through cytochrome b_5 reductase and cytochrome b_5 (*15*).

The catalytic cycle of cytochrome P450 (displayed in Figure 2) has been object of remarkable research for more than four decades. The iron (III) resting state binds the substrate that displaces a water molecule as the sixth heme ligand. The reduction of the iron (III) complex with one electron from CPR leads to the (deoxy-) iron (II) state, which is then able to bind molecular oxygen. Binding of molecular oxygen subsequently forms an oxyiron (II) complex. The addition of the second electron from CPR and a proton to oxyferrous cytochrome P450 results in a hydroperoxo-iron (III) intermediate ($Fe^{3+}OOH^-$ or Compound 0). The second protonation leads to O-O bond cleavage with

concomitant loss of water and is thought to generate the active oxygen π-cation radical oxoferryl state (Fe^{4+}=O or Compound I). Similar to Compounds I and II, this is a highly electrophilic intermediate that leads to the insertion of the oxygen into the substrate to form the oxidized product, and cytochrome P450 returns to its initial resting state *via* unbinding of the product (*17*).

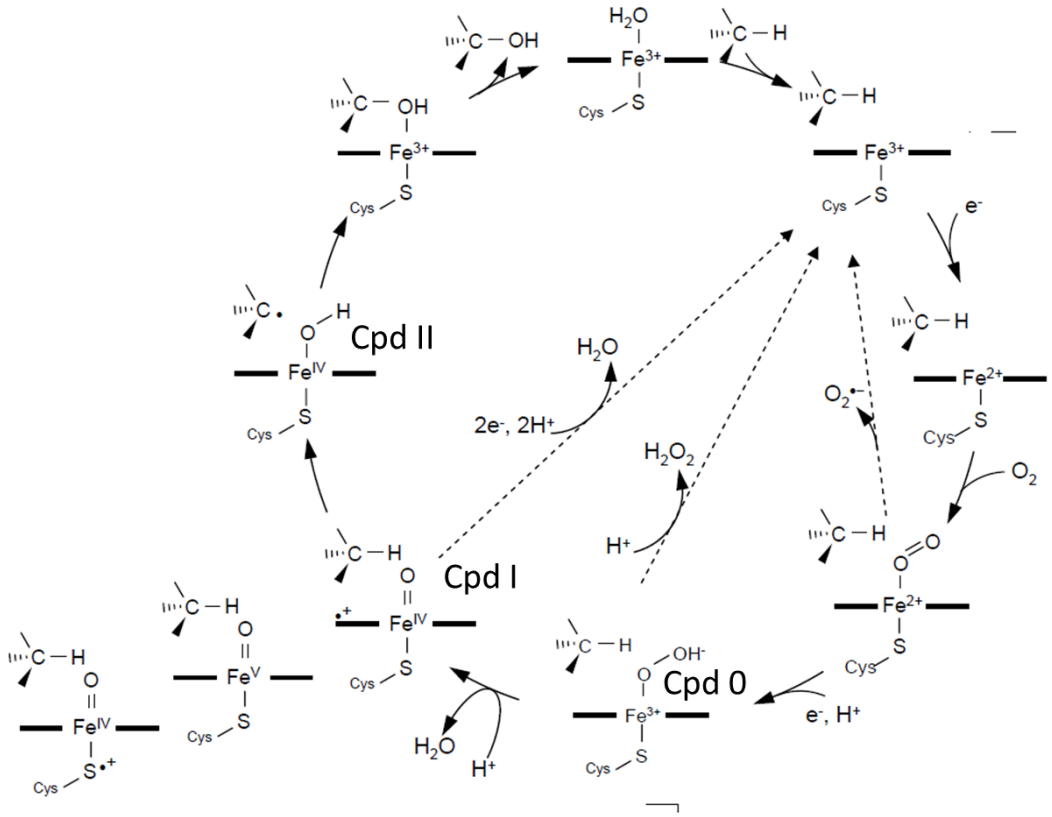

Figure 2: Catalytic cycle of cytochrome P450 showing the various iron oxygen intermediates. Unproductive pathways are depicted with dashed arrows (reproduced with permission of Willem H. Koppenol).

All intermediates of the reaction cycle except Compound II have been observed (Compounds 0, and I only under non-physiological conditions though) and most of them have been thoroughly characterized (*17-22*). It has been generally agreed that oxoferryl cytochrome P450 is the key intermediate in alkane hydroxylations, but it has also been proposed that multiple electrophilic oxidants other than the oxoferryl state may be involved in P450-catalyzed reactions, such as the peroxo- and hydroperoxo- iron (III) state in olefin epoxidations (*17, 23*) as well as in hydroxylations (*24*). The terminal electrophilic species, i.e. the oxoferryl state, has remained elusive until recently.

It has been generated by reacting iron (III) CYP119 with *m*-chloroperbenzoic acid (*21*) or by oxidizing CYP119 or CYP2B4 to their Compound II species (the iron(IV) hydroxide or iron(IV)-oxo intermediate) with peroxynitrite and then irradiating with 355 nm light (*25-28*). The relative importance of the individual oxidative intermediates for substrate oxidations has remained subject to controversial discussions.

1.3 NADPH CYTOCHROME P450 OXIDOREDUCTASE

The enzyme NADPH-cytochrome P450 oxidoreductase, abbreviated as CYPOR or CPR (here we will use the notation CPR), is essential for electron donation to microsomal cytochromes P450 (reference (*29*) pp. 115 – 148). It receives electrons from NADPH and transfers them via FAD and FMN. FMN hydroquinone transfers the electrons, one at a time, to CYP3A4 or other redox partners, which include microsomal heme oxygenase, cytochrome b_5 and, although not in a physiological environment (*in vivo*), cytochrome *c (30).* The latter is commonly used in oxidised form for quantification of CPR contents in complex samples where a spectroscopic determination is impossible (see also chapters 2 and 3) (*31*). Similar to microsomal cytochrome P450, CPR has two functional domains: a hydrophobic membrane-binding domain at the *N*-terminus and a hydrophilic *C*-terminal catalytic domain, which in turn is comprised of several structural domains. The *N*-terminal domain of CPR is a hydrophobic 6 kDa polypeptide that anchors the protein to the endoplasmatic reticulum and nuclear envelope (*32*) and facilitates spatial interaction for electron transfer from CPR to P450. Without the hydrophobic anchor, the hydrophilic and soluble *C*-terminal domain still passes electrons to cytochrome *c*, but is not capable of reducing cytochrome P450 (*30*).

CYP3A4 receives electrons from CPR at two separate steps in the reaction mechanism (see chapter 1.2) (*33*). Deletion of the *POR* gene that encodes CPR essentially leads to inactivation of all microsomal cytochromes P450. This has been exploited in evaluating cytochrome P450 function in normal homeostasis, drug pharmacology, and chemical toxicity *in vivo* (*29*). Twenty-six missense mutations/polymorphisms of the *POR* gene have been described and were associated with the Antley-Bixer syndrome and/or disordered steroidogenesis, which lead to defects in bone development and sexual dimorphisms (*33-36*).

1.4 CYTOCHROME P450 3A4 (CYP3A4)

Cytochrome P450 3A4 (CYP3A4) is the most abundant form in most adult humans. It metabolizes about 50% of all marketed drugs (*37*), which is a huge number in view of the list of the approved drugs by the U.S. Food and Drug administration, a report that currently contains ~3600 drug products[2]. CYP3A4 has the heme group in the active site and consists of a small *β*-strand *N*-terminal and a larger *α*-helical *C*-terminal domain (*38*), and adopts the typical fold of the cytochrome P450 superfamily (*39*). The three other members of the 3A family are CYP3A5, CYP3A7, and CYP3A43. CYP3A5 has 85% sequence identity with CYP3A4 and is thought to have a much lesser pharmacological importance than CYP3A4, as are the other two. However, CYP3A5 has a polymorphic and racial distribution with possible relevance to clinical issues (*29*). CYP3A7 is the major cytochrome P450 in human fetal liver and also present in other fetal tissues, but decreases in abundance during the first week of life and plays no major role in the metabolism of adults (*29*). CYP3A43 makes most likely contribution to drug metabolism, even though it may have specialized roles in extrahepatic tissues.

The heme iron in CYP3A4 is ligated by the side-chain group of the conserved cysteine residue Cys442 at its proximal ligand binding site. The propionates of the heme are in contact with the side chains of Arg105, Trp126, Arg130, Arg375 and Arg440 (*38*). The structure of CYP3A4 (Figure 3) differs in a number of features from other cytochrome P450 structures (*38, 40*). A hydrophobic region (residues 36 – 50) is located around the loop following a helix that is not observed in other cytochrome P450 structures, helix A''. This region is thought to mediate the interaction of CYP3A4 with the microsomal membrane along with the G'-helix and the hydrophobic GG' loop. Another unexpected structural feature of CYP3A4 is the F-helix that is markedly short compared with other cytochrome P450 structures. It is followed by an ordered polypeptide stretch that does not conform to any secondary structure motif. This stretch is perpendicular to the I-helix and contains several amino acid residues that play a direct or indirect role in CYP3A4 function. Leu211, Asp214, and Leu210 are implicated in allostery as well as regio- and stereoselectivity of CYP3A4 (*41-44*) and are situated in this region. The side chains of these residues are pointing away from the active site in the structure 1W0G (see Figure 3*b-c*) (*38*). Two other residues in this extended loop region that were shown by site-directed mutagenesis to have no role in cooperativity (*42*), Phe213 and Phe215, point toward the active site and form the "phenylalanine cluster" along with Phe108, Phe219, Phe220, Phe241, and Phe304. This

[2] http://www.fda.gov/Drugs/default.htm

phenylalanine cluster is another characteristic feature of CYP3A4 and lies above the active site. Its aromatic side chains stack against each other to form a highly ordered hydrophobic core. The position of the phenylalanine cluster causes a closed conformation of the active site in the first reported x-ray structure of CYP3A4 (1W0G) (*38*) similar to the closed conformation of cytochrome P450 EryF (*39*). However, the spatial arrangement of the F-G loop and the F helices is not conserved. The F-G region is part of a portion of CYP3A4 that is predicted to reside within the lipid bilayer along with the N-terminal membrane anchor α-helix (*11*). Helices F and G and the intervening loops underwent the most prominent conformational changes upon binding of erythromycin (CYP3A4 substrate and inhibitor) and ketoconazole (CYP3A4 inhibitor) (*45*). The F-F'-G-G'-sequence of α-helices is assumed to be the primary interaction site of CYP3A4 with substrates.

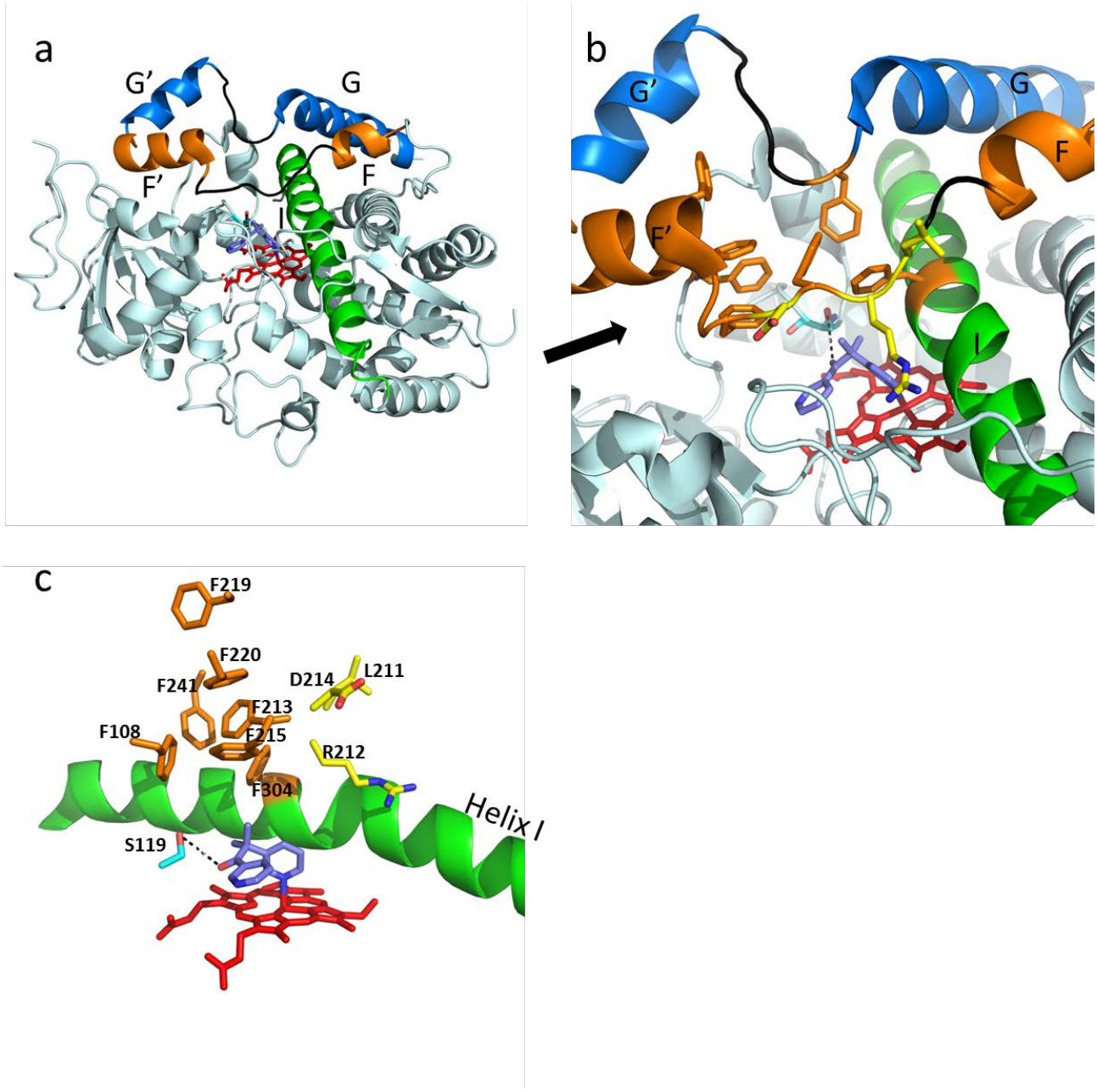

Figure 3: X-ray structure 1W0G of CYP3A4 (*38*). Some of the most important structural features are highlighted. Panel (*a*) shows the overall structure of CYP3A4 with the F/F'-helices (orange), the G'/G-helices (marine) and the I-helix (green). The FF'- and GG'-loops are shown in black. In panel (*b*), residues of the FF'/GG' region important for substrate recognition are highlighted (Phe residues are shown in orange, Leu211, Arg212, and Asp213 are shown in yellow). The inhibitor metyrapone (shown in violet) is ligated to the heme iron (shown in red) via direct *N*-ligation and is likely to be hydrogen-bonded to the side chain hydroxyl of Ser119 (shown in light blue). In panel (*c*), a view of the structure along the axis of the black arrow in (*b*) is presented. Side chains of residues discussed in the text are shown and labelled; the Phe residues constituting the Phe-cluster are shown in orange, residues Leu211, Arg212 and Asp214 of the FF'-loop involved in allostery are shown in yellow, Ser119 is shown in light blue.

Molecular dynamics simulations have predicted this sequence to undergo large-scale movements upon interaction with the lipid bilayer, which allow for opening and closing of the substrate access channel (*46*, *47*). This region has also been suspected to harbor a peripheral effector binding site (*48*, *49*) close to the progesterone binding site identified in the 1W0F X-ray structure (*38*). It is however likely that this area binds potentially harmful hydrophobic substances (such as toxins) non-specifically, which are then directed to the active site for possible oxidation and neutralization (*11*).

An important feature is the accessibility of the heme in the active site of CYP3A4, which is greater than in, for instance, CYP2C9 (*38*). This allows CYP3A4 to accommodate either large ligands or several smaller ligands, which may all have access to the activated distal oxygen. This is in agreement with a large body of data indicating that CYP3A4 can simultaneously bind and/or metabolize several molecules of certain substrates or inhibitors, such as pyrene (forming pyrene-pyrene complexes with excimer emission) (*50*) or ketoconazole (*45*) (see also chapter 1.5). The total solvent-accessible volume of the active site undergoes large changes depending on the presence and identity of a ligand (*45*). The volume in the ligand-free structures was estimated to amount to ≈ 950 Å^3. In a complex with ligands, the volume increased to 1650 Å^3 for erythromycin (structure 2J0D) and to ≈ 2000 Å^3 in the presence of two ketoconazole molecules in the binding pocket (structure 2V0M).

As a consequence of its flexibility and its large active site, CYP3A4 is a highly unspecific and promiscuous enzyme and can accommodate and metabolize substrates of large diversity in size and chemical structure. This makes CYP3A4 a key player in drug metabolism and gives rise to a sensitivity of drug metabolism to changes in CYP3A4 activity (e.g. due to inhibition or activation of its metabolism) and expression level. Through fast or slow degradation, CYP3A4 can lower or increase the drug disposition or bioavailability of pharmaceuticals. One of the co-administered drugs may increase the plasma concentration of another drug and lead to toxic drug plasma levels, but may also induce cytochrome P450 gene expression and thus upregulate protein production or directly activate drug metabolism and lead to low, ineffective drug levels. For instance, low levels of an immunosuppressant (e.g. cyclosporine) will not prevent organ tissue rejection after transplantation, but high levels may cause renal toxicity (*29*). Because many pharmaceuticals have narrow therapeutic indices and are CYP3A4 substrates, their dose needs to be adjusted for optimal therapy; preferably their concentrations are monitored continuously to prevent adverse drug reactions (see p. 29). Interactions between simultaneously administered drugs may affect drug clearance and the outcome of drug therapies and are therefore also of major importance for the pharmaceutical industry.

Carbamazepine, an anticonvulsive and CYP3A4-substrate (Figure 4), is an example of a narrow therapeutic index drug with a target blood plasma concentration of 17 – 70 μM (*51*). The CYP3A4-dependent metabolism of carbamazepine is the subject of chapter 4. CYP3A4 is furthermore involved in steroid biosynthesis and bioactive metabolite production, for instance vitamin D and retinoic acid metabolites (reference (*29*) pp. 423 – 430). Atypical functional properties of CYP3A4 are addressed in chapter 1.6 (see p. 19).

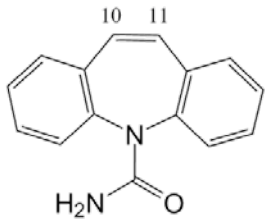

Figure 4: Chemical structure of carbamazepine (CBZ). The numbered carbon atoms mark the epoxidation site in the CYP3A4-dependent reaction.

1.5 LIGAND BINDING TO CYP3A4 AND REGULATION

Iron catalysis in biology is potentially dangerous, because lethal levels of reactive oxidants can be formed. Such catalysis is not restricted to hemoproteins and iron thus needs to be tightly regulated by the organism. In cytochromes P450, catalytic activity is regulated through the change in the electrode potential of the heme iron that accompanies the spin transition upon binding of the substrate in the active site of the enzyme. In the substrate-free resting state of most cytochromes P450, heme iron (III) is predominantly present in the (S = 1/2) low-spin state. Some exceptions (e.g. CYP1A2) are predominantly isolated in the high-spin state (S = 5/2) in the absence of substrates. They are therefore not amenable to the typical spectral analysis methods of substrate binding to cytochromes P450 that are based on a change of spin state (*52*). In the resting state in the absence of ligand, the coordination of water at the sixth (distal) ligand position stabilizes Fe (III) in the low-spin hexacoordinated state (S = 1/2). Type I substrates bind to the active site near to the distal ligand binding site with a hydrophobic moiety and can displace the bound water molecule. They account for the common type of substrates that are metabolized by cytochromes P450. Binding of type I ligands effect a shift in the Soret band from ~ 416 nm to ~ 391 nm, and induces a change in the spin state of the heme iron from low-spin (S=1/2) to high-spin (S=5/2). For most soluble bacterial cytochromes P450, the substrate-induced spin shift is correlated with a change in the electrode potential of the protein (*53-55*). For CYP3A4 incorporated into nanodiscs, a protein

scaffold that simulates a native-like membrane bilayer (*56*), the type I spin shift accompanies a shift in the reduction potential of the heme (iron (III) → iron (II)) of ~ +80 mV for substrates such as bromocriptine and testosterone that are capable to induce a strong spin shift (see chapter 5) (*57*). Binding of a type I ligand therefore facilitates the reduction of heme, which then favors binding of molecular dioxygen. Substrate binding also contributes to a stabilization of the iron adduct with the activated oxygen species (*58*). In most cases, O_2 only binds at the sixth iron coordination site when substrate is bound to the active site. This ensures that highly oxidizing species are only formed in the presence of substrate and, therefore, that only the substrate is oxygenated. The stronger the type I ligation of heme (the higher its ability to perturb water ligation), the larger is the spin shift. The reduced oxyiron (II) CYP3A4 is predominantly present in the high-spin pentacoordinated state. The local dielectric constant at the heme can also affect the electrode potential of the heme protein. Iron (II) heme is neutral, while iron (III) heme exhibits a net positive charge (*57*). Additionally, the local dielectric constant may also interfere with the spin equilibrium of iron (III) CYP3A4 via disruption of the water network that provides the (sixth) water ligand (see chapter 5).

Inhibition of CYP3A4 is an issue for the pharmaceutical industry due to a number of clinically important drug-drug interactions. A well-known example is the inhibition of CYP3A4 by grapefruit juice with its furanocoumarins bergamottin and 6',7'-dihydroxybergamottin, both mechanism-based inhibitors, such that warning labels contain this contraindication for many drugs (*29*). Herbal medicines often interact with cytochrome P450 metabolism. One of the most studied examples is St. John's wort, which is a strong inducer of CYP3A4 and reduces the effectiveness of oral contraceptives. The induction of CYP3A4 expression led to pregnancies, which were the result of an increase in the rate of elimination of 17α-ethynylestradiol, previously also reported for the induction caused by rifampicin and barbiturates.

Inhibitors of CYP3A4-dependent metabolism (see (*29*) pp. 247 – 325) can be divided into three groups: (a) reversible inhibitors, (b) quasi-irreversible inhibitors (that form complexes with the heme iron), and (c) mechanism-based inhibitors (that irreversibly bind to the cytochrome P450 or accelerate degradation or oxidative fragmentation of the heme). Reversible inhibitors show one or more of the following characteristics: they bind to the hydrophobic regions of the active site, they engage into hydrogen bonding or ionic interaction with active site residues, they directly coordinate to the heme iron. Most of the time, reversible inhibition encompasses two or more types of interactions. Ligands that undergo direct ligation to the heme iron atom *via* nitrogen - provided by imidazole, pyridine or primary amino groups - are called type II ligands. Binding of type II ligands induces a shift in the Soret band from ~ 416 nm to 420 – 424 nm and concomitantly lowers the electrode potential of cytochrome P450, which prevents both electron donation by a redox partner

and oxygen binding (*11*). Some antidepressants, steroids, macrolide antibiotics and other types of drugs are CYP3A4 inhibitors that do not act through nitrogen ligation, but inhibit the enzyme *via* reversible or irreversible binding and mechanism-based inhibition (*11, 59*).

Two very potent inhibitors of CYP3A4 are ketoconazole, a widely used antifungal drug, and ritonavir, a peptidomimetic HIV protease inhibitor that is also administered as a booster for the enhancement of the pharmacokinetics of other HIV protease inhibitors that are otherwise quickly metabolized by CYP3A4 (*11, 60, 61*) (Figure 5). For both inhibitors, X-ray structures of their complexes with CYP3A4 have been solved. Both inhibitors ligate active-site heme iron *via* their azole nitrogens. While ritonavir binds to CYP3A4 as one molecule in the X-ray structure 3NXU (*62*), the most interesting feature of the crystal structure of the ketoconazole-bound CYP3A4 (2V0M) is the presence of two drug molecules in the active site in antiparallel tandem configuration (*45*). Notably, in both structures, residue S119 contributes to the stabilization of ligand binding *via* hydrogen bonding to the ligand.

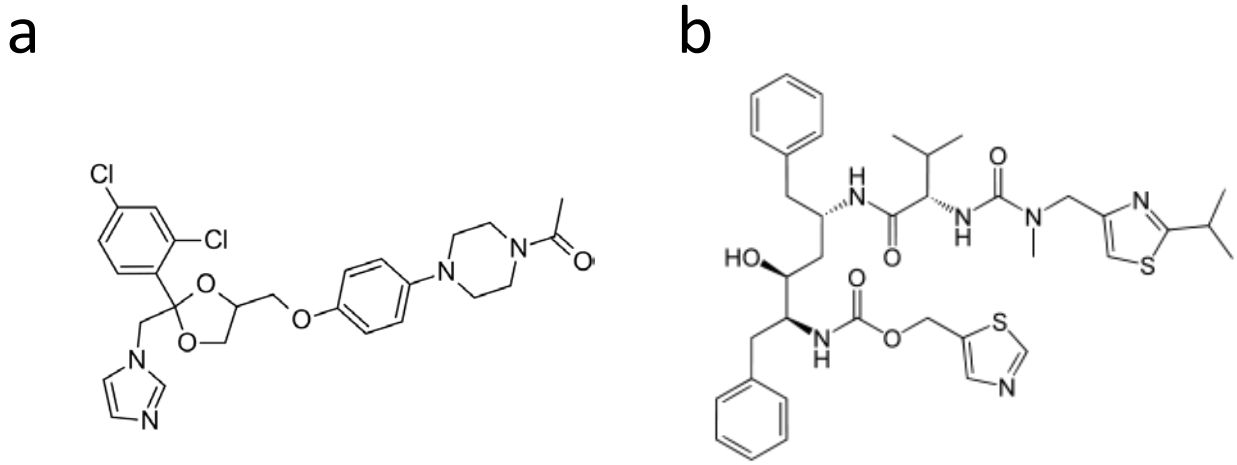

Figure 5: Structures of the two CYP3A4 type-II ligands (inhibitors) ketoconazole (a) and ritonavir (b).

Cytochrome P420 (*63-69*) is a cumulative term used to designate several stable, but inactive species with a changed sphere of ligation of the heme iron that can be produced spontaneously and generated via numerous chemical and physical means, such as increased temperature or pressure or addition of salts, denaturants or organic solvents (*64*). All these species have the Soret band of the ferrous iron (II) carbonyl complex positioned around 420 nm, instead of its positioning at 447-452 nm as in the P450 state of the heme protein. The nature of the proximal heme ligand of P420 has been subject to speculations. Still, it is generally accepted that the major P420 state represents the protonated form of the native cysteinate ligand, and it has been suggested that a ligand switch

replaces the protonated cysteine for a histidine to form a myoglobin-like heme coordination (*64, 69*). In the oxidized, ferric iron (III) state, both type II-ligated cytochrome P450 and the major, most commonly occurring cytochrome P420 form exhibit a similar Soret band maximum at 424-426 nm (*63, 70*) and discrimination between the P420 and the type-II ligand-bound cytochrome P450 state requires the examination of the spectra of the reduced carbonyl complex.

1.6 COOPERATIVITY AND ATYPICAL KINETICS IN CYP3A4

1.6.1 COOPERATIVITY AND ALLOSTERY

A large number of comprehensive reviews have been published on atypical kinetics in cytochrome P450. For a deeper understanding, the reader may wish to consult these reviews (*58, 71-75*). Most key biological processes are highly cooperative. Examples are as diverse as the formation of native biomolecules and their functional assemblies or cellular signalling and regulation (*58, 76*). Cooperativity and allostery result from a mutual perturbation of the functional properties of a biological macromolecule interacting with two or more ligands. This feature is exploited by many living systems to improve the sensitivity to perturbations and to amplify the response of their receptors and macromolecular transporters (*58*).

Cooperative functional properties and allosteric regulation play important roles in xenobiotic metabolizing systems, including cytochromes P450, and are regarded as one of the main underlying mechanisms of drug-drug interactions (*58*). In numerous biochemical and biophysical experiments with cytochrome P450 including NMR, calorimetry, surface plasmon resonance, time-resolved fluorescence, rapid kinetic approaches, and equilibrium spectroscopy, more diverse complex functional responses have been discovered and summarized under the term *atypical*, or *non-Michaelis-Menten* kinetics (*71, 77*). However, the plethora of data that has been published has rendered the term inappropriate. Manifestations of non-Michaelis-Menten kinetics in cytochrome P450 include substrate cooperativity (i.e. the stimulation of substrate turnover or substrate binding of an enzyme) and substrate inhibition. *Homotropic* cooperativity is revealed in sigmoidal (S-shaped) dependencies of the rate of metabolism (or of a spin shift upon substrate binding) on the concentration of the substrate. In *heterotropic* cooperativity, the functional response of the enzyme (in cytochrome P450 in terms of substrate binding or turnover) to ligand A is stimulated in the presence of ligand B. In this sense, homotropic cooperativity may be seen as the special case where the two molecules are identical (A = B). In heterotropic cooperativity, the functional response of the

P450 system is modulated in the presence of a molecule, which can be a substrate itself, such as α-naphthoflavone (ANF) (*78-81*) or testosterone (TST) (*79, 82, 83*), or an alternative ligand (non-substrate) such as glutathione (*84, 85*). If the binding of molecule B is not involved in catalytic action for the case of substrate turnover, it is referred to as *allosteric*: B is an *allosteric effector* that binds to an *allosteric binding site*. The effector is called *activator* if the catalytic activity of the enzyme towards the substrate is enhanced, and it is called *inhibitor*, if the activity is reduced. Cooperativity represents one possible type of allosteric regulation. Unfortunately, cooperativity and allostery are often used interchangeably in the literature on cytochrome P450. An important characteristic of cytochromes P450 is, in contrast to the vast majority of allosteric proteins discovered so far, that they show cooperative behavior also in their monomeric form (*58, 86*).

Protein as well as non-protein effectors are involved in *allostery* of microsomal cytochromes P450, including cytochrome b_5 (*87-91*) and glutathione (*84*), or inhibitors such as erythromycin and ketoconazole. Some divalent metal ions were also reported to enhance catalysis in microsomal cytochromes P450 (*92*). In the case of CYP3A4, in particular Mg^{2+} and Ca^{2+}, and to a lesser extent Sr^{2+}, stimulate some of the CYP3A4-catalyzed reactions (*85, 92, 93*). Mg^{2+} appears to increase the rate of electron transfer from NADPH-P450 oxidoreductase to cytochrome b_5 and CYP3A4 (*85*). The effect of the specific mutations L211F/D214E in CYP3A4 abolished cooperativity in CYP3A4 with the effectors ANF or testosterone (*44*). While wild-type CYP3A4 showed cooperativity in spectral binding studies with testosterone (as shown by a sigmoidal binding curve), the double mutant displayed hyperbolic behavior. The latter also displayed increased rates of testosterone and progesterone 6β-hydroxlation at low substrate concentrations and a decreased level of heterotropic stimulation by ANF.

Human CYP3A4 is a textbook example of a cooperative cytochrome P450, along with human CYP2C9 and CYP107 of *Bacillus subtilis* (*94*). CYP3A4 has a large and flexible substrate binding pocket capable of binding relatively large substrates with molecular weights >1000 Da (e.g. erythromycin, M_r = 1203 Da). The size and the flexibility of the binding pocket also allow for the simultaneous binding of several small (identical or different) organic molecules like carbamazepine (M_r = 236 Da, chapter 4) instead of one large molecule (*45*). The common conclusion in studies of CYP3A4 cooperativity is therefore that two or possibly more ligands co-occupy the large binding site as a requirement for one of the molecules to adopt a productive binding mode. Indeed, for some substrates, the simultaneous presence of several molecules has been established (*72, 95, 96*). This model is able to explain most cases of homotropic cooperativity, but fails to account for some cases of heterotropic cooperativity, where the turnover is stimulated many times (*74*). In such a case, an increase in activity towards a substrate occurs at low concentration of the other ligand (effector), but

this effect vanishes (or substrate turnover may even be inhibited) at saturating concentrations of the effector. The particular type and mechanism of allostery in CYP3A4 therefore depends on the specific substrate(s) or effector(s). As the homotropic and heterotropic cooperativity models are mutually incompatible, it is not possible to explain all instances of allostery in cytochromes P450 by a single mechanism.

From EPR and absorbance spectroscopy experiments, Roberts et al. concluded that binding of the first testosterone molecule occurs with the highest affinity and is "spectrally silent", i.e. it does not lead to a significant spin shift (*96*). Following their conclusion, the binding of the second testosterone molecule induces only a partial spin shift, and a third molecule is required for the maximum shift. Independently, Denisov and co-workers applied global analysis to equilibrium substrate binding and steady-state NADPH consumption kinetics, which resolved the fractional contributions to turnover of CYP3A4 with one, two, and three testosterone molecules bound. The first binding led to an increase in NADPH consumption, but did not induce a strong spin shift nor did it lead to significant product formation. A second testosterone molecule was required to reach maximum rate in catalysis, whereas the third molecule mainly increased the coupling efficiency of redox equivalent usage (*72*).

In normal vernacular, cooperativity implies changes in ligand affinity induced at one site in a macromolecule by binding at one or more additional sites (*94*). It was however suggested that a sigmoidal, seemingly cooperative effect can also be explained without the requirement of functional cooperativity (*58, 72, 79, 96-98*). A non-hyperbolic response only requires several binding sites for the substrates and/or effectors and the catalytically active binding site to have the lowest affinity for the substrate (*58*). In this model, the high-affinity sites are saturated first during substrate titration but only offer a small fractional contribution to the total spectral response in spin shift or a negligible fraction of the total product formation rate. The binding of a second molecule to a lower affinity site would result in the formation of a catalytically competent enzyme-substrate complex. Only when the substrate binds to the immediate vicinity of the catalytically active heme can this be detected by spectral or functional responses (such as spin shift, NADPH consumption, or appearance of product). All of these functional readouts unambiguously indicated non-hyperbolic, apparently cooperative responses in the case of testosterone. In this example, an apparently cooperative effect (sigmoidal substrate dependence) may be explained by the differential functional contributions of the individual enzyme states, namely CYP3A4 with one, two or three testosterone molecules bound. This model provides a robust foundation to explain sigmoidal dose-response functions in the case of steroids. The model may however not be applicable to other substrates. In particular, the assumption that the spectrally silent binding site is associated with high affinity

binding is not maintained in the case of Nile Red, a fluorescent allosteric substrate of CYP3A4. Nile Red was found to exert a sigmoidal spin shift in CYP3A4 (*99*). However, with the help of a fluorochromic effect upon binding to CYP3A4 in the active site (emission maximum is blue-shifted: λ_{red} ~ 660 nm to λ_{blue} ~ 620 nm), but not at the peripheral site, the authors concluded that the high-affinity binding site ($K_D \approx 50$ nM) is in the active site, whereas the low-affinity binding site ($K_D \approx 2.2$ μM) lies at the periphery of CYP3A4 (*100*). In chapter 5, we report multiple binding of cooperative substrates to the CYP3A4 S119A mutant and their bidirectional effects on the spin state.

An X-ray structure of a complex of CYP3A4 with progesterone established a location in the flexible FF'GG' region on the CYP3A4 globular surface as a potential place for a peripheral binding site (*38*) for an allosteric effector. The two helices F' and G' are absent in cytochrome P450 BM3, EryF, and other structures of the bacterial forms (*38*). A study involving Förster resonance energy transfer (FRET) suggested that the peripheral ligand binding site is in a region close to the progesterone binding site (*49*). High-affinity binding at the periphery may exert important effects on the functional response of CYP3A4 and be involved in heterotropic cooperativity (*48, 49*). For CYP3A4 incorporated into the lipid bilayer of microsomes, this site is likely located at the solvent/membrane interface and is therefore thought to interact with the components of native membranes such as lipid head groups, steroids and fatty acids (*58*). The interaction of this site with the lipid bilayer or effector molecules is expected to affect the large-scale conformational change ('open-close' movement) of CYP3A4 that is thought to be important for substrate binding and release (*101-103*). On the other hand, direct participation of the tentative peripheral ligand binding site in substrate turnover or spin shift is thought to be insignificant, as studies on testosterone binding suggest (*58, 72, 79, 97, 98*). In fact, binding to the tentative peripheral ligand binding site caused only a negligible perturbation of the spin state of the heme iron (less than 20% spin shift for TST (*72*) and less than 4 % for ANF (*79*)) and did not lead to product formation.

Observations of several-fold increased substrate turnover in the presence of allosteric effectors (heterotropic cooperativity) have been attributed to an effector-induced redistribution of a pool of cytochrome P450 conformers with dissimilar activity and substrate specificity (*74, 78, 81*). Evidence for conformational heterogeneity was obtained from kinetics studies on the reduction of the heme iron in cytochrome P450 by sodium dithionite ($Na_2S_2O_4$, tetraoxidodisulfate sodium) (*104-106*) or other artificial electron donors, or the kinetics of CO binding (*107*). Some allosteric effectors may induce a conformational change in CYP3A4. The existence of non-interconverting subpopulations suggests that the expression 'spin equilibrium' is not applicable to the pool of

CYP3A4 taken as a whole, but rather to the several stable subpopulations of the enzyme. In chapter 7.2, some of the results of ref. (*105*) are reproduced, but with the mutants generated for this thesis.

The formation of cytochrome P450 oligomers in membranes has been shown in several studies on rotational diffusion (*74*). Recently, the effect of oligomerization of CYP3A4 on the kinetics of the reduction of the enzyme with the flavin domain of cytochrome P450-BM3 (BMR) as a model electron donor partner (*108*) and on the degree of activation by the heterotropic activator ANF (α-naphthoflavone) (*78*) have been studied. Besides homo-oligomerization, CYP3A4 also forms hetero-oligomers with CYP1A1, CYP2B4 or CYP1A2. For instance, CYP3A4-mediated metabolism of testosterone was stimulated when co-reconstituted with CYP1A1 or CYP1A2, but no effect was found in reconstitutions with CYP2C9, CYP2D6, or CYP2E1 (*109*). For detailed discussions on the formation of cytochrome P450-P450 complexes in membranes and their effect on the function of the enzymes, the reader is referred to recent review articles (*16, 73, 74*).

Whereas CYP3A4 cooperativity has initially been understood as a case of pseudo-allostery due to multiple substrates binding into a large, rather static, binding pocket, the allosteric mechanism is now acknowledged to be much more complex. The mechanism is most likely a combination or overlay of the results of multiple substrate binding (space-filling mechanism) combined with ligand-induced changes in the conformation and redistribution of a set of enzymatic states that are maintained in the membrane due to oligomerization (*74*).

1.6.2 MATHEMATICAL FRAMEWORKS FOR ALLOSTERY IN CYTOCHROMES P450

Mathematical frameworks for the handling of multi-site substrate binding have been proposed in the form of sequential ordered binding or sequential random binding models. We will consider the simplest case of a two-site sequential ordered model of substrate binding to one macromolecule (*96*). Since binding affinities of the individual binding sites in CYP3A4 are often assumed to substantially differ, the use of the simplified sequential ordered model in these cases is permissible (Scheme 1).

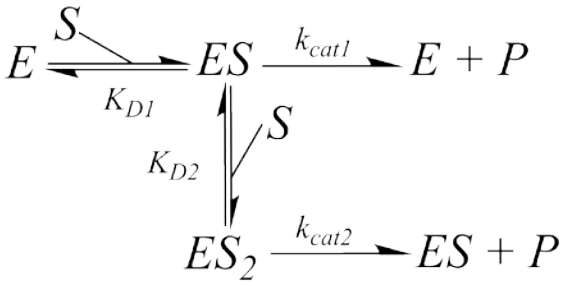

SCHEME 1

An enzyme *E* can bind a single substrate *S* to form a complex *ES* with an equilibrium dissociation constant $K_{D1} = K_1$. The complex *ES* can then bind a second substrate molecule *S* to form *ESS*, a ternary complex with a dissociation constant $K_{D2} = K_2$. As per definition the two binding sites in a single cytochrome P450 are non-identical, binary and ternary complexes may be denoted by writing *SES* or ES_1S_2 instead of $ESS \equiv ES_2$. However, for simplification, we forego the distinction between the binding sites in the formalism of the derivation. *ES* and *SES* can both react to irreversibly form product *P* with rate constants k_{cat1} and k_{cat2}, respectively. In the following, the derivation for the functional responses of a system according to the sequential ordered two-site or three-site model is reproduced (*58, 77, 96*).

Via transformations, the concentrations of $[ES]$ and $[ESS]$ are obtained from the definition of the dissociation constants:

$$K_1 = K_{D1} = \frac{[E][S]}{[ES]} \tag{1.1}$$

$$\Rightarrow [ES] = \frac{[E][S]}{K_1} \tag{1.2}$$

$$K_2 = K_{D2} = \frac{[ES][S]}{[ESS]} \tag{1.3}$$

$$\Rightarrow [ESS] = \frac{[ES][S]}{K_2} = \frac{[E][S]^2}{K_1 K_2} \tag{1.4}$$

The fractions of singly- and doubly-occupied enzymes can be expressed as:

$$\frac{[ES]}{[E_T]} = \frac{[ES]}{[E]+[ES]+[ESS]} = \frac{\frac{[S]}{K_1}}{1+\frac{[S]}{K_1}+\frac{[S]^2}{K_1K_2}} \tag{1.5}$$

$$\frac{[ESS]}{[E_T]} = \frac{[ESS]}{[E]+[ES]+[ESS]} = \frac{\frac{[S]^2}{K_1K_2}}{1+\frac{[S]}{K_1}+\frac{[S]^2}{K_1K_2}} \tag{1.6}$$

$[E_T]$ is the total concentration of enzyme in free form and in the binary and ternary complex ($[E_T] = [E] + [ES] + [ESS]$). The total functional response (in this case the enzymatic *turnover*) for the system is given by:

$$V = \frac{v_1\frac{[S]}{K_1} + v_2\frac{[S]^2}{K_1K_2}}{1+\frac{[S]}{K_1}+\frac{[S]^2}{K_1K_2}} \tag{1.7}$$

$$v_i = k_{cat_i} \cdot [E_T] \tag{1.8}$$

If v_1 (for the binary complex *ES*) is much higher than v_2 (for the ternary complex *ESS*), the equation predicts substrate inhibition kinetics. If v_2 is much higher than v_1, sigmoidal kinetics will be observed.

Equation 1.7 holds true for the turnover by an enzyme with two binding sites for a substrate with different reactivities from the two states [*ES*] and [ES_2]. It can easily be adapted to obtain the equilibrium binding equation by replacing all v_i parameters with appropriate scaling factors a_i for the observed signal. In the case of substrate binding to CYP3A4 (monitored *via* spin shift), a_1 and a_2 represent the fractional contributions to the total spin shift of singly- and doubly-occupied CYP3A4 (Eq. 1.9)

$$A = \frac{a_1 \frac{[S]}{K_1} + a_2 \frac{[S]^2}{K_1 K_2}}{1 + \frac{[S]}{K_1} + \frac{[S]^2}{K_1 K_2}} \tag{1.9}$$

In the case of three sequential ordered binding steps, Scheme 2 applies.

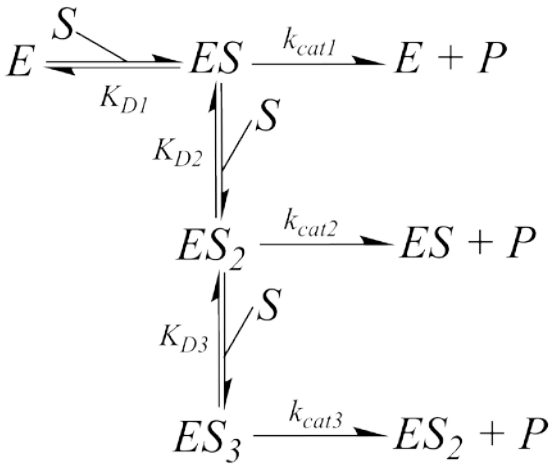

SCHEME 2

Accordingly, the overall reaction velocity (1.10) and equilibrium binding (1.11) of the three-site binding model are given as:

$$V = \frac{v_1 \frac{[S]}{K_1} + v_2 \frac{[S]^2}{K_1 K_2} + v_3 \frac{[S]^3}{K_1 K_2 K_3}}{1 + \frac{[S]}{K_1} + \frac{[S]^2}{K_1 K_2} + \frac{[S]^3}{K_1 K_2 K_3}} \tag{1.10}$$

$$A = \frac{a_1 \frac{[S]}{K_1} + a_2 \frac{[S]^2}{K_1 K_2} + a_3 \frac{[S]^3}{K_1 K_2 K_3}}{1 + \frac{[S]}{K_1} + \frac{[S]^2}{K_1 K_2} + \frac{[S]^3}{K_1 K_2 K_3}} \tag{1.11}$$

The two-site and three-site models are useful in cases where binding of two or three substrate molecules occurs, respectively. In some cases with S-shaped binding isotherms and turnover profiles (*v vs.* [TST]) on the basis of three binding sites, such as in testosterone (TST) binding and hydroxylation by CYP3A4, the predicted functional response conforms well with the data (*72*). However, in general, the exact number of binding sites for specific small and moderate-sized substrates is not known.

If the number of binding sites and therefore the binding stoichiometry is unknown, the Hill equation (*110*) is often applied for fitting of sigmoidal data in cytochromes P450. Fitting yields an averaged binding parameter, the Hill coefficient *h*. The Hill equation was originally derived to describe the binding of oxygen and carbon monoxide by haemoglobin (*110*). The protein was correctly assumed to consist of *h* of subunits which bind ligands simultaneously (Scheme 3).

$$E + hS \underset{}{\overset{K_{Eq}}{\rightleftharpoons}} ES_h$$

SCHEME 3

K is the dissociation constant for the *h*-th order binding equilibrium. In the original formalism of Hill this constant is substituted with the parameter S_{50}, which is defined as $S_{50} = \sqrt[h]{K_D}$. The Hill equation describes the binding isotherm for such a binding:

$$Y = \frac{[ES_h]}{[E_0]+[ES_h]} = \frac{[S]^h}{S_{50}+[S]^h} \qquad (1.12)$$

By definition, the Hill coefficient *h* represents the number of the molecules of ligand which bind to the enzyme (or an oligomer consisting of *h* subunits) *simultaneously* (*110*). This is the case of infinite cooperativity, which represent an ultimate simplification and barely occurs in the real mechanisms. However, the fitting of titration curves to the Hill equation provides a convenient means to judge as to how much the system deviates from the hyperbolic binding model and to presume the number of binding sites. It was shown that the Hill coefficient is always less than or equal to the number of subunits or binding sites, and therefore may be used to assess the *minimal* number of binding sites involved in the cooperativity mechanism (*94*). The parameter S_{50} on the other hand represents the midpoint of the binding isotherm. It does not correspond to any individual

dissociation constant, but rather represents a composite of the real dissociation constants that characterizes the averaged affinitiy.

Importantly, the Hill equation has been developed for an aggregate system that consists of *identical* subunits with identical binding affinities. In the case of cytochrome P450, neither conditions of the original model of hemoglobin are met, since sigmoidal behavior is seen in monomers of cytochrome P450 that do not comprise identical binding sites (*72, 86*), and since it is known that these binding sites usually exhibit different affinities for the substrate. Despite major limitations, the Hill equation is a common and simple model often used for the fitting of cooperative functional aspects of cytochromes P450 in order to obtain information about the extent to which a system is "cooperative" (*111*).

Chapter 4 addresses cooperativity in cases, when the number of substrate binding sites is unknown, such as for carbamazepine. An equation is derived that combines the phenomenological nature of the Hill equation with substrate inhibition (see p. 54). In this model, substrate inhibition by an additional substrate molecule occurs upon cooperative binding of an unknown number *h* of substrates (Scheme 4).

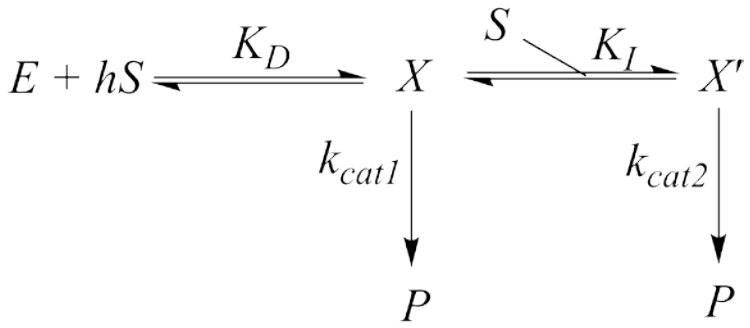

SCHEME 4

The law of mass action is expressed as:

$$K_D = \frac{[E][S]^h}{[X]} \tag{1.13}$$

$$K_I = \frac{[X][S]}{[X']} \tag{1.14}$$

The equation for turnover as a function of substrate concentration is given as (a complete derivation is shown on p. 54ff):

$$V = \frac{k_{cat} \cdot [E]_0 \cdot [S]^h \cdot (\alpha \cdot [S] + K_I)}{[S]^h \cdot (K_I + [S]) + S_{50}^h \cdot K_I} \quad (1.15)$$

1.7 RECONSTITUTION OF THE ACTIVITY OF PURIFIED CYTOCHROME P450

In order to study the activity of individual hepatic microsomal cytochromes P450, it is necessary to isolate and purify a particular isozyme, and to reconstitute its activity. The activity of microsomal cytochromes P450 can be reconstituted by mixing purified cytochromes P450, NADPH and cytochrome P450 reductase (CPR) with purified phospholipids and certain detergents. Optimal conditions for reconstitution of activities vary with the studied cytochrome P450 isozyme (see ref. (*112*)). The activity of CYP3A4 has been found to be a complex function of diverse factors: a particular lipid environment, cytochrome b_5, divalent metal ions such as Mg^{2+}, and reduced glutathione (GSH) all enhance catalytic activity of CYP3A4 (*85, 88, 92, 93, 113, 114*). Most additives (except for phospholipids) are, however, not required to study the activity of CYP3A4, and may even alter the complex kinetics, e.g. GSH (*84*) or Mg^{2+} (D. R. Davydov, personal communication). For the reconstitution of CYP3A4, a detergent such as sodium cholate or 3-[(3-cholamidopropyl)-dimethylammonio]-1-propanesulfonate (CHAPS; Figure 6) is usually added. In some instances, the use of detergent has been made unneccessary by incubating purified CYP3A4 with commercial microsomal lipid preparations (Supersomes) containing CPR (*78, 105*). Under suitable conditions, CYP3A4 co-integrates into the reductase-containing microsomes during incubation and establishes monooxygenation activity.

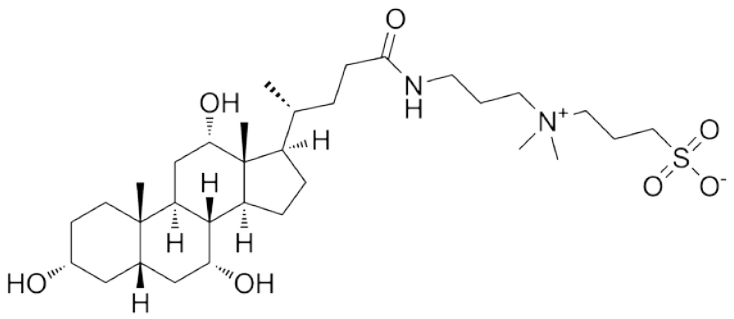

CHAPS

Figure 6: Structure of the detergent (CHAPS) that is commonly used for reconstitution of the activity of microsomal cytochromes P450 such as CYP3A4.

1.8 COUPLING OF CYTOCHROME P450 TO ELECTRODES

The requirement of cytochrome P450-dependent monooxygenation for NADPH-cytochrome P450 reductase (CPR) and NADPH as a source of reducing equivalents can be circumvented through immobilization of the enzyme on solid electrode supports that serve as electron donors (*115-118*) (Figure 7). In some cases, the detection of the reaction products (in addition to the catalytic currents to the immobilized cytochrome P450) in the presence of substrates has been achieved (*118-121*). The broad spectrum of substrates that are metabolized by cytochromes P450 make these enzymes interesting for the application as a recognition element for biosensing. On the other hand, the broad substrate-specificity of some cytochromes P450 hampers the development of specific biosensors. A further limitation is the low native or target plasma concentration of most analytes in humans that could be relevant to cytochrome P450-based biosensing, such as steroid hormones or most pharmaceutical drugs, respectively. Nevertheless, adverse effects in multi-drug treatments as a result from complex drug-drug interactions or polymorphisms in drug-metabolizing enzymes are of high importance and represent a major problem for the pharmaceutical industry. Biosensors that employ electrodes with immobilized cytochromes P450 may therefore eventually be used for detection of drug substrates as an enabling technology in drug development and for therapeutic monitoring in clinical settings (*115, 118, 122*).

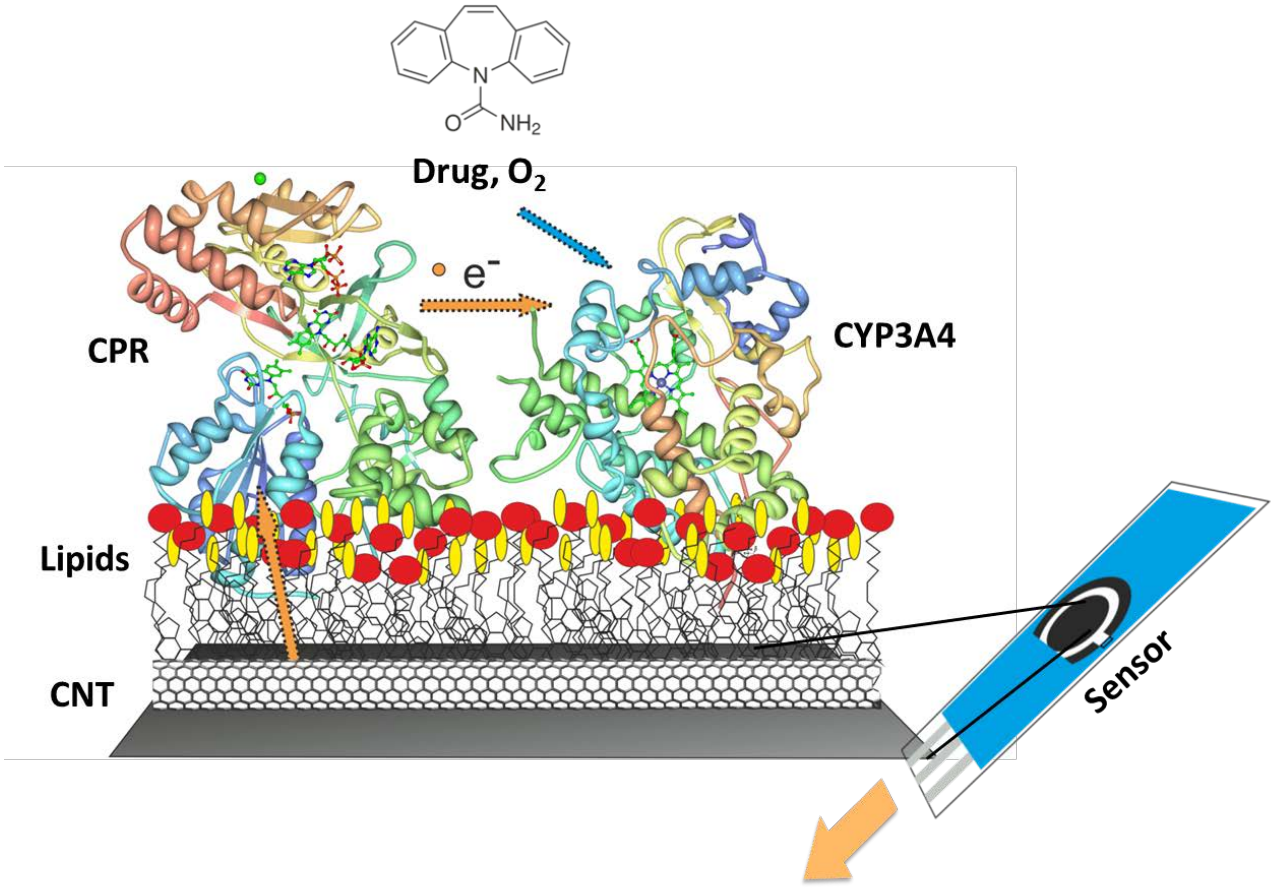

Figure 7: Coupling of CYP3A4 and CPR to electrodes. Membrane-bound CYP3A4 and CPR deposited onto screen-printed electrodes that were covered with carbon nanotubes (CNT). Small orange arrows denote electron flow via CPR to CYP3A4 to initiate metabolism upon substrate binding (small blue arrow, carbamazepine in the figure). The blue sensor is connected to a potentiostat (fat orange arrow).

1.9 SCOPE OF THIS THESIS

The aim of this work was to probe the interaction of CYP3A4 with carbamazepine by an approach of simulation-guided cloning of CYP3A4 (active-site) point mutants in order to generate variants of CYP3A4 with higher activity and/or affinity towards the anticonvulsive drug carbamazepine (CBZ), a small molecule drug prescribed for the treatment of epilepsy and bipolar disorder (Figure 4). CBZ has a therapeutic blood plasma target concentration of 17 – 70 µM (*51*). Since this qualifies CBZ as a narrow therapeutic index drug (*123*), continuous therapeutic monitoring is desirable for the optimal outcome of a therapy that involves the prescription of CBZ. Failure in maintaining the target plasma range may cause toxic side-effects in the course of the

treatment of epilepsy known under the name *anticonvulsant hypersensitivity syndrome*, a multi-organ syndrome with potentially fatal outcome (*124, 125*).

The engineered CYP3A4 variants were intended to be ultimately incorporated into biosensors for CBZ detection and for continuous therapeutic monitoring during the administration of CBZ to patients. Parts of the data presented in chapter 4 involve *in silico* studies such as molecular dynamics (MD) simulations and the derivation of distance trajectories or pose clustering. The data obtained from simulations were generated by members of our scientific collaboration (T. Knehans, Prof. A. Caflisch)[3]. The generation of the mutants relied on a simulated molecular structure of a binary complex of CYP3A4 with CBZ.

The engineered CYP3A4 mutants were also applied to binding studies with other CYP3A4 ligands, such as bromocriptine, erythromycin, testosterone, estradiol, and 7-benzyloxyquinoline (chapters 5-7). We also studied the kinetics of the reduction of Fe (III) → Fe (II) heme in the CYP3A4 mutants by sodium dithionite ($Na_2S_2O_4$; chapter 7.2). In Chapter 2, computational, experimental, and analytical methods that were used to obtain the presented data are described. In chapter 3, the generated enzymes CPR and CYP3A4 including mutants of CYP3A4 are characterized *via* biochemical and biophysical techniques and the chapter also provides further insight into the application of some of the used methods. Chapter 8 wraps up the work and summarizes the major achievements of the thesis, relates them to the initial scope, and provides an outlook for future work.

[3] Amedeo Caflisch, PhD, and Tim Knehans, Institute of Biochemistry, University of Zürich, Switzerland.

2 MATERIALS AND METHODS

The methods are organized with respect to their first occurrence in the chapters of the thesis.

2.1 REAGENTS

Compound	**Company**	**Place (Group)***
L-α-phosphatidyl choline L-α-phosphatidyl ethanolamine L-α-phosphatidic acid	Avanti Polar Lipids	Alabaster, AL, USA
3-[(3-cholamidopropyl)-dimethylammonio]-1-propanesulfonate (CHAPS) nicotinamide adenine dinucleotide phosphate (NADPH and NADP+) glucose 6-phosphate (GSP) sodium cholate butane-2,3-diol-1,4-dithiol (dithiothreitol, DTT)	Applichem GmbH	Darmstadt, Germany
Vivid® BOMR (benzyloxy-methoxy-resorufin)	Life Technologies	Carlsbad, CA, USA
tetraoxidodisulfate sodium (sodium dithionite, $Na_2S_2O_4$)	Riedel-de Haën	Morriston, NJ, USA (Honeywell International)
Pfu DNA polymerase	Fermentas	Waltham, MA, USA (Thermo Fisher Scientific)
potassium phosphate monobasic potassium phosphate dibasic 2-[4-(2-hydroxyethyl)piperazin-1-yl]-ethanesulfonic acid (HEPES) isopropyl β-D-1-thiogalactopyranoside (IPTG) propane-1,2,3-triol (glycerol)	Fisher Reagents	
Tris(hydroxymethyl)aminomethane hydrochloride (TRIS) 5H-dibenzo[b,f]azepine-5-carboxamide (CBZ)	Acros Organics	

Compound	Company	Place (Group)*
D(+)-sucrose erythromycin (ERY)		
HisPur Ni-NTA beads	Thermo Fisher	
CM macro-prep ion exchange support Biobeads	Biorad	Hercules, CA, USA
Escherichia coli (*E. coli*) HMS 174 (DE3)	Calbiochem	Darmstadt, Germany (Merck)
5-amino-4-oxo-pentanoic acid (δ-aminolaevulinic acid, δ -ALA)	Merck	
carbamazepine-10,11-epoxide DEAE sepharose fast flow ion exchange adenosine 2',5'-diphosphate agarose Igepal-CO630 glucose 6-phosphate dehydrogenase (GSPDH) testosterone (TST) estradiol (EST) bromocriptine (BCT) cytochrome *c* imidazole ampicillin	Sigma	St. Louis, MO, USA (Sigma Aldrich)
sulfanylethan-1-ol (2-mercaptoethanol) riboflavin 5'-monophosphate sodium salt dehydrate potassium chloride D-histidine ethylenediaminetetraacetic acid (EDTA) Triton X-100	Fluka	
Oligonucleotide primers	Microsynth AG	Balgach, Switzerland
10-methoxy-carbamazepine	TLC PharmaChem	Vaughan, Ontario, Canada

Compound	Company	Place (Group)*
Human CYP3A4HR EasyCYP Bactosomes (Bactosomes with a high CPR:CYP3A4 ratio)	CYPEX Ltd	Dundee, UK

* In case the group name is not identical with the company name.

***E. coli* TOPP 3** cells for the expression of the CYP3A4 gene were provided by D. R. Davydov (UCSD, CA, USA). ***E. coli* XL1-Blue** cells were obtained from Dr. Algirdas Ziogas (Obstetrics Research Department, University Hospital of Zurich, Switzerland).

2.2 EXPERIMENTAL METHODS

2.2.1 RECOMBINANT DNA MANIPULATIONS

The construct pSE3A4 encoding an *N*-terminally modified human cytochrome P450 3A4 with a tetra-histidine tag attached at the *C*-terminus was described previously (*42*) and was provided by Prof. James R. Halpert[4]. A plasmid map of pSE3A4 is shown in Figure 8. Site-directed mutagenesis was performed by means of the polymerase chain reaction (PCR) with the QuikChange Site-Directed Mutagenesis Kit (Agilent Technologies, Stratagene Products Division, La Jolla, CA). Table 2 lists the primers that were used in the PCR protocol.

The highly thermostable *Pfu* DNA polymerase from the hyperthermophilic archaeon *Pyrococcus furiosus* was used for PCR. *Pfu* DNA polymerase catalyzes the polymerization of nucleotides into duplex DNA in the 5'→3' direction and has 3'→5' exonuclease activity for proofreading (correction of nucleotide incorporation errors). The error incorporation frequency during PCR by *Pfu* DNA polymerase is given as $2.6 \cdot 10^{-6}$ errors per nucleotide per cycle[5]. The average number of incorporated incorrect nucleotides per site-directed mutagenesis experiment with *Pfu* polymerase and the plasmid pSE3A4 is given as:

[4] James R. Halpert, Skaggs School of Pharmacy, The University of California San Diego, 9500 Gillman Drive, PSB, room 2226, La Jolla, CA, 92093-0703.

[5] According to the product description of *Pfu* DNA Polymerase Fermentas #EP0501.

$$P_{error} = P_{error/nt} \cdot L \cdot N_c = \frac{5661 \cdot 15}{2.6 \cdot 10^6} = 0.033 \qquad (2.1)$$

with *nt*, nucleotide; *L*, length of plasmid; N_c, number of PCR cycles.

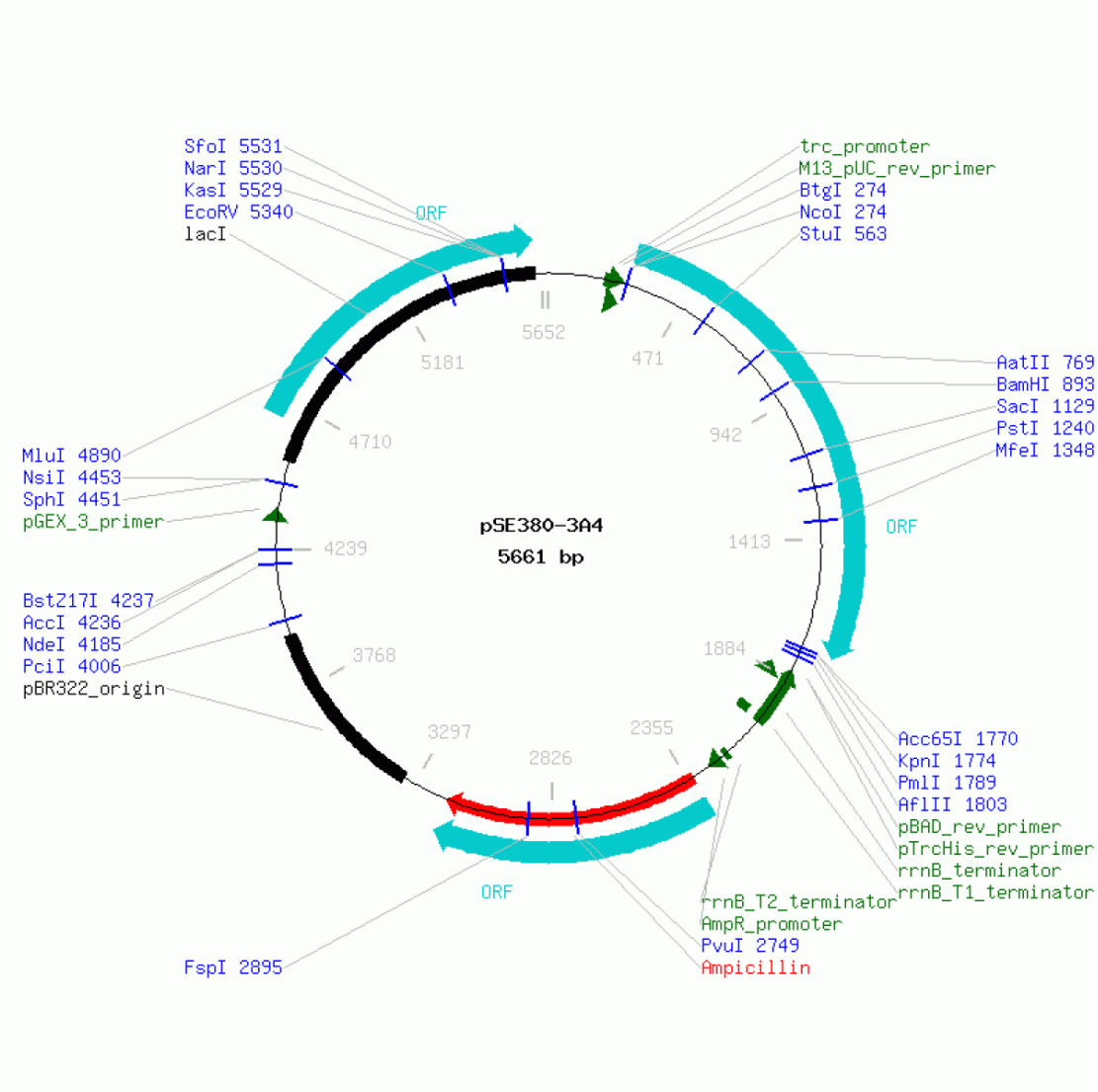

Figure 8: Plasmid map of the CYP3A4 expression plasmid pSE3A4. The map shows restriction sites (blue), primers, promoters and terminators (green), open reading frames (ORFs; light blue), the ampicillin resistance gene (red), and the pBR322 origin of replication and the *lac* operon (black). This plasmid map was generated from a web application of the website www.lablife.org[6].

[6] This platform was later incorporated into *Labguru*: www.labguru.com

Table 2: List of primers that were used for the generation of site-directed mutants.

Mutant		Forward (F) and Reverse (R) Primer
Ser119Ala	F	5'-GAT TTA TGA AAA GTG CCA TCG CGA TAG CTG AGG ATG AAG AAT G-3'
	R	5'-CAT TCT TCA TCC TCA GCT ATC GCG ATG GCA CTT TTC ATA AAT C-3'
Ile369Leu	F	5'-ACG CTC AGA TTA TTC CCA CTG GCT ATG AGA CTT GAG AGG GT-3'
	R	5'-ACC CTC TCA AGT CTC ATA GCC AGT GGG AAT AAT CTG AGC GT-3'
Ile369Phe	F	5'-CGC TCA GAT TAT TCC CAT TTG CTA TGA GAC TTG AGA GGG T-3'
	R	5'-ACC CTC TCA AGT CTC ATA GCA AAT GGG AAT AAT CTG AGC G-3'
Ala370Val	F	5'-CTC AGA TTA TTC CCA ATT GTT ATG AGA CTT GAG AGG GTC TG-3'
	R	5'-CAG ACC CTC TCA AGT CTC ATA ACA ATT GGG AAT AAT CTG AG-3'
Ala370Leu	F	5'-CGC TCA GAT TAT TCC CAA TTC TTA TGA GAC TTG AGA GGG TCT GC-3'
	R	5'-GCA GAC CCT CTC AAG TCT CAT AAG AAT TGG GAA TAA TCT GAG CG-3'

For the incorporation of point mutations into the pSE3A4 plasmid, we followed the strategy described in the QuikChange Site-Directed Mutagenesis Kit (Agilent Technologies, Santa Clara CA, USA). Briefly, two synthetic oligonucleotide primers that contained the desired mutations were designed and synthesized through a third-party DNA synthesis provider (Microsynth, Balgach, Switzerland). The oligonucleotide primers, each complementary to opposite strands of the vector (see Table 2), were extended during PCR cycling by the *Pfu* DNA polymerase. Due to the incorporation of the oligonucleotide primers, a mutated plasmid containing staggered nicks was generated. Treatment of the PCR product with the *Dpn*I endonuclease was used to digest parental (methylated and hemi-methylated) DNA, thereby selecting for the mutation-containing synthesized DNA. The nicked vector DNA containing the mutation was then transformed into and amplified by *E. coli* XL1-Blue cells. The nicks in the mutagenized plasmids were repaired intracellularly. The mutagenesis strategy is illustrated in Figure 9.

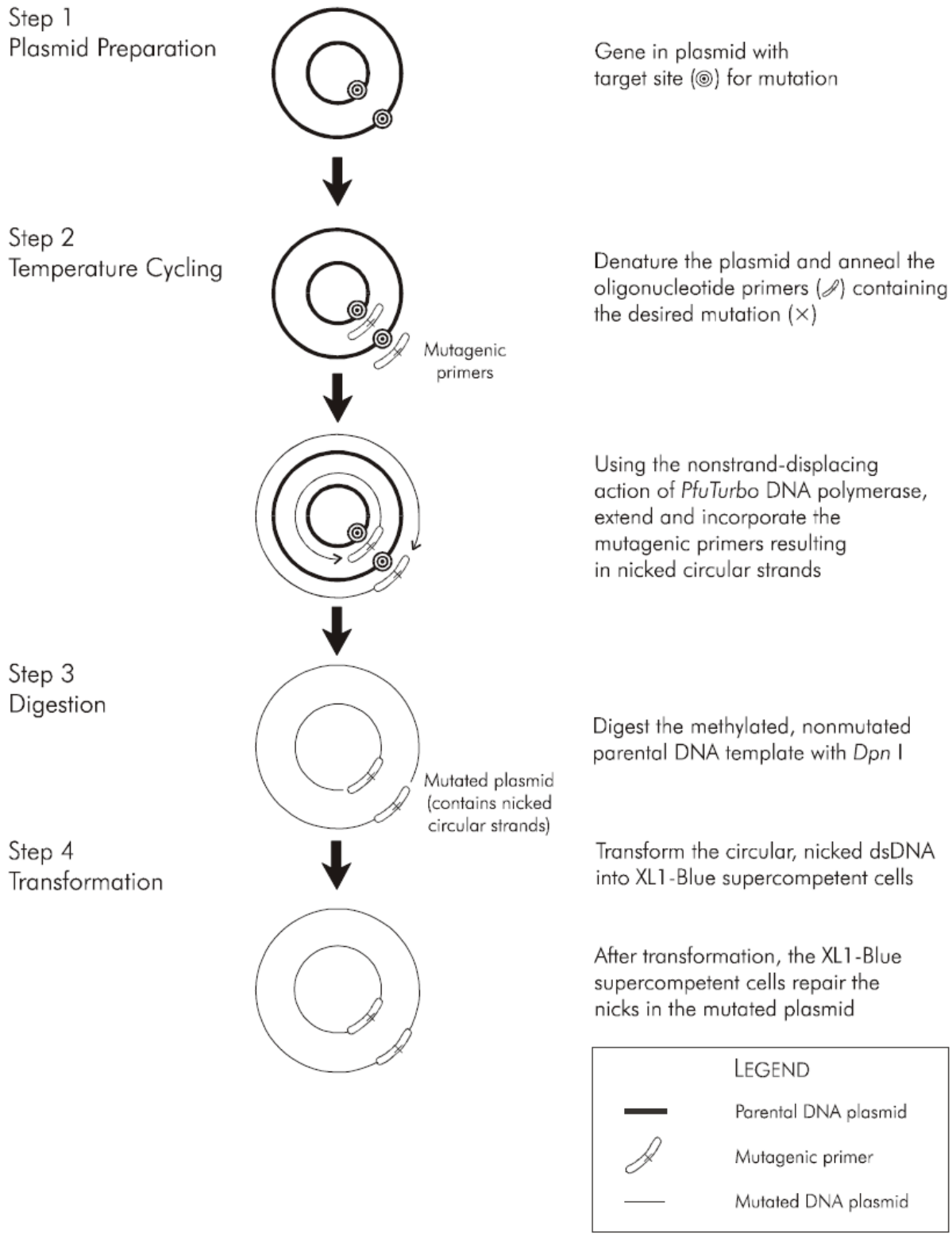

Figure 9: Illustration of the mutagenesis strategy. The illustration is reproduced from the QuikChange Site-Directed Mutagenesis Kit instruction manual (Catalog #200518, Agilent Technologies).

Protocol: *Polymerase chain reaction (PCR)*

The components listed in Table 3 were placed into 0.2 ml PCR micro-reaction tubes on ice. The forward and reverse primers used in the reactions are presented in Table 2. Tubes were thoroughly mixed by vortexing prior to the addition of *Pfu* polymerase. After the addition of *Pfu* polymerase, the samples were placed into the thermo-block of the thermocycler and the PCR program was started immediately (Table 4).

Table 3: List of components used in site-directed mutagenesis experiments:*

Component	Volume, µl	Final Amount
dsDNA template	1	50 ng
Primer 1	1	125 ng
Primer 2	1	125 ng
dNTP mix	1	10 mM each
H_2O	to 49	
Pfu Polymerase	1	2.5 U
Total	50	

*dsDNA; double-stranded DNA template (plasmid), dNTP mix; mix of the four deoxynucleotide triphosphates.

Table 4: PCR programme used in site-directed mutagenesis experiments:

Part	Cycles	Temperature	Time
1	1	95°C	30 sec
2	15	95°C 55°C 68°C	30 sec 1 min 12 min
3	1	4°C	Pause

After the PCR, the reaction tubes were placed on ice and a sample from each PCR tube was loaded onto a 1% agarose gel stained with ethidium bromide. 1 µl of 10 U/µl *Dpn*I was added to the remainder of the sample and incubated at 37 °C for 1 h. A sample of *Dpn*I-treated DNA was loaded onto an agarose gel and the gel was run at 140 V for ~ 45 min. An aliquot of the remaining sample was used to transform chemically competent *E. coli* XL1-Blue cells. All single-point mutants listed in Table 2 and the four double-point mutants that are obtained by combining the

described point mutations of Ile369 and Ala370 were generated. Only the single-point mutants were expressed.

The products from the site-directed mutagenesis PCR were loaded on a 1% agarose gel to verify the amplification. For sizing of the DNA in the loaded samples, aliquots of GeneRuler 1 kb DNA ladder were loaded on the gel (Thermo Scientific). The ladder contains fourteen DNA fragments of the sizes (in base-pairs): 10,000, 8,000, 6,000, 5,000, 4,000, 3,500, 3,000, 2,500, 2,000, 1,500, 1,000, 750, 500, and 250. A sample of the PCR product after restriction digestion with the enzyme *Dpn*I was also loaded on the gel to verify the presence of the desired mutated DNA fragment.

Amplified mutagenized plasmid was transformed into chemically competent cells of the strain *E. coli* XL1-Blue. Nicks in the PCR-amplified DNA are repaired *in vivo*. The DNA was purified using a commercial plasmid purification kit (GeneJET Plasmid Miniprep Kit, Thermo Scientific). All purified mutagenized plasmids were sequenced.

Protocol: *Transformation of chemically competent cells*

> 50-100 µl of chemically competent *E. coli* XL1-Blue cells were thawed on ice and transferred to 1.5 mL microreaction tubes. 10-100 ng of plasmid of the PCR reaction were added, carefully mixed with the cells, and incubated on ice for 5-60 minutes. Tubes were then placed into a thermoblock set at 42 ºC for 45 sec (heat-shock) and then again placed on ice for ≥ 2 minutes. A 100-200 µl sample was plated onto LB-agar plates containing 50 µg/ml sodium ampicillin. The plates were incubated overnight at 37 ºC.

Amplified plasmids were sent for DNA sequencing by a third-party sequencing service (GATC Biotech AG, Constance, Germany). The received chromatograms were carefully checked to confirm and the DNA sequence called by the sequencing service. Nucleic acid sequences were translated into amino acid sequences with the genetic code. The human wild-type CYP3A4 nucleic acid and amino acid sequences were retrieved from the homepage of The UniProt Consortium (*126*)[7]. The amino acid sequences of the pSE3A4 expression construct was aligned with the retrieved sequence of human CYP3A4 using the Pairwise Sequence Alignment tool LALIGN (*127*) of the European Bioinformatics Institute (EMBL-EBI) (*128, 129*) (default settings).

[7] Website of The UniProt Consortium: http://www.uniprot.org/

2.2.2 EXPRESSION AND PURIFICATION OF RAT NADPH-P450 REDUCTASE AND HUMAN CYTOCHROME P450 3A4

CYP3A4 are purified and stored preferably in Good's buffers such as MOPS or HEPES due to the excellent buffering capacities at near-neutral pH of the latter two: $pK_{a\ MOPS}$ = 7.15 and $pK_{a\ HEPES}$ = 7.55 at 20 °C (*130*). In this work, we used mostly HEPES buffer during purification and HEPES or phosphate buffer in the kinetics measurements. In the titration experiments, we used HEPES supplemented with 1 mM dithiothreitol (DTT) and 1 mM of the multidentate chelating agent EDTA.

2.2.2.1 EXPRESSION OF HUMAN CYTOCHROME P450 3A4

Freshly transformed *E. coli* TOPP 3 cells were induced with 0.5 mM IPTG, and the construct was expressed for 48 – 72 h before cells were lysed by sonication. The expression levels were quantified *via* binding of CO to Fe^{2+}-heme (*4*). The enzyme was purified from solubilized membranes via nickel-affinity chromatography by using Ni-NTA beads and anion exchange chromatography on a CM macro-prep ion exchange support, as described previously (*80, 108*). A detailed protocol of the procedure is given below.

***Protocol*:** *Expression and purification of human CYP3A4:*

Expression of human CYP3A4 - Chemically competent cells of the strain *E. coli* TOPP 3 were thawed on ice and incubated with a small aliquot of the plasmid pSE3A4 (and its derivatives) for 30 – 60 min. The mixture was then subjected to heat-shock transformation. An aliquot of the mix was then plated on agarose petri dishes containing 50 µg/ml sodium ampicillin. Plates were incubated overnight at 37 °C. The grown cells were transferred from the plates into lysogeny broth (LB) medium (5 g/l yeast extract, 5 g/l NaCl, 10 g/l tryptone) supplied with 50 µg/ml sodium ampicillin and the cultures were grown for 2.5 – 3 h at 200 rpm in a incubation shaker (*Multitron Standard*, Infors AG, Bottmingen, Switzerland). Grown cultures were diluted into terrific broth (TB)[8] medium and the cells were grown at 37 °C

[8] Terrific broth (TB): 12 g of tryptone, 24 g of yeast extract and 4 ml of glycerol were dissolved in 900 ml H_2O and autoclaved for 20 min at 121 °C. After cooling, 100 ml of an autoclaved solution of 0.17 M KH_2PO_4, 0.72 M K_2HPO_4 were added.

and 200 rpm until cell density reached an OD_{550} = 0.8 – 1.5. IPTG and 5-aminolaevulinic acid (ALA) were added to final concentrations of 1 mM and 80 mg per l of culture, respectively (stock solution: of 1.19 g IPTG and 0.4 g ALA in 10 ml water, addition of 0.5 ml of the stock to each flask). Cultures were grown at 30°C, 190 rpm for 48 – 72 h and then placed on ice. The cultures were centrifuged at 5,000 rpm at 4 °C for 15 min and the supernatant was decanted. The cell pellet was resuspended in 10 ml buffer A (see below) per 250 ml culture with 1 mM phenylmethanesulfonyl fluoride (PMSF) added just before resuspension. The suspension was sonicated in 2 cycles of 45 s to 2 min per round, 80% time, 60% power in small volumes on a VCX 750 Ultrasonic Processor (Sonics & Materials, Inc., Newton CT, USA) such that the temperature of the sample thereby never exceeded 15 °C. The samples were centrifuged at 31,000 rpm, 4 °C, for 30 min. The pellets were resuspended in 10 ml of buffer A with 1 mM PMSF (without CHAPS) per 250 ml culture. The suspension was stored in a glass vessel saturated with argon gas, CHAPS added to 1% (*v*/*v*) followed by stirring at 4 °C with a magnetic stir bar for 2 – 12 h. The sample was then centrifuged at 31,000 rpm, 4 °C, for 30 min. The supernatant was saved for further purification. The content of CYP3A4 was measured by CO-difference spectroscopy in microsome solubilization buffer (see below).

Buffer A: 100 mM HEPES, pH 8.0, 10% glycerol.

Microsome Solubilization Buffer (MSB): 100 mM potassium phosphate (pH = 7.3), 10% glycerol, 0.5% sodium cholate, 0.4% Igepal CA-630, 1 mM EDTA.

Purification of CYP3A4 using a three-column procedure

Ni-column I:

The solubilized CYP3A4 was loaded onto a Ni-sepharose column (1 ml column support per 60 nmol P450) in 100 mM HEPES, pH 8.0, containing 0.5 M KCl and 0.5% CHAPS. The column was washed with 3 volumes of 20 mM imidazole in the same buffer, followed by washing with 15-20

volumes of 100 mM HEPES, pH 8.0, containing 0.5 M KCl and 0.5% Igepal. An additional washing step with 3 volumes of 100 mM HEPES, pH 8.0, containing 0.2% Igepal (no KCl) was followed by the elution of P450 with 100 mM HEPES, pH 8.0, containing 0.2% Igepal and 200 mM imidazole.

CM-Macroprep column

The P450 solution was diluted to obtain an imidazole concentration < 10 mM (at least 20 times) with, in the case of CYP3A4 wild type, 100 mM HEPES, pH 7.4 (20 mM for mutants), containing 0.2% Igepal. The concentration of CYP3A4 was optimally adjusted to < 5 µM. The solution was loaded onto a column containing the CM-Macroprep anion exchange material (1 ml per 100 nmol CYP3A4 wild type or 60 nmol mutant) at a loading rate of 10 ml/h. The column was washed with 10 volumes of the same buffer. Cytochrome P450 was eluted with 150 mM KCl (threshold of elution ca. 100 mM).

Ni-column II:

The eluate was loaded onto a Ni-column (1 ml column support per 100 nmol P450) at a protein concentration of 5 µM in 100 mM HEPES, pH 7.4, 0.2% Igepal. The column was washed with 5 volumes of 100 mM HEPES, pH 7.4, containing 0.5% CHAPS, (150 mM KCl for the purification of mutants). The column was washed with 30 volumes of 100 mM HEPES, pH 7.4, in the absence of detergent (150 mM KCl for the mutants). The enzyme was eluted with the same buffer additionally containing 150 mM histidine-HCl and 200 mM imidazole. The eluate was concentrated to ~100-150 µM P450 and dialyzed against 100 mM HEPES, pH 7.4, containing 1 mM EDTA, 1 mM DTT, and 10% glycerol (150 mM KCl in the case of mutants). The dialysis was repeated three times with 100 volumes of fresh buffer used each time. All buffers contained 2 mM 2-mercaptoethanol (70 µl neat/100 ml), except for the buffers used for the 2nd Ni column and the dialysis, which contained 1 mM DTT instead. All buffer solutions used were saturated with Argon.

The purified protein was loaded onto a sodium dodecyl sulphate (SDS) gel and an SDS polyacrylamide gel-electrophoresis (SDS-PAGE) was run until clear separation of all bands of the protein sizer (PageRuler^{TM} Prestained Protein Ladder Plus, Thermo Scientific) on the gel was obtained. The purity of the enzymes was also analysed by absorption spectroscopy and protein concentrations were quantified by comparison with spectral standards of CYP3A4 (CYP3A4 high-spin, low-spin and P420 species) using the SpectraLab software package (*131*).

2.2.2.2 PRODUCTION OF RAT NADPH-CYTOCHROME P450 REDUCTASE

The rat NADPH-cytochrome P450 reductase (CPR) gene was expressed from the construct pETOR262 that was provided by James R. Halpert. The construct was generated by Greg R. Harlow and James R. Halpert (*42*) from cDNA obtained by Todd Porter. The construct is a T7 expression plasmid created by moving the *Xba*I – *Hin*dIII fragment from pOR262 (*132*) into pET29a(+) (Novagen, Madison, WI). This fragment contains the *N*-terminally modified rat reductase with a fused *omp*A-encoded signal peptide and ribosome binding site. The sequence of the amino-terminal region of the cloned reductase construct shown in Figure 10 displays the last 6 amino acids of the signal peptide from *omp*A. The arrow indicates the signal peptide cleavage site. It is followed by 8 added amino acids from cloning (*italics*). The first three *N*-terminal amino acids of rat liver reductase are highlighted in grey:

```
GCTACCGTAGCGCAGGCCGGAATTCCCGGGGATCCGACCAACATGGGGGAC
AlaThrValAlaGlnAla GlyIleProGlyAspProThrAsnMetGlyAsp
                   ↑
```

Figure 10: Sequence of the amino-terminal region of the cloned CPR expression construct (see text for details).

The construct was expressed in *E. coli* HMS 174 (DE3) and purified *via* ionic exchange and affinity chromatography as described previously (*42*). Briefly, solubilized protein from a lysate of bacterial cultures was captured on a DEAE sepharose fast flow anion exchange support. The eluate was purified *via* affinity chromatography with an adenosine 2',5'-diphosphate agarose support. The detailed protocol for the purification of CPR is described below.

Protocol: *Expression and purification of rat NADPH-cytochrome P450 reductase*

Fresh *E. coli* HMS174 (DE3) cells were transformed with the plasmid pETOR262 and plated onto agar plates containing kanamycin (50 μg/ml) and incubated overnight. The grown colonies on the agar plates were resuspended in 100 ml LB medium containing kanamycin (50 μg/ml) in a 250 ml flask at 37 °C and 250 rpm for 2-3 h. The culture was used to inoculate 250 ml TB medium (225 ml TB + 25 ml TB salts + 0.25 ml kanamycin (50 μg/ml) in a 1 L flask) and grown at 37 °C, 250 rpm, for ca. 4 h, until the OD_{550} was > 0.8. IPTG was added to a final concentration of 0.5 mM and the culture grown at 30 °C, 190 rpm, for 48 h. Cells were harvested by centrifugation at 5000 rpm, 15 min, and 4 °C. Cells were resuspended in 2 flasks of 100 ml buffer A (see below). 4 mg lysozyme was added and the solution stirred at 4 °C for 30 min. The solution was centrifuged at 5000 rpm at 4 °C for 30 min to pellet the spheroblasts. The pellets were resuspended in 130 (2x 65) ml affinity buffer without detergent. The cells were sonicated twice for 45 s (80% of time, 60% of power) on a VCX 750 Ultrasonic Processor. Igepal CO-630 to a final concentration of 0.3% was added and the sample was shaken on ice for 1 h. The sample was then centrifuged at 32,000 rpm for 45 min and the supernatant was saved.

Buffer A: 100 mM Tris-HCl, pH 8.0, 0.25 M sucrose, 0.5 mM EDTA (1 ml 0.5 M stock).

Affinity Buffer: 100 mM Tris-HCl, pH 7.7, 0.5 mM EDTA, 1 mM DTT (add from 1 M stock before using), 0.3% Igepal.

A new column containing DEAE-sepharose was prepared by mixing 125 g (125 ml bed volume) of DEAE–sepharose with 8-10 bed volumes of 100 mM Tris (pH 7.7). The column material was allowed to settle and the buffer was decanted. This was repeated for four buffer exchanges. The gel was washed in 10 bed volumes of H_2O. After the gel had settled, an aliquot of the supernatant was taken and the pH was checked. If the pH was not 7.7, the column was washed again with 100 mM Tris buffer (pH 7.5) and the gel resuspended 1:3 in H_2O. The column was then packed.

The DEAE-Sepharose column was equilibrated with 500 ml Affinity Buffer at 100 ml/h. The sample (250 ml) was loaded overnight and the column washed with 500 ml Affinity Buffer containing 1 µM FMN at 80-100 ml/hr. The column was washed with 125 mM KCl in Affinity Buffer containing 1 µM flavin mononucleotide (FMN). The flavoprotein was eluted with Affinity Buffer containing 300 mM KCl and 1 µM FMN.

A small column was prepared with 2.5 g of 2'5' ADP Sepharose 4B in 150 ml H_2O. The supernatant was decanted and the gel resuspended in 25 ml of Affinity Buffer. The column was packed and equilibrated with 120 ml Affinity Buffer containing 1 µM FMN at 30 ml/h. The sample was applied at 9 ml/h and the column washed with 100 ml of Affinity Buffer containing 1 µM FMN at 20 ml/h. The column was washed with 100 ml of Affinity Buffer containing 0.1% deoxycholate and 1 µM FMN. The sample was eluted from the column with 50 ml of 4 mM 2'-AMP or 8 mM of a 2'-/3'-AMP mix in Affinity Buffer containing 1 µM FMN at 9 ml/h and small fractions were collected. OD_{455} was measured and the absorbing fractions were collected. Samples were concentrated on a 100,000 molecular weight cut-off concentrator to an OD_{455} of ca. 1.5-2. The concentrated flavoprotein was dialysed twice against 1 l of Dialysis Buffer. An absorbance spectrum from 250-700 nm was taken in a 1 mm cell and the protein concentration determined using SpectraLab.

Dialysis Buffer: 100 mM HEPES, pH 7.4, containing 10% glycerol, and 1 mM DTT (1 l, two changes, 1x overnight and 1x during the day).

The purity of the enzymes was analyzed via SDS-polyacrylamide gel electrophoresis. The concentrations of the protein were quantified before and after all purification steps *via*:

(1) Cytochrome *c* reduction kinetics in non-purified samples.

(2) Spectral decomposition of recorded spectra using a linear least-squares fitting procedure with spectral standards of rat reductase by using the SpectraLab software package (*131*).

Comments about the procedures for the CPR quantification assays:

(1) Spectra of samples were recorded from 340 – 700 nm. The spectral standard of CPR that was used in combination with spectral decomposition and determination of CPR concentrations in the samples is shown in Figure 11. CPR exhibits an absorption maximum at $\lambda = 454\ nm$ ($\epsilon_{454} = 21.4\ mM^{-1}cm^{-1}$).

(2) CPR-dependent cytochrome *c* reduction kinetics were determined under the following conditions: 50 µl of a 1 mM aqueous cytochrome *c* solution (stored at -20 °C) was mixed with 945 µl of 0.27 M potassium phosphate buffer solution, pH 7.4, in a 1 cm quartz cuvette. 0.1 - 1 µl of a purified CPR sample was added and the spectrophotometer was set on time-drive. The reaction was started *via* the addition of 5 µl of a 20 mM aqueous NADPH solution and a time series of difference spectra (550 – 541 nm) was recorded. The amount *m* of reduced CPR in the cuvette was calculated with the extinction coefficient $\Delta\varepsilon_{550-541} = 18\ mM^{-1}cm^{-1}$ according to Eq. 2.2 (*133*) (in nmol of reduced cytochrome *c* min^{-1}):

$$m = \frac{\Delta A_{550-541}}{\varepsilon_{550-541} \cdot t} \tag{2.2}$$

The concentration of rat reductase was calculated with a reaction rate for rat P450 reductase of (*134*):

$$k_{cyt.c\ reduction} = 2840\ \text{min}^{-1} \tag{2.3}$$

2.2.2.3 ABSORBANCE SPECTROSCOPY AND SPECTRAL ANALYSIS

Spectra were recorded on a Specord S 250 UV-VIS spectrophotometer equipped with a Peltier thermostat and a stirring device (Analytik Jena, Jena, Germany) at 28 °C. The concentrations and the spin state of CYP3A4 were quantified based on the approximation of the heme protein absorbance spectra with a set of the prototype spectra of absorbance of the CYP3A4 (Fe^{3+}) high-spin, low-spin, and the ‘P420’ states (*135*). The concentration of CPR was determined based on the

prototypic spectrum of the pure enzyme. In these calculations, the linear least-squares approximations of the spectra with combinations of the absorbance standards were performed with the SpectraLab software package (*131*).

2.2.2.4 SPECTRAL STANDARDS OF CYP3A4 AND CPR

Spectral standards of CYP3A4 species published in the Supplemental to ref. (*95*) and P450 oxidoreductase were downloaded together with the SpectraLab software package[9] (*131*), which includes, among others, the spectral standards shown in the following figures. The spectral standards of oxidised CPR, CYP3A4 high-spin, low-spin, and "P420" in solution shown in Figure **11** were used to determine the concentrations of purified CPR, CYP3A4 and the mutant species of purified CYP3A4. The same standards were also used in the titration experiments with ligands. The CYP3A4 species exhibit absorption maxima at 417 nm (low-spin) or 391 nm (high-spin). The absorption spectrum with the peak at 425 nm is representative of a set of CYP3A4 species that consists of active CYP3A4 bound to a type-II ligand and inactivated cytochrome P420 forms of CYP3A4.

The spectral standards of iron (II) carbonyl complexes of the P450 and P420 states of CYP3A4 were used for the assignment of the concentrations of iron (II) cytochrome P420 and CO-bound cytochrome P450 in mixed samples.

[9] SpectraLab (SpLab) software package by D. R. Davydov: http://cyp3a4.ucsd.edu/spectralab.html.

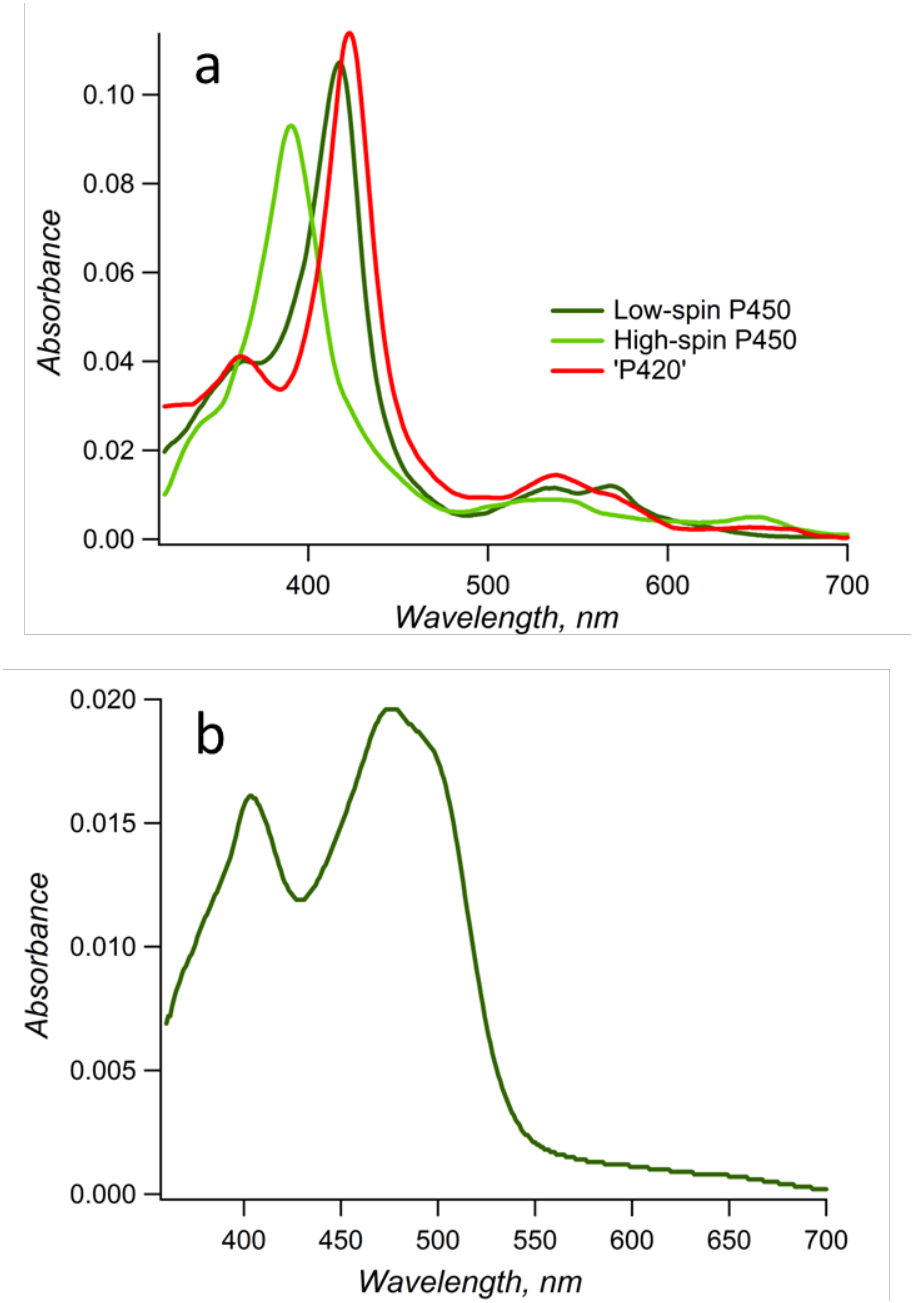

Figure 11: Absorbance spectra of (*a*) cytochrome P450 high- and low-spin, and cytochrome P420 and (*b*) NADPH-P450 oxidoreductase (CPR) used for the determination of the enzyme concentrations in purified samples. The spectra shown here correspond to a concentration of 1 µM of purified enzyme measured in a cuvette with an optical path length of 10 mm.

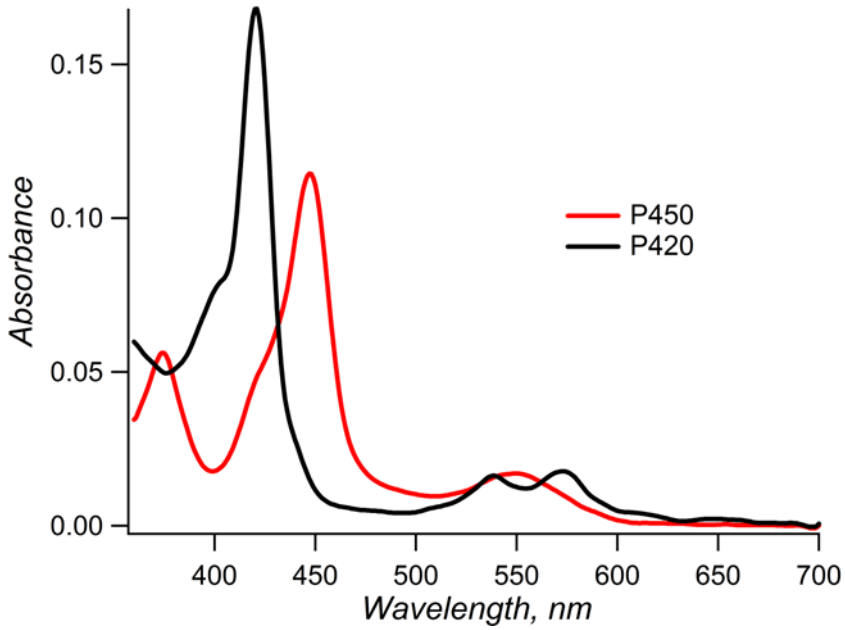

Figure 12: Absorbance spectra of the iron (II) carbonyl complexes of the P450 (red) and P420 (black) states of CYP3A4. These spectra were used to determine the concentrations of iron (II) P450 and P420 in CO-saturated buffer. The spectra presented correspond to concentrations [P450] = 1 µM purified CYP3A4 measured in a cuvette with an optical path length of 10 mm.

2.2.3 FUNCTIONAL RECONSTITUTION OF PURIFIED CYP3A4 AND CPR

A functional mono-oxygenation system with CYP3A4 and CPR was reconstituted in a micellar system containing phospholipids – added as chloroform solutions of L-α-phosphatidyl choline, L-α-phosphatidyl ethanolamine, and L-α-phosphatidic acid mixed at a molar ratio of the phospholipids of 1:2:0.6 (*108*) – and 0.4% CHAPS. The pellet of phospholipids obtained after removal of the solvent under a flow of argon gas was resuspended in buffer A (100 mM HEPES, pH 7.4, 150 mM KCl, 0.5 mM EDTA, 1 mM DTT containing 10% (*v*/*v*) glycerol) to the final concentration of 10 mg/mL (13.3 mM) by vigorous shaking on a Vortex mixer. The resulting suspension was homogenized by extrusion through a 200 nm pore-size filter with a mini-extruder (Avanti Polar Lipids, Alabaster, USA). A mixture of CYP3A4 and CPR containing 10 µM of each protein was then supplemented with the 6.5 mM phospholipid suspension to a final concentration of 1.5 mM, and buffer A containing 1.5% CHAPS was added to a final concentration of 0.4% CHAPS. The mixtures were incubated overnight at 4 °C under continuous shaking in a table-top thermomixer (Eppendorf, Hamburg, Germany; see Chapter 3.8).

The activities of the reconstituted CYP3A4 enzymes were compared in high-throughput CYP3A4 activity assays in 96-well plates on a Thermo Release Varioskan Flash Spectral Scanning Multimode Microplate Reader (Thermo Fisher Scientific, Waltham, MA, USA). In each well, an aliquot of a specified CYP3A4 reconstitute was incubated with either one of the fluorogenic substrates Vivid® BOMR (Figure 13a) or 7-benzyloxyquinoline (Figure 13b) and the fluorescence was monitored over time.

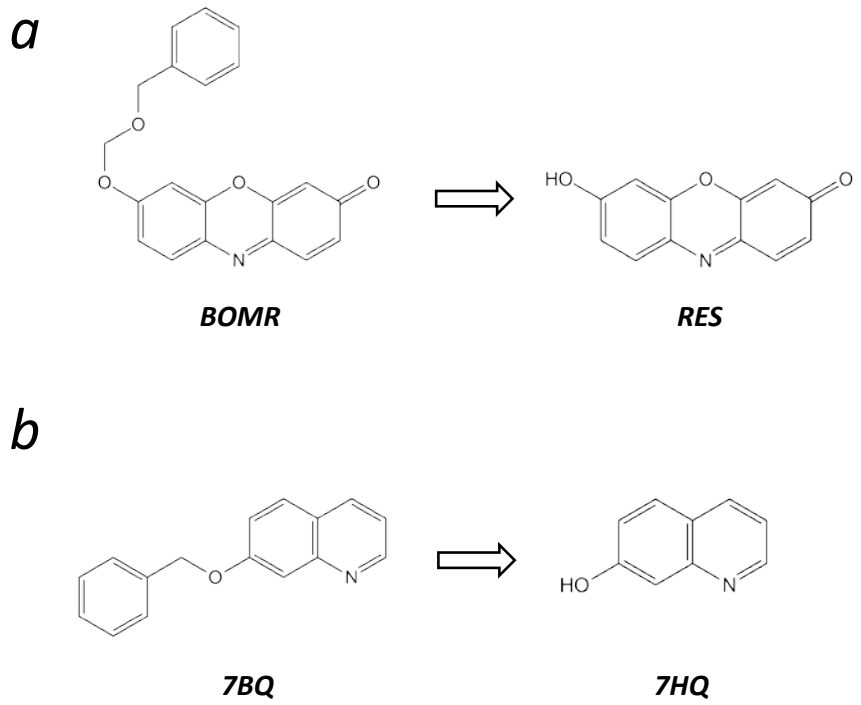

Figure 13: Fluorogenic test substrates and reaction products used in the determination of the activity of reconstituted enzyme. (*a*) The resorufin derivative BOMR is metabolized by CYP3A4 to resorufin (RES), which is fluorescent (λ_{Abs} = 530 nm, λ_{Em} = 585 nm). 7-benzyloxyquinoline (7BQ) undergoes metabolism to 7-hydroxyquinoline (7HQ), a fluorescent dye with λ_{Abs} = 410 nm, λ_{Em} = 538 nm.

BOMR is a resorufin derivative that is metabolized to resorufin (RES) by CYP3A4. BOMR exhibits negligible fluorescence at optimal excitation and emission conditions for RES (λ_{Exc} = 530 nm, λ_{Em} = 585 nm) (*156*) and is therefore a powerful fluorogenic indicator of CYP3A4 activity. 7BQ is metabolized to 7HQ (*157*, *158*), which exhibits fluorescence around λ_{Em} = 538 nm upon

excitation at λ_{Exc} = 410 nm [10]. Since excitation of the fluorescence of 7HQ interferes with NADPH fluorescence, the substrate BOMR was preferably used in most CYP3A4 activity assays

2.2.4 FORMATION OF CARBAMAZEPINE-10,11-EPOXIDE (CHAPTER 4)

Kinetics assay: formation of carbamazepine-10,11-epoxide – Reactions were carried out at 37 °C in micro-reaction tubes in a table-top thermomixer. The reconstituted enzymes were diluted 20-fold into 0.1 M HEPES buffer, pH 7.4. The final concentrations of CYP3A4 and CPR were 0.5 μM in all experiments, except for the incubations with CYP3A4 Bactosomes, where they were 0.05 μM. The working concentration of CHAPS was 0.02% or 325 μM. CBZ was added from methanol stock solutions such that in each incubation, a final methanol concentration of 1% was obtained. The addition of 20 μl of a 5× NADPH regeneration system containing 25 mM glucose 6-phosphate (GSP), 5 U/ml glucose 6-phosphate dehydrogenase (GSPDH), and 5 mM $NADP^+$ in 50 mM potassium phosphate buffer, pH 7.4, brought the reaction volume to 100 μl at final concentrations of the regeneration system components of 5 mM, 1 U/ml, and 1 mM, respectively. The reaction mixture was buffered at pH 7.4 with 75 mM HEPES and 10 mM potassium phosphate.

The linear ranges of product formation as a function of time were determined for each mutant by taking aliquots of the reaction mixture at 0, 5, 10, 15, 20, 25, and 30 min after initiation of the reaction. All incubations were conducted in triplicate. The enzymatic reactions were stopped by adding an equal volume of ice-cold methanol containing 20 μM of the internal standard 10-methoxy-carbamazepine, followed by 1:1 dilution with deionized water for a final methanol concentration of 25%. The samples were analyzed by reversed-phase HPLC on an Ultimate 3000 system (Thermo Fisher Scientific, Waltham, MA, USA) on a 150 mm × 4.5 mm diameter C18 *Gravity* column (Macherey-Nagel GmBH & Co. KG, Düren, Germany) with 30:70 acetonitrile:water containing 0.1% formic acid as the mobile phase.

The rates of reactions as a function of substrate concentration were fit to either the regular Hill equation or the Hill equation complemented with an allowance for partial substrate inhibition by means of a combination of the Nelder-Mead and Marquardt non-linear regression algorithms as implemented in the SpectraLab software package by Davydov (*131*).

[10] Conditions and settings for a 7BQ plate reader assay were retrieved from http://www.cypex.co.uk/3a4plate.htm, January 8, 2013.

*2.2.5 DERIVATION OF AN EQUATION THAT COMBINES AN ALLOWANCE FOR PARTIAL SUBSTRATE INHIBITION WITH AN APPROXIMATION OF COOPERATIVE INTERACTIONS IN TERMS OF THE HILL EQUATION**

**D. R. Davydov is acknowledged for the derivations in this chapter*

The Hill equation was first introduced in 1910 by A. Hill (Hill, A.V. (1910), J. Physiol. 40 (Suppl): iv–vii) to depict the interactions of hemoglobin with oxygen. It is based on a simple model where the complex of a protein with ligand is formed via simultaneous binding of *h* molecules of ligand. Although the initial model considered the interactions of a protein oligomer (*h*-mer) with *h* molecules of ligand, the assumption of oligomerization of the protein is not necessary for this formalism to be applicable. The Hill equation in its modern representation may be obtained considering an equilibrium of simultaneous binding of *h* molecules of ligand *S* to protein *E* (either monomer or oligomer, or a subunit of an oligomer) with the formation of complex *X* (Scheme 5):

SCHEME 5

The equilibrium constant K_D that defines the steady-state concentration of the complex [*X*] may be represented as:

$$K_D = \frac{([E]_0 - [X]) \cdot [S]^h}{[X]} \tag{2.4}$$

Resolving this equation for [*X*] for the case where the total concentration of the ligand ($[S]_0$) is much higher than the total concentration of the protein ($[E]_0$), so that [*X*] << $[S]_0$ and [S] ≈ $[S]_0$, we obtain:

$$[X] = \frac{[E]_0 \cdot [S]^h}{K_D + [S]^h} \tag{2.5}$$

Now introducing a new parameter S_{50}, defined as $S_{50} = \sqrt[h]{K_D}$, we get the Hill equation in its most common representation:

$$[X] = \frac{[E]_0 \cdot [S]^h}{S_{50}^h + [S]^h} \tag{2.6}$$

Let us complement this model with a binding of one more substrate molecule to the complex *X* resulting in the formation of complex *X′* (Scheme 6):

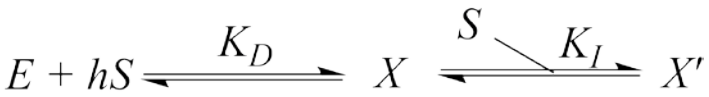

SCHEME 6

Considering the case where $[S]_0 >> [E]_0$ so that $[S] \approx [S]_0$, we obtain the following relationship for the dissociation constant K_D of the complex *X*:

$$K_D = \frac{([E]_0 - [X] - [X']) \cdot [S]^h}{[X]} \tag{2.7}$$

The dissociation constant of the (inhibitory) complex *X′* (K_I) may be defined as:

$$K_I = \frac{[X] \cdot [S]}{[X']} \tag{2.8}$$

Resolving the system of equations (2.7) and (2.8) for [*X*] and [*X′*] and introducing the parameter S_{50}, which is defined as $S_{50} = \sqrt[h]{K_D}$, we obtain the following equations:

$$[X] = \frac{K_I \cdot [E]_0 \cdot [S]^h}{[S]^h \cdot (K_I + [S]) + S_{50}^h \cdot K_I} \tag{2.9}$$

and

$$[X'] = \frac{[E]_0 \cdot [S]^{h+1}}{[S]^h \cdot (K_I + [S]) + S_{50}^h \cdot K_I} \tag{2.10}$$

Let's now consider the case when the protein E is an enzyme, ligand S is a substrate, the complex *X* is the enzyme-substrate complex with the maximal rate of catalytic turnover, and the complex *X´* is an inhibitory complex, where the rate of catalysis is decreased due to the binding of an additional (inhibitory) molecule of substrate. We define the parameter α as a ratio of the turnover numbers (apparent catalytic constants) characteristic of the complexes *X* (k_{cat}) and *X´* (k'_{cat}):

$$\alpha = \frac{k'_{cat}}{k_{cat}} \tag{2.11}$$

We may represent the overall rate of catalysis (*V*) as a function of [*X*] and [*X´*]:

$$V = k_{cat} \cdot [X] + k'_{cat} \cdot [X'] = V_{\max} \cdot ([X] + \alpha \cdot [X']) \tag{2.12}$$

Combining equations (2.9), (2.10) and (2.12) we obtain:

$$V = \frac{k_{cat} \cdot [E]_0 \cdot [S]^h \cdot (\alpha \cdot [S] + K_I)}{[S]^h \cdot (K_I + [S]) + S_{50}^h \cdot K_I} \tag{2.13}$$

Considering the case when cooperativity of the interactions is eliminated ($h = 1$) and replacing S_{50} with K_M we can obtain Equation 4.1 of chapter 4.3.1.

Similar to the regular Hill equation, equation (2.13) is based on the presumption that the binding of several ligand molecules to the protein takes place simultaneously. Due to this outermost simplification, the parameter *h* (the Hill coefficient) cannot be straightforwardly considered as a number of binding sites involved in the formation of complex *X*. However, similar to the case of the regular Hill equation, it may be shown that, for a mechanism with a positive cooperativity ($h > 1$), this parameter is less or equal to the actual number of binding sites involved in the interactions (see reference (*136*), Chapter 7).

2.2.6 SPECTRAL BINDING TITRATIONS (CHAPTERS 5-7)

Substrate binding to ferric CYP3A4 was monitored by spectrophotometry at 28 °C under aerobic conditions. The spectra were recorded on a Specord 250 UV-VIS spectrophotometer with

an incorporated peltier thermostat (Analytik Jena, Jena, Germany). Substrate-free CYP3A4 wild type and mutants were diluted into HEPES buffer (0.1 M Na-HEPES, pH 7.4, 0.5 mM EDTA) into a 1 cm quartz cell to final concentrations specified in the respective results sections (≈ 1 – 3 μM). Small aliquots of stock solutions were added to the cuvette under continuous stirring.

Table **5** shows the stock solutions that were employed in spectral binding titrations.

Table 5: Stock solutions used in spectral binding titration experiments:

Ligand	[Ligand], mM	Solvent
Bromocriptine	0.3	20 mM Na acetate, pH 4.0
Erythromycin	50	methanol
Testosterone	30	methanol
Estradiol	20	methanol
7-benzyloxyquinoline	20	methanol
CHAPS	150	ddH_2O

The absorbance spectra were generally recorded in the wavelength range of 340 – 700 nm. The series of absorbance spectra obtained during the titration experiments were background-corrected using the principal component analysis (PCA) combined with the fitting of the principal component spectra to a set of spectral standards, as described in chapter 2.2.7 on p. 58 and in ref. (*135*). The total volume of added methanol did not exceed 1% (*v/v*). Where the contributions of the solvent methanol to the spin perturbations were significant compared to the total spin-shift (as for the minimal spin-shifts in peripheral binding of allosteric substrates to CYP3A4 S119A in chapter 6), spectra were corrected with the background signal obtained from titration series with pure methanol. Methanol induced a low-spin shift with ~linear [MeOH] dependence of (2.2 ± 0.4) $\%_{HS\rightarrow LS}$ $(\%_{v/v}\ \text{methanol})^{-1}$ (calculated for $p = 0.05$). Titration curves obtained with the substrate BCT were fit to the equation for equilibrium of binary association, also known as “tight binding or “square root” equation (ref. (*137*), p. 73, Eq. II-53):

$$[ES] = \frac{[E]_0 + [S]_0 + K_D - \left\{\left([E]_0 + [S]_0 + K_D\right)^2 - 4[E]_0[S]_0\right\}^{1/2}}{2} \qquad (2.14)$$

In the case of allosteric substrate binding (except for bidirectional spin-shifts), data were fit to the Hill equation. For instances of bidirectional spin-shifts, data were fit to the equation for a two-site sequential ordered binding model:

$$A = \frac{a_1 \frac{[S]}{K_1} + a_2 \frac{[S]^2}{K_1 K_2}}{1 + \frac{[S]}{K_1} + \frac{[S]^2}{K_1 K_2}} \quad \mathrm{A} = \frac{\mathrm{a_1}\frac{[S]}{\mathrm{K_1}} + \mathrm{a_2}\frac{[S]^2}{\mathrm{K_1 K_2}}}{1 + \frac{[S]}{\mathrm{K_1}} + \frac{[S]^2}{\mathrm{K_1 K_2}}} \tag{2.15}$$

In order to measure the presence and formation of cytochrome P420, the enzymes were diluted into 100 mM HEPES buffer, pH 7.4, containing 0.5 mM EDTA and saturated with carbon monoxide by slowly bubbling CO through the buffer for 10 minutes. Absorbance spectra from 340 – 700 nm were recorded before and after addition of a few crystals of sodium dithionite. Spectral transition of the Soret band absorbance maximum to 447 nm was monitored *via* time-series of the difference spectra Δ_{Abs} (450-490 nm). After Δ_{Abs} (450-490 nm) reached a temporary maximum, the full spectra were recorded and evaluated by fitting it to spectral standards of the corresponding states of cytochrome P450 (CO bound to Fe^{2+}-heme of cytochromes P450 and P420).

2.2.7 PRINCIPAL COMPONENT ANALYSIS (PCA)

For the quantitation of the substrate-induced changes in the series of spectra obtained in absorbance titrations, we used the Principal Component Analysis (PCA) method as implemented in SpectraLab (*131*). PCA is a mathematical procedure that is used to convert a set of data containing possibly correlated variables into a set of values of linearly uncorrelated variables via orthogonal transformation. In other terms, PCA is an orthogonal linear transformation of an N-by-M matrix. In our case, N is the number of spectra in the series and M is the number of data points in each spectrum. Through PCA, the data are transformed to a new coordinate system in a way that the greatest variance by projection of any sort comes to lie on the first coordinate, the second greatest variance on the second coordinate etc. The first principal component hence accounts for the largest correlated variability in the dataset. The uncorrelated variables are called principal components. The total number of principal components is equal to N-1. Each principal component comes along with N-dimensional vectors of so-called loading factors, which define its representation in each of the spectra in the series. An important feature of PCA is that the high-order principal components may be exempted from the analysis as accounting for “occasional”, non-systematic changes. In this way, the data may conveniently be compressed by reducing the number of dimensions without losing much information. PCA is very powerful for finding patterns in data of high dimension such as absorbance spectra and expressing data in such a way as to highlight similarities and differences in

the data-set. PCA is the optimal orthogonal transformation for reducing the dimensionality of the data while keeping the subspace with the largest variance in the data-set.

The principal component spectra were analysed by approximation with a linear combination of spectral standards of the three major cytochrome P450 states found under the given conditions (low-spin and high-spin cytochrome P450, and cytochrome P420), and a low-order, i.e., 2-nd to 4-th order, polynomial (for the approximation of the changes in turbidity), as described in ref. (*138*). After suppression of the turbidity changes by subtracting the polynomial components multiplied by the corresponding loading factors, the corrected data set was subjected to a second round of PCA. The spectra of the principal components hence obtained were approximated with linear combinations of the spectral standards of the P450 states, and the stoichiometric coefficients deduced from these approximations were used to determine the changes in concentrations of high-spin, low-spin cytochrome P450 and cytochrome P420, from the set of loading factors of the significant principal components.

2.2.8 CO BINDING TO IRON (II) CYP3A4 (CHAPTER 6)

For the determination and quantification of the concentrations of functional and inactivated cytochrome P450, we monitored the binding of carbon monoxide to (ferrous) iron (II) heme of the enzyme via absorbance spectroscopy. The enzyme was diluted into 100 mM HEPES buffer, pH 7.4, containing 0.5 mM EDTA, saturated with CO by bubbling for 5 min. Where indicated, a CYP3A4 ligand was added to a specified concentration and a spectrum was recorded. A few crystals of $Na_2S_2O_4$ were directly added to the cuvette, the solution stirred, and the appearance of the absorption peak at 450 nm was monitored continuously via the difference spectrum ($A_{450} - A_{490}$), which selectively measures binding of CO to the reduced iron (II) form of functional cytochrome P450. The data were analysed via spectral decomposition in the SpectraLab software package.

2.2.9 KINETICS OF DITHIONITE-DEPENDENT REDUCTION OF CYP3A4 (CHAPTER 7)

Scanning stopped-flow kinetic experiments were performed on an Olis stopped-flow apparatus equipped with a rapid scanning monochromator (Olis, Bogart, GA, USA). The device has a mixing time of 1-2 ms and can record up to 1000 spectra per second within a range of 75 - 400 nm centered at a chosen wavelength. Experiments were carried out in 100 mM HEPES buffer, pH 7.4, containing 1 mM EDTA at 25 °C. The concentration of dithionite in the cell was 12.5 mM. The two syringes connected to the stopped-flow apparatus contained either 5 μM CYP3A4 enzyme or 25 μM

$Na_2S_2O_4$ in HEPES buffer saturated with CO by bubbling for 5 min (Figure 14). Spectra were recorded from 380 – 600 nm with a spectral resolution of ~1.1 nm and a time-resolution of 12 to 16 ms to a total of 40 s (2500 spectra).

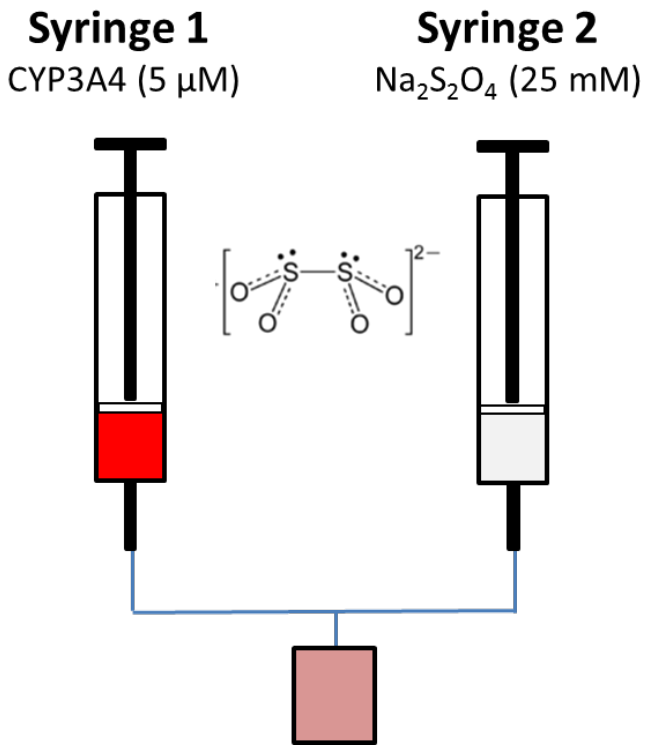

Figure 14: Schematic depiction of the mixing process and the compounds in the stopped-flow measurement.

Data processing:

Time-dependent changes were monitored by plotting the absorbance at 418 nm (low-spin Fe III) and 448 nm (CO-bound Fe II) against time. The kinetic curves were fit to a multiexponential equation:

$$A_t = A_\infty - \left(A_\infty - A_0\right)\sum_{i=1}^{n} F_i e^{-k_i t} \qquad (2.16)$$

with A_0, A_t and A_∞ corresponding to the absorbances at the beginning of the reaction, at time t, and at an infinite time, respectively. F_i and k_i are the fractions and rate constants of the i-th exponential phase. The number of exponentials n was chosen to be three, as at least three exponentials were needed for fitting without systematic bias in the fit from the data. Hence, Eq. 2.16 can be written as:

$$C(t) = C_{t_1} - \left(C_{t_1} - C_{t_0}\right)\left[F_1 \cdot e^{-k_1 t} + F_2 \cdot e^{-k_2 t} + F_3 \cdot e^{-k_3 t}\right] \quad (2.17)$$

*2.3 COMPUTATIONAL METHODS (CHAPTER 4)**

**This chapter describes methods used in simulation experiments that were performed by T. Knehans*

Molecular dynamics simulations - The simulations were performed with the coordinates extracted from the structure of the CYP3A4 complex with metyrapone (1W0G) (*38*). CBZ was superimposed on the bound structure of metyrapone, and water molecules, ions, and the metyrapone molecule were removed. Due to a lack of crystallographic density in flexible segments, spurious *N*- and *C*-termini were neutralized with acetyl groups at Asp270 and Ala289 and with *N*-methyl-amide groups at Glu262 and Ile276, while the natural termini were considered charged. Missing side-chain atoms were added with CHARMM (*139*). Parameters for CYP3A4 and HEME were derived from the CHARMM27 force field (*140*). The partial charges of the Cys442 side chain thiolate were set as developed by Foloppe et al. (*141*). CBZ was parameterized according to the CHARMM general force field (*142*) and Paramchem (*143, 144*).

To determine the modes of binding of CBZ to CYP3A4, five independent MD simulations of 50 ns each were carried out with GROMACS (v 4.5.6) (*145*). First, the CYP3A4/CBZ complex was placed in a dodecahedral box, the size of which was set for a margin of at least 13 Å from any atom of the complex. The box was then filled with pre-equilibrated TIP3P water molecules (*146*), and the system was neutralized with Na and Cl ions at a concentration of 150 mM. Van der Waals and short-range electrostatic interactions were calculated up to a cutoff of 10 Å, long-range electrostatics were evaluated with the particle mesh Ewald method (*147*), and periodic boundary conditions were applied. All bonds involving hydrogen atoms were constrained by the LINCS algorithm (*148*), and a 2 fs time step was used. The temperature was kept constant at 310 K by means of the velocity rescaling algorithm implemented (*149*) in GROMACS, and the pressure was kept constant at 1 atm with a Parinello Raman barostat (*150, 151*). Mutations at the respective residue indices were introduced by simple remodeling in Pymol (*152*). For the simulations with multiple copies of CBZ bound to CYP3A4, the starting positions were generated by manually positioning two, three, or four molecules of CBZ in the active site so that no steric clashes were introduced. All systems were energy minimized for 10000 steps of the conjugate gradient algorithm

before starting the MD. Subsequently, the system was equilibrated in an NPT simulation for 1 ns. From the resulting atomic positions, the production runs were started with different random seeds for the initial assignment of the velocities.

Clustering - The WORDOM (*153*) (version 0.22) implementation of the leader algorithm was used to cluster the snapshots saved along the MD trajectories by a criterion based on the root mean square deviation (RMSD) of the CBZ non-hydrogen atoms. Only the last 10 ns of each 50-ns run were used for clustering, i.e., the first 40 ns of each run were considered equilibration time. First, the CYP3A4 C_α atoms were used to structurally overlap the coordinate sets in the five 10-ns segments with the X-ray structure. Starting from one of the snapshots at 40 ns, which was taken as the first cluster, the leader algorithm proceeded iteratively by comparing each snapshot with the representative of the previously defined clusters. A snapshot was assigned to a cluster when the root mean square deviation was smaller than a threshold value, set equal to 2 Å. Simulations with two CBZ molecules positioned in the active site were clustered with a tree-based algorithm as provided in CAMPARI (*154, 155*)**.** RMSD-based clustering over the entire 200 ns was performed for each of the two CBZ molecules separately with a threshold radius (CRADIUS) of 2 Å, a tree height (BIRCHHEIGHT) of 16, and a coarsest threshold (CMAXRAD) of 10 Å. CYP3A4 C_α atoms were aligned before clustering. All figures were prepared with the PyMol package (*152*).

3 CYTOCHROME P450 3A4 AND NADPH-P450 REDUCTASE: MOLECULAR BIOLOGY AND BIOCHEMISTRY

3.1 SEQUENCING RESULT OF THE EXPRESSION PRODUCT

The expression of the rat CPR gene produces a membrane-bound ~77 kDa protein that contains 1 mol of flavin adenine dinucleotide (FAD) and flavin mononucleotide (FMN) each per mol of enzyme. The expression of the human CYP3A4 gene produces a membrane-bound 57 kDa protein that contains 1 mol heme per mol of enzyme (Table 6) (*44*).

Table 6: Key characteristics of CYP3A4 and CPR*

Characteristic	CYP3A4	CPR
Mass, Da	57,343	76,690
Cofactors	1 heme	1 FAD, 1 FMN
$\#_{(Residues)}$	503	677
$\#_{(Basepairs)}$	1509	2031

*$\#_{(Residues)}$, number of amino acids of the encoded protein; $\#_{(Basepairs)}$, number of nucleotides of the gene.

The entire open reading frame of each generated CYP3A4 construct was verified *via* DNA sequencing through a third-party sequencing service. In Figure 15, deviations of the amino acid sequence between the CYP3A4 version encoded by the expression plasmid pSE3A4 and the authentic human CYP3A4 are shown.

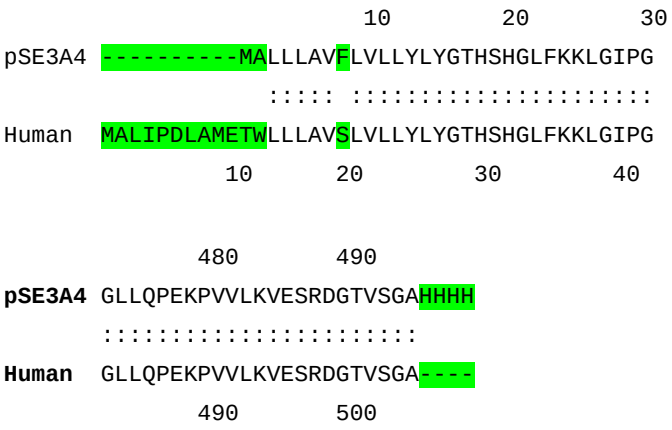

Figure 15: Differences in amino acid sequences of pSE3A4-encoded CYP3A4 from authentic human CYP3A4. Upper alignment: The *N*-terminal alpha-helix encoded on pSE3A4 is truncated by 10 amino acids; amino acids 11, 12 and 18 are mutated. Lower alignment: The *C*-terminus of the recombinant protein contains a 4-histidine-tag to facilitate purification *via* Ni-affinity chromatography. Differences in the sequences are highlighted in green.

Figure 16 presents a complete amino acid sequence alignment of the translated open reading frames (ORFs) of the construct pSE3A4 (*44*), that expresses *N*-terminally modified CYP3A4, and authentic human CYP3A4.

```
                      10        20        30        40        50
pSE3A4 ----------MALLLAVFLVLLYLYGTHSHGLFKKLGIPGPTPLPFLGNILSYHKGFCMF
                 :::::  ::::::::::::::::::::::::::::::::::::::::
Human  MALIPDLAMETWLLLAVSLVLLYLYGTHSHGLFKKLGIPGPTPLPFLGNILSYHKGFCMF
                10        20        30        40        50        60

                60        70        80        90       100       110
pSE3A4 DMECHKKYGKVWGFYDGQQPVLAITDPDMIKTVLVKECYSVFTNRRPFGPVGFMKSAISI
       ::::::::::::::::::::::::::::::::::::::::::::::::::::::::::::::
Human  DMECHKKYGKVWGFYDGQQPVLAITDPDMIKTVLVKECYSVFTNRRPFGPVGFMKSAISI
                70        80        90       100       110       120

               120       130       140       150       160       170
pSE3A4 AEDEEWKRLRSLLSPTFTSGKLKEMVPIIAQYGDVLVRNLRREAETGKPVTLKDVFGAYS
       ::::::::::::::::::::::::::::::::::::::::::::::::::::::::::::::
Human  AEDEEWKRLRSLLSPTFTSGKLKEMVPIIAQYGDVLVRNLRREAETGKPVTLKDVFGAYS
               130       140       150       160       170       180

               180       190       200       210       220       230
pSE3A4 MDVITSTSFGVNIDSLNNPQDPFVENTKKLLRFDFLDPFFLSITVFPFLIPILEVLNICV
       ::::::::::::::::::::::::::::::::::::::::::::::::::::::::::::::
Human  MDVITSTSFGVNIDSLNNPQDPFVENTKKLLRFDFLDPFFLSITVFPFLIPILEVLNICV
               190       200       210       220       230       240

               240       250       260       270       280       290
pSE3A4 FPREVTNFLRKSVKRMKESRLEDTQKHRVDFLQLMIDSQNSKETESHKALSDLELVAQSI
       ::::::::::::::::::::::::::::::::::::::::::::::::::::::::::::::
Human  FPREVTNFLRKSVKRMKESRLEDTQKHRVDFLQLMIDSQNSKETESHKALSDLELVAQSI
               250       260       270       280       290       300

               300       310       320       330       340       350
pSE3A4 IFIFAGYETTSSVLSFIMYELATHPDVQQKLQEEIDAVLPNKAPPTYDTVLQMEYLDMVV
       ::::::::::::::::::::::::::::::::::::::::::::::::::::::::::::::
Human  IFIFAGYETTSSVLSFIMYELATHPDVQQKLQEEIDAVLPNKAPPTYDTVLQMEYLDMVV
               310       320       330       340       350       360

               360       370       380       390       400       410
pSE3A4 NETLRLFPIAMRLERVCKKDVEINGMFIPKGVVVMIPSYALHRDPKYWTEPEKFLPERFS
       ::::::::::::::::::::::::::::::::::::::::::::::::::::::::::::::
Human  NETLRLFPIAMRLERVCKKDVEINGMFIPKGVVVMIPSYALHRDPKYWTEPEKFLPERFS
               370       380       390       400       410       420

               420       430       440       450       460       470
pSE3A4 KKNKDNIDPYIYTPFGSGPRNCIGMRFALMNMKLALIRVLQNFSFKPCKETQIPLKLSLG
       ::::::::::::::::::::::::::::::::::::::::::::::::::::::::::::::
Human  KKNKDNIDPYIYTPFGSGPRNCIGMRFALMNMKLALIRVLQNFSFKPCKETQIPLKLSLG
               430       440       450       460       470       480

               480       490
pSE3A4 GLLQPEKPVVLKVESRDGTVSGAHHHH
       ::::::::::::::::::::::
Human  GLLQPEKPVVLKVESRDGTVSGA----
               490       500
```

Figure 16: The full alignment of amino acid sequences of the construct pSE3A4 (CYP3A4 ORF) with human CYP3A4. The alignment was generated using a web-based alignment tool on: https://www.ebi.ac.uk/Tools/psa/lalign/. The used parameter settings were: matrix file: BLOSUM50, gap open/ext: -100/ -4. Result returned from Lalign: 96.6% identity in 507 amino acid overlap; Global score: 3248.

3.2 RECOMBINANT DNA MANIPULATIONS

pSE3A4 plasmid mutants containing the following variants of CYP3A4 were created *via* the strategy described in Chapter 2.2.1: the I369L, I369F, A370V, A370L, and S119A point mutants and the I369F/A370V, I369F/A370L, I369L/A370V, and I369L/A370L double mutants. The mutagenized PCR products produced according to the described strategy were loaded on a 1% agarose gel and the DNA fragments were separated *via* gel electrophoresis according to their size. The amplified DNA constructs ran at their expected length of ca. 6000 base-pairs. Figure 17 contains photographs of ethidium bromide-stained agarose gels after the separation of the PCR products. Panels (a) and (b) contain each two gel parts, a top and a bottom segment, both of which were loaded with the products of the respective PCR reactions. In the top part, unprocessed PCR product of finished reactions was loaded on the gel. In the bottom parts, *Dpn*I-digested PCR product was loaded. Since the original (methylated) DNA templates added to the PCR reactions are selectively fragmented during *Dpn*I digestion, the presence of bands at 6,000 bp in the bottom part of panels (a) and (b) indicates that DNA amplification during PCR was successful. On both sides of the gel, a mix of DNA fragments of variable lengths was loaded for size comparison (GeneRuler 1 kb DNA ladder). The insets in Figure 17 show that the DNA in the sample was separated according to the expectations based on the sizer (DNA ladder).

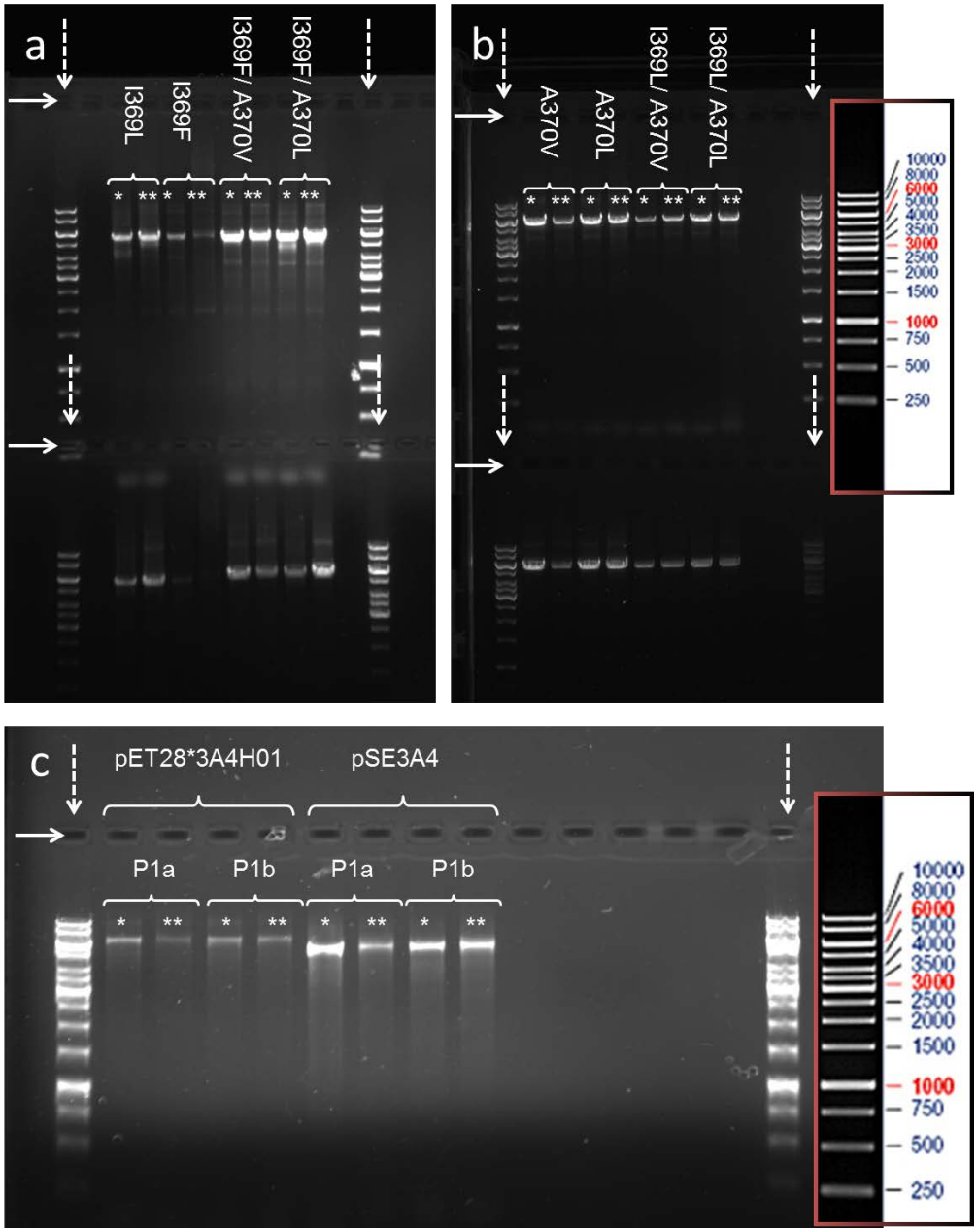

Figure 17: Photograph of 1% agarose-gels containing the products of the PCR-based site-directed mutagenesis. The desired mutations are indicated above the wells. Panel (a) and (b) show the separation of PCR products containing the indicated mutants. The gels in these two panels contain two separations each (top and bottom). Top: separations of the products of the undigested whole plasmid site-directed mutagenesis, bottom: the product of the *Dpn*I-digested whole plasmid site-directed mutagenesis. The gel in panel (c) shows a separation of the PCR-generated DNA of the S119A mutant, both with templates pSE3A4 and pET28*3A4H01 (the latter is a plasmid based on the pET28 vector (Novagen, Merck Millipore, Darmstadt, Germany) and was designed for the expression of the authentic human CYP3A4). The wells containing GeneRuler 1kb DNA ladder are indicated with white dashed arrows. The insets in the red-black frames are shown for comparison of expected and actual separations of the marker. The white full arrows indicate the sample loading wells. * and ** stand for 3% and 10% dimethyl sulfoxide (DMSO) concentration in the PCR. The gels are not uniformly stained due to electrophoretic migration of the ethidium bromide gel stain towards the cathode.

Plasmid DNA from the transformants was isolated using the GeneJET Plasmid Miniprep Kit and submitted for sequencing to GATC biotech (Constance, Germany). The sequenced DNA was aligned with the sequence of the parent plasmid pSE3A4 and the presence of the desired mutations verified. The sequences of the mutagenized plasmids were translated into their amino acid sequences and were aligned with the sequence of human wild-type CYP3A4, analogously to the primary structure alignments of the protein shown in Figure 15 and Figure 16. The focus was set on the amino acids that were targeted for mutagenesis. Out of 24 PCR reactions, the DNA of 22 reactions contained the desired mutations. One clone did not yield a readable sequence and another clone had the wild-type sequence instead of the desired mutation (A370L). Figure 18 shows excerpts of the alignments of the sequencing results with the original wild-type CYP3A4 sequence (as encoded on the PCR template DNA). Due to the already substantial alterations in the biophysical and biochemical properties of the generated point mutants, no double mutants were expressed.

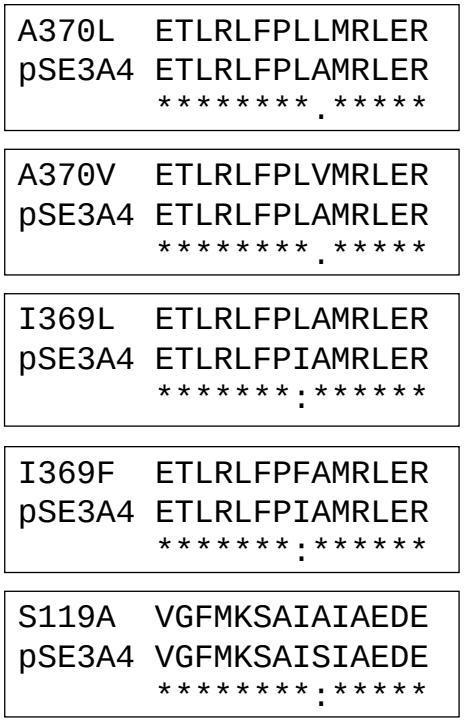

Figure 18: Alignments of the obtained amino acid sequences from mutagenized pSE3A4 plasmids with the sequence of the original pSE3A4 template (wild type). Due to space constraints, only the excerpts of the relevant amino acid sequences are shown. The 1st lines contain the obtained sequences (mutagenized plasmids), and the 2nd lines contain the sequences of the parent plasmid pSE3A4. The 3rd lines contain the symbols used in alignment tools to visualize identities (*) or replacements (:)/(.).

3.3 SPECTRAL CHARACTERISATIONS OF RECOMBINANT ENZYMES

The presence of CYP3A4 was verified in partially purified or non-purified samples. In crude protein extracts, cytochrome P450 is commonly detected *via* binding of CO to Fe^{2+}-heme. The absorbance spectra before and after addition of $Na_2S_2O_4$ of a sample containing wild-type CYP3A4 in a 100 mM HEPES buffer solution, pH 7.4, that is saturated with CO and contains 0.5 mM EDTA, are shown in Figure 19.

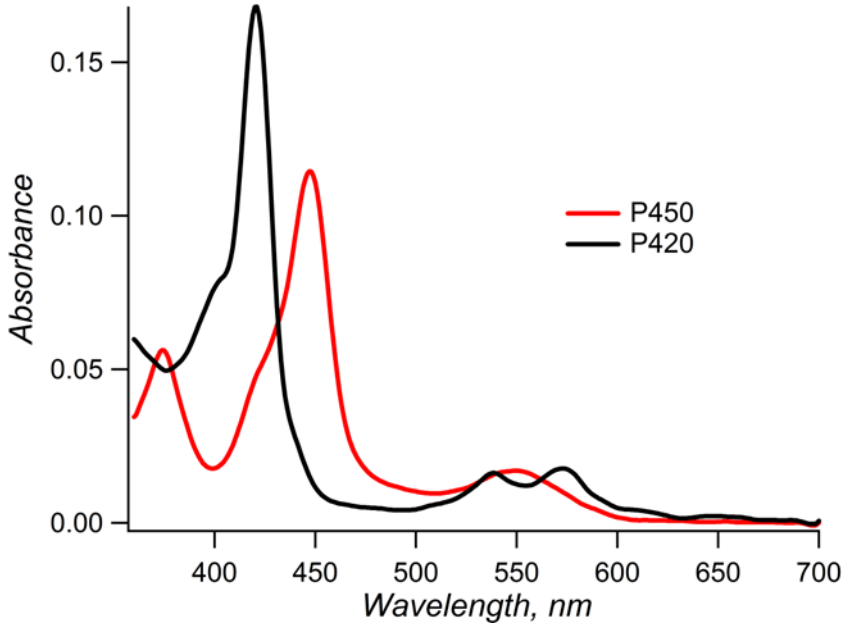

Figure 19: Absorbance spectra of CYP3A4 in CO-saturated buffer solutions before (black) and after (red) reduction with sodium dithionite. Upon reduction, CYP3A4 binds CO with a concomitant shift in the Soret absorbance band from 417 nm to 447 nm. The conditions of the experiment were: 2 µM CYP3A4 wild type in CO-saturated 100 mM HEPES, pH 7.4, 0.5 mM EDTA before and after addition of $Na_2S_2O_4$ (here shown for a purified enzyme sample).

Absorbance spectra of the purified recombinant CYP3A4 enzymes (WT and mutants) and CPR are shown in Figure 20. All five substitutions probed in this study caused a notable increase in the amplitude of the heme protein absorbance band at 391 nm relative to the amplitude of the band at 417 nm. This is indicative of a displacement of the spin equilibrium towards the ferric high-spin state. A peculiarity of the two mutants A370V and A370L is the red-shift in the maximum of the Soret band in the low-spin state by ca. 1 nm.

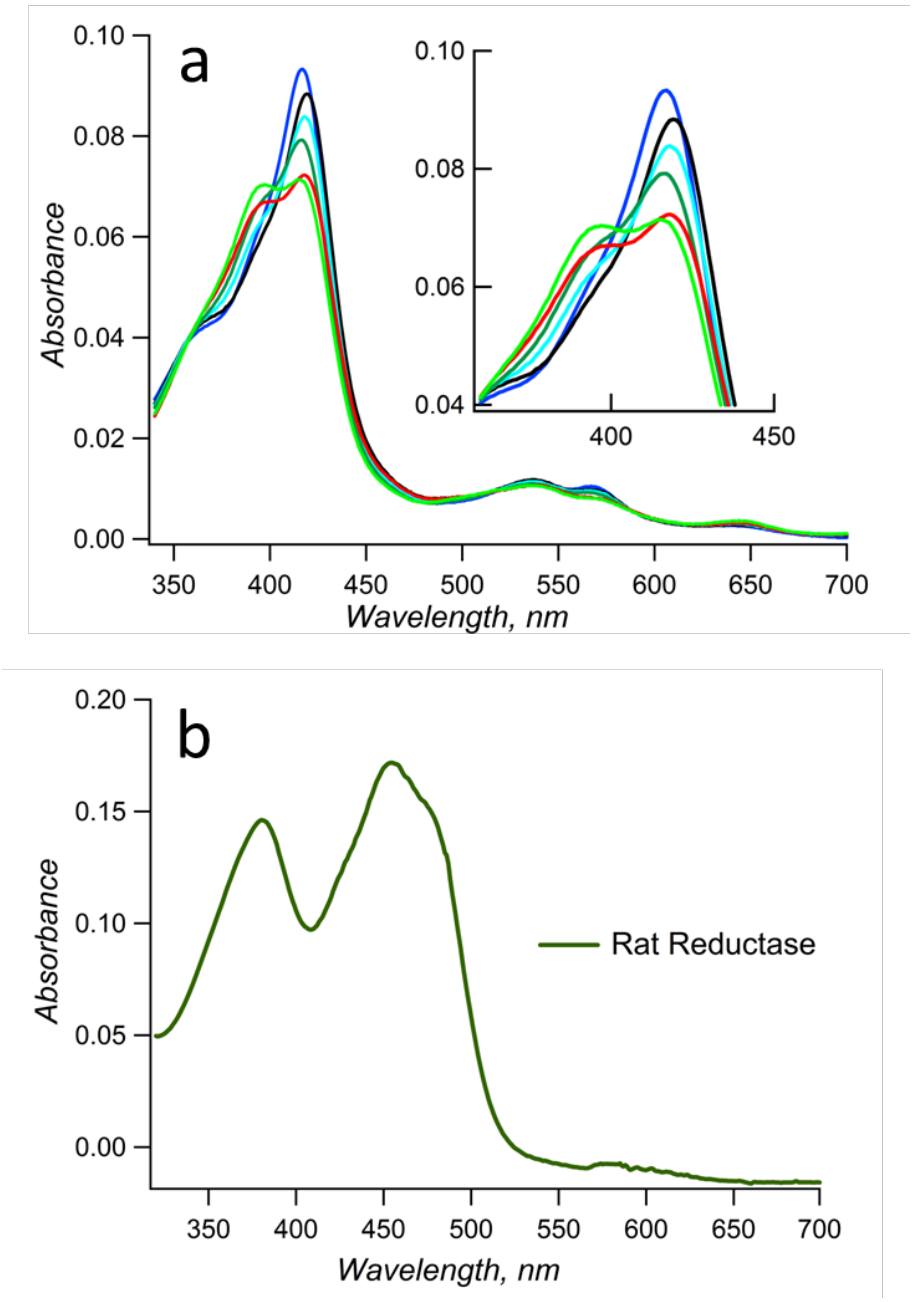

Figure 20: Absorption spectra of the purified enzymes. Panel (a) shows the absorbance spectra of the wild-type CYP3A4 (blue) and its I369F (red), I369L (green), S119A (light green), A370V (turquoise), and A370L (black) mutants. The spectra were normalized to correspond to a heme protein concentration of 1 µM for comparison. The inset in panel (a) shows a zoom of the Soret band of the same spectra and displays the red-shift in the A370V and A370L mutants. Conditions: 100 mM HEPES, pH 7.4, 1 mM DTT, 10% glycerol. The concentration of P450 was in the range of 1.5 – 2.5 µM. Panel (b) shows a spectrum of NADPH-P450 reductase (CPR).

The absorbance spectra were reproduced with a combination of the spectral standards (see p. 49) of CYP3A4 high-spin, low-spin, and ‘P420’, in combination with a low-order polynomial. This allowed the determination of the respective species in the total enzyme pool. An example of how the individual species of cytochrome P450 present in the ensemble were quantified is shown in Figure 21, which shows the absorbance spectrum of a sample containing purified CYP3A4 I369L.

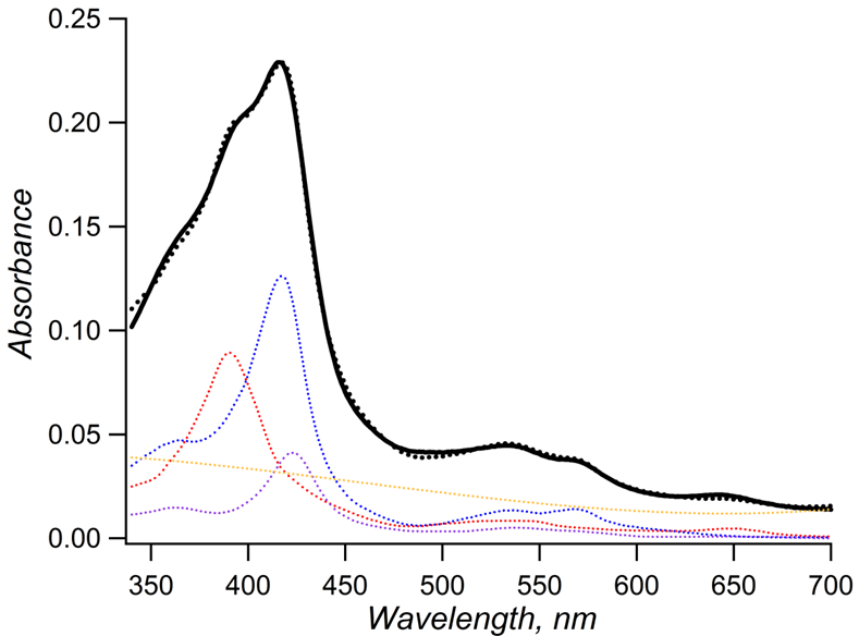

Figure 21: Background-correction and quantification of the cytochrome P450 species that are present in an ensemble of purified hemoprotein of CYP3A4 I369L. The recorded spectrum of the purified CYP3A4 I369L mutant (black line) is approximated with the spectral standards for CYP3A4 high-spin (dotted red line), low-spin (dotted blue line), ‘P420’ (dotted violet line), and a low-order polynomial (dotted orange line). The dotted black line represents the approximation of the recorded spectra, i.e., the sum of the polynomial and the weighted spectral standards as shown in the figure.

The analysis of the high-spin contents in the CYP3A4 mutants in the absence of substrate is shown in Figure 22. The displacement in the spin equilibrium is most pronounced in the mutants I369F and S119A, where the fraction of high-spin heme protein approaches 50%, in sharp contrast to the spin state of the wild-type CYP3A4, where the high-spin fraction at 28 °C does not exceed 20%.

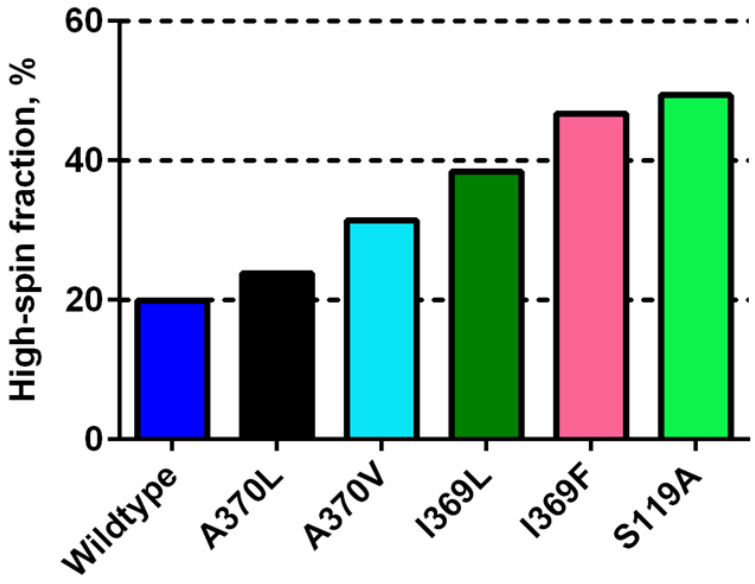

Figure 22: Effect of mutations on the spin state distribution in purified CYP3A4 proteins. Illustrated are the high-spin fractions of the expressed CYP3A4 variants.

3.4 SDS-PAGE OF RECOMBINANT ENZYMES

An SDS polyacrylamide gelelectrophoresis (SDS-PAGE) analysis of the purified enzymes is shown in Figure 23. As it is apparent from the gel, the recombinant enzymes were produced in high purity. In the peripheral wells to both sides, an aliquot containing proteins of known length was run for sizing the protein (PageRuler^{TM}; contains a prestained mixture of ten recombinant proteins of sizes that range from 10 kDa to 170 kDa). The enzymes ran at their expected sizes of ca. 55-60 kDa (CYP3A4) and ca. 70-80 kDa (CPR).

The obtained yields were low, which is typical for the expression of human CYP3A4 genes. The yields are shown in Table 7.

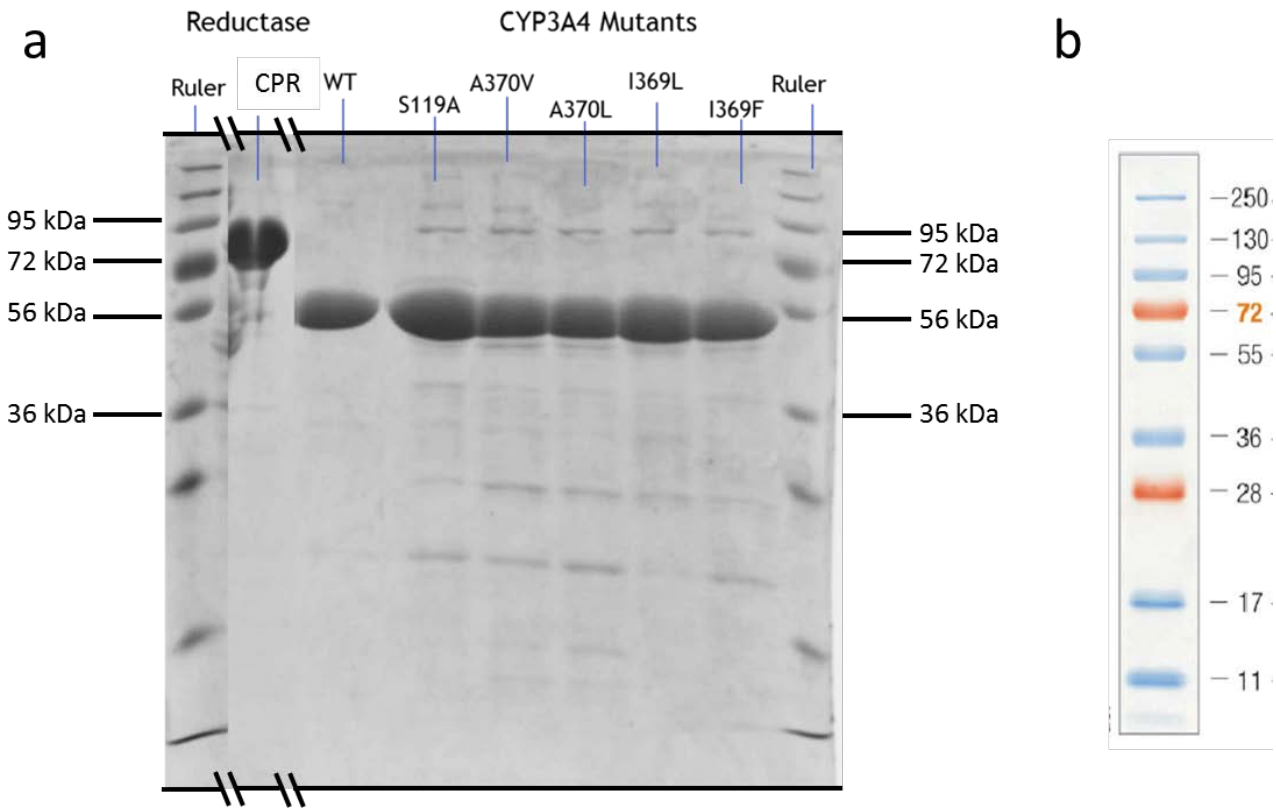

Figure 23: Separation of purified enzymes *via* sodium dodecyl sulphate polyacrylamide gel electrophoresis (SDS-PAGE). Panel (a) shows a polyacrylamide gel loaded with the recombinant purified enzymes after electrophoresis. Protein bands of wild-type (WT) CYP3A4 and its mutants ran at a mass of ca. 55 kDa, CPR (= POR) ran at a molecular mass of ca. 75 kDa. These values are in accordance with the calculated molecular masses of 57 kDa and 77 kDa of the enzymes, respectively. For size comparison, the leftmost and rightmost wells were each loaded with PageRuler™ Prestained Protein Ladder Plus, a commercial mixture of proteins of known length. (b) SDS-PAGE profile of the commercial protein mix.

Table 7: Recombinant expression and purification yields of the enzymes*

Enzyme (CYP3A4 variant)	Volume, l (culture)	Yield cell lysate, mg		Yield pure enzyme, mg	
		total	per l	total	per l
(WT)	4	620	155	257	**64**
(A370V)	2	260	130	60	**30**
(A370L)	2	240	120	55	**28**
(I369F)	4	386	97	120	**30**
(I369L)	4	600	150	170	**43**
(S119A)	4	320	80	38	**10**
CPR	4	429	107	32	**8**

* The yields are shown both for the crude cell lysate and the purified enzyme and are given in mg and mg/l.

3.5 KINETIC CHRARACTERIZATION OF RECOMBINANT CYP3A4 AND CPR

The activities of enzymes that had been reconstituted at 4 °C for 30 min or overnight were determined in an activity assay with the resorufin derivative Vivid® BOMR and compared (see p. 51). The reproducibility of the procedure with overnight incubation was as good or even better than that with 30 min incubation. The subsequent activity measurements showed no decrease in the activity of the reconstituted enzyme after overnight compared to 30 min incubation in the thermomixer (Figure 24). The enzymes were henceforth reconstituted overnight in further experiments.

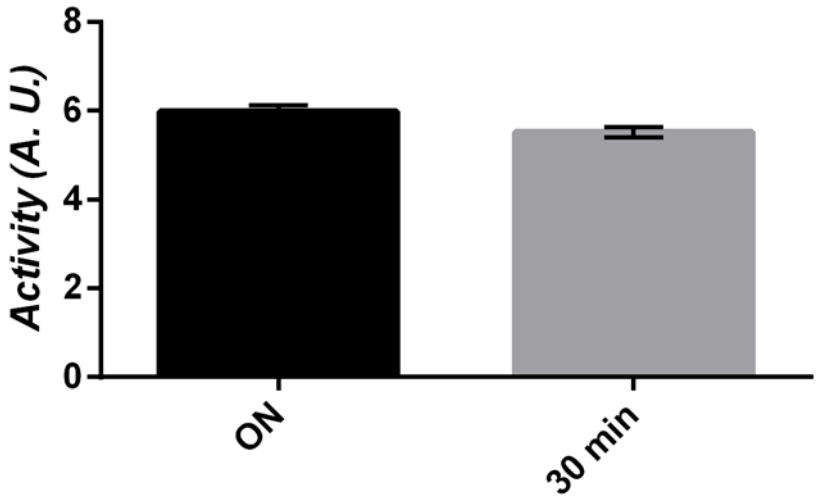

Figure 24: Activity of CYP3A4 WT reconstituted either overnight (ON) or during 30 min in a thermomixer at 4 °C (turnover of Vivid® BOMR). The data represent the mean activities and the error bars represent the standard deviations from 3-4 experiments.

In order to prove the presence of an active flavoprotein NADPH-P450 reductase (CPR) in crude cell lysates and along the purification steps, we applied a cytochrome *c* reduction assay to quantify CPR in non-purified samples as described in ref. (*31*). Although CPR donates electrons to P450, P450-based assays are uncommon due to the tendency of reduced P450 to react with air. A convenient approach is therefore the coupling of the reduction reaction to air-stable dyes or redox components such as cytochrome *c*. CPR accepts electrons from its native hydride donor NADPH and transfers them to cytochrome *c*, which acts as an electron acceptor surrogate. Even though the bacterial strains used for heterologous expression of cytochrome P450 genes contain other reductases that can accept electrons from NADPH and transfer them to cytochrome *c*, many of these

reductases are not membrane bound. Therefore, they do not interfere with the reduction of cytochrome *c* in partially purified cell lysates in the downstream processing of P450 isolations. The reduction of cytochrome *c* generates a prominent narrow absorption peak at λ = 550 nm (*31*), the emergence of which is detected *via* the monitoring of the difference in absorption between 550 nm and the isosbestic point at 541 nm.

Figure 25 shows a sample cytochrome *c* reduction experiment (0.4 µl of a purified CPR sample to be quantified in 1 ml potassium phosphate, pH 7.4, containing 50 µM cytochrome *c* and 100 µM NADPH).

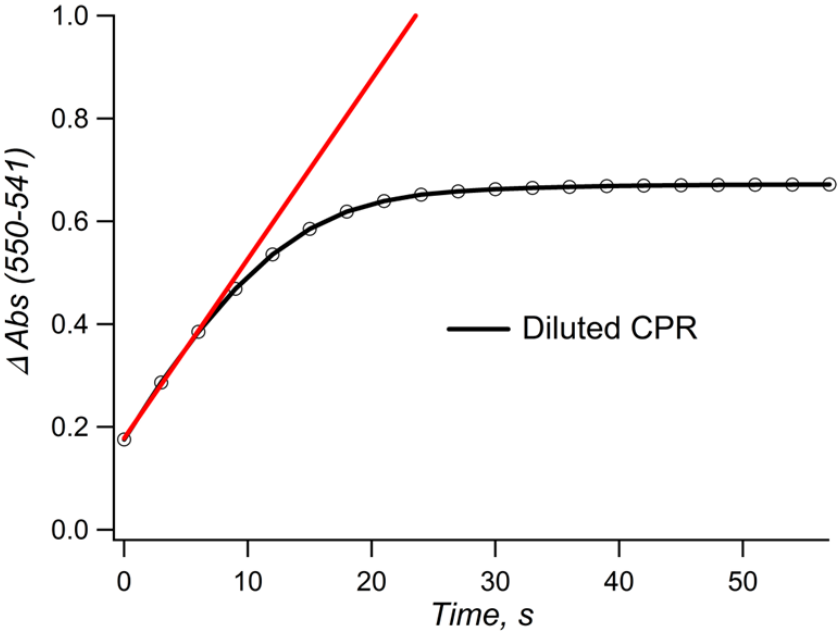

Figure 25: Time-series of absorbance difference spectra (*ΔAbs*$_{550\text{-}541}$) versus time in the CPR activity assay. The concentration of the CPR stock can be calculated from the initial slope (red) of the $\Delta A_{550\text{-}541\ nm}$ vs. time curve (black).

With the extinction coefficient of reduced cytochrome *c* ($\varepsilon_{550\text{-}541}$ = 0.018 mM^{-1} cm^{-1}), the CPR content in mixed samples can then be calculated by assuming a cytochrome *c* reduction rate of ca. $3.0 \cdot 10^3$ min^{-1} at room temperature (*133*, *134*). Masters et al. reported a rate of 2380 – 2840 min^{-1} in 100 mM potassium phosphate, pH 7.7, 20% glycerol, 0.2 mM EDTA (*134*). In this example, the concentration of the CPR stock is calculated through (with dilution factor *D*):

$$[CPR] = \frac{\Delta A_{550-541} \cdot D}{0.018\ mM^{-1} cm^{-1} \cdot 3.0 \cdot 10^3\ min^{-1}} \approx 100\ \mu M \qquad (3.1)$$

Conversely, the activity of a CPR stock of known concentration can be determined by transforming equation 3.1.

3.6 ILLUSTRATION OF THE PRINCIPAL COMPONENT ANALYSIS METHOD

In substrate titrations of an enzyme, the number of principal components in theory corresponds to the number of the titration-associated transitions with distinct spectral signatures. In the case of CYP3A4, binding of type-I substrates or changes in temperature result in a shift of the equilibrium between the ferric high-spin and low-spin states of the hemoprotein component and yield a difference spectrum with prominent maxima and minima at ~390 nm and ~420 nm, respectively (Figure 26). In the presence of a temperature gradient and the absence of any other titration process, PCA is expected to yield only one significant principal component that corresponds to the temperature-induced equilibration of the spin state in cytochrome P450.

In titrations with substrate, the changes in the spin state often overlap with the changes caused by the inactivation of the enzyme via its conversion into the so-called P420 state. A further important contribution to spectral changes in absorbance titration experiments is caused by changes in turbidity of the sample due to the limited solubility of substrates and substrate-induced changes in the aggregation state of the enzyme. In most titration data, at least these three independent sources of spectral changes are therefore present: (1) substrate-induced spin changes; (2) time- and/or substrate-dependent inactivation through the transition to the P420 state, and (3) changes in light scattering induced by increasing turbidity of the sample. Accordingly, titration-related spectral changes are distributed between three principal components. Each of these components represents a linear combination of the three types of spectral changes (Figure 27).

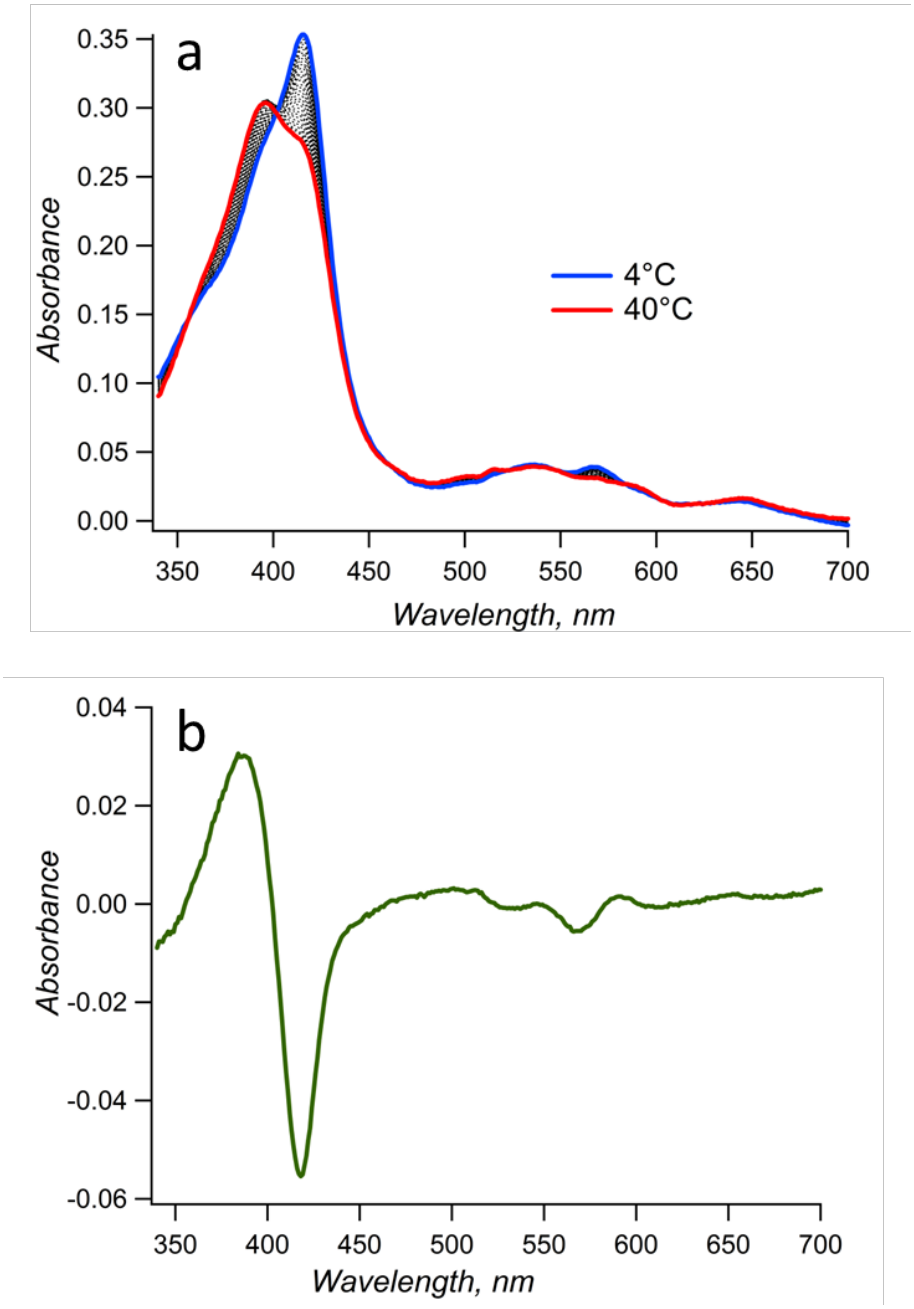

Figure 26: PCA of a temperature-gradient experiment with the CYP3A4 mutant S119A. (a) Corrected absorbance spectral series of the CYP3A4 mutant S119A recorded at temperatures increasing incrementally by 1 degree from 4 °C to 40 °C (spectra at 4 °C and 40 °C are presented as blue and red lines, respectively; the spectra between the extreme values are shown in black dotted curves). (b) The first principal component of the spectral series dataset taken in the temperature gradient experiment of CYP3A4 S119A. This principal component amounts to 99.84% of the total changes in the spectra. The spectrum clearly shows a difference spectrum characteristic of a type-I spin shift (HS – LS) with a minimum at 417 nm (absorbance maximum of LS P450). Whereas the Soret band at 417 nm shifts to ~391 nm, the α-band (absorbance maximum 562 nm) and to a lesser extent the β-band (absorbance maximum 534 nm) are attenuated in the course of the (LS → HS) spin shift.

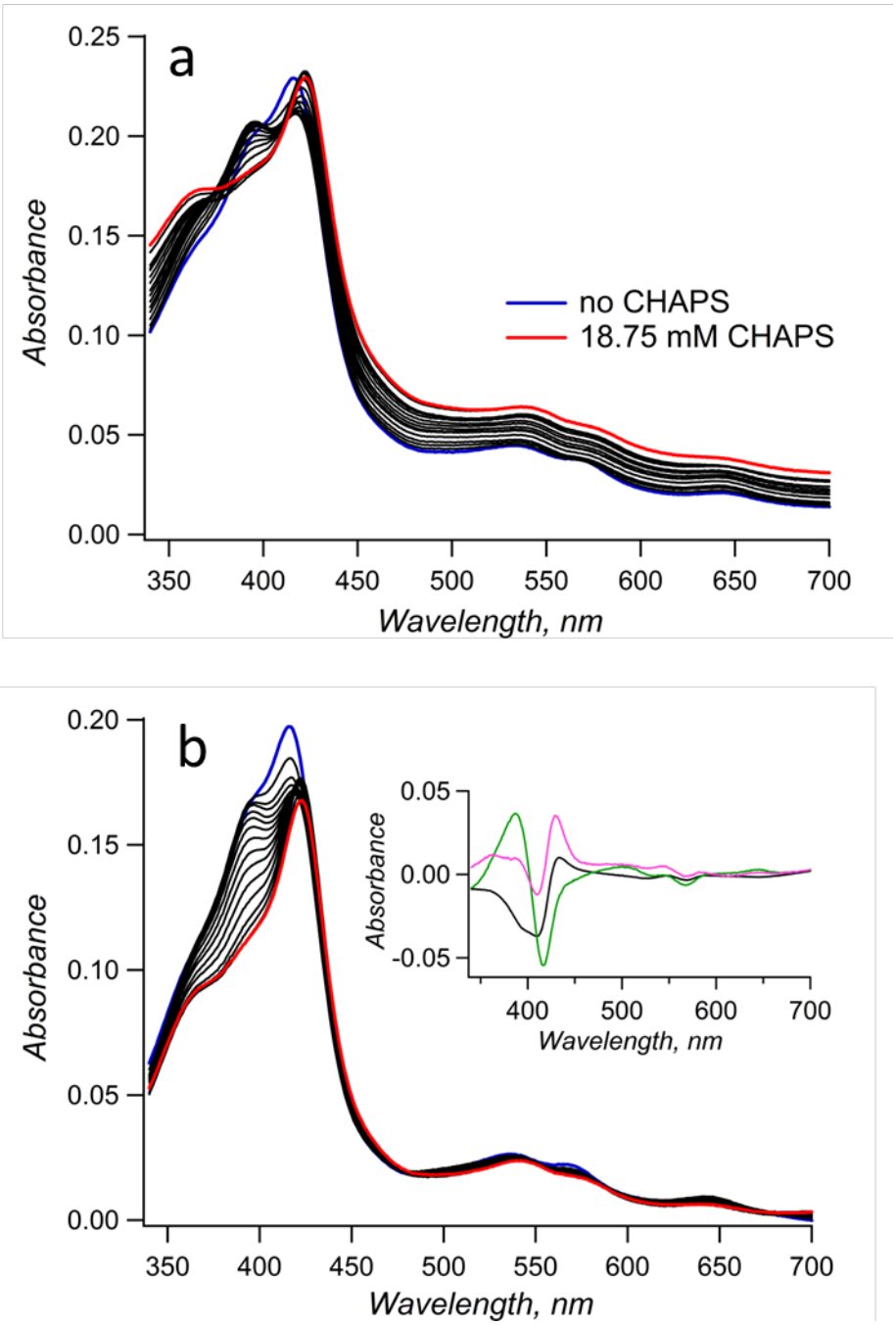

Figure 27: Absorbance titration spectra of CYP3A4 I369L with the zwitterionic detergent CHAPS (a) before and (b) after correction. Panel (a) shows the unprocessed data of the titration experiment. Panel (b) shows this data after correction for background. The inset shows the three first principal components, which hold 93.6% (black), 5.9% (green) and 0.5% (magenta) of the total variation in the data. The components contain the changes [LS+HS] → ['P420'], [LS] → [HS], and [LS]→['P420'], respectively. The sample contains 2.5 µM P450 in 100 mM HEPES buffer and CHAPS was incrementally added from 0 to a total concentration of 18.75 mM.

3.7 EFFECT OF SOLVENTS ON THE CYP3A4 S119A SPIN EQUILIBRIUM

In titration experiments, diverse polar solvents, such as acetone, methanol, DMSO, or ethyl acetate are commonly used as stock solvents. The optimal solvent exhibits titrant solubility above the desired concentration of the stock solution and negligibly perturbs the spin equilibrium in the heme iron (III) cytochrome P450. In order to determine the best stock solvent for the titration experiments, we investigated the effect of the two solvents acetone and methanol on the spin state of the mutant S119A. Acetone and methanol have a similar effect on the spin equilibrium of CYP3A4 S119A (Figure 28). However, since evaporation of the stock solvent due to high gas pressure of acetone cannot be excluded, methanol was preferred as stock solvent due to its lower evaporation rate.

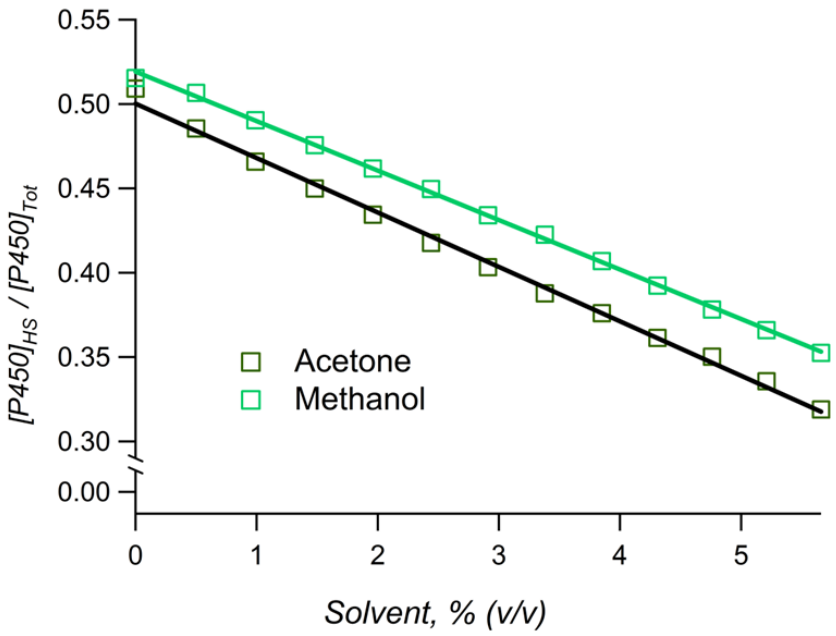

Figure 28: High-spin proportion of total cytochrome P450 for the titration of the CYP3A4 S119A mutant with the solvents acetone and methanol.

3.8 DISCUSSION

The purified enzymes CYP3A4 and P450 reductase (CPR) were used in studies of the epoxidation kinetics of carbamazepine (Chapter 4), which resulted in a manuscript by Müller C. S., Knehans T., Davydov D.R., Bounds P.L., von Mandach U., Halpert J.R. Caflisch A., and Koppenol W.H. entitled *"Concurrent Cooperativity and Substrate Inhibition in the Epoxidation of Carbamazepine by Cytochrome P450 3A4 Active Site Mutants Inspired by Molecular Dynamics Simulations"*. The produced enzymes were also immobilized on electrodes, characterized and employed for the sensing of the cytostatic drug iphosphamide. The results from this work were submitted for a publication entitled *"Faradic Peaks Enhanced by Carbon Nanotubes on P450 Based Electrochemistry by Microsomes"* by Baj-Rossi, C., Müller, C., von Mandach, U., De Micheli, G., and Carrara, S.

4 CONCURRENT COOPERATIVITY AND SUBSTRATE INHIBITION IN THE EPOXIDATION OF CARBAMAZEPINE BY CYTOCHROME P450 3A4*

** This chapter was adapted from a manuscript by Müller C. S., Knehans T., Davydov D.R., Bounds P.L., von Mandach U., Halpert J.R. Caflisch A., and Koppenol W.H., submitted to Biochemistry. Data and figures that were generated by T. Knehans (TK) are marked accordingly.*

4.1 ABSTRACT

Cytochrome P450 3A4 (CYP3A4) is the major human P450 responsible for the metabolism of carbamazepine (CBZ). To explore the mechanisms of interactions of CYP3A4 with this anticonvulsive drug, we performed multiple molecular dynamics (MD) simulations starting from the complex of CYP3A4 with manually docked CBZ. Based on these simulations, we engineered the CYP3A4 mutants I369F, I369L, A370V, and A370L, in which the productive binding orientation was expected to be stabilized, thus leading to increased turnover of CBZ to the 10,11-epoxide product. In addition, we generated S119A as a control construct with putative destabilization of the productive binding pose. The evaluated kinetic profiles of CBZ epoxidation demonstrate that the CYP3A4-containing bacterial membranes (Bactosomes) as well as purified CYP3A4 wild type and I369L/F mutants in reconstituted systems exhibit substrate inhibition. In contrast, the mutants S119A and A370V/L exhibit S-shaped profiles indicative of homotropic cooperativity. MD simulations with two to four CBZ molecules provide evidence that the substrate binding pocket of CYP3A4 can accommodate more than one molecule of CBZ. Analysis of the kinetic profiles of CBZ metabolism with a model combining the formalism of the Hill equation with an allowance for substrate inhibition demonstrates that the mechanism of interactions of CBZ with CYP3A4 involves multiple (most likely three) substrate-binding events. Despite the retention of the multisite binding mechanism in the mutants, its functional manifestations reveal an exquisite sensitivity to even minor structural changes in the binding pocket introduced by such conservative substitutions as I369F, I369L, or A370V.

4.2 INTRODUCTION

Cytochrome P450 3A4 (CYP3A4) is the most abundant cytochrome P450 enzyme in the liver of most adult humans (*159*). This enzyme, which metabolizes about 50% of drugs on the market (*37*), is the main hepatic cytochrome P450 involved in the metabolism of 5*H*-dibenzo[*b,f*]azepine-5-carboxamide (carbamazepine or CBZ). CBZ is a commonly prescribed anti-convulsive drug, and its major metabolite is carbamazepine-10,11-epoxide (Figure 29) (*160, 161*). CBZ, for which the target for plasma concentration is 17 – 70 µM (*51*), qualifies as a "narrow therapeutic index drug" (*123*). As failure to maintain the target plasma range may cause toxic side-effects, continuous therapeutic monitoring is desirable for optimal outcome of CBZ therapies. A potential approach to continuous monitoring are biosensors constructed from electrodes with immobilized P450 enzymes to detect drug substrates such as CBZ (*115, 118, 122*).

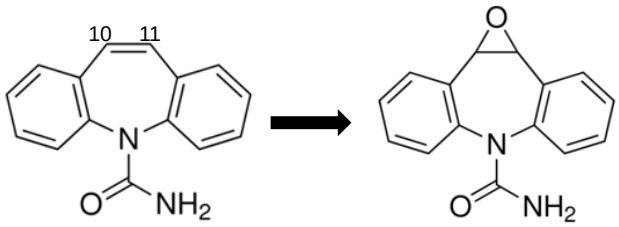

Figure 29: Structures of carbamazepine (left) and the major product of its CYP3A4-dependent oxidation, carbamazepine-10,11-epoxide (right).

Numerous studies on *in vitro* CBZ epoxide formation that include data from incubations with human liver microsomes (HLM) (*51, 83, 161-163*), recombinant enzyme expressed in microsome fractions from insect cells (*164, 165*), and reconstituted purified enzyme preparations (*77, 161, 166*) have been published: both hyperbolic and sigmoidal dependencies of the reaction rate on the substrate concentration have been observed. Differing degrees of homotropic cooperativity have been reported for HLM (*51, 83, 161, 162*) and microsomes from insect cells expressing recombinant human CYP3A4 (*163, 164*). Michaelis-Menten kinetics (*161*) as well as sigmoidal profiles (*51*) have been reported for purified and reconstituted CYP3A4. The apparent inconsistency among these reports demonstrates that epoxidation of CBZ by CYP3A4 is very sensitive to the experimental conditions and the enzyme source. Such inconsistencies in kinetic profiles have also been reported for other substrates, such as amitriptyline, nifedipine, and testosterone (*167*).

In this study, we sought to explore the mechanism of interaction of CYP3A4 with CBZ by engineering CYP3A4 variants with enhanced affinity for CBZ and/or increased epoxidation turnover. These studies were targeted towards elaboration of a CYP3A4-based electrochemical biosensor with improved capacity for determining CBZ concentration in clinical samples. Our approach to the optimization of CYP3A4 for CBZ binding encompasses explicit solvent MD simulations of the structure of the CYP3A4 complex with CBZ in combination with site-specific protein engineering to incorporate amino acid alterations in the enzyme active site. Based on our MD simulations, we cloned, expressed, and purified four CYP3A4 mutants with putative stabilization of the CBZ molecule in a predicted productive binding mode for increased affinity for CBZ and turnover to the epoxide product. As a negative control with putative disruption of a critical hydrogen bond, we also constructed the S119A mutant, for which we expected enzyme turnover with CBZ to be diminished.

We report herein that the point mutations S119A, I369L, I369F, A370L, and A370V produce dramatic effects on the kinetic parameters of CBZ oxidation. These results demonstrate a profound sensitivity of the reaction kinetics of CYP3A4 to minor structural changes in the binding pocket. The observation of both homotropic cooperativity and substrate inhibition in the kinetics of CBZ epoxidation by the cloned CYP3A4 mutants suggests that the interactions of CYP3A4 with the drug involve the binding of at least two, but more likely three CBZ molecules to the enzyme. This conclusion is supported by multiple MD simulations, which demonstrate possible accommodation of multiple CBZ molecules in the CYP3A4 binding pocket.

4.3 RESULTS

4.3.1 CBZ EPOXIDATION BY CYP3A4-CONTAINING BACTOSOMES

In good agreement with previous studies of CYP3A4-dependent metabolism of CBZ, we detected no product other than carbamazepine-10,11-epoxide in significant amounts (*161*). Upon examination of the substrate concentration dependence of the kinetic profiles, we extended the range of CBZ concentrations used in our analyses to 0 – 2000 μM, which includes considerably higher concentrations than reported in previous studies (*161-164*). The kinetic profile reveals a moderate but clearly pronounced substrate inhibition that becomes evident at CBZ concentrations > 700 μM (Figure 30). The fit of the initial parts of the titration curves ([CBZ] ≤ 1000 μM) with the Hill equation (Figure 30, dashed line) is consistent with positive cooperativity, with a Hill coefficient h of 1.4 ± 0.4 (S_{50} = 162 ± 4 μM, k_{cat} = 1.9 ± 0.3 min^{-1}), in

agreement with a previous report in which CYP3A4-dependent epoxidation of CBZ was characterized as exhibiting inherent homotropic cooperativity with *h* of 1.4 – 1.7 (*51*).

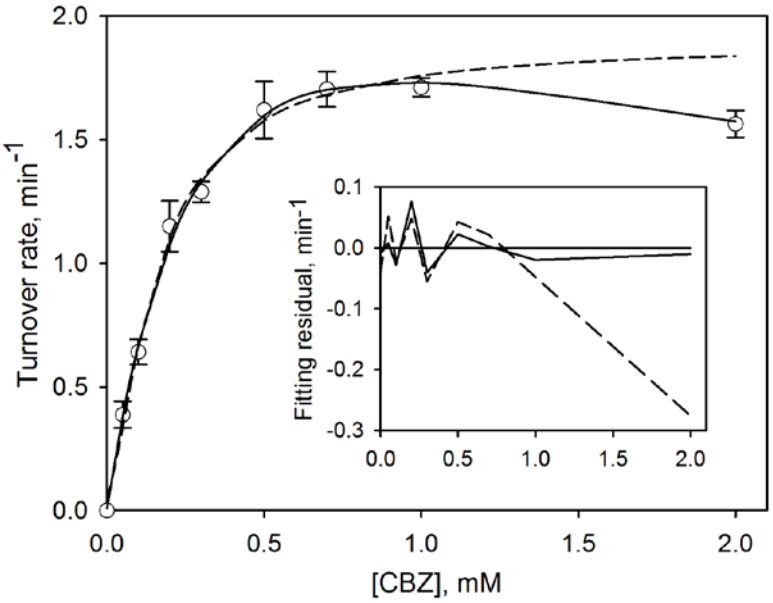

Figure 30: Substrate dependence of the rate of formation of carbamazepine-10,11 epoxide catalysed by recombinant CYP3A4 in Bactosomes. Data points represent the mean values of the results of three individual measurements and the error bars show the respective standard deviations. Fitting to the Hill equation (dashed line) and the Equation (4.1) are shown with dashed and solid lines, respectively. The inset shows the respective plots of the fitting residuals.

However, the Hill equation fits of the titration curves are satisfactory only up to CBZ concentrations of ca. 700 µM; at higher concentrations, there is evident systematic deviation of the experimental data from the equation curve (Figure 30, inset). In an attempt to achieve an appropriate approximation of the experimental data over the entire range of CBZ concentrations, we fit the data sets to the Michaelis-Menten equation adapted for partial substrate inhibition:

$$V = \frac{k_{cat} \cdot [E]_0 \cdot [S] \cdot (\alpha \cdot [S] + K_I)}{K_M \cdot K_I + [S] \cdot (K_I + [S])} \qquad (4.1)$$

Here V and k_{cat} designate the reaction rate at substrate concentration [S] and the catalytic constant, respectively. The Michaelis constant and the dissociation constant of the enzyme complex with the inhibitory substrate molecule are designated as K_M and K_I, respectively, and the coefficient

α represents the fraction of k_{cat} that is retained in the inhibitory complex with a second molecule of bound substrate. The derivation of this equation is described in the methods section (Chapter 2).

As shown in Figure 30 (solid line), the fitting of the experimental data sets with Eq. 4.1 results in a satisfactory approximation ($\rho^2 \geq 0.982$) with no systematic deviations over the entire range of CBZ concentrations studied (Figure 30, inset). The parameters for fitting Eq. 4.1, representing the averages of the results obtained in three individual experiments, are: $k_{cat} = 3.1 \pm 0.5$ min^{-1}, $K_M = 140 \pm 10$ µM, $K_I = 1600 \pm 300$ µM, and $\alpha = 0.21 \pm 0.08$. Therefore, the data obtained with bactosomes are consistent with a model whereby the maximal rate of CBZ metabolism is obtained in the complex of CYP3A4 with one substrate molecule, and subsequent low-affinity binding of a second CBZ molecule to this complex results in a ca. 5-fold decrease in the rate of CBZ metabolism. It appears probable, therefore, that earlier reports of positive cooperativity in the CYP3A4-dependent CBZ metabolism should be questioned, whether the titration curves thought to fit the Hill equation (Figure 30, dashed line) were recorded over a range of CBZ concentrations too low to effect pronounced substrate inhibition.

4.3.2 PROBING THE CBZ BINDING MODE TO CYP3A4 WITH MD SIMULATIONS

According to the above analysis, we infer that the complex of CYP3A4 with one substrate molecule in the substrate binding pocket may serve as an adequate initial model of the catalytically competent complex of the enzyme with CBZ. Thus, we selected a binary complex of CYP3A4 with one CBZ molecule as the subject for initial MD simulations aimed to elicit the structure of the CBZ-CYP3A4 complex and the orientation of the substrate molecule in the active site.

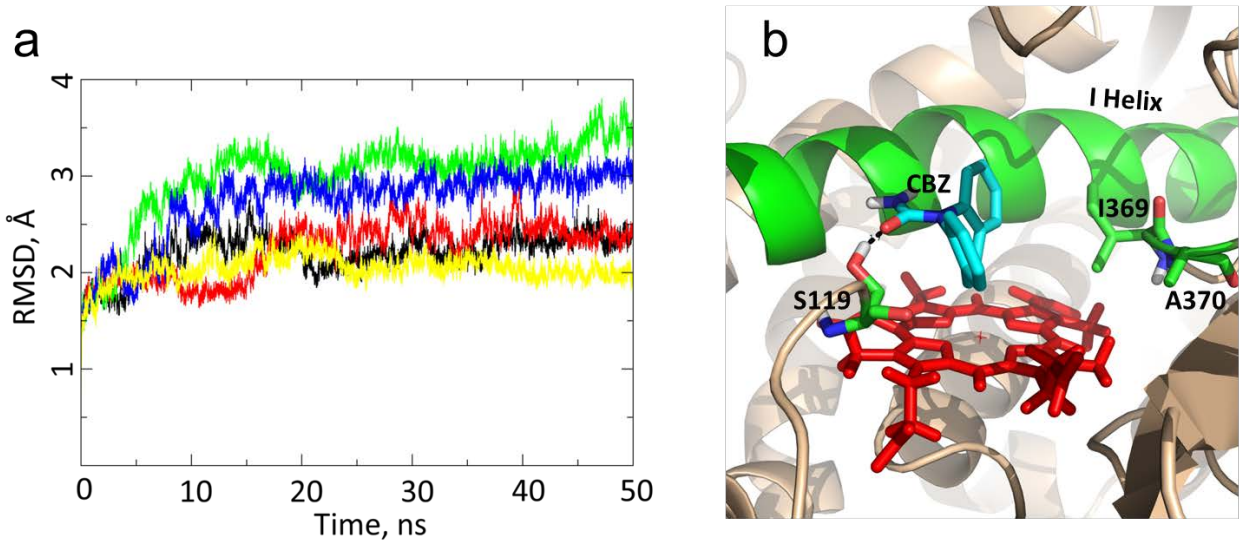

Figure 31: Results of MD simulations with the complex of wild-type CYP3A4 with one molecule of CBZ. Panel (a) shows the time series of the RMSD from the crystal structure (PDB code 1W0G) of the protein backbone after alignment of the C_α carbons. The RMSD reaches a plateau after about 20 ns in the five independent runs, which are plotted with different colors. Panel (b) shows a representative snapshot of the most populated cluster. The residues selected for mutation (S119, I369, and A370), CBZ, and the heme group are shown with stick models in green, cyan, and red, respectively. The protein backbone is shown in transparent grey, and the I-helix is shown in green. *Panel (a): data and figure by T.K., panel (b): data by T.K., figure by C.M.*

Figure 31b shows that the time series of the backbone RMSD from the X-ray structure of CYP3A4 (1W0G) (*38*) reaches a plateau between 2 and 3 Å after about 10 ns (equilibration phase). We determined the binding modes of CBZ in five independent MD runs of 50 ns each, whereby only the last 10 ns of each run were evaluated. In the most populated, i.e., largest, cluster of the CBZ poses, the heme iron is located within 5 Å of the center of the bond between the carbon atoms 10 and 11 (C10,11), compatible with the CYP3A4-catalyzed epoxidation of CBZ (Figure 31b). It should be noted, however, that the relevance of this binding mode to the actual mechanism of interactions is difficult to assess as it was primarily sampled in only one of five MD runs. The CBZ molecule that was initially superimposed at the position of the removed metyrapone did not exit the CYP3A4 binding site in any of the runs. The cluster representatives of the 5 most important clusters of the simulation are shown in Figure 32.

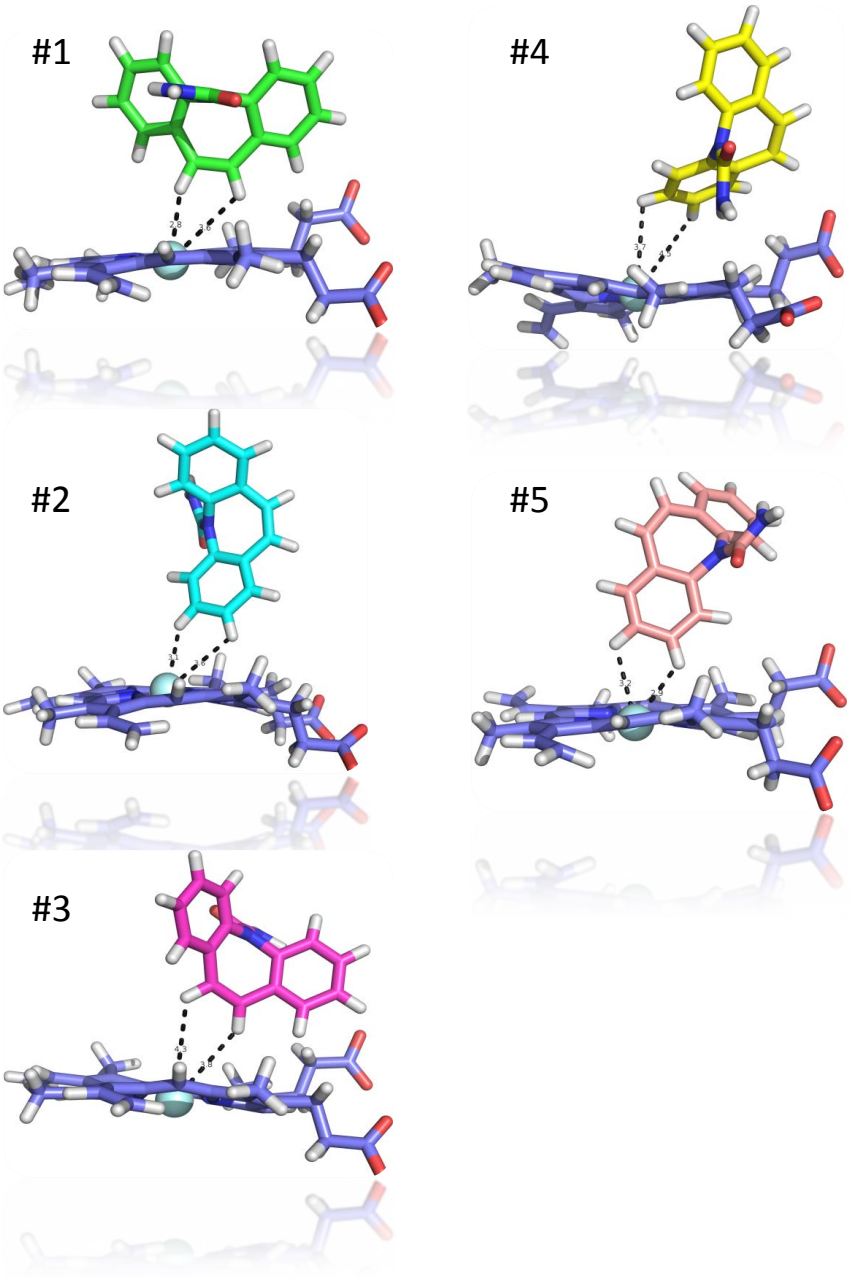

Figure 32: Relative orientations of CBZ and the heme in the cluster representatives of the five most populated clusters of the MD simulations of the CYP3A4 WT-CBZ complex. Cluster # 1 corresponds to the structure shown in Figure 29b. *Data and figure by T.K.*

4.3.3 SELECTION AND SUGGESTION OF MUTANTS

Based on the binding mode of CBZ in the largest cluster of poses deduced from MD simulations (Figure 31b), we suggested five single-point mutants on the basis of the mean distances between the center of mass (COM) of the respective residues and the COM of CBZ in this cluster. The prime notion was that the effect of methylation of small molecules, which is done in iterations of drug optimizations to increase potency, can also be achieved by increasing the hydrophobic

surface of the protein, since the structure of the ligand CBZ was to be maintained. Table 8 shows the centre of mass distances for the CBZ molecule in the largest cluster and the surrounding residues. While side chains featuring a hydrogen bond donor/acceptor were excluded from mutation due to unforeseeable influences on the charge distribution of the active site, only residues with a hydrophobic side chain in a certain distance were considered. Phe residues (already at maximal hydrophobic surface) were not considered either. Only residues close to the 5H-dibenzo[b,f]azepine moiety featuring a side chain which would be closer after mutation could potentially increase VdW interactions with the substrate. Considering these criteria, only Ala370 and Ile369 were left for mutagenesis. We predicted that the mutations I369L, I369F, A370V, and A370L would lead to improved steric complementarity, i.e., van der Waals interactions, between CYP3A4 and the 5H-dibenzo[b,f]azepine ring system of CBZ. Mutation S119A was selected as a negative control, devised to disrupt the structural stability of the productive binding mode by eliminating the hydrogen bond between the carbonyl oxygen of CBZ and the Ser119 side-chain hydroxyl group. Ile301, Ala305, and Gly306 were not considered for mutation since an increase in the side-chain volume was assumed to introduce steric clashes and thus obstruct the binding mode. Ile120 was on the side opposite to the 5H-dibenzo[b,f]azepine moiety and too close to the hydrogen bond with Ser119 to be considered for mutation.

Table 8: Mean distance of center of mass (COM) for the respective residues to the COM of carbamazepine in the largest cluster.*

residue	mean	residue	mean
Arg105	8.97	Ala297	12.72
Arg106	14.09	Gln298	12.1
Pro107	14.41	Ser299	13.19
Phe108	9.46	Ile300	11.47
Gly109	14.28	Ile301	6.85
Phe110	16.28	Phe302	9.95
Val111	12.12	Ile303	11.43
Gly112	15.41	Phe304	6.01
Phe113	15.19	Ala305	5.45
Met114	10.86	Gly306	9.15
Ile118	9.82	Tyr307	11.96
Ser119	5.83	Glu308	8.28
Ile120	8.5	Thr309	7.85
Ala121	11.79	Leu366	20.52
Leu210	10.36	Phe367	16.9
Leu211	11.05	Pro368	13.16
Arg212	6.38	Ile369	8.01
Phe213	8.81	Ala370	8.74
Asp214	13.47	Met371	12.88
Phe215	13.62	Arg372	14.33
Leu221	20.75	Leu373	11.59
Ser222	22.02	Leu479	21.44
Ile223	18.59	Gly480	16.69
Thr224	19.09	Gly481	13.45
Val225	23.88	Leu482	10.76
Phe226	25.67	Leu483	13.48
Pro227	23.87	Gln484	14.24
Phe228	27.1	Pro485	17.97

*Based on the binding mode, the decision was made to investigate an increase of hydrophobic contacts without introducing either steric clashes or changing the biochemical property of the residue (e.g. a change of polarity). Thus, only Ala370 and Ile369 were left for consideration since other residues were either too close to CBZ or already large enough in terms of VdW size of the side chain.

4.3.4 ENZYME PRODUCTION, PURIFICATION, AND RECONSTITUTION

Based on the results of the MD simulations, we elected to probe the effect of the mutations S119A, I369L, I369F, A370L, and A370V on the metabolism of CBZ by CYP3A4. Expression of all five constructs in *E. coli* provided stable P450 holoproteins, in good agreement with earlier reports on the expression and purification of the mutants S119A (*41*), A370V (*168*), and I369F

(*169*). The expression yields obtained with the mutants were generally somewhat lower than the yield of wild-type CYP3A4.

4.3.5 EFFECT OF MUTATIONS ON CYP3A4-DEPENDENT EPOXIDATION OF CBZ

For most mutants, we obtained linear profiles for the increase in the product concentration in the time ranges longer than 20 min. The S119A and I369F mutants were exceptions because the product formation was linearly dependent on time for only ca. 15 min (Figure 33). Consequently, the incubations with wild-type CYP3A4, the I369L and the A370V/L variants were carried out for 20 min and for 15 min with the S119A and the I369F mutants.

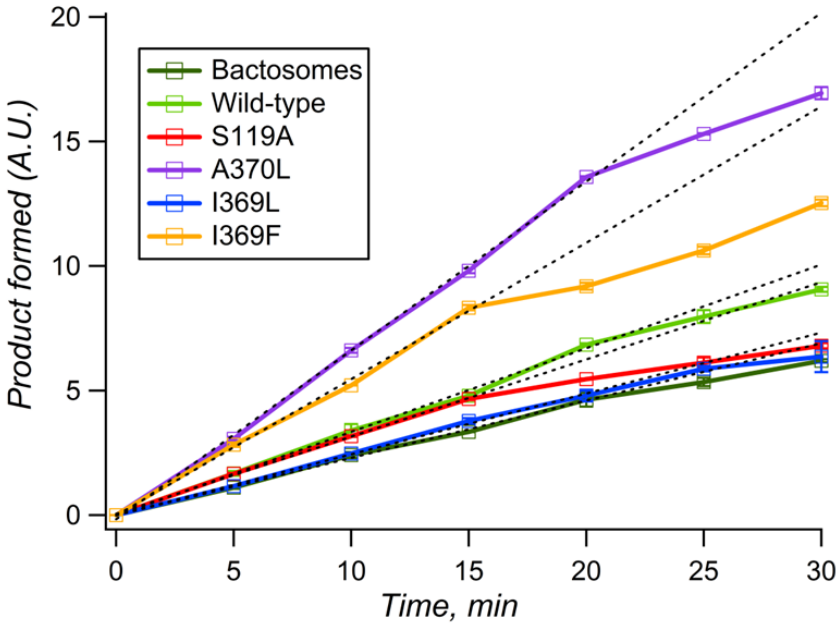

Figure 33: Formation of carbamazepine-10,11-epoxide by CYP3A4-containing Bactosomes, purified wild-type, and purified mutants of CYP3A4. The graph shows the total product formation within 30 min. The black dotted lines represent linear extrapolations of the initial slopes from the first 20 min of incubation (first 15 min in the case of the S119A and the I369F mutants).

In initial experiments, we assessed the turnover rate of CBZ epoxidation in the reconstituted system with the purified mutants and the wild-type CYP3A4 (rCYP3A4) at apparent subsaturating (0.1 mM) and saturating (1 mM) substrate concentrations (Figure 34, Table 9). When measured at subsaturating substrate concentration, the activities of the A370V and I369L mutants were essentially similar to that of the wild type, whereas a substantial increase in activity was observed with the I369F mutant and a substantial decrease was observed with the A370L mutant. The S119A

substitution, which was devised to abolish the putative hydrogen bond to the CBZ carbonyl oxygen, caused the most pronounced decrease in enzyme activity at subsaturating substrate concentration. However, at saturating CBZ concentration (1 mM), the activity of the S119A mutant became similar to that of the wild type and approximately two-fold the activity of the I369L variant. The A370V mutant exhibited the highest activity, and the activities of the A370L and I369F mutants were also higher than that of the wild type.

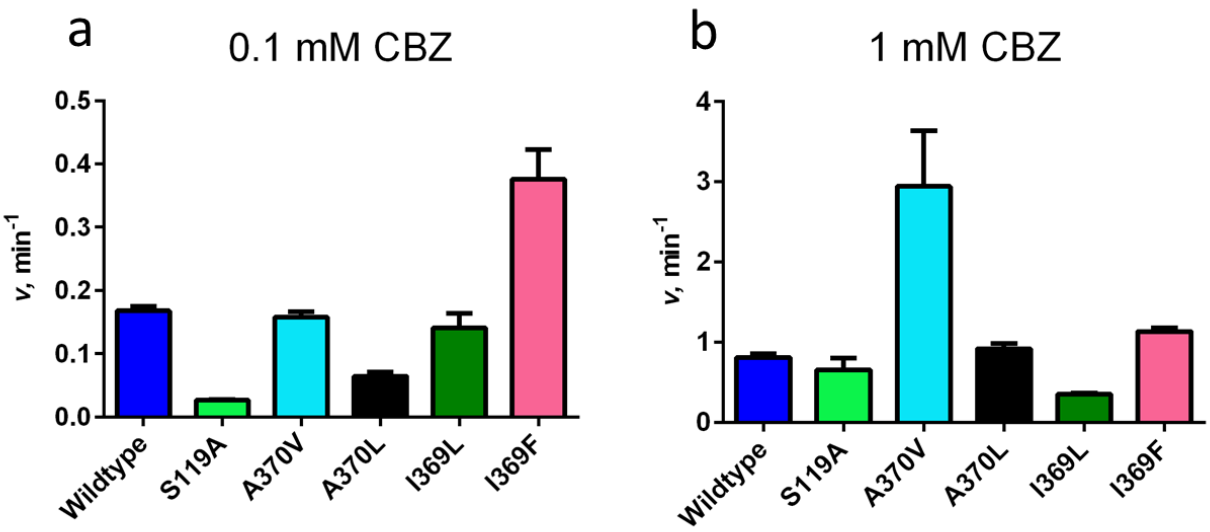

Figure 34: Turnover rates of CBZ epoxidation by purified CYP3A4 wild type and mutants measured at CBZ concentrations of 0.1 (a) and 1 mM (b). The columns represent the means of three individual measurements and the error bars represent the respective standard deviations.

Table 9: Turnover of CBZ by rCYP3A4 wild type and mutants*.

Enzyme		Wild type	S119A	A370V	A370L	I369L	I369F
100 µM	***v***	0.17 ± 0.02	0.027 ± 0.001	0.16 ± 0.02	0.07± 0.01	0.14 ± 0.06	0.4 ± 0.1
	(%)	(100%)	(16%)	(94%)	(39%)	(84%)	(224%)
1 mM	***v***	0.8 ± 0.1	0.7 ± 0.4	3 ± 2	0.9 ± 0.2	0.35 ± 0.04	1.1 ± 0.1
	(%)	(100%)	(81%)	(362%)	(113%)	(43%)	(140%)

*The values given in the table represent the means of three individual measurements, and the "±" values show the respective confidence interval calculated for $p = 0.05$.

To analyze the effects of these substitutions in more detail, we evaluated full kinetic profiles of the wild-type enzyme and the mutants in the reconstituted system, increasing the range of CBZ concentration studied up to 2 mM (Figure 35).

Although the overall quality of the fit (dashed line) of the substrate titration curves obtained with the wild-type CYP3A4 to the Hill equation (h = 2.0 ± 0.9, S_{50} = 300 ± 100 µM and k_{cat} = 1.0 ± 0.3 min^{-1}) appears acceptable (ρ^2 = 0.957), systematic deviations of the experimental points (Figure 35a, circles) suggest the presence of substrate inhibition at higher concentrations, similar to that observed with the CYP3A4-containing Bactosomes. While for the I369F and I369L mutants substrate inhibition is much more evident than in the wild type (Figure 35a), S119A, A370V, and A370L mutants show no visible signs of substrate inhibition (Figure 35b). In contrast, the S-shaped kinetic profiles obtained with these mutants are indicative of a high degree of cooperativity.

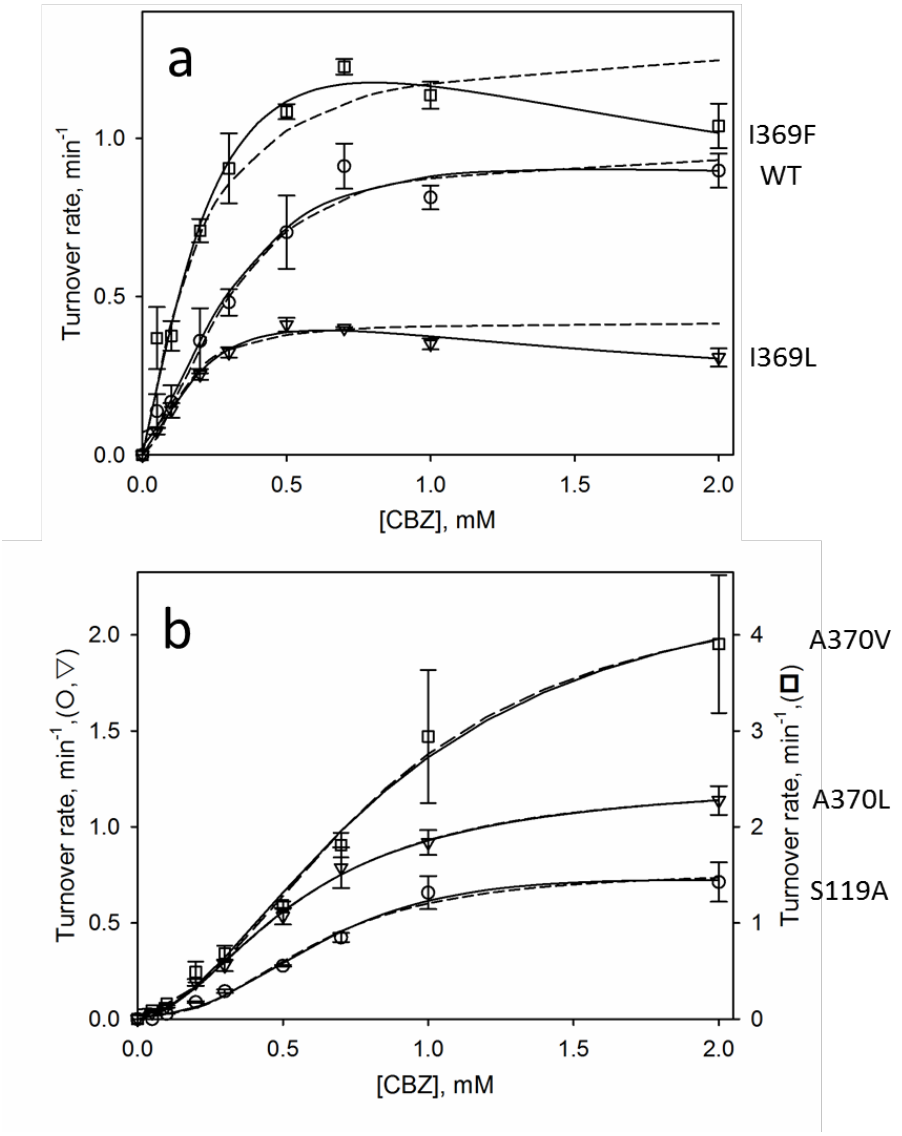

Figure 35: Substrate dependence of the carbamazepine-10,11 epoxide formation rate catalyzed by purified CYP3A4 and its mutants in the reconstituted system. Incubations were carried out with 0.5 µM CYP3A4. Data points represent the mean values of three individual measurements and the error bars show the respective standard deviations. Fits to the Hill equation (dashed line) and to Eq. 4.2 (solid line) are shown. Panel (a) shows the plots obtained with the wild-type enzyme (circles) and the I369F (squares) and I369L (triangles) mutants; panel (b) shows the data obtained with the mutants S119A (circles), A370V (squares), and A370L (triangles).

Table 10: Parameters of CYP3A4-dependent epoxidation of carbamazepine*

System	Hill equation[a]			
	k_{cat}, min^{-1}	S_{50}, mM	*h*	ρ^2
Bactosomes	1.9 ± 0.3	0.16 ± 0.04	1.4 ± 0.4	0.979
rCYP3A4 WT	0.9 ± 0.3	0.3 ± 0.1	2.0 ± 0.9	0.957
rCYP3A4 I369L	0.42 ± 0.06	0.14 ± 0.02	1.80 ± 0.10	0.884
rCYP3A4 I369F	1.4 ± 0.2	0.20 ±0.07	1.3 ± 0.5	0.932
rCYP3A4 S119A	0.8 ± 0.1	0.61 ±0.07	2.5 ± 0.4	0.985
rCYP3A4 A370V	5 ± 1	1.0 ±0.3	2.1 ± 0.9	0.991
rCYP3A4 A370L	1.3 ± 0.4	0.6 ±0.3	2.0 ± 0.6	0.993

System	Hill equation complemented with substrate inhibition (Eq. 4.2)					
	k_{cat}, min^{-1}	S_{50}, mM	*h*	K_i, mM	α	ρ^2
Bactosomes	2.9 ± 0.7	0.3 ± 0.2	1.06 ± 0.08	1.3± 0.8	0.3 ± 0.3	0.991
rCYP3A4 WT	1.4 ± 0.4	0.50 ± 0.04	1.4 ± 0.4	0.79 ± 0.04	0.6 ± 0.5	0.964
rCYP3A4 I369L	0.8 ± 0.4	0.3 ± 0.2	1.4 ± 0.3	1.1 ± 0.5	0.2 ± 0.1	0.989
rCYP3A4 I369F	3 ± 1	0.6 ± 0.4	1.2 ± 0.3	1.1 ± 0.6	0.2 ± 0.4	0.971
rCYP3A4 S119A	1.2 ± 0.1	0.94 ± 0.08	2.1 ± 0.3	1.0 ± 0.2	0.5 ± 0.1	0.990
rCYP3A4 A370V	4.6 ± 0.9	1.1 ± 0.3	1.9 ± 0.6	5 ± 8	0.96 ± 0.07	0.991
rCYP3A4 A370L	1.2 ± 0.2	0.77 ± 0.07	1.7 ± 0.2	5 ± 9	1.4 ± 0.7	0.993

*The values given in the table represent the averages of 3 individual measurements, and the "±" values show the confidence intervals calculated for $p = 0.05$. [a] In the cases with clearly pronounced substrate inhibition (CYP3A4 bactosomes, reconstituted systems with I369L and I369F mutants), the fitting to the conventional form of the Hill equation was performed with the data subsets corresponding to the CBZ concentration range of 0 – 1 mM. The square correlation coefficients given in the table correspond to the fitting to the entire CBZ concentration range (0 – 2 mM) in all cases.

To justify the apparent combination of positive cooperativity and substrate inhibition mechanisms observed in the mutants, we approximated the experimental data with an equation that combines the Hill formalism with an allowance for substrate inhibition:

$$V = \frac{k_{cat} \cdot [E]_0 \cdot [S]^h \cdot (\alpha \cdot [S] + K_I)}{S_{50}^h \cdot K_I + [S]^h \cdot (K_I + [S])} \qquad (4.2)$$

The derivation of Eq. 4.2 is described in the methods section (see Chapter 2.2.5, p. 54). The S_{50} term in Eq. 4.2 is defined in a way similar to the definition in the regular Hill equation, as the *h*-th root of the apparent dissociation constant of the catalytically competent enzyme-substrate complex. In the case where $h = 1$, Eq. 4.2 reduces to Eq. 4.1, and S_{50} is equivalent to K_M.

The fits of Eq. 4.2 to the data are shown in Figure 35 (solid lines), and the respective parameters are summarized in Table 10. Eq. 4.2 clearly provides a better model for fitting datasets obtained with the wild-type enzymes, whether in the form of Bactosomes or in reconstituted systems, and with the I369L and I369F mutants. For the data obtained with the A370L and A370V mutants, the fit to Eq. 4.2 is as good as to Eq. 4.1. The values obtained for the parameter α with the A370L and A370V mutants are close to unity, which suggests that the binding of additional substrate molecules does not affect the activity of these enzymes. Hence, we conclude that substrate inhibition is completely abolished in these mutants.

The analysis of the kinetic parameters suggests that, over the five mutants probed in this study, only the I369F and especially the A370V substitution cause considerable increases in enzyme turnover with CBZ compared to wild type (Table 10). In the case of I369F, the increase in the k_{cat} value is attenuated by enhanced substrate inhibition caused by a decrease in the fraction of activity retained in the inhibitory complex (α). However, for the A370V mutant, where substrate inhibition is eliminated, the increase in the CBZ turnover is substantial Figure 35b, Table 10).

Clearly pronounced positive cooperativity in CBZ metabolism observed with the mutants A370V, A370L, and S119A suggests that the formation of the catalytically competent complex with CBZ in these mutants requires the binding of at least 2 substrate molecules per molecule of the enzyme. At the same time, in contrast to A370V and A370L, where substrate inhibition is eliminated, the fit of the data obtained with S119A to Eq. 4.2 indicates that the metabolism of CBZ by this mutant is characterized by a combination of a prominent positive cooperativity ($h = 2.1 \pm 0.3$) with a moderate degree of substrate inhibition ($\alpha = 0.5 \pm 0.1$). It further suggests that the mechanism of interactions with CBZ involves at least three separate substrate binding events.

4.3.6 MD SIMULATIONS OF 2-4 CBZ MOLECULES IN CYP3A4 BINDING POCKET

Based on the analysis of the kinetic profiles for CBZ metabolism, we concluded that changes in CBZ metabolism caused by the mutations at positions 369, 370, and 119 cannot be accurately described by simulations with a single CBZ molecule bound. Therefore, we conducted MD simulations with two, three, or four CBZ molecules positioned in the CYP3A4 binding pocket. Five MD simulations each with two copies of CBZ in the active site were performed with CYP3A4 wild type, I369F, and A370V. Cluster analyses yielded non-identical largest clusters for both mutants and wild type. The simulation times of 0.2 µs per MD run – equal to a total sampling time of 1 µs for each of the three CYP3A4 variants – were intended to achieve convergent data. Importantly, similar to the single-CBZ simulations, the obtained clusters stem mainly from only one of the five runs, which is indicative of a lack of convergence. The largest clusters for each of the wild type, A370V, and I369F variants are shown in Figure 36. For the A370V mutant only (Figure 36b) is the binding mode, i.e., the position and orientation, of the CBZ closest to the heme essentially identical to that of the most populated cluster in the single-CBZ wild-type run with the C10–C11 bond close to the heme iron (Figure 32, cluster #1). Interestingly, the hydrogen bond observed between Ser119 and the carbonyl oxygen of one CBZ molecule is retained in all panels in Figure 36. This lends further evidence that Ser119 plays an important role in substrate binding.

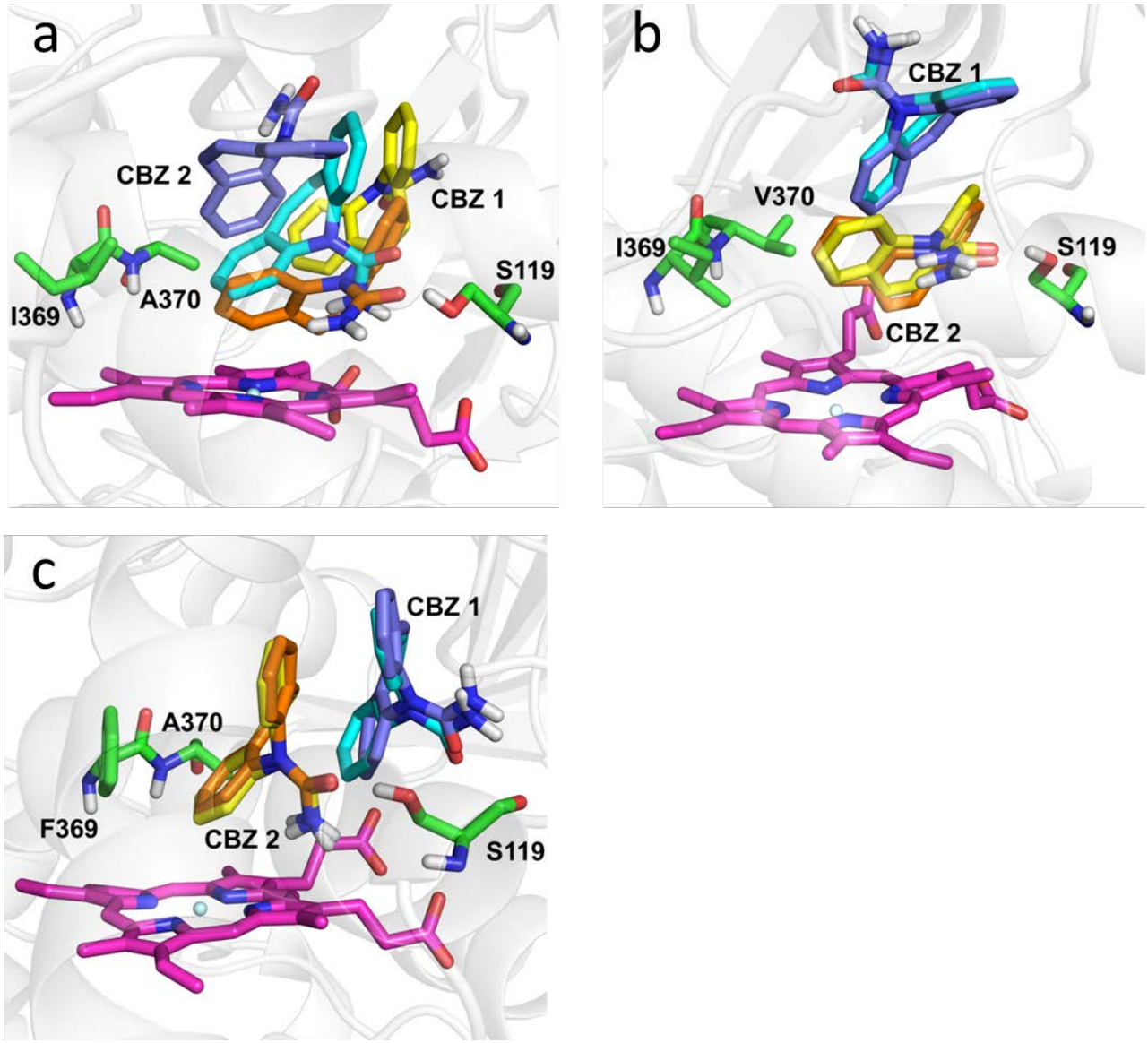

Figure 36: Results of MD simulations with the complex of two molecules of CBZ and wild-type CYP3A4 (a), A370V (b), and I369F (c). Each panel shows two representatives corresponding to the most populated clusters obtained with each of the two CBZ molecules for clustering. Clustering of the non-hydrogen atoms of the CBZ molecules was carried out upon structural alignment of all snapshots of the MD trajectories to the X-ray structure via the Cα atoms of the α-helical residues of CYP3A4. Only in panel (a) are the orientations of the CBZ molecules different depending on which of the two CBZ molecules was subjected to clustering, which indicates that the sampling did not converge. *Data and figure by T.K.*

Partial dissociation of a single CBZ molecule was observed in one of the MD simulations (Figure 37 and Figure 38). Analysis of the unbinding pathway reveals that the CBZ molecule moves to the periphery of CYP3A4 through the F'-helix β-sheet-1 putative substrate binding channel predicted by Williams et al. (*38*). To assess the ability of CYP3A4 to accommodate more than two CBZ molecules, we performed five independent MD runs of 100 ns each with wild-type CYP3A4

plus three or four CBZ molecules (Figure 37). No dissociation events were observed, and the distance of the CBZ molecule furthest from the heme iron was never larger than 18 Å. These results indicate that the CYP3A4 binding pocket is large enough to accommodate up to four CBZ molecules, and that the A370V and I369F mutations considerably affect the mobility of CBZ molecules bound in the binding pocket.

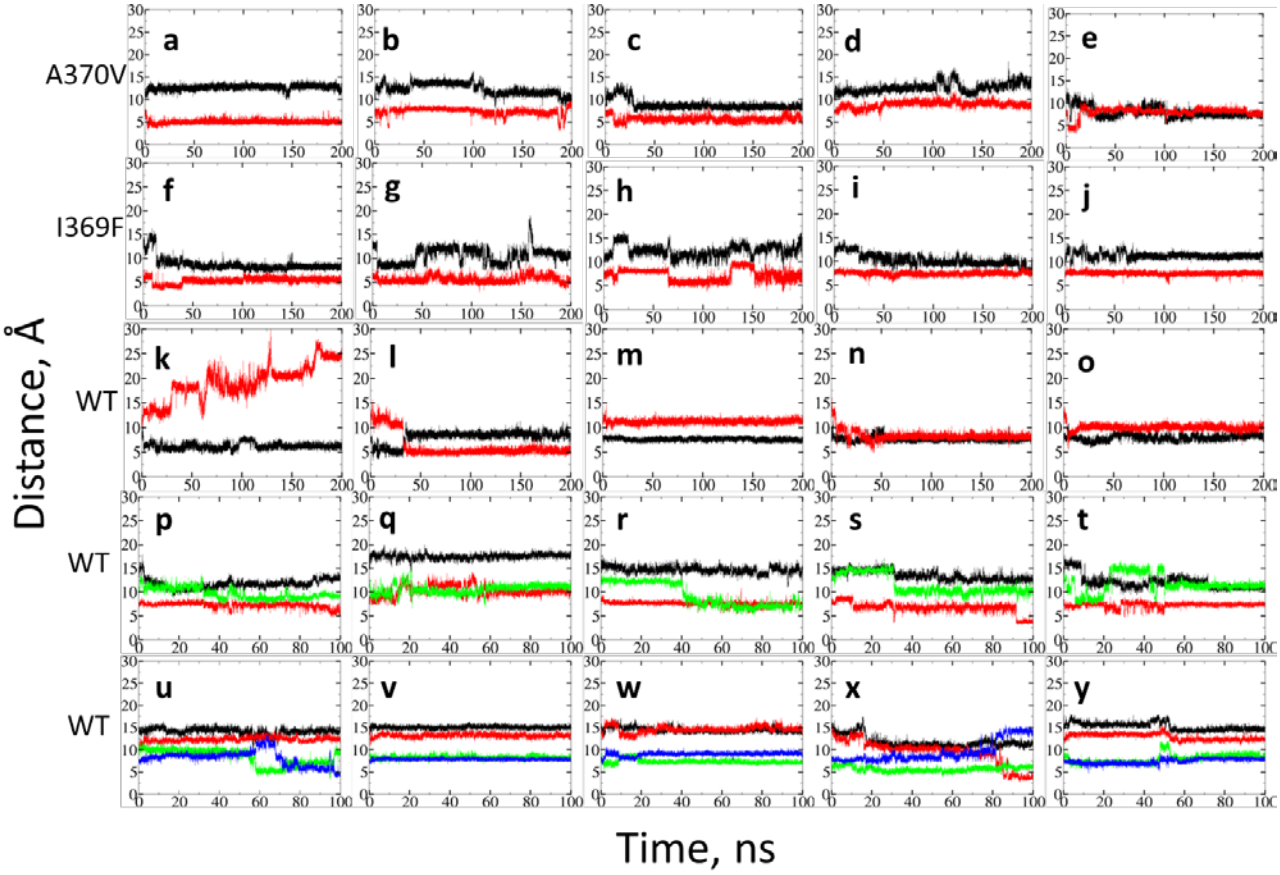

Figure 37: Time series of the distance between the center of the C10-C11 bond in CBZ and the heme iron. Each color corresponds to a single CBZ. Five 200 ns simulations were performed with two CBZs with the A370V mutant (a-e), the I369F mutant (f-j), and the wild-type CYP3A4 (k-o); five 100-ns simulations were performed with the wild type with three (p-t) and four (u-y) CBZ molecules. All figures were generated with xmgrace. No full dissociation event is observed in the MD runs. The largest separation of CBZ from the heme is observed in panel (k) and several snapshots from the corresponding MD run are combined in Figure 38. *Data and figure by T.K.*

4.4 DISCUSSION

This study represents the first attempt to employ MD simulations to suggest CYP3A4 mutants with enhanced activity of epoxidation of carbamazepine combined with subsequent *in vitro* corroboration of the impact of the mutations on kinetics parameters. Our initial studies of the kinetics of CBZ epoxidation by CYP3A4-containing Bactosomes reveal pronounced substrate inhibition. This leads us to suggest that the apparent positive cooperativity reported in earlier studies of CBZ metabolism might be due to the limited range of substrate concentrations examined. We demonstrate that the kinetic profiles obtained with bactosomes adequately approximate the Michaelis equation complemented with an allowance for partial substrate inhibition (Eq. 4.1). The complex of CYP3A4 with one substrate molecule bound in the substrate binding pocket (Figure 31) may be taken as an adequate model of the catalytically competent complex.

In the MD simulations performed with a single CBZ molecule, the most populated cluster displays a productive CBZ binding mode compatible with substrate epoxidation. The distance between the COM of CBZ carbon atoms 10 and 11 to the heme iron is less than 5 Å. On the basis of the analysis of the structure in this cluster, we identified mutants I369L, I369F, A370V, and A370L that could lead to improved steric complementarity *via* Van der Waals interactions of the enzyme with the three-ring system of CBZ. The S119A mutation was devised to abolish the hydrogen bond to the carboxyl function of CBZ to decrease the stability of the binding mode and, thus, the overall binding affinity.

Although the approach based on MD-simulations with one CBZ molecule was successful in constructing mutants with a considerable increase in maximal CBZ turnover rate (in the case of the I369F and A370V mutants), our examination of the kinetic profiles of CBZ metabolism with the full series of our mutants reveals certain limitations of this simplified model. We demonstrate that the best approximation of the kinetic profiles obtained *in vitro* with the wild type or the mutants is obtained by means of a model that combines the positive cooperativity mechanism with an allowance for partial substrate inhibition (Eq. 4.2). According to our analysis with this model, the cooperativity exhibited by the wild type and with the I369L and I369F mutants is only marginal, but is clearly pronounced ($h \approx 1.7 – 2.1$) in the S119A, A370V, and A370L mutants. On the other hand, substrate inhibition is quite modest in the wild type and the S119A mutant ($\alpha \approx 0.5$) and eliminated in the A370V and A370L mutants ($\alpha \approx 1$), but is considerably enhanced in the I369L and I369F mutants ($\alpha \approx 0.2$). This complex mix of positive cooperativity and substrate inhibition in CBZ metabolism is consistent with the results of Egnell and co-workers (*51*), who compared the kinetic profiles for CBZ epoxidation by HLM to those obtained with purified CYP3A4 in a reconstituted

system. They demonstrated that, although data obtained with HLM are consistent with a two-site model where binding of the first CBZ molecule increases the enzyme affinity for binding of a second substrate molecule, the reconstituted system instead exhibits substrate inhibition (*51*).

On the basis of our findings, we suggest that the CYP3A4-CBZ interaction is best explained with a model that involves binding of three or more CBZ molecules in the active site. MD simulations of the complex of CYP3A4 with two to four CBZ molecules provide strong support for this suggestion; no complete egress of substrate was observed in five MD simulations involving three or four CBZ molecules bound to CYP3A4. In the simulations of two molecules of CBZ bound to the CYP3A4 wild-type enzyme or the I369F or A370V mutants (Figure 36), the most populated binding mode of the single-copy simulations of CBZ was observed only for A370V: in this case, one of the two CBZ molecules is bound in a putative catalytic pose. The finding that this pose appears to be stabilized by the second CBZ molecule provides a plausible explanation for homotropic cooperativity in CBZ epoxidation. Indeed, the A370V mutant is the only one of the three enzyme variants probed with simulations that exhibits prominent homotropic cooperativity (Figure 35 and Table 10). However, given the limited sampling in the simulations, we caution that this observation may be coincidental.

In the 15 simulations – 5 simulations each with wild type, A370V, and I369F – of 2 CBZ molecules in the active site of CYP3A4, only one partial egress of substrate was observed in the case of wild-type CYP3A4 (Figure 38). We compared the cumulative volume of the dissociation trajectory of the egress of CBZ via the sampled volume of the COM of C10/11 (Figure 38c) to the position of the substrate access channel predicted by Williams et al. on the basis of the x-ray structure (1W0G) of CYP3A4 (*38*). We found that the volumes largely match; hence, our simulation supports the geometry of the substrate- and solvent-accessible binding pocket of CYP3A4 previously proposed.

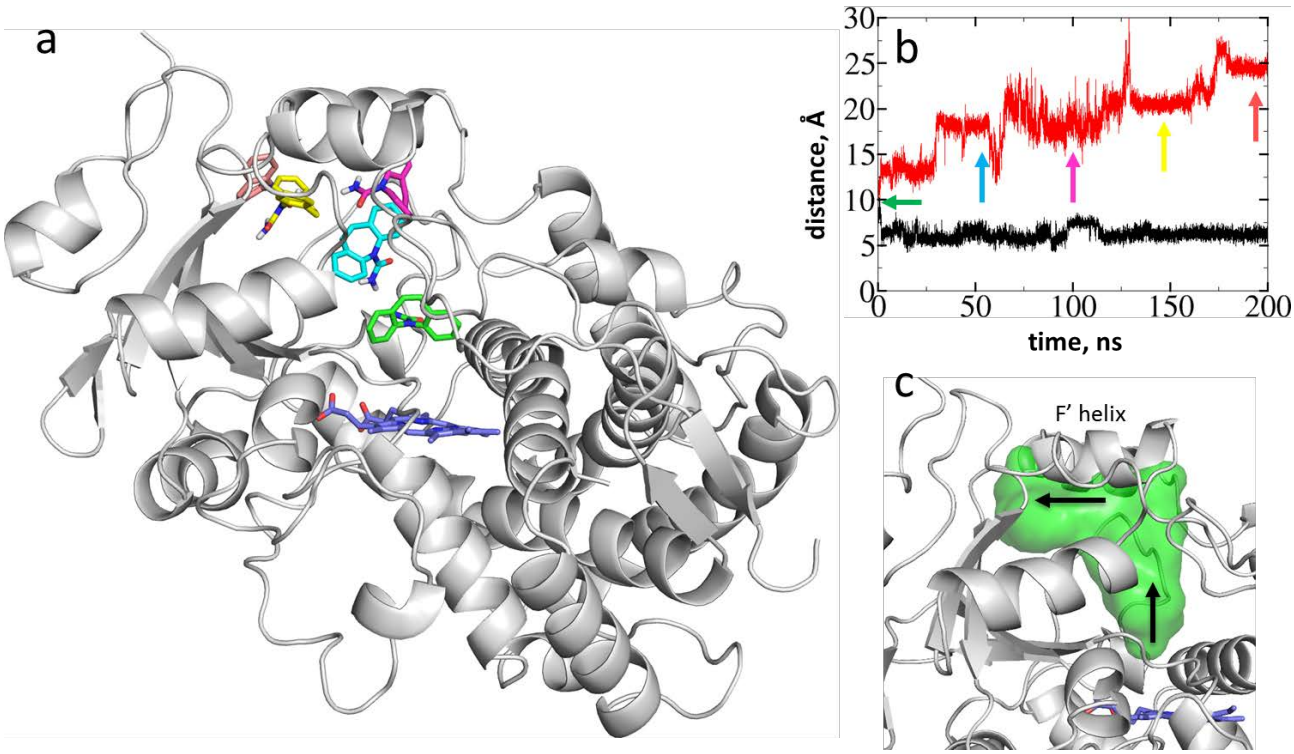

Figure 38: Egress pathway of one of the two bound CBZ molecules from the heme pocket of the wild-type CYP3A4 to a distance > 20 Å from the heme iron. (a) Structure of CYP3A4 showing the positions of the CBZ molecule during its dissociation: The initial position of the CBZ molecule is highlighted in green and the positions after 50 ns, 100 ns, 150 ns, and 200 ns are shown in cyan, magenta, yellow, and maroon, respectively. The second CBZ molecule is not shown. (b) Time series of the COM distance between the CBZ C10-C11 bond and the heme iron. The distance of the bound CBZ molecule is shown in black, whereas the distance of the unbinding CBZ molecule is shown in red with colored arrows indicating the positions on the time axis corresponding to the colored structures shown in panel (*a*). The green arrow indicates the starting position of the molecule. (c) Surface circumscribed by the central nitrogen atom of the dissociating CBZ molecule over the course of a single 200 ns simulation. The protein backbone from the first snapshot of the simulation is shown in white and does not account for changes during the simulation. The arrows indicate the general direction of the movement of the CBZ molecule. *Data and figure by T.K.*

Although a multisite binding mechanism in the mutants is retained, the enzyme is exquisitely sensitive to the minor structural changes in the binding pocket introduced by the point mutations S119A, I369F, I369L, A370L, and A370V. The observation of the hydrogen bond between the CBZ molecule adjacent to the heme and the Ser119 residue (Figure 36) provides a clue to the effects of the S119A substitution (Figure 35). Importantly, this bond is found in the structures of all simulated variants (wild type, A370V, and I369F). The absence of the stabilizing hydrogen bond in the S119A mutant may explain the reduced affinity of this mutant for CBZ. Furthermore, enhancement of homotropic cooperativity in CBZ epoxidation by this mutation reveals an increased role for the binding of a second substrate molecule in stabilizing the catalytically competent complex. These results further support the conclusion that the residue Ser119 plays a key role in substrate binding in CYP3A4 (*11, 40, 45, 62, 168, 170*), in agreement with a recent study in which it was shown that the association of CYP3A4 with ritonavir analogues is strongly facilitated by polar interactions mediated by Ser119, even in cases where the ligand does not engage in hydrogen bonding to this serine (*170*).

Possible effects of the mutations on the structure of CYP3A4 are illustrated in Figure 39, which shows the largest clusters obtained in simulations with two CBZ molecules of the wild type and the I369F and A370V mutants compared to the X-ray crystal structure of CYP3A4 with metyrapone (1W0G) (*38*). The π-π stacking interactions between residues Phe316 and Phe367 found in most X-ray structures are likely to be structurally important. The residues Ile369 and Ala370 reside in the 1.4 K/β-loop (residues 368–372), which connects the α-helix K (shown in violet) with the subsequent β-strand (shown in blue) and adjoins the active site in Van der Waals contact to the α-helix I (shown in green). The structural changes upon substitution of Ile369 by phenylalanine are apparently important for the increased substrate inhibition observed in the I369F mutant (Figure 35, Table 10). The replacement of Ile369 with phenylalanine (or leucine) is likely to affect hydrophobic interactions in the active site and, thereby, promote inhibitory substrate-binding and/or steric or conformational effects. The I369F substitution may reduce the volume of the active site and concomitantly restrict access to the heme (Figure 39c). The bulky phenylalanine residue 369 in the vicinity of the heme is likely to destabilize the association of a water molecule to the iron (III) and may be the source of the observed increase in the proportion of high-spin cytochrome P450 in the substrate-free I369F mutant. The I369F substitution may also reduce the free space between the 1.4 K/β-loop and the I-helix that face each other in the active site. An analysis of the trajectories of Phe304 and residue 369 in the MD simulations (Figure 40) reveals a decrease of the mean distance between the side chains (SC) of these residues (blue dashed line) from $\Delta_{SC(WT)} \approx 11.6$ Å in

the wild type (Figure 39b) to $\Delta_{SC(I369F)} \approx 8.0$ Å in I369F (Figure 39c) averaged over the total simulation. The corresponding distance in the A370V mutant was $\Delta_{SC(A370V)} \approx 13.0$ Å (Figure 39d).

The formation of a kink in the helix near the Phe304 residue indicated with a black arrow in Figure 39*c* may further restrict access to the active site in the I369F mutant (the conformational change was however only seen in one out of five simulations). Furthermore, although not revealed in the simulations, a direct interaction of the I369F phenylalanine with residue F304 may be possible and contribute to the changes in the kinetics observed with this mutant. In the I369L mutant, the side-chain γ-methyl groups of leucine may more closely interact with the T309 side chain to move the K/β -loop and to induce a similar conformational change in the I-helix as seen in the simulation of the I369F mutant. A direct effect of the leucine on the accessibility to the heme may also be plausible.

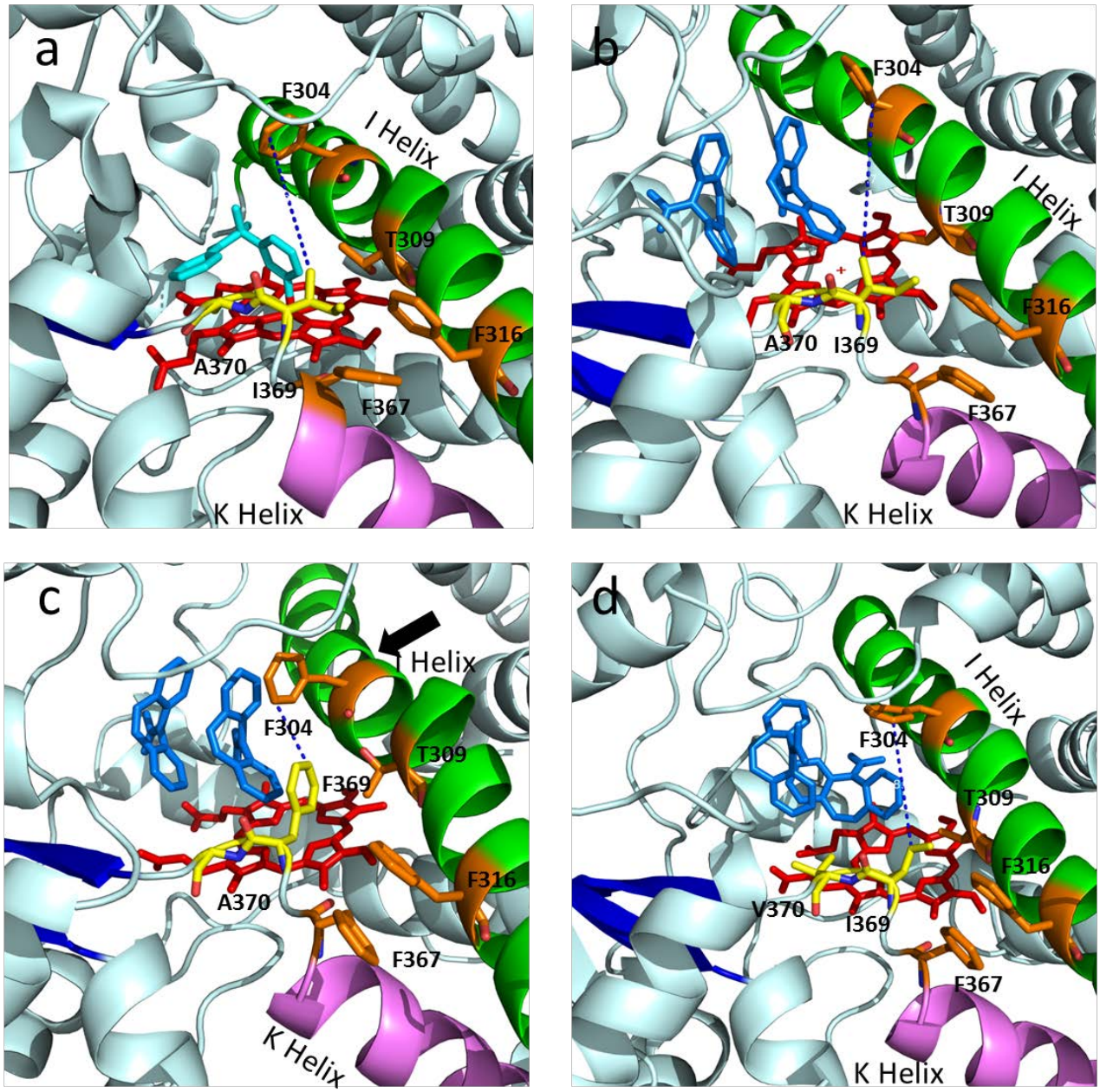

Figure 39: Comparison of the X-ray structure 1W0G with the simulated structure (cluster representatives). (*a*) The active site of CYP3A4 structure 1W0G with metyrapone (light blue) bound (*38*). Panels (*b-d*) show cluster representatives of MD simulations of CYP3A4 (*b*) wild type and the (*c*) I369F and (*d*) A370V mutants with two CBZ molecules (marine blue). Residues Phe316 and Phe367 shown in orange apparently engage in π-π stacking interactions. The K-β-(1.4) loop consisting of residues 368–372 (PIAMR) that joins the K-helix (violet) to the sequential β-sheet (blue) makes Van der Waals contacts with the long I-helix (green). Mutated residues are shown in yellow. Note in panel (*c*) that the bulky phenylalanine in the I369F mutant projects into the active site to reduce accessibility of the heme. Over the length of one simulation of the I369F mutant, the I-helix exhibits a kink (black arrow) around residue Phe304 and additionally constricts the access to the active site due to a dramatic decrease in the distance between the side chains of F304 and residue 369 (blue dashes). *Data by T.K., figure by C.M.*

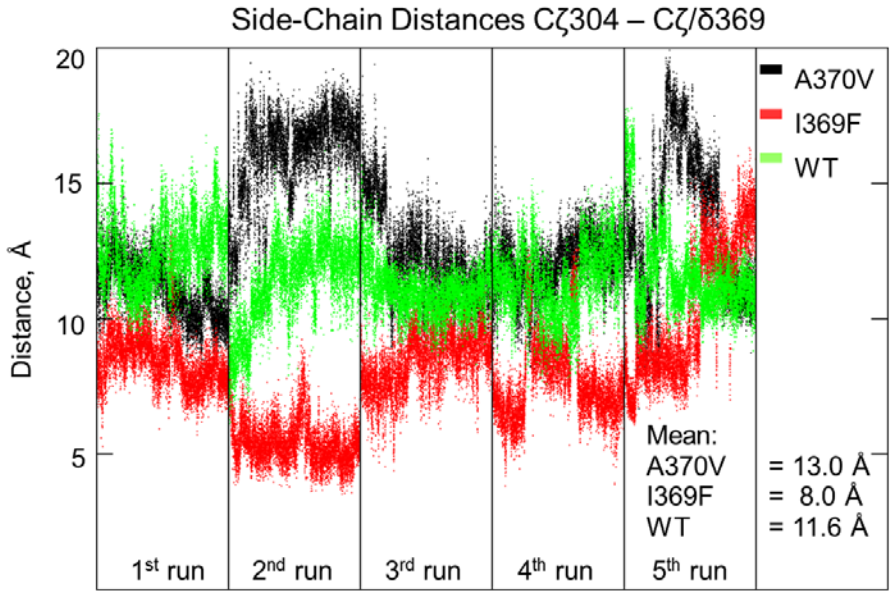

Figure 40: Time-series of distances between the ends of the side chains of residues 369 and Phe304 of the five simulations with complexes of two CBZ molecules with the wild type (light green) and the mutants A370V (black) and I369F (red). The data stems from the analysis of the simulations that are also the matter of Figure 37 (a-o). *Data and figure by T.K.*

Stabilization of substrate binding by the additional phenylalanine residue near the heme moiety in the I369F mutant *via* stacking interactions of the aromatic rings may contribute to the high rate of CBZ turnover observed with this mutant at low CBZ concentrations (Table 9). At higher CBZ concentrations, stacking of several CBZ molecules above the heme may prevent dissociation of product and be responsible for the observed substrate inhibition (Table 10).

Elimination of substrate inhibition in the mutants A370V and A370L (Figure 35, Table 10) is associated with a significant increase in the S_{50} value for these mutants compared to the wild type. The decreased affinity for CBZ provides further support for the importance of the K/β loop region for CBZ binding. It seems plausible that the steric clashes between the larger aliphatic side chains of the valine and leucine of these mutants and the metabolized or stabilizing CBZ molecule may disfavor substrate stacking, which is hypothesized to be a potential reason for substrate inhibition. The observation that the mutants with higher affinity for CBZ display more pronounced substrate inhibition provides additional support for the above hypothesis that the mechanism of substrate inhibition is based on binding of additional CBZ molecules that impede egress of product. In contrast, the finding that the mutants with lower affinity for CBZ exhibit homotropic cooperativity is consistent with the stabilization of the catalytically competent enzyme-substrate complex upon binding of a second CBZ. Whether these correlations are specific to metabolism of CBZ or represent a general characteristic of CYP3A4-catalyzed reactions requires further experimentation.

Determination of crystal structures of the CYP3A4 variants investigated in this study, such as I369F and S119A, is expected to yield important insights regarding the relevance of structural aspects to mechanisms of substrate inhibition and homotropic cooperativity in CYP3A4. In spite of the structural plasticity of CYP3A4 (*45, 48*), we have been able to use MD simulations to identify plausible productive and non-productive binding modes for one or more substrate molecules in the substrate binding pocket of the enzyme. In particular, the combination of MD simulations and pose clustering to guide site-directed mutagenesis has resulted in the generation of enzyme variants that exhibit altered functional properties, such as homotropic cooperativity, substrate inhibition, and substrate affinities *in vitro*. This approach may prove to be generally applicable to other enzyme-substrate pairs as a means to probe binding interactions and mechanisms and modulate functionality.

5 BROMOCRIPTINE AND ERYTHROMYCIN REVEAL INVERSE TYPE-I TRANSITION IN CYP3A4 S119A

5.1 ABSTRACT

The presence of a water network in the binding pocket of cytochromes P450 stabilized *via* polar interactions is crucial for the proper function of the enzyme. Failure in maintaining the regulation of reactivity can lead to futile redox cycling and to the generation of the oxidising compounds in the absence of substrates that can harm the enzyme and the surrounding tissue. In the case of type-I substrates, the interactions upon ligand association modulate the spin equilibrium of the enzyme, which is assumed to be a determinant of redox coupling and catalytic efficiency. In cytochrome P450 3A4 (CYP3A4), we suspected that the maintenance of its native water network in the active site relies on polar interactions to hydrophilic amino acid residues lining the active site such as Ser119 and Thr309, which facilitate water access to its hydrophobic binding pocket.

In order to investigate the role of the active site residues S119, I369 and A370 for substrate binding, we exploited the characteristic spectral shift in the Soret band upon binding of the prototypic type-I substrate bromocriptine (BCT), a dopamine agonist and substrate of CYP3A4. We analyzed the spectral changes upon association of BCT to the five CYP3A4 mutants S119A, I369F, I369L, A370V, and A370L, and the wild type. While affinities of several mutants for BCT were considerably altered, S119A exhibited the lowest affinity and a unique inverse type I-shift in a substrate-concentration dependent manner, which is not commonly associated with CYP3A4. The S119A mutant also exhibited a spin equilibrium shifted towards the high-spin state in the absence of substrateas a result of a decreased probability of a water molecule ligating to the heme iron (III) at the distal ligand site. In order to investigate whether the unusual behaviour of the S119A mutant in ligand binding is not an isolated feature that is restricted to binding of BCT, we extended our studies to titrations with the type-I ligand erythromycin (ERY), which confirmed this peculiar inverse spin shift in the S119A mutant. Our data therefore present evidence for the crucial role of Ser119 in both the association of ligands and the native regulation of enzymatic activity *via* stabilization of a water network in the CYP3A4 active site in the absence of substrate.

5.2 INTRODUCTION

Bromocriptine (BCT), an ergot alkaloid and dopamine receptor agonist, is prescribed for the treatment of pituitary tumors, Parkinson disease, type 2 diabetes, hyperprolactinaemia and neuroleptic syndrome. It is a type-I substrate that does not exhibit cooperativity in binding to microsomal or recombinant CYP3A4, but they form a high-affinity complex ($K_D \approx 0.3 - 1$ μM) (*171*). It consists of a lysergic acid part and a cyclic tripeptide, which is important for the specific

interaction with cytochromes P450 of the 3A family. Binding of BCT to CYP3A4 was studied in several publications (*48, 171, 172*) and a crystal structure of the CYP3A4-BCT complex showing a productive binding mode of BCT has been presented recently (*171*). The CYP3A4-BCT interactions were found to be predominantly non-polar (*171*). Extensive Van der Waals interactions were reported between the tripeptide group of BCT and the residues Ile301, Ph304, and Ala305 of the I-helix, as well as residues Arg105, Arg212, Ala370, and Arg372, whereas the lysergic moiety of BCT was sandwiched between the side chains of Arg106 and Phe215 and H-bonded to Thr224. In titration experiments, monitored *via* the spectral transition in the Soret band from 416 nm to 391 nm that accompanies the low- to high-spin shift, the substitution of Thr224 for alanine reduced the affinity for BCT ca. 6-fold (*171*).

In order to investigate the role of the amino acids S119, I369, and A370 in the association of BCT, we performed equilibrium binding titrations with the mutants S119A, I369F, I369L, A370V, and A370L. Whereas the wild type and all mutants except for S119A exhibited a regular type-I spin shift, the latter underwent an inverse (i.e. high to low-spin) shift. In order to study whether this peculiarity of the CYP3A4 S119A mutant is restricted to the association with BCT, we also studied the binding of erythromycin (ERY). ERY is a macrolide antibiotic drug used in the treatment of a number of bacterial infections and it is a substrate of CYP3A4. A structure of the CYP3A4-ERY complex has been presented with the drug in a non-productive configuration (*45*). ERY is known to form inactive protein accumulates with CYP3A4 due to its formation of metabolite complexes (C-nitroso:iron, R-N=O:Fe) (*29*). The structures of BCT and ERY are shown in Figure 41. In this chapter, we report that the CYP3A4 S119A mutant appears to exclusively undergo reverse type-I spin transitions upon binding of non-allosteric substrates, such as ERY and BCT. The abnormal transition in the S119A mutant provides support for the importance of the side chain of Ser119 in the control of redox cycling and enzymatic activity of CYP3A4.

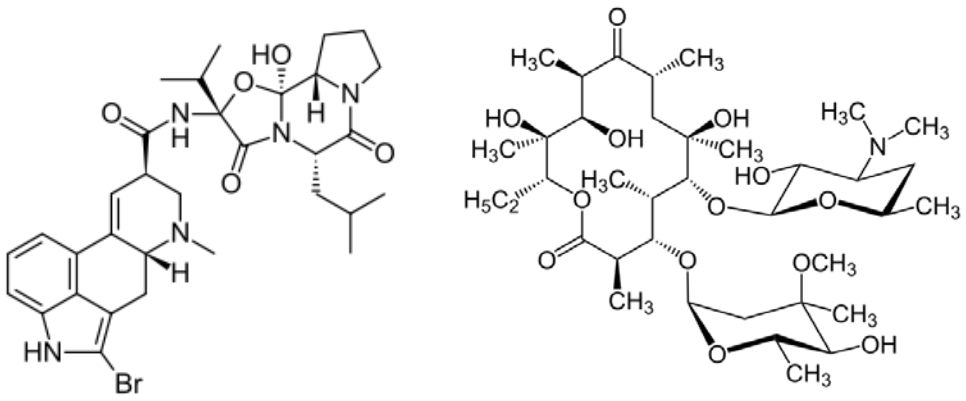

Figure 41: Structures of the two CYP3A4 type-I ligands bromocriptine (BCT) and erythromycin (ERY).

5.3 RESULTS

5.3.1 BROMOCRIPTINE TITRATIONS

The association of BCT to CYP3A4 induced spin shifts that were sufficient to obtain reproducible fitting parameters for CYP3A4 wild type and all tested mutants. The strongest spin shift was obtained in wild-type CYP3A4 (48%) and the least was found for the S119A mutant (24%, Table 11). All recombinantly produced CYP3A4 variants displayed type-I spin shifts as reported for CYP3A4 (*67, 82, 171*), except for S119A, which exhibited an inverse type-I spin-shift (Figure 42 and Figure 43). Titration of the S119A mutant with BCT resulted in an increase in low-spin at the expense of high-spin enzyme. The mutants I369F and I369L exhibited 2.4-fold and 1.5-fold higher affinities to BCT than the wild type, respectively, whereas the affinities of the A370V, A370L, and S119A mutants were decreased by 1.8-fold, 7.0-fold, and 11-fold, respectively. All results of the fits to the data are shown in Table 11.

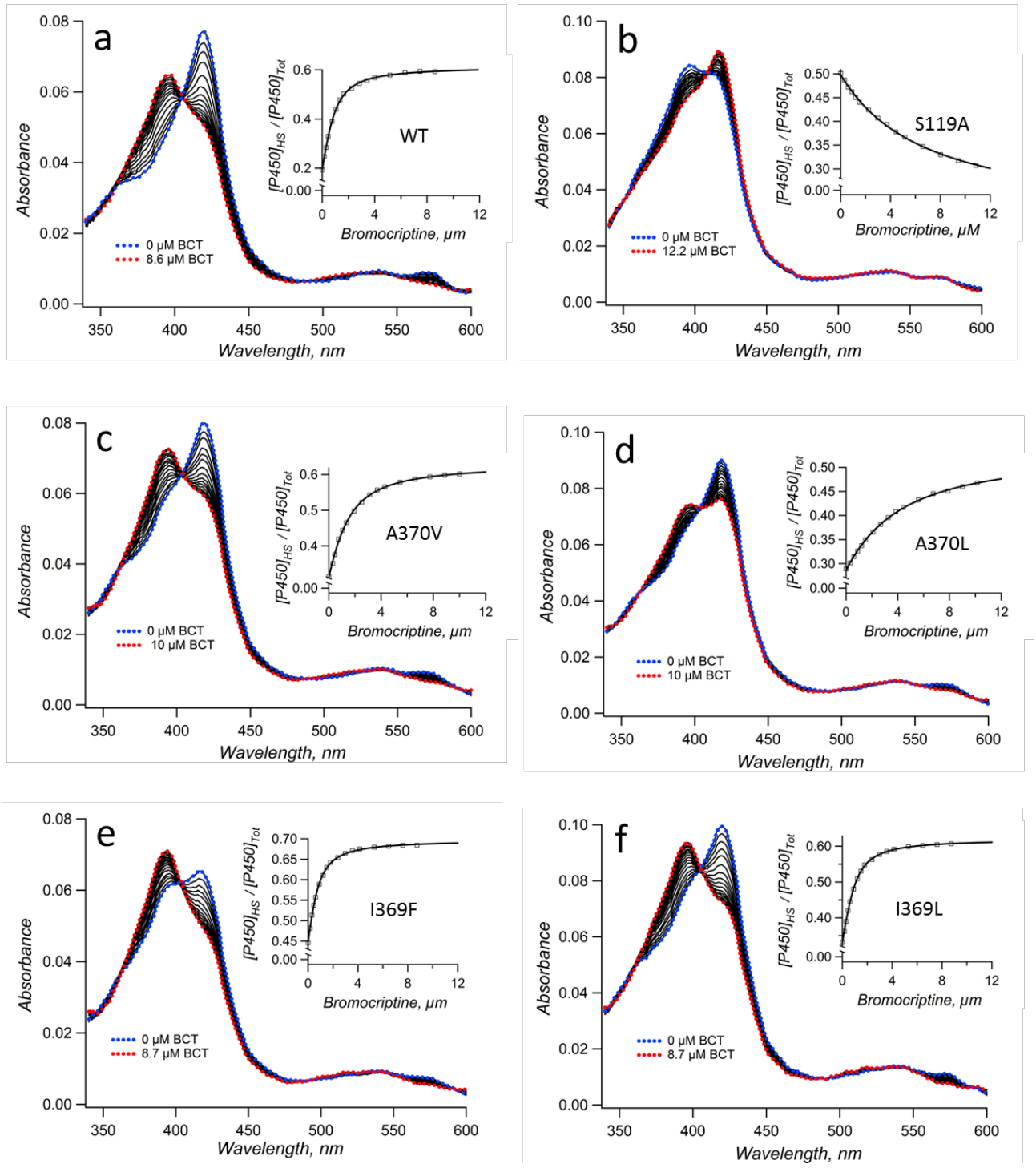

Figure 42: BCT Titrations of (a) purified CYP3A4 wild type, and the mutants S119A (b), A370V (c), A370L (d), I369F (e), and I369L (f) in solution. In the corrected series of absorbance spectra, the initial spectra of BCT-free enzyme are shown with blue dots, titration end-points are shown with red dots. Insets: High-spin fractions are plotted against BCT concentrations; solid lines represent fits to the equation of bimolecular association.

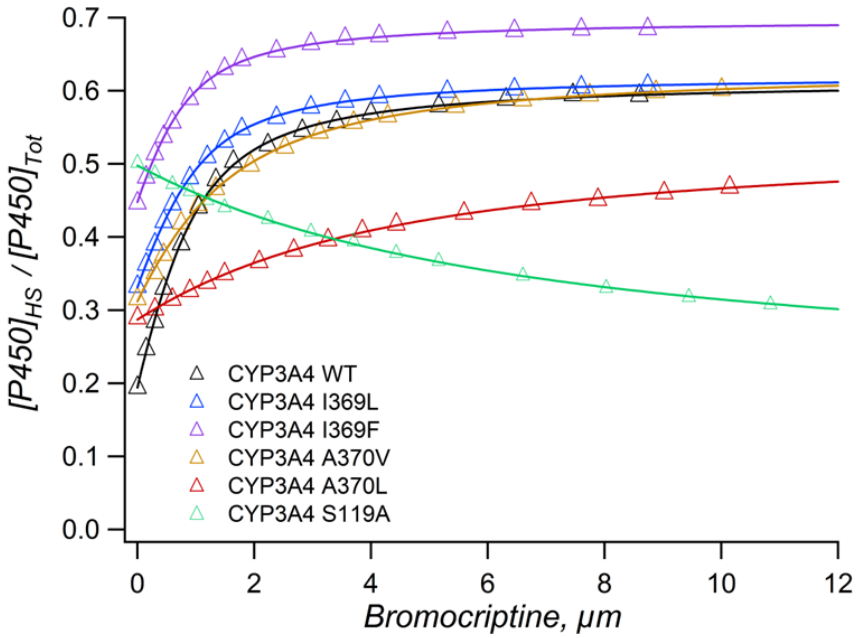

Figure 43: Comparison of all titration curves (black, wild type; blue, I369L; purple, I369F; beige, A370V; red, A370L; green, S119A). The data represents a compilation of the data of Figure 42.

Table 11: Bromocriptine titrations of CYP3A4 wild type and five mutants*.

	Fitting Results		
Mutant	**K_D, µM**	**Spin Shift**	**HS_{Fin}**
WT	0.6 ± 0.2	0.48 ± 0.05	0.62 ± 0.02
S119A	6.3 ± 1.0	-0.24 ± 0.04	0.22 ± 0.07
A370V	1.1 ± 0.4	0.32 ± 0.04	0.65 ± 0.04
A370L	4.2 ± 1.7	0.26 ± 0.07	0.56 ± 0.05
I369F	0.25 ± 0.07	0.25 ± 0.03	0.70 ± 0.02
I369L	0.40 ± 0.15	0.30 ± 0.04	0.63 ± 0.02

*Results for the parameters K_D (affinity constant), total spin shift and (asymptotic) endpoints of the high-spin fractions are shown. Spin shifts are given in fractions of the total cytochrome P450; HS_{Fin} denotes the (theoretic) asymptotic estimation of the proportion of high-spin P450 for BCT-saturated CYP3A4. The values given in the table represent the mean values of triplicates, and the "±" values show the respective confidence interval calculated for $p = 0.05$.

The UV-VIS spectrum recorded at saturating BCT conditions revealed a maximum of the Soret band at 417 nm, a characteristic of low-spin heme iron (III). Consistent with this, the first principal component obtained in the analysis of the titration series (which accounts for the highest variability in the data) exhibited a maximum at ca. 420 nm (Figure 44). In order to confirm that the nature of the spin-shift in S119A is inverse type-I, we investigated the binding of CO to Fe^{2+}-heme.

This revealed no involvement of the inactivated P420 form in BCT titration, as we concluded from the essentially identical levels of [‘P420’] in the absence of substrate and at saturating BCT concentration (20 µM).

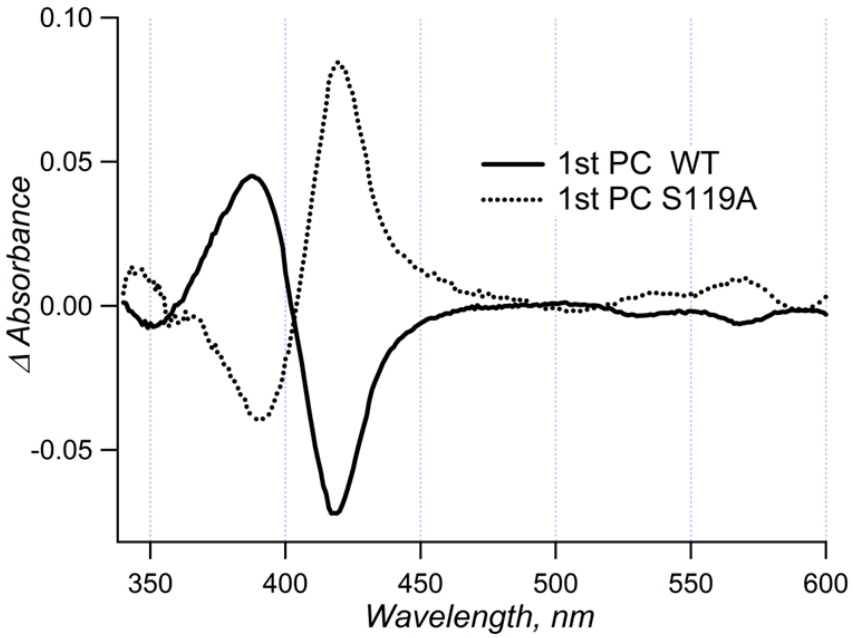

Figure 44: The first principal components, which represent the highest variation in the respective titrations, are shown for CYP3A4 wild type and the S119A mutant.

5.3.2 ERYTHROMCYCIN TITRATIONS

In order to examine whether the inverse type-I binding of the CYP3A4 S119A mutant is restricted to BCT, we explored the transition upon binding of ERY, another ligand that shows no cooperativity in its association to CYP3A4. The results of the titrations of the S119A mutant with ligands that exhibit cooperativity in association or turnover of CYP3A4 are reported in Chapter 6. In the titration with CYP3A4 wild type, ERY did not induce a type-I spin shift, but induced a red-shift of ca. 1 nm (417 nm → 418 nm) in the absorption maximum of the Soret band (Figure 45, panels a/c). This shift was captured and quantified via spectral decomposition with the help of the spectral species that exhibits a Soret band maximum at 424-426 nm. The ‘P420’ spectral standard represents either type-II ligated CYP3A4 or one of the inactivated cytochrome P420 forms of CYP3A4, which are spectrally not distinguishable due to their similar position of the Soret band maximum. The shift in the absorbance maximum was concentration dependent and was fit to the equation of bimolecular association (Eq. 2.14, Figure 45a, c). Similar to BCT, ERY titration

resulted in an inverse spin shift in the S119A mutant (Figure 45b). The extent of total spin shift amounted to (-33 ± 2)%, which exceeds the total apparent type-II transition in the wild type (18 ± 2)% (Table 12). The 1st principal component of the spectral titration series of the S119A mutant exhibited a maximum and a minimum at 389 nm and 421 nm, respectively, and reveals an inverse type-I spin perturbation. The first principal component obtained from the analysis of the wild-type titration data exhibited a maximum at 426 nm (Figure 45d). This supports the findings that the wild type exhibits a red-shift in the Soret band indicating an apparent type-II transition (max = 426 nm). The S119A mutant showed an inverse type-I spin shift (max = 421 nm).

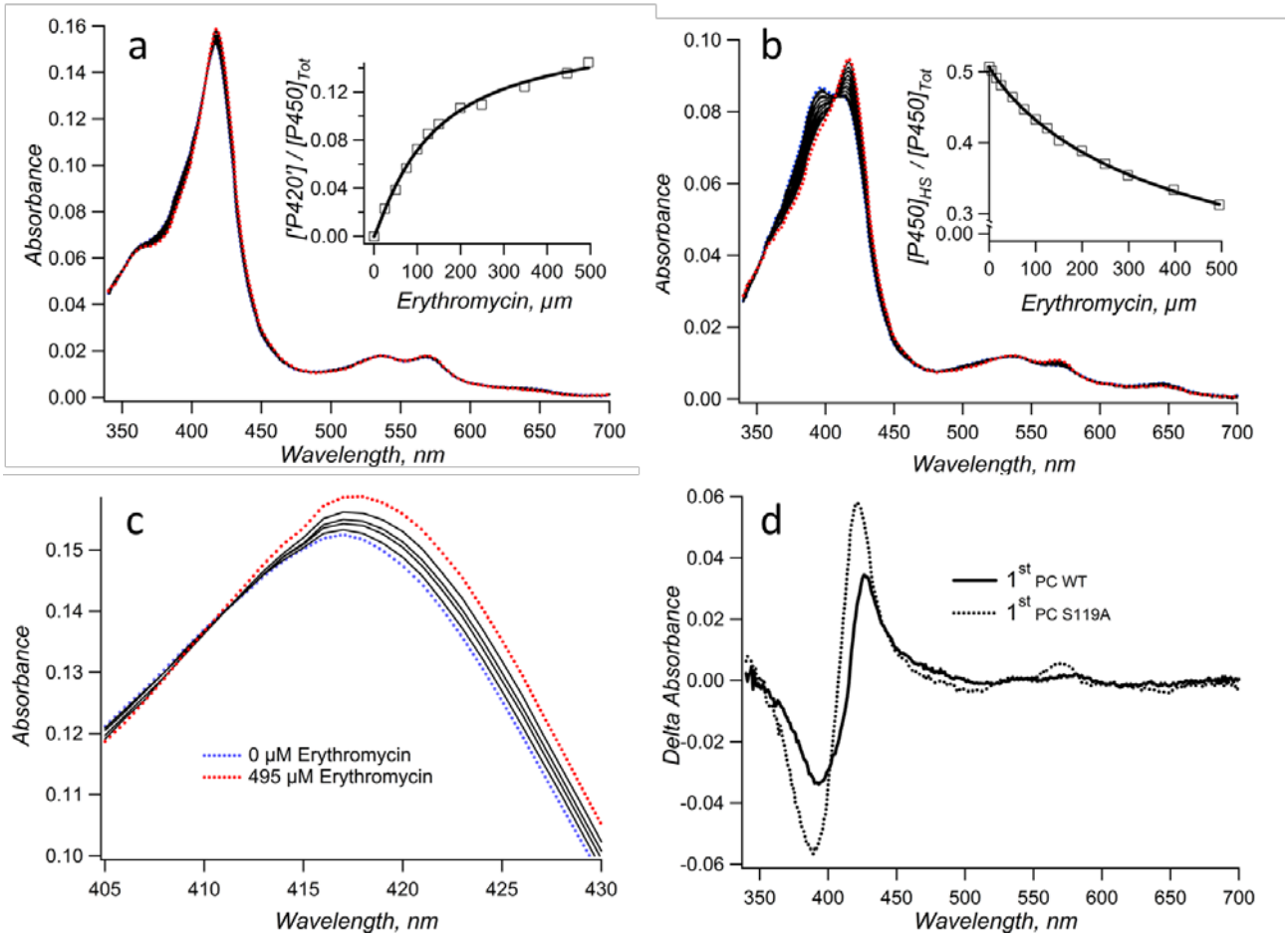

Figure 45: Titrations of CYP3A4 wild type (a) and S119A (b) with erythromycin. In panel (a) and its zoom into the Soret band (c), titration data with wild-type CYP3A4 reveals a spectral red-shift in the absorbance maximum. This was captured in the form of an apparent type-II shift in the analysis. The data for the S119A mutant in panel (b) indicates a pure inverse type-I spin-shift. Insets represent the dependence of the respective spectral species on ERY concentration ($[P450_{HS}]$ / $[P450]_{Tot}$ or ['P420'] / $[P450]_{Tot}$ *vs.* [ERY], respectively). Panel (d) shows the first principal components of the analysis of the two spectral titration series.

Table 12: Fitting parameters for the ERY titrations.*

	Fitting Results		
Mutant	**K_D, μM**	**Spin Shift**	**Endpoint**
WT	$(1.9 \pm 0.7) \cdot 10^3$	0.18 ± 0.02	0.23 ± 0.06[1]
S119A	$(3.5 \cdot \pm 0.3)\ \ 10^3$	-0.33 ± 0.02	0.17 ± 0.02

*Results are presented for the affinity parameter K_D, for the total spin shift in fractions of total cytochrome P450, and the (asymptotic) endpoints of the transition. [1]The values were determined for the analysis with respect to the appearance of the spectral 'P420' species in the case of wild-type CYP3A4 due to absence of type-I transition. Endpoint denotes the (theoretical) asymptotic endpoint proportions of the respective spectral species in ERY-saturated solution. The values given in the table represent the mean values of four measurements and the "±" values show the respective confidence interval calculated for $p = 0.05$.

Table 13: Positions of the maxima and minima of the first principal components that were obtained in the principal component analysis of the spectral titration series (see Figure 42g and Figure 45d).

Substrate	CYP3A4	Max., nm	Min., nm
Bromocriptine	WT	387	417
	S119A	420	389
Erythromycin	WT	426	392
	S119A	421	389

5.4 DISCUSSION

The calculated affinity of BCT for wild-type CYP3A4 (K_D = 0.6 μM) is in accordance with previous reports on the formation of a complex with CYP3A4 (K_D of 0.3 - 1.0 μM) (*171*). The affinities of the generated mutants are between 0.25 μM and 6.1 μM, which corresponds to an overall variation factor of ca. 25. The considerable variation in affinities can be explained on the basis of the X-ray structure of the BCT-CYP3A4 complex shown in Figure 46 (PDB-code 3UA1) (*171*).

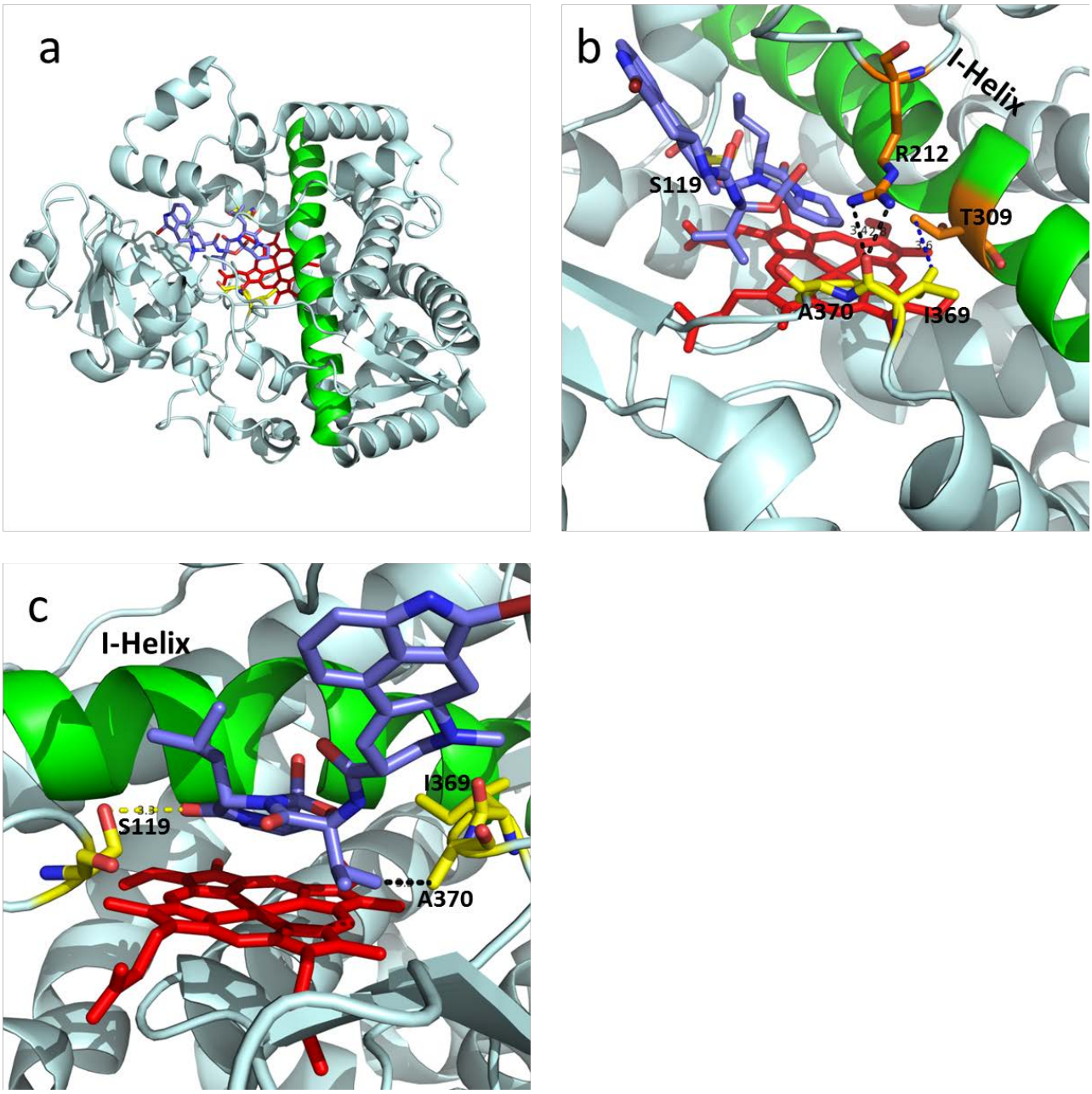

Figure 46: X-ray structure of the binding mode of BCT in a CYP3A4-BCT complex (structure ID 3UA1): Panel (a) displays the entire structure, and panels (b-c) zooms into the active site. Residue Ile369 interacts with Thr309 of the adjacent I-helix through hydrophobic interactions. The side chain of Arg212 projects into the active site and makes possible contacts with the Ile369 backbone carbonyl. Ser119 and Ala370 form a hydrogen bond and engage in hydrophobic interactions with BCT, respectively. BCT is in VdW contact to Ala370 and forms an H-bond to Ser119.

In 3UA1, no direct interactions of Ile369 with BCT can be identified; in fact, the side chain of Ile369 is separated from BCT by > 6 Å. This allows substitution of Ile369 with a residue that comprises a larger hydrophobic side chain and explains why the I369F and I369L substitutions are

both well tolerated. The affinities of these mutants for BCT are both increased, in the case of the I369F mutant ca. 2.5-fold. We concluded from the evaluation of the distance trajectory between the side chains of residue 369 and Phe304 in the respective MD simulations (see chapter 4, Figure 40) that the substituted phenylalanine residue projects further into the active site cavity than Ile369. A possible shift of the I-helix is seen in one of five MD simulations of the 2CBZ-CYP3A4 I369F complex along with direct hydrophobic interactions of Phe369 with the tricyclic peptide of BCT. This shift may allow for a tighter fit of BCT and result in the increased affinity obtained in the equilibrium titrations. Arg212 of the FF'-loop (residues 210-214) and Thr309 of the I-helix are in close contact with Ile369 in the CYP3A4-BCT X-ray structure (side-chain distances $\leq$ 4 Å). The I369L substitution may affect the hydrophobic interactions with the two residues mentioned above and may account for the slight increase in affinity seen in the titrations. Ala370 is in close contact with the valine of the tricyclic tripeptide of BCT ($\Delta_{(BCT:A370)}$ = 3.3 Å in the X-ray structure in Figure 46c). Extension of the side chain of A370 by two or three methyl groups (which corresponds to the A370V or A370L substitutions, respectively) is expected to cause steric clashes in the binding mode of BCT shown in Figure 46. Therefore, this is in agreement with the 2- and 7-fold decreased BCT affinities obtained for the two mutants A370V and A370L, respectively. Based on the interatomic distances between the β-hydroxyl oxygen atom of Ser119 and the backbone amide oxygen atom of the tricyclic peptide of BCT ($\Delta_{(BCT\text{-}O:O\text{-}S119)}$ = 3.3 Å), a hydrogen bond is likely to be formed. The substitution of Ser119 for an alanine abolishes the hydrogen-bonding partner of the amide oxygen and may account for the major portion of the strong, 10-fold decrease in affinity with respect to the wild type.

In our BCT titrations carried out in solution, the high-spin content does not exceed 70% at saturating ligand concentration (Figure 42), which is in agreement with earlier reports (*105, 171*). In CYP3A4 associated to native-like membrane bilayer mimics (Nanodiscs), BCT and testosterone binding have completely converted CYP3A4 to the high-spin state (> 90% high-spin content) (*86*). However, in reconstituted or detergent-solubilised CYP3A4, the conversion to high-spin does usually not exceed 2/3 (*44, 173*) due to interactions between the enzyme monomers to form oligomers. This suggests that only a portion of the total enzyme pool participates in substrate binding (*105*).

In the titrations of wild-type CYP3A4 with ERY, we detected a spectral red-shift of ca. 1 nm upon ligand association. Whether this represents a type-II transition or the formation of some species of cytochrome P420 was not determined by binding of carbon monoxide to the reduced heme iron (II) enzyme. It may be of interest to mention that the absorption maximum of the Soret band was displaced by ca. 1 nm in the absorbance spectra of the A370V and A370L mutants in the

substrate-free form. Titration curves obtained with the substrates BCT and ERY fit well to the isotherm of bimolecular association and allow the determination of affinity constants (Table 11).

Our data of the mutant S119A exhibiting inverse spin shifts with BCT and ERY confirm a major role of Ser119 for the configuration of the active site of CYP3A4. The S119A mutant was shown to be a functional CYP3A4 enzyme (*41*). In chapter 4, we demonstrated that the mutant is capable of catalysing the turnover of the substrate carbamazepine to its epoxide product. In chapter 7, we will show that the mutant also catalyzes the conversion of the fluorogenic quinoline and resorufin derivatives used in this work to probe for active CYP3A4 enzymes. The S119A mutant equilibrates into approximately equivalent proportions of low and high-spin P450 in solution in the absence of ligands, whereas the wild type exhibits less than 20% high-spin cytochrome P450 under identical conditions (see chapter 4, Figure 22 on p.72). Modulation of the spin equilibrium in the heme iron (III) of the enzyme is thought to be an important determinant of its redox coupling and catalytic efficiency. Partitioning into similar proportions of the two most common spin states of iron (III) cytochrome P450 requires a substantial decrease in the occupancy of the heme iron (III) ligand site *trans* to the cysteinate ligand by a water molecule. Strikingly, the increase in low-spin iron upon titration with the substrates ERY and BCT appears to re-establish the native water network in the active site of CYP3A4 S119A, which is decisive for the predominant low-spin form of the heme iron of CYP3A4 in the absence of substrate.

There is an increasing interest in the role of Ser119 in ligand association to CYP3A4 demonstrated by several recent studies involving experiments with the S119A mutant (*11, 170, 174*). In addition to an apparent alteration of the mechanism of ligand association, S119A generally exhibits reduced affinity to the probed substrates. The example of BCT showed a 10-fold decrease in affinity in the S119A mutant with respect to the wild type. Sevrioukova and coauthors studied the effect of the mutation of S119A on equilibrium binding as well as the kinetics of the association and inhibitory binding of a series of ritonavir analogues to CYP3A4. The S119A mutation reduced the affinity to all investigated ligands by at least three-fold and up to two orders of magnitude. The kinetics of association of the ritonavir analogues to the mutant were significantly perturbed (*170*).

The S119A substitution may involve considerable reorganization of the active site in the substrate-free form, leading to (i) thermodynamically unfavorable ligation of water that leads to partial water displacement and a concomitant high-spin transition and (ii) some restriction to the access of large ligands to the active site. We argue that the residue Ser119 is of critical importance for the hydration of the active site of CYP3A4 *via* the formation of a *meta*-stable water network. Its absence appears to involve a reorganization of the hydrophobic binding pocket to form an energetically favorable conformation that is less suitable for the turnover of some of the substrates

probed here at low concentration (see Figure 34, p. 92; note also the reduced activity towards 7-benzyloxyquinoline at $[S]_{7BQ}$ = 5 µM in Figure 59 on p. 153). Support for the hypothesis stated above is provided by studies in which the thermal stability of wild-type CYP3A4 and the S119A mutant were compared (*174*). It is known that tight-binding ligands often increase the melting temperatures T_m of their target proteins. The melting temperature of the ligand-free S119A mutant was increased by 1.4 °C with respect to the wild-type enzyme. This led the authors to conclude that the protein fold of the mutant is somewhat stabilized upon mutation of Ser119 to an alanine. Surprisingly, the stabilization through association with ritonavir analogues obtained for the wild-type enzyme, that was considerable for some of the analogues (ΔT_m = 1.1 – 6.7 °C), was mostly or completely eliminated (ΔT_m = (-0.2) – 1.6 °C) in the mutant. These authors concluded that the Ser119-mediated H-bond both assists the association of ritonavir analogues and stabilizes the resulting complexes (*170*).

It is therefore of interest to examine existing structural data with respect to Ser119 in order to obtain further insight into its functional relevance. A distance of 4.1 Å between *O*-atoms of metyrapone and Ser119 was reported in the crystal structure 1W0G (*38*) of the CYP3A4-metyrapone complex. In an MD simulation study of Park et al. in which the X-ray coordinates of the 1W0G structure were employed, the hydrogen bond to Ser119 was rapidly formed and remained stable over the course of the simulations (*40*). The evolution of the enzyme *in silico* therefore suggests that distances up to and possibly larger than 4 Å can account for hydrogen bonds. X-ray structures of complexes of CYP3A4 with several ligands (e.g. BCT (3UA1) (*171*), ritonavir (3NXU) (*62*), or ketoconazole (2V0M) (*45*)) show shorter separations between the β-hydroxyl oxygen atom of Ser119 and H-bond donating/accepting atoms of ca. 3 Å and therefore represent hydrogen bonding (Table 14). In the MD simulations of the complex of wild-type CYP3A4 with CBZ (see Figure 31, p. 87 of chapter 4), Ser119 was also identified to engage in a hydrogen bond to the CBZ ligand. In summary, Ser119 is directly involved in ligand binding in most of the available X-ray structures of CYP3A4 complexes with ligands.

On the other hand, in one of the available structures of ligand-free CYP3A4 (PDB-ID 4I3Q) (*174*), only three water oxygen atoms are resolved in the active site of the enzyme. Interestingly, the resolved water oxygen atoms appear to connect Ser119 to the heme iron (see Figure 47). This seems to be important for the stabilization of a fully functional active site and to be affected upon the elimination of the β-hydroxyl of Ser119.

Table 14: Currently available X-ray structural data of CYP3A4*

Structure (PDB)	Ligand	S119-O···O-L, Å
3NXU	Ritonavir	3.0
2J0D	Erythromycin	3.3
3UA1	Bromocriptine	3.3
2V0M	Ketoconazole	2.7
1W0G	Metyrapone	4.0
1TQN	water	3.3
4I3Q	water	4.1

*Indicated are the distances of the Ser119 β-hydroxyl oxygen atom to the closest oxygen atom of the ligand or the water molecule in cases where no ligand is present.

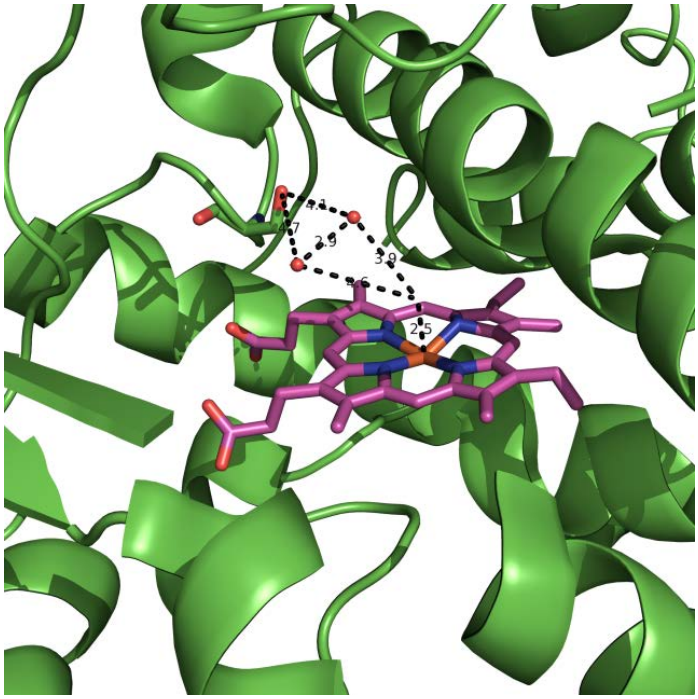

Figure 47: Close-up of the active site of CYP3A4 in the ligand-free X-ray structure 4I3Q. The three resolved water oxygen atoms in the binding pocket (shown as red spheres) connect Ser119 to the heme iron. The oxygen atoms of the water molecules are connected with black dashed lines and the distances between the oxygen atoms are indicated in the figure. This figure was prepared with the X-ray structural coordinates published with ref. (*174*).

In summary, we report herein that CYP3A4 S119A exhibits inverse type-I spin transition upon binding of the type-I ligands BCT and ERY. To the best of our knowledge, there is no previous account on mutants of CYP3A4 that exhibit similarly intriguing effects on the mechanism of ligand association. CYP3A4 S119A is therefore a unique point mutant of CYP3A4 that engages in inverse spin transition upon titration with native type-I ligands of CYP3A4. In chapter 6, our

spectral titration studies of CYP3A4 S119A will be extended to substrates that are known for their sigmoidal, or cooperative, binding curves. The fast growth in the number of X-ray structures in the last decade along with the mutagenesis studies presented here as well as recent experimental work with ritonavir analogues (*170, 174*) altogether disclose important roles for Ser119 in the association of ligands and the stabilization of the water network in the binding pocket of substrate-free CYP3A4. A crystal structure of the S119A mutant would give additional decisive insight into the atypical function of this mutant and may reveal important conformational changes.

6 EVIDENCE FOR SPECTRALLY SILENT ALLOSTERIC LIGAND BINDING IN CYP3A4

6.1 ABSTRACT

The binding of allosteric ligands to the periphery of the microsomal cytochromes P450 is predicted to be the basis for many important occurrences of atypical kinetics in CYP3A4 that lead to drug-drug interactions. Binding of multiple molecules of steroids that exhibit homotropic cooperativity in binding to CYP3A4 has been predicted to occur at spatially separate binding sites in the active site and at the periphery of CYP3A4. However, this has never been directly observed. In order to elucidate peripheral ligand binding of cooperative CYP3A4 ligands, we studied the spectral effects of ligand association to CYP3A4 wild type and the S119A mutant. The results presented in chapter 5 showed a unique inverse spin shift upon binding of the type-I ligands bromocriptine (BCT) and erythromycin (ERY) to this mutant, which were not found for the wild type. While these two non-allosteric substrates ERY and BCT induced a simple reverse type-I shift upon ligand association to CYP3A4 S119A, we report here bidirectional spin-shifts for the allosteric substrates testosterone (TST), estradiol (EST), and 7-benzyloxyquinoline (7BQ). Minor initial high-spin shifts were followed by transitions to the low-spin iron (III) cytochrome P450, the extents of which varied among the substrates. The phenomenological cooperative behaviour was often attributed to the fact that several substrate molecules are required to bind within a large binding pocket in order to overcome the loose binding and to attain the formation of a productive complex with at least one of the substrate molecules. The most common conclusion from data with several simultaneously metabolized substrates was, however, that most likely several substrate molecules have simultaneous access to the oxidizing species in cytochrome P450, which requires direct binding to the active site. The data presented in this chapter provide evidence for initial binding of these cooperative ligands to a high-affinity binding site that does not induce a substantial spin transition and therefore is ‘spectrally silent’. This feature, which appears to be exclusively related to the CYP3A4 S119A mutant, promotes the notion of a ‘true allosteric’ effect, i.e. binding to an allosteric site that does not take part in catalysis itself, but promotes substrate metabolism in the active site.

6.2 INTRODUCTION

Cytochrome P450 3A4 (CYP3A4), the most abundant human cytochrome P450 expressed in liver and small intestine (*37*), is a prominent example of a cytochrome P450 showing functional variability. CYP3A4 metabolizes about 50% of all currently marketed drugs and is a determinant of important drug-drug interactions. Many reactions catalysed by CYP3A4 obey non-hyperbolic

kinetics indicative of homo- and heterotropic cooperativity, as seen from sigmoidal substrate turnover or binding *in vitro*. Important examples of non-hyperbolic substrate dependencies were documented in CYP3A4-dependent oxidations of native steroids (e.g. testosterone 6*β*-hydroxylation, estradiol 2-hydroxylation, and progesterone 6*β*-hydroxylation) or of xenobiotic compounds and pharmaceutical drugs (e.g. aflatoxin B1, amitriptyline *N*-demethylation, carbamazepine 10,11-epoxidation, or diazepam 3-hydroxylation) (*166*). However, it is still not understood how and to what extent putative peripheral ligand binding translates into drug-drug interactions that can lead to adverse drug interactions. The complex non-hyperbolic kinetics and ligand binding may though in many instances be explained *via* allosteric ligand binding to a "spectrally and functionally silent" peripheral ligand binding site (*58*).

Recent studies of the function and regulation of cytochrome P450 have revealed increasing attention to the functional significance of the mechanism of substrate binding to such a putative peripheral binding site (*38, 46, 49, 100, 171*). Peripheral binding is thought to cause an effector-induced conformational rearrangement in the enzyme along with multiple ligand binding (*67, 71, 166, 172, 175*). We studied the spectral effects of the spin transition upon binding of cooperative substrates to the CYP3A4 S119A mutant. It has been shown that this mutant involves inverse type-I spin transitions along with the binding of the type-I substrates BCT and ERY. Specifically, we studied the effect of the binding of the substrate 7BQ, and the steroid hormones TST and EST to CYP3A4 (Figure 48). 7BQ is a fluorescent substrate and activity marker that is used in activity assays that are aimed at the investigations involving novel drug candidates (*176-179*). The substrate is metabolized by CYP3A4 *via* debenzylation to 7-hydroxyquinoline (7HQ), which exhibits altered fluorescent properties. The compound is used by the pharmaceutical industry for testing of the potency of new chemical drugs for CYP3A4 inhibition in order to predict potential drug-drug interactions of the novel drug candidates (*176, 178*). TST and EST are both endogenous CYP3A4 substrates that are metabolized to their predominant native products 6β-hydroxytestosterone and 2-hydroxyestradiol, respectively.

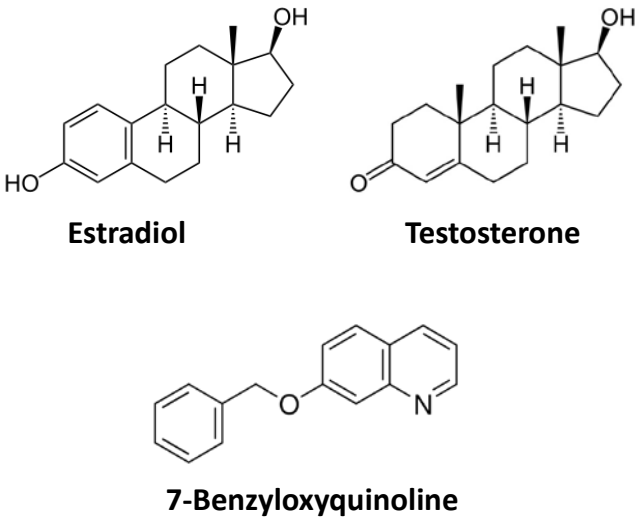

Figure 48: Structures of the CYP3A4 ligands studied in this chapter.

6.3 RESULTS

6.3.1 EFFECT OF SOLVENTS ON SPIN EQUILIBRIUM

As reported in the following section, titrations of the CYP3A4 S119A mutant with allosteric substrates may initially induce minimal spin perturbations. Even the minor contributions from the methanol used as stock solvent may significantly bias the obtained spin transitions and conceal the effects caused by the actual substrates. For this reason, the spectra needed corrections for the solvent background effect. Obtained titration curves were therefore corrected for solvent contributions. To this end, control titrations with methanol were performed with CYP3A4 S119A and the obtained spectra analysed for the quantification of the induced spin shift. An example of a spectral series of methanol titration and the analysed titration curve are shown in Figure 49. Panel (b) in this figure shows a plot of the high-spin proportion as a function of methanol concentration. The linear dependence of the high-spin (HS) cytochrome P450 fraction on [MeOH] allowed a linear fitting of the data, from which the following parameters were obtained ($y = ax + b$, the shown parameters represent the mean of three independent measurements and the "±" values represent the confidence interval calculated for $p = 0.05$):

$$a = \frac{\partial \frac{[\mathrm{P450}_{HS}]}{[\mathrm{P450}_{Tot}]}}{\partial [MeOH]} = -0.022 \pm 0.004 \tag{6.1}$$

$$b = \left(0.494 \pm 0.007\right) = \left.\frac{[P450_{HS}]}{[P450_{Tot}]}\right|_{[MeOH]=0} \tag{6.2}$$

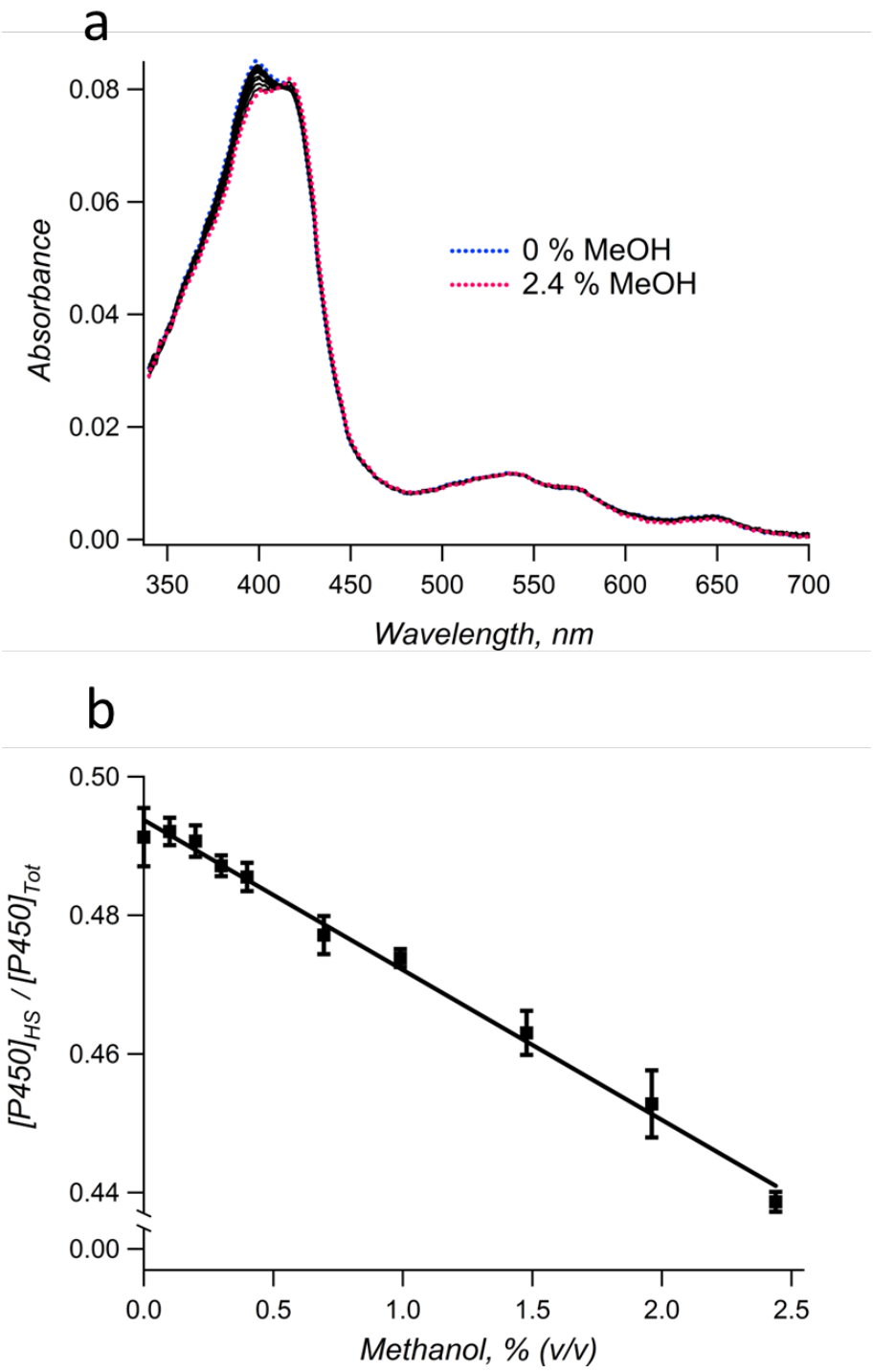

Figure 49: Methanol background: titrations of CYP3A4 S119A. (a) Series of absorbance spectra of titrations of CYP3A4 with methanol as the solvent. (b) Dependence of high-spin P450 on methanol content. The markers and error bars show the mean and standard deviations of the experimentally determined high-spin fractions of P450, respectively. Titrations were performed in triplicate. Linear fitting of the data yielded a concentration dependence of – (2.2 ± 0.4) % high-spin (% methanol (*v*/*v*))$^{-1}$.

6.3.2 TITRATIONS OF CYP3A4 WILD TYPE AND S119A WITH ALLOSTERIC SUBSTRATES

Titration with the native substrate testosterone (TST) induced a strong spin-shift of (45 ± 2) % in wild-type CYP3A4, with an S_{50} = (56 ± 14) μM, which is in agreement with data from previous studies (*82*). Binding of TST was found to occur with a moderate cooperativity with a Hill coefficient h = (1.15 ± 0.08; Figure 50a). Titration of the wild-type enzyme with estradiol (EST) led to a considerably smaller spin-shift of (19 ± 4) %, compared to the one obtained with TST, and exhibited increased affinity with an S_{50} = (39 ± 7) μM. Homotropic cooperativity in EST binding was somewhat more pronounced than with TST: h = 1.24 ± 0.12 (see Table 12). In order to explore the binding of a non-steroidal cooperative CYP3A4 ligand, we extended our titrations to 7-benzyloxyquinoline (7BQ). Analysis of the spectral series of the titrations of wild-type CYP3A4 revealed an S_{50} of (75 ± 16) μM and a spin-shift of (38 ± 6) %. Cooperativity was considerably higher compared to the probed steroids: h = 1.73 ± 0.12 (Figure 50c).

Table 15: Fitting parameters for the analysis of the titrations of CYP3A4 wild type with cooperative substrates.*

Fitting Results (CYP3A4 Wild type)				
Substrate	**S_{50}, μM**	**Spin Shift**	***h***	**Endpoint**
TST	56 ± 14	0.45 ± 0.02	1.15 ± 0.08	0.59 ± 0.03
EST	39 ± 7	0.19 ± 0.04	1.24 ± 0.12	0.33 ± 0.01
7BQ	72 ± 17	0.36 ± 0.03	1.70 ± 0.08	0.54 ± 0.01

*Results for the parameters S_{50}, the Hill parameter h, total spin shift, and (asymptotic) spin transition endpoints for the titrations of wild-type CYP3A4 with the cooperative substrates testosterone (TST), estradiol (EST), and 7-benzyloxyquinoline (7BQ). Spin shifts and titration endpoints are given in fractions of total cytochrome P450. The values given in the table represent the mean values of at least three experiments, and the "±" values show the respective confidence interval calculated for p = 0.05.

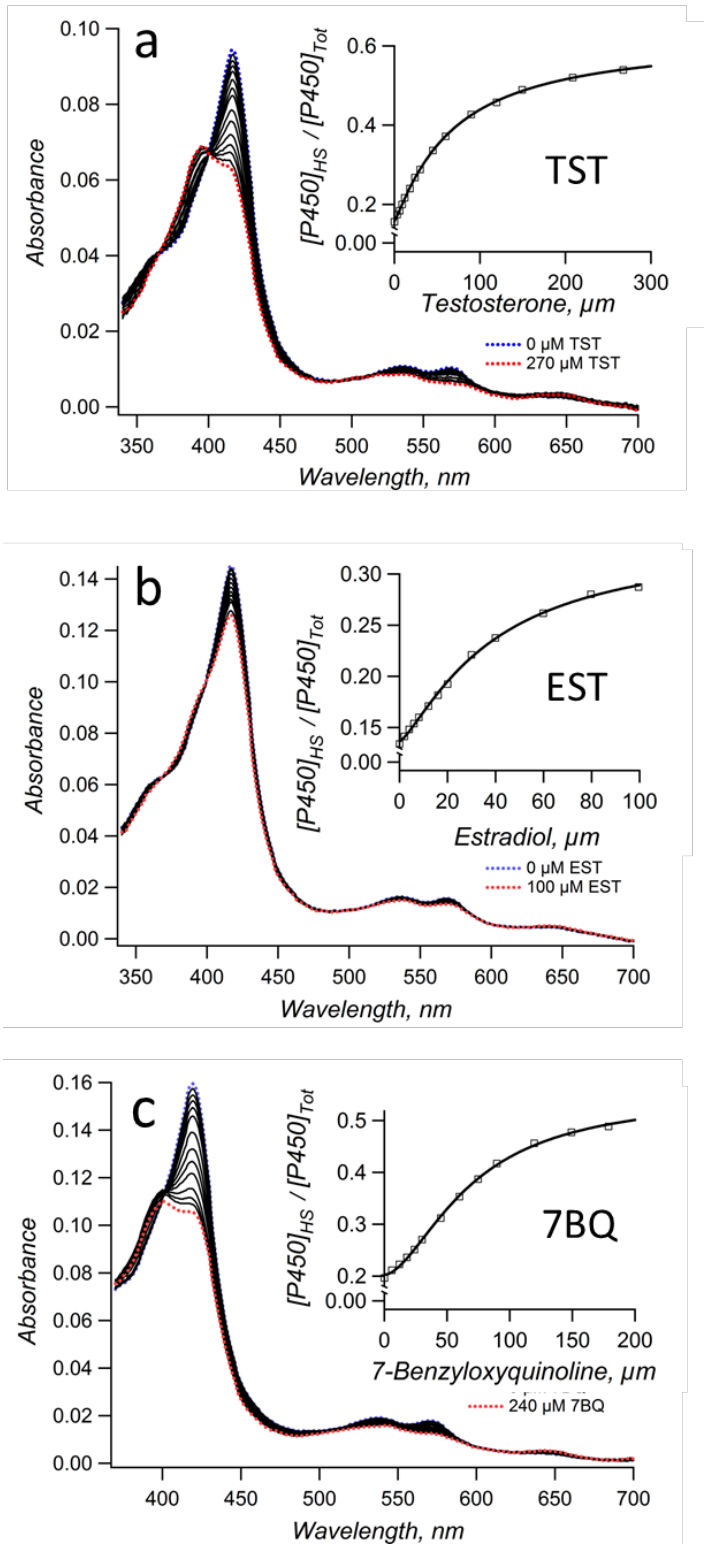

Figure 50: Titrations of CYP3A4 WT with testosterone (a) (TST), (b) estradiol (EST), and 7-benzyloxyquinoline (7BQ). Spectral series of the titrations insets show plots of the high-spin fractions total cytochrome P450 ([HS]/[P450]$_{Tot}$) as a function of ligand concentration. The analysis of the spectral series of the 7BQ-titrations of the wild-type enzyme reveals a pronounced homotropic cooperativity (h = 1.7).

In contrast to the titrations with ERY shown in chapter 5, the mutant S119A exhibited only minor perturbations of the spin equilibrium upon TST binding. Most notably, the analysis of the data of the S119A mutant showed a bidirectional spin shift, i.e. a combination of an initial type-I spin shift followed by an inverse spin transition. The initial "regular" transition leads to a maximum for the high-spin content of total cytochrome P450 at ca. 45 μM TST. The corresponding spectrum Figure 51 is shown in green. Further titration beyond [TST] ≈ 45 μM led to an inverse type-I transition, such that this part of the titration resulted in spectral changes similar to those obtained for the non-cooperative substrates BCT and ERY (chapter 5). A spectral analysis of the titration data with respect to an apparent type-II transition resulted in a concentration dependent increase in the population of this species (Figure 51b). Since the absolute amounts of the individual spin perturbations were minor (in the range of ca. 1-7%, see Figure 51b and c), we expanded our studies to the substrate EST, a steroid hormone closely related to TST. Interestingly, in contrast to TST binding, the overall spin shift for EST binding to the S119A mutant was clearly inverse type-I, although comprising a "lag-phase" in which the spin state was hardly perturbed ([EST] ≈ 0 – 15 μM; Figure 52c). Inspection of this range of substrate concentration revealed a maximum of the high-spin portion at *ca*. 10-20 μM. Analogous data were obtained for the titrations of the S119A mutant with 7BQ, the analysis of which yielded a minor increase in high-spin with a maximum at *ca*. 6 μM that was followed by a ca 20% inverse spin-shift (Figure 53).

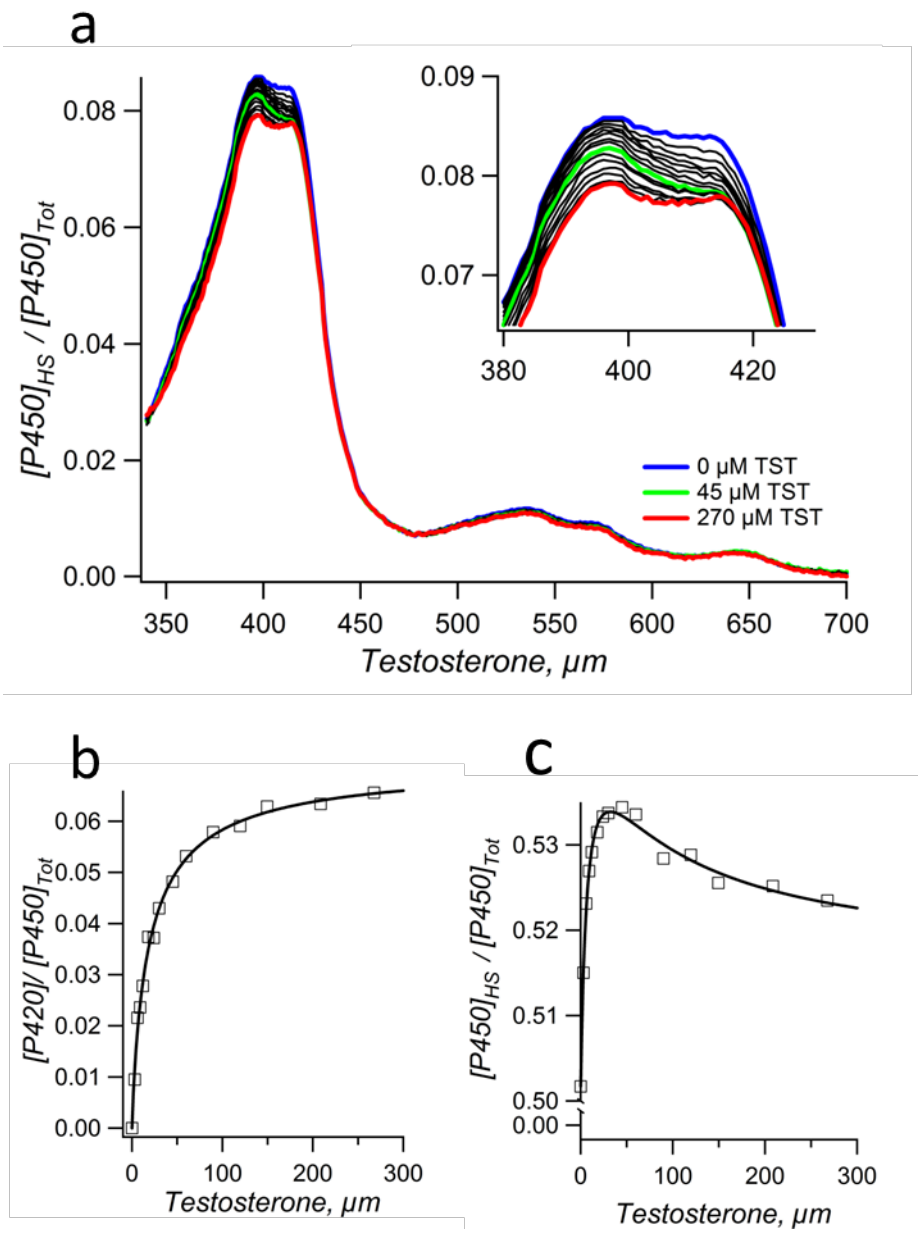

Figure 51: Testosterone (TST) binding to CYP3A4 S119A. Panel (*a*) shows a series of spectra of CYP3A4 S119A titrations with TST, and the inset to this panel displays a zoom of the Soret band; the blue and the red dotted line depict the starting and end points of the titration, respectively. The spectrum recorded at 45 μM TST is shown in green in order to highlight the transient maximum in high-spin cytochrome P450. Panels (*b*) and (*c*) display the proportions of the apparent type-II and the high-spin form of total cytochrome P450 as a function of [TST], respectively. The data in panel (*b*) were fit to the Hill equation; the data shown in (*c*) were fit to the equation of the two-site model (Eq. 1.9).

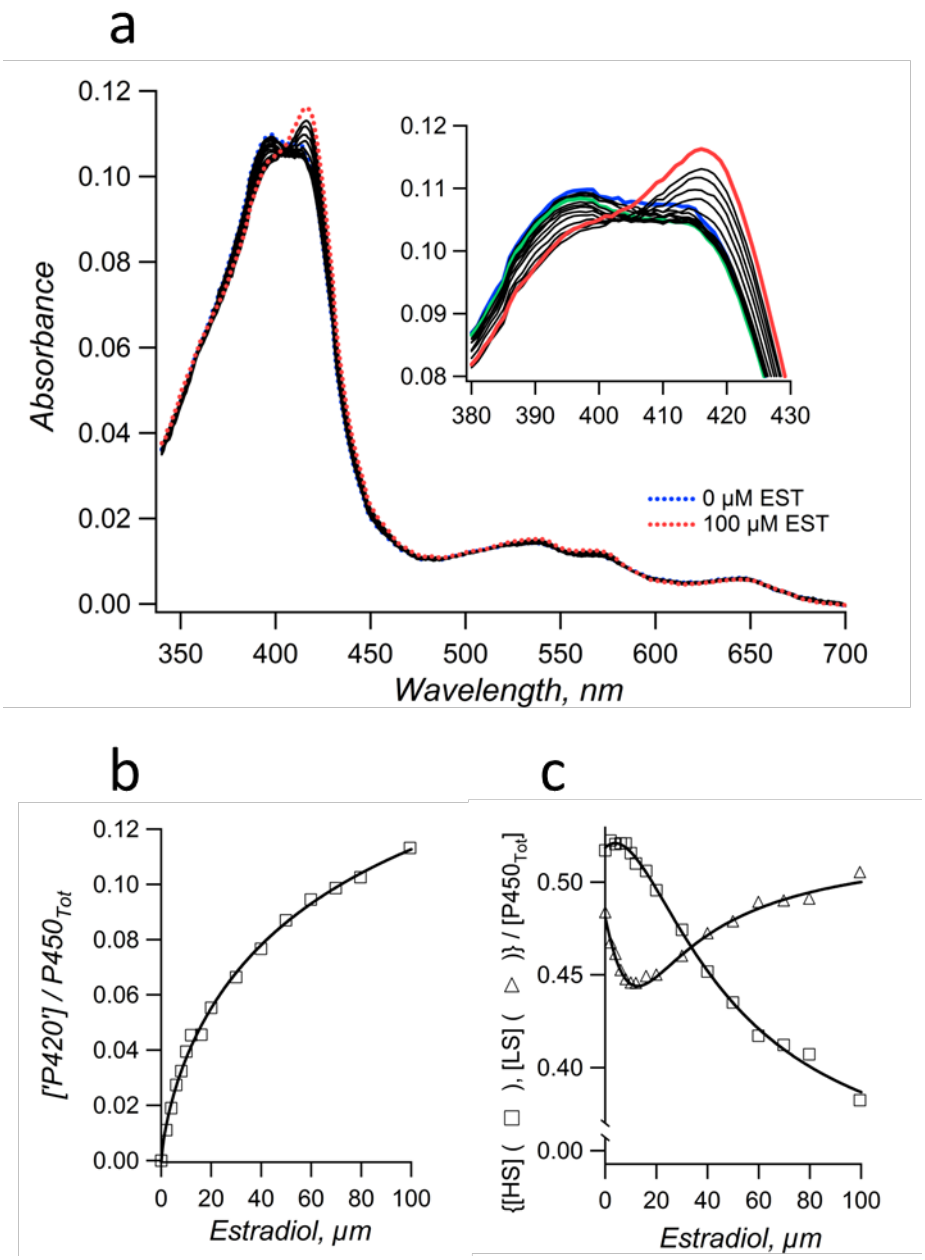

Figure 52: Estradiol (EST) binding to CYP3A4 S119A. Panel (*a*) shows a series of spectra of CYP3A4 S119A titrations with EST, and the inset to this panel displays a zoom of the Soret band; the blue and the red dotted line depict the starting and end points of the titration, respectively. The spectrum recorded at 8 µM EST is shown in green in order to highlight the transient maximum in high-spin cytochrome P450. Panels (*b*) and (*c*) display the contents of the 'P420' (*b*) and the high-spin (squares) and low-spin (triangles) forms (*c*) of the total cytochrome P450 as a function of [EST]. The data in (*b*) were fit to the Hill equation; the data shown in (*c*) were fit to the equation of the two-site model (Eq. 1.9).

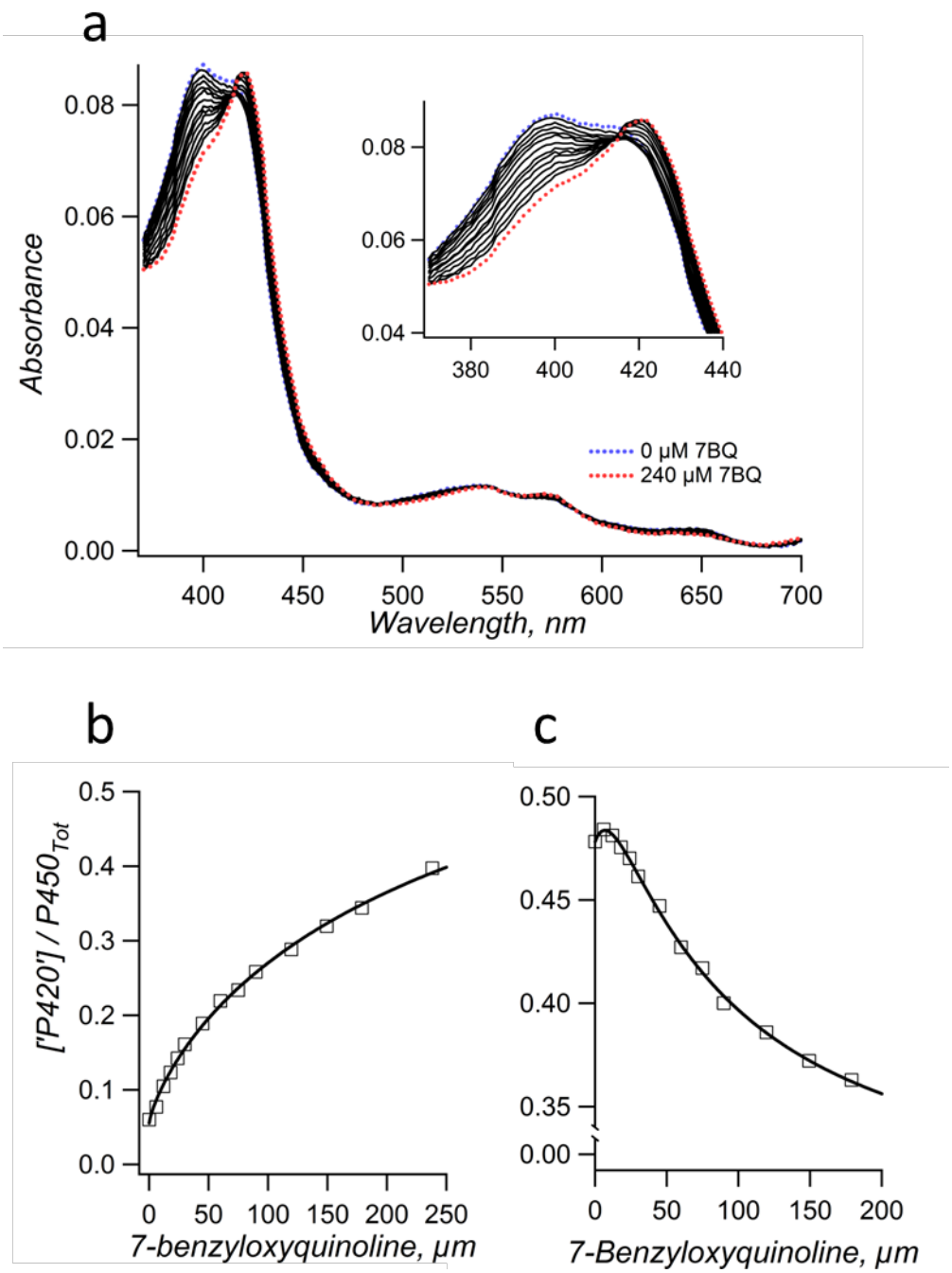

Figure 53: 7-benzyloxyquinoline (7BQ) binding to CYP3A4 S119A. Panel (*a*) shows a series of spectra of CYP3A4 S119A titrations with EST, and the inset to this panel displays a zoom of the Soret band; the blue and the red dotted line depict the starting and end points of the titration, respectively. Panels (*b*) and (*c*) display the contents of the 'P420' (*b*) and the high-spin (*c*) forms of the total cytochrome P450 as a function of [7BQ]. The data in (*b*) were fit to the Hill equation; the data shown in (*c*) were fit to the equation of the two-site model (Eq. 1.9).

In order to explore the nature of the uncommon spin transition exhibited by the S119A mutant, the results from the principal component analysis (PCA) are shown in Figure 54 and the position of the maxima of the first principal components (PC) are shown in Table 13. The first PC

of the spectral titration series of the wild type with testosterone reveals a pure type-I spin-shift. Analysis of the first two PCs of the titration data of the S119A mutant demonstrates that a decrease in both high- and low-spin cytochrome P450 accounts for the bulk of the difference (1st PC), whereas the 2nd most variation in the data is due to a common type-I spin shift similar to the case of wild-type CYP3A4. PCA of the tirations with EST and 7BQ illustrate a nearly inverse spectral transition in the S119A mutant, but in both cases, the peak positions of the maximum values are somewhat red-shifted with respect to the peak position of the minimum obtained from the analysis of the wild-type data (Table 16).

Table 16: Maxima and minima extracted from the 1st principal components after principal component analysis (PCA) of the substrate titrations of CYP3A4 wild type and S119A.*

Substrate	Mutant	Max., nm	Min., nm
Estradiol	WT	385	418
	S119A	**423**	**389**
7-Benzyloxyquinoline	WT	388	420
	S119A	**430**	**391**
Testosterone	WT	387	418
	S119A	-[1]	411

*The positions of the extreme values that were extracted from the 1st principal components shown in Figure 54 are listed. [1]In the titration of S119A with TST, a minor overall spin shift was obtained, which led to a broad minimum in the 1st principal component due to a high noise level. Whereas in the case of BCT and ERY the maximum for the S119A mutant coincides with low-spin CYP3A4 (inverse type-I transition, see chapter 5, Table 13 on p. 117), the binding of 7-benzyloxyquinoline and estradiol appears to induce a type-II transition starting from high-spin iron (III).

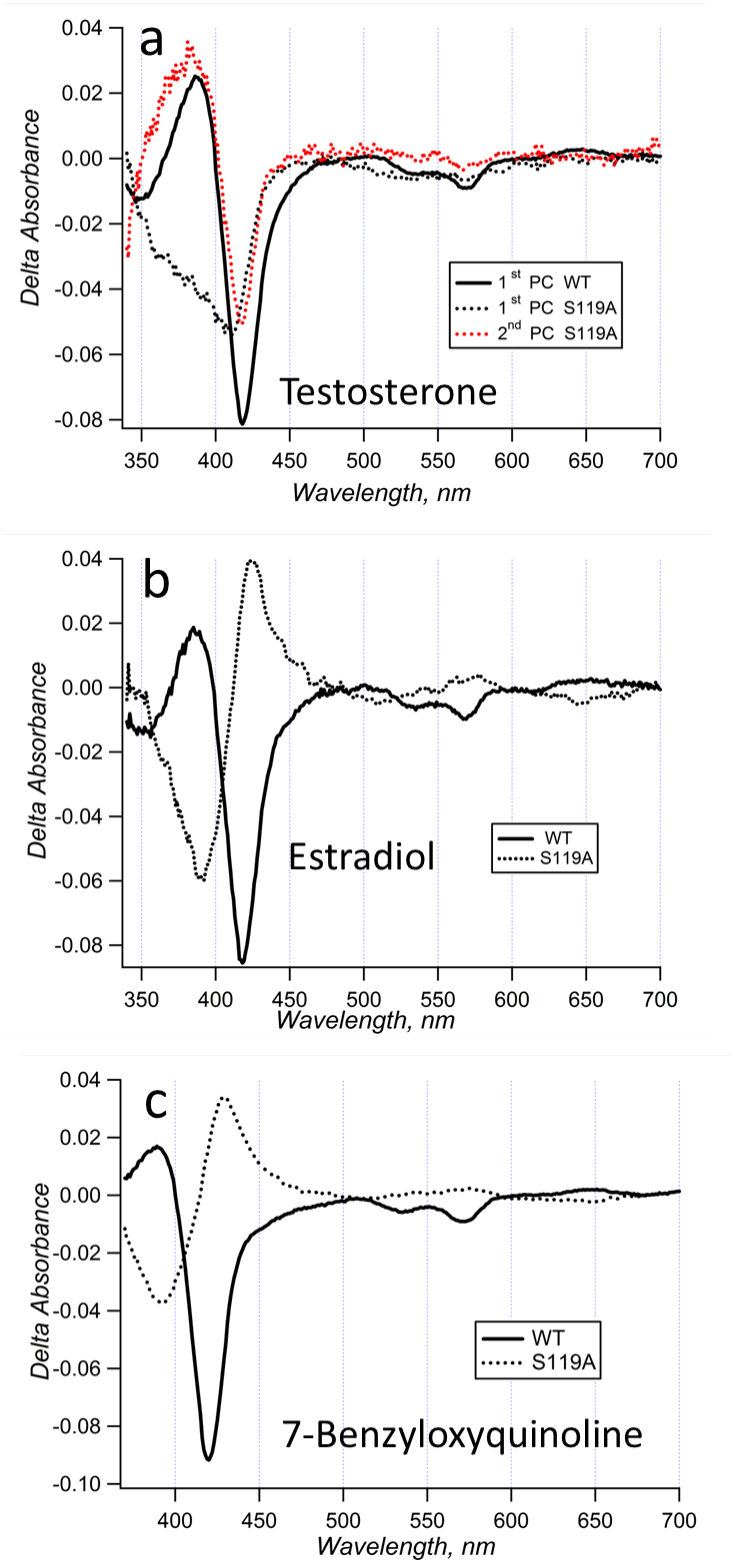

Figure 54: First principal components (PC) of the titration data. The first PCs of the data from the titration with (*a*) TST, (*b*) EST, and (*c*) 7BQ are compared. In (*a*), the second PC of for the data with the S119A mutant is shown, too. The first PC contains a decrease in low- as well as high-spin cytochrome P450, and the second PC contains regular type I shift. In (*c*), the maximum of the principal component shows a red-shift with a maximum at ~430 nm which may reflect either inactivation to a cytochrome P420 form of the enzyme or a type-II transition.

The titration experiments of the CYP3A4 S119A mutant with the cooperative substrates probed here do not comprise simple inverse type-I spin shift as in the titrations with BCT and ERY (chapter 5). This can be concluded from the displacement of the maxima of the first principal components. The maximum of the 1st PC appears red-shifted with respect to low-spin cytochrome P450 ($\lambda_{max} \approx 417$ nm), in particular in the case of the titration data with 7BQ ($\lambda_{max} \approx 430$ nm), and to a lesser extent in the binding of estradiol ($\lambda_{max} \approx 423$ nm).

6.3.3 FORMATION OF CYTOCHROME P420 UPON BINDING OF 7BQ

In order to explore whether binding of 7BQ leads to the transition of cytochrome P450 to the cytochrome P420 form, we studied binding of CO to Fe^{2+}-heme in the presence and absence of 7BQ in both the wild-type CYP3A4 and the S119A mutant. The spectra that were obtained from a sample containing CYP3A4 wild-type enzyme in buffer solution saturated with CO before and after adding $Na_2S_2O_4$ to the sample are shown in the absence of substrate (*a*) and in the presence of 150 µM (*b*) and 300 µM (*c*) of 7BQ for CYP3A4 wild type and the S119A mutant in Figure 55. The proportion of cytochrome P420, which does not exhibit a Soret band absorption maximum at ca. 450 nm upon binding of CO, was calculated with the respective standards. The data show that titration of both enzyme variants with 7BQ leads to the inactivation of CYP3A4 with the emergence of an absorption peak at ca. 424 nm. The spectra were decomposed with the help of spectral standards for the CO-bound cytochrome P450 and the cytochrome P420 form of CYP3A4 (see chapter 2.2.2.4 on p. 51). The results from this analysis are shown in Table 17.

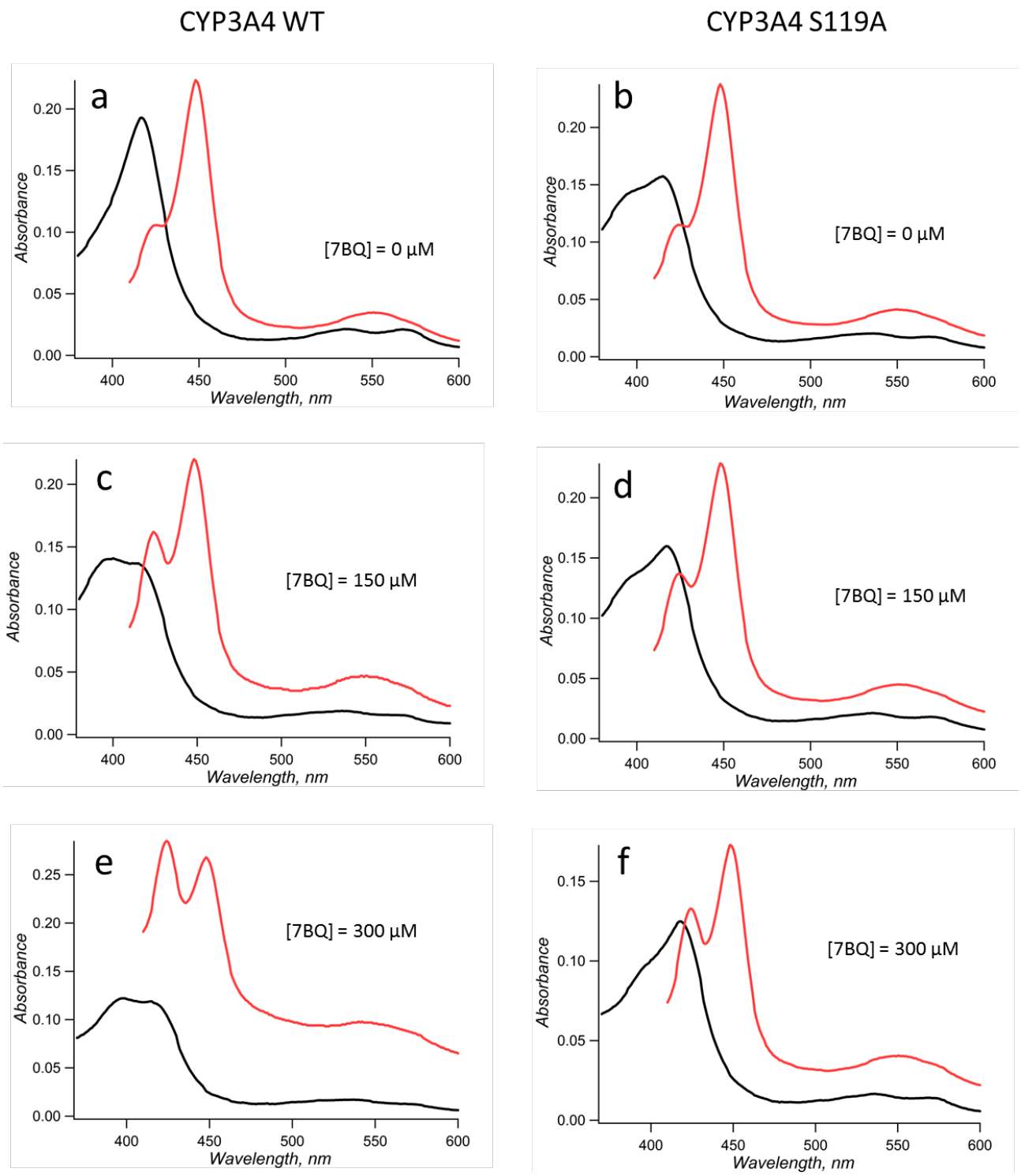

Figure 55: Absorbance spectra of (*a, c, e*) CYP3A4 wild type and (*b, d, f*) the S119A mutant in buffer solution containing CO before (black) and after (red) the Fe (III) → Fe (II) reduction of the heme iron by the addition of $Na_2S_2O_4$. The portion of the total heme protein that is inactivated through the transition to a cytochrome P420 form of CYP3A4 increased with the concentration of the titrant 7BQ and was determined via spectral decomposition (Table 17).

The CO-binding data identified a process that entails the formation of the inactivated cytochrome P420 form of CYP3A4 both in the wild type and in the S119A mutant enzyme. Strikingly, upon binding of the 7BQ ligand to the wild type, the proportion of cytochrome P420 strongly increased. For instance, at 300 µM 7BQ, the CYP3A4 wild type only exhibited (11 ± 3)% of inactivated enzyme. Upon reduction with sodium dithionite, the portion of cytochrome P420 increased to (34 ± 1)%. In strong contrast, the proportions of inactivated enzyme in the S119A mutant were not affected during reduction of the heme iron with $Na_2S_2O_4$ (see Table 17).

Table 17: Proportion of cytochrome P420 in the total enzyme pool determined before and after reduction of the heme iron by the addition of $Na_2S_2O_4$.*

7BQ, µM	Wild type		S119A	
	- $Na_2S_2O_4$	+ $Na_2S_2O_4$	- $Na_2S_2O_4$	+ $Na_2S_2O_4$
0	0	0.061 ± 0.002	0	0.06 ± 0.01
150	0.06 ± 0.02	0.23 ± 0.03	0.13 ± 0.01	0.15 ± 0.01
300	0.11 ± 0.03	0.34 ± 0.01	0.21 ± 0.02	0.24 ± 0.02

*The values given in the table represent the mean values of at least three experiments, and the "±" values show the respective confidence interval calculated for $p = 0.05$.

6.4 DISCUSSION

Titration with the two steroids EST and TST and the marker substrate 7BQ are in contrast to the simple inverse type-I spin shifts that result from the association of ERY and BCT to the S119A variant (chapter 5). Principal component analysis of a spectral series of substrate titrations was employed in order to monitor the fractions of the different cytochrome P450 species in the total enzyme pool during the course of the titration experiment. Initial binding causes a minor high-spin shift, whereas additional substrate leads to a low-spin shift, the extent of which depends on the substrate. The variant S119A exhibits contrary effects of substrate binding to the putatively distinguishable binding sites in CYP3A4: initial binding causes normal type-1 spin-shift, whereas further increase in ligand concentration leads to an inverse type-1 shift, most likely due to binding in the active site of CYP3A4.

The analysis of the spectral series was therefore employed to demonstrate the binding of cooperative ligands to spatially separated locations of the enzyme *via* the identification of different spectral transitions. This allows us to differentiate the binding of 2-3 molecules of the steroids testosterone, estradiol, and the CYP3A4 marker substrate 7BQ. Theoretically, the data allow us to

calculate and obtain three different affinity constants, which may correspond to the binding of up to three, but at least two, substrate molecules to the S119A mutant: The first substrate binding event appears almost spectrally silent and leads to a slight LS → HS transition (type-I shift) similar to the first binding of these substrates to the CYP3A4 wild type. The binding of a second substrate leads to an inverse type-I spin shift (HS → LS) with a stronger spectral response with both EST and 7BQ than with TST. A third spectrally different transition similar to a type-II transition may be assigned to binding of an additional substrate molecule. The apparent spectral type-II transition may be caused by binding of the third steroid molecule, or it may be caused by the combined effects of the binding of the first two ligand molecules.

The predominant human hepatic microsomal P450 isoform CYP3A4 has been studied extensively with regard to atypical kinetics, (*58*). Models used to explain the cooperative behavior of this enzyme rely on the binding of multiple substrates to different sites in CYP3A4. The initial binding of the ligand to a high-affinity, "spectrally silent" and/or "functionally silent" binding site has been proposed (*72, 95, 98, 100*). This binding has been suggested to occur at a site on the protein globule in the region of the progesterone binding site in the X-ray structure 1W0F (*38, 49*).

Often, evidence for separate binding sites has remained elusive with the exception of very few cases. The mechanism(s) of cooperative behavior have therefore remained obscure in most cases. In particular cases, there are both evidence of multiple binding sites in the binding pocket (*45, 50*) and binding at a peripheral site on the surface of the protein globule in the F-G loop region (*38, 49, 100*). Homotropic cooperativity of TST has been extensively studied in both equilibrium binding and turnover (*44, 166, 173*). It has been indirectly shown in several works in the lab of Sligar and others (*58, 72, 79, 86, 94, 97, 98*) that binding of individual TST molecules to CYP3A4 differentially influence functional properties of the enzyme, such as spin state, NADPH consumption, and the rate of substrate hydroxylation. The binding of the first TST is assumed to have a minor effect on the spin equilibrium, but to induce a critical conformational change in the protein (*80*). The binding of the second molecule is likely to cause the largest part of the spin-shift *via* binding within the active site and this leads to maximal turnover of TST. The Formation of a quaternary complex does not further increase the turnover rate, but improves coupling of NADPH consumption with product formation. The quantitative contributions of the binary, tertiary, and quaternary complexes to the observables spin equilibrium, NADPH consumption and/or TST turnover were derived with a global fitting approach (*58, 72, 86, 94*).

The initial binding of the other cooperative substrates, such as Nile Red (*100*), α-naphthoflavone (*79*), and 1-pyrenebutanol (*95*), have also been proposed to occur without significant contribution to spin-shift or turnover of the substrate. Nile Red, a fluorescent CYP3A4

substrate that is sequentially metabolized to the *N*-monoethyl and *N*-desethyl products, binds to the active site of CYP3A4 with a concomitant blue-shift in the maximum of the fluorescence emission band from ~ 660 nm to ~ 620 nm (*100*). The binding of an additional red-shifted spectral component emitting at 660 nm is selectively eliminated by the titration with the known allosteric effectors of CYP3A4, α-naphthoflavone and TST. The affinity of the blue spectral component to the active site was much higher (K_D = 0.05 μM) than that of the red spectral component (K_D=2.2 μM) to the allosteric site. This is in contrast to the affinities of TST, where peripheral binding occurs prior to active site binding. In contrast to Nile Red, no spectral resolution of TST binding to different binding sites has been achieved. A conformational transition upon first ligand binding was supported by the finding of an increase in the spatial separation between the α- and β-domains of CYP3A4 induced by α -naphthoflavone and TST in a study involving luminescence resonance energy transfer (LRET). If substrate binding is spectrally silent, initial binding takes place without perturbing the water network that stabilizes distal water ligation of the heme iron and occurs therefore either at a site distant from the heme in the binding pocket or at a peripheral ligand binding site. In summary, previous work hypothesized that initial binding of TST is spectrally silent to a high-affinity binding site that is likely to reside at the periphery of the protein globule close to the progesterone binding in the reported X-ray structure (*38, 49*).

We reported here for the first time a direct observation of a differential effect of binding of steroids and 7BQ on the spin equilibrium in a CYP3A4 variant. We infer that the mutation S119A leads to a significant interference with binding of a water ligand to the sixth ligand-binding site in the heme iron. It is possible that the perturbation of the water ligation entails a structural change in the flexible binding pocket of CYP3A4. In the case of CYP3A4 S119A, addition of substrates that bind tightly in the vicinity of heme may lead to an opening of a channel that allows water molecules to access the distal ligand site. A stark decrease in substrate affinity to the active site leads to an alteration of the occupancy of the individual binding sites. As a result, the binding site close to the heme iron becomes saturated only at high substrate concentration. Similar to the model for apparent binding cooperativity that was recently presented by Denisov and coworkers (*58*), a high relative occupancy at an unproductive binding site distant from the heme produces a more sigmoidal binding curve.

Our experimental data demonstrate that all type-I substrates studied in chapters 5 and 6 induce an inverse spin-shift in the S119A mutant, either initially or as the result of multiple substrate binding in the case of cooperative ligands. CYP3A4 S119A therefore represents an intriguing enzyme variant that is useful in the identification of allosteric substrates due to its unique properties

of inducing bidirectional spin shifts. In addition to the alteration in the mechanism of substrate binding, S119A generally exhibits lower affinity to the probed substrates than the wild type. One possible explanation is that the general affinity of the substrates to the active site strongly decreases as a result of the active site mutation in the S119A mutant, while the affinity of allosteric substrates to the periphery remains largely unaffected. The strong relative separation in affinities together with the opposite direction of spin shifts lead to a clearly visible maxima and inflection points in the high-spin proportions of total cytochrome P450. Our data with the cooperative substrates TST, EST, and 7BQ therefore convincingly demonstrate the existence of a binding site distant from the heme, most likely at the periphery of the enzyme, and provide support for a true allosteric ligand binding mechanism.

7 ADDITIONAL STUDIES

This chapter contains additional studies involving the CYP3A4 mutants introduced in the previous chapters. Specifically, the two following projects:

- A study of ligand binding to the I369F mutant of CYP3A4 involving the substrates introduced earlier and the discussion of potential applications of this mutant in drug detection with biosensors.
- A study of the kinetics of heme iron (III) → iron (II) reduction in CYP3A4 by dithionite and its implication for conformational diversity of the enzyme.

7.1 CYP3A4 I369F - AFFINITY AND ACTIVITY STUDIES

This chapter contains references and figures generated based on MD simulation data that were performed by T. Knehans.

7.1.1 INTRODUCTION

Despite fundamental advances in the development of pharmaceutical drugs with intensive drug testing and expensive clinical trials, still a majority of the available drugs exhibit a beneficial therapeutic effect in less than half of the treated individuals (*180, 181*). There are several causes that potentially affect treatment success, such as pathogenesis and severity of the treated disease, drug interactions, nutritional status, renal and liver function, age, and concomitant illnesses (*182*). Therapies based on information about the individual's drug metabolising capability would aid to increase the success rate in drug therapies and reduce adverse drug reactions (*180*). Hence, there has been a rising demand for the development of personalized therapy. Glucose sensors can be viewed as prototypic biosensors that are increasingly used to monitor glucose levels in diabetes therapy. The need for long-term implantable automatic glucose sensors are acknowledged by the diabetes care community. Continuous glucose monitoring has been achieved with percutaneous glucose sensors that are inserted with needle introducers into subcutaneous tissues (*183*), but these sensors face drawbacks such as the need for frequent replacement (every 3 – 7 days) due to adverse reactions, e.g. encapsulation of the subcutaneous sensor part by the body (*184*). They are however generally capable of reliably measuring glucose levels and have been developed to the commercial product stage. Such advances in the diabetes care have translated into a stimulation of the research on electrochemical biosensors for the detection of other human metabolites, or xenobiotic compounds such as drugs. It was suggested that electrochemical biosensors based on cytochromes P450 should be combined with chip-based assays on marker genes in the next generation of diagnostic sensing devices (*115, 180*).

Cytochromes P450 have the third position after glucose oxidase and cytochrome *c* in the number of publications on protein electrochemistry (*180*). Because they cover a broad substrate range, they theoretically offer intriguing opportunities for the application in drug detection and therapeutic monitoring. The first cytochrome P450-based enzyme electrode was presented in 1978, and a whole spectrum of P450-dependent sensors have been characterized since that were targeted at the detection of drugs, metabolites, or environmental pollutants (*115, 180*). In contrast to glucose sensors, the major limitation of drug sensors based on cytochromes P450 are their low sensitivity to their target drugs. Whereas normal plasma glucose levels lie in the range of 4-8 mM, the therapeutic

target concentrations of most drugs are in the low micromolar or even nanomolar range[11]. Since most drugs exhibit affinity parameters (e.g. S_{50}, K_D, or K_M) to the microsomal cytochromes P450 that are >> 1 μM, they are in most cases not suitable for the detection of drugs in the therapeutic window and hence for therapeutic drug monitoring. Novel enzyme variants that exhibit improved affinity to target pharmaceuticals on the basis of the extensively studied wild-type enzymes are therefore required for applications in the novel enabling technologies for cytochrome P450-based therapeutic drug monitoring.

The original scope of this thesis was the development of CYP3A4 mutants with improved activity or affinity towards pharmaceuticals such as the model compound carbamazepine (CBZ) for the implementation of the enzymes as recognition elements in drug sensing. In view of our original goal to generate CYP3A4 variants to be used in CBZ biosensors, the A370V variant may seem to be the best candidate, as it exhibits the highest maximal rate of CBZ turnover among the probed enzyme variants (see chapter 4). However, taking into account that the target therapeutic concentrations of CBZ in blood plasma should fall in the range of 17 – 70 μM (*51*), we argue that the decreased affinity of A370V to CBZ (S_{50} = 1.1 mM) undermines its practical utility. We believe that the most promising enzyme variant for practical use is the I369F mutant, where the rate of CBZ turnover was increased two-fold and the S_{50} value obtained with the use of Eq. 4.2 remained unaffected p. 94). Moreover, the CBZ epoxidation kinetics showed that the turnover at 100 μM and 50 μM CBZ is 2.2- and 2.7-fold that of the wild type, respectively (see Table 9 on p. 92).

The two CYP3A4 mutants, I369F and I369L, exhibited increased affinities to bromocriptine (BCT; see Table 11, chapter 5, on p. 114). The K_D of the mutants I369F and I369L was reduced 2.5-fold and 1.5-fold compared to the wild type, respectively. For further exploration of alterations in substrate affinities in the mutants, we performed titrations of the I369F mutant with the cooperative ligands testosterone (TST), estradiol (EST), and 7-benzyloxyquinoline (7BQ) and compared the data to CYP3A4 wild type. We also probed the activities of all generated mutants with the fluorogenic marker substrates 7BQ and BOMR in a screening assay. The results are discussed with respect to the potential application of the generated enzyme variants to drug detection and drug monitoring.

[11] The Vademecum 2007 contains a list of therapeutic levels of many drugs (Institute of Clinical Chemistry, University Hospital Zürich, Switzerland).

7.1.2 RESULTS

Titrations of the CYP3A4 I369F mutant with cooperative substrates resulted in type-I spin shifts that were fit to the Hill equation for determination of the affinity parameter S_{50}. EST did not induce a spectral transition that was sufficient for the analysis. The fitting parameters are presented in Table 18 below and compared to the results of the titrations of the wild-type enzyme. The S_{50} parameter for the titrations with TST, 7BQ, and BCT of the I369F mutant was, on average, 2.1 times smaller than the wild type. The titrations were not performed with ERY, as this non-cooperative ligand does not induce a type-I transition in the wild-type enzyme (see chapter 5).

Table 18: Comparison of investigated ligand affinities to CYP3A4 wild type and the I369F mutant.*

		Fitting Results			
Substrate		**S_{50}, µM**	**Spin Shift**	***h***	**HS_{Fin}**
Testosterone	**w/t**	56 ± 14	0.45 ± 0.02	1.15 ± 0.08	0.59 ± 0.03
	I369F	28 ± 10	0.21 ± 0.03	1.2 ± 0.3	0.67 ± 0.01
Estradiol	**w/t**	34 ± 6	0.18 ± 0.02	1.22 ± 0.07	0.32 ± 0.02
	I369F	-	-	-	-
7-Benzyloxy-quinoline	**w/t**	72 ± 17	0.36 ± 0.03	1.70 ± 0.08	0.54 ± 0.01
	I369F	40 ± 5	0.17 ± 0.02	1.58 ± 0.14	0.62 ± 0.03
		K_D, µM	**Spin Shift**		**HS_{Fin}**
Bromocriptine[§]	**w/t**	0.6 ± 0.2	0.48 ± 0.05		0.62 ± 0.02
	I369F	0.25 ± 0.07	0.25 ± 0.03		0.70 ± 0.02

*The titration data with the cooperative substrates testosterone, estradiol, and 7-benzyloxyquinoline were fit to the Hill equation for the comparison of the affinity parameters. [§] The bromocriptine titration data were presented in chapter 5 (see p. 114) and are shown here for the completeness of the data. The values given in the table represent the mean values of at least three experiments, and the "±" values show the respective confidence interval calculated for $p = 0.05$.

The series of spectra obtained upon titration of the CYP3A4 I369F mutant with testosterone, estradiol, and 7-benzyloxyquinoline are shown in Figure 56, Figure 57, and Figure 58, respectively.

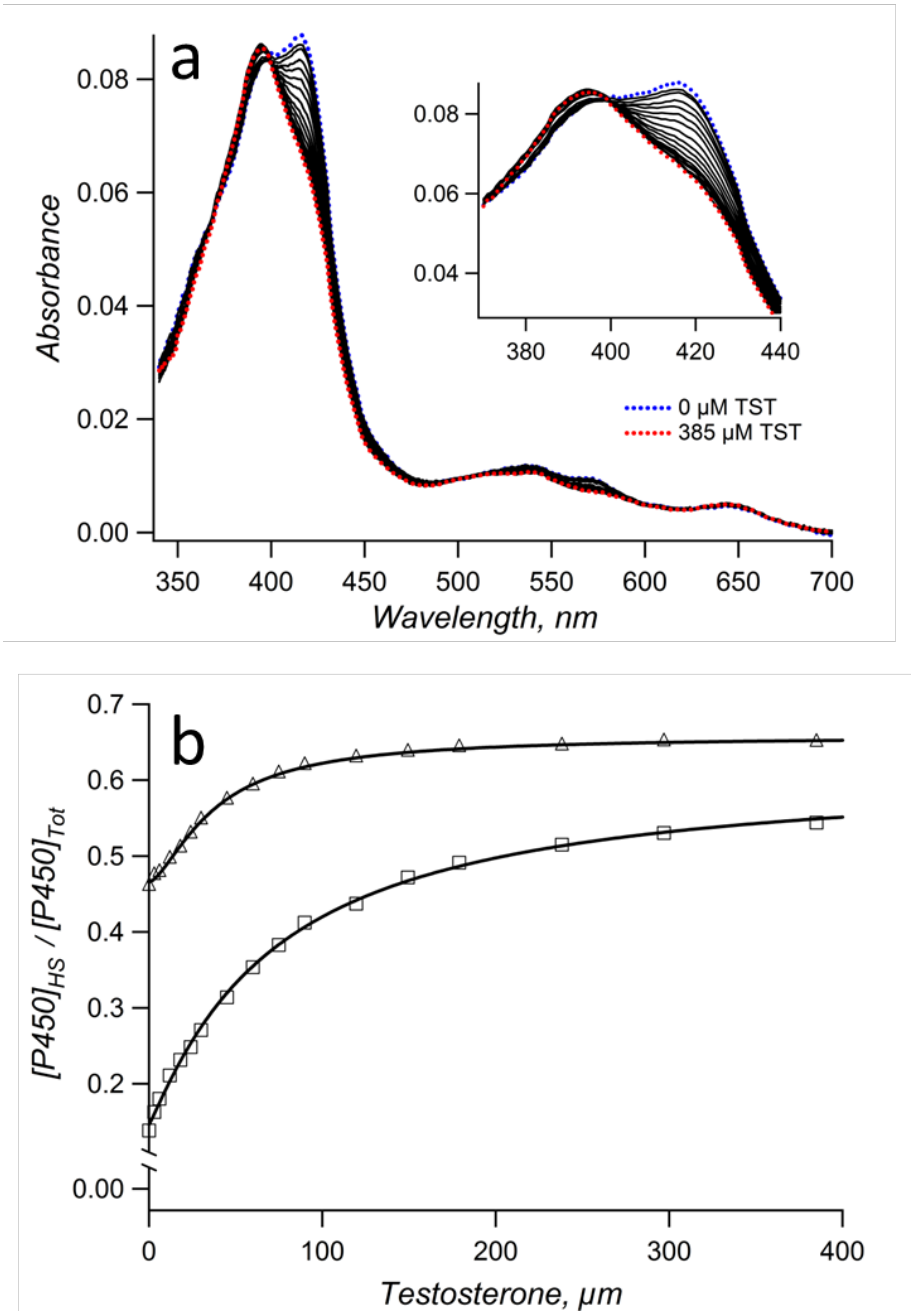

Figure 56: Titration of the CYP3A4 I369F mutant with testosterone (TST). Panel (a) shows the spectral series of the titration with the substrate and a zoom into the peak of the Soret band in the inset. Panel (b) represents a comparison between the titrations of the I369F mutant (triangles) and of the CYP3A4 wild type (squares). The parameters from the fitting of the Hill equation are shown in Table 18.

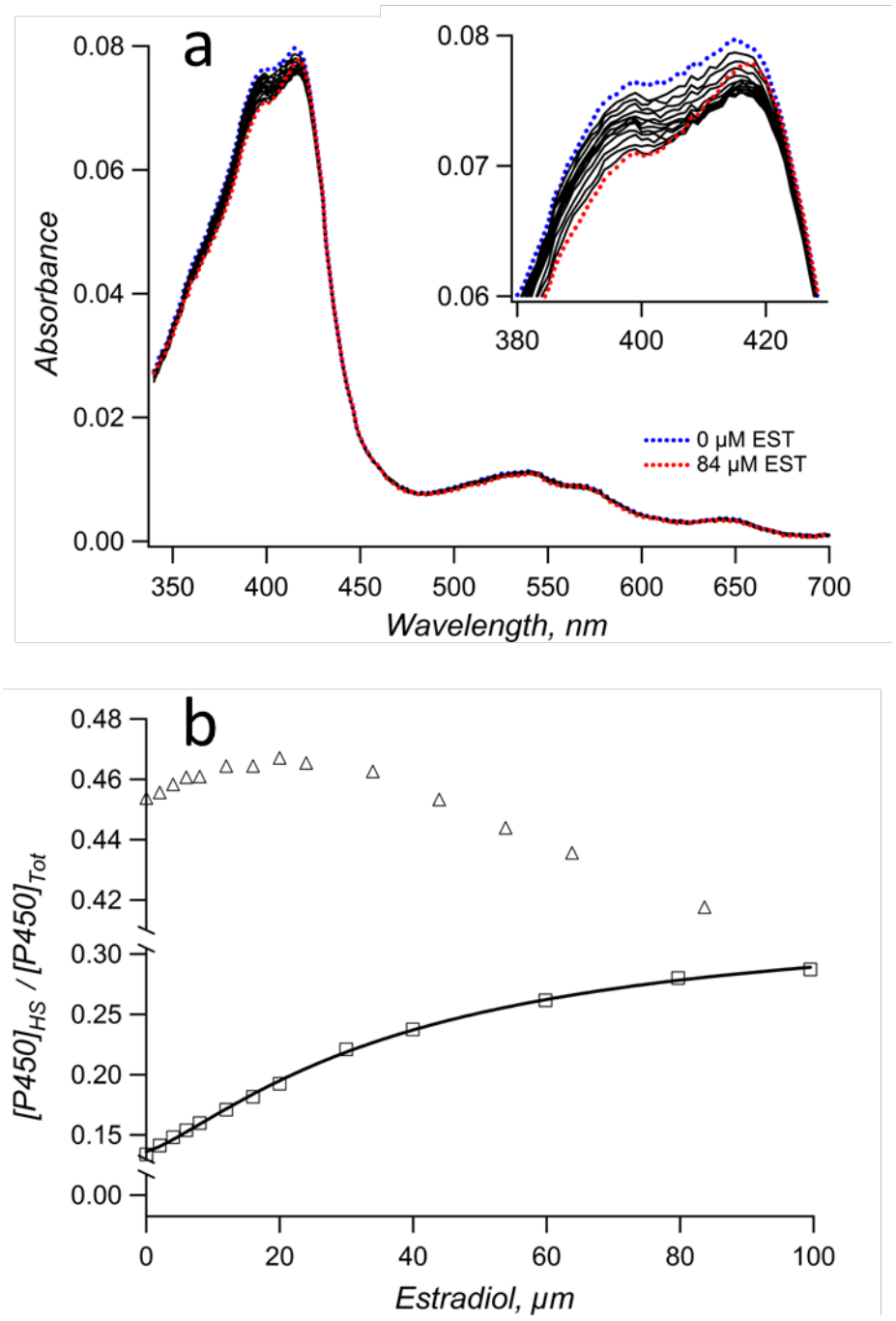

Figure 57: Titration of the CYP3A4 I369F mutant with estradiol (EST). Panel (a) shows the spectral series of the titration with the substrate and a zoom into the peak of the Soret band in the inset. Panel (b) represents a comparison between the titrations of the I369F mutant (triangles) and of the CYP3A4 wild type (squares). The parameters from the fitting of the Hill equation are shown in Table 18. The analysed spin shift in the I369F mutants was not sufficient for the determination of affinity parameters.

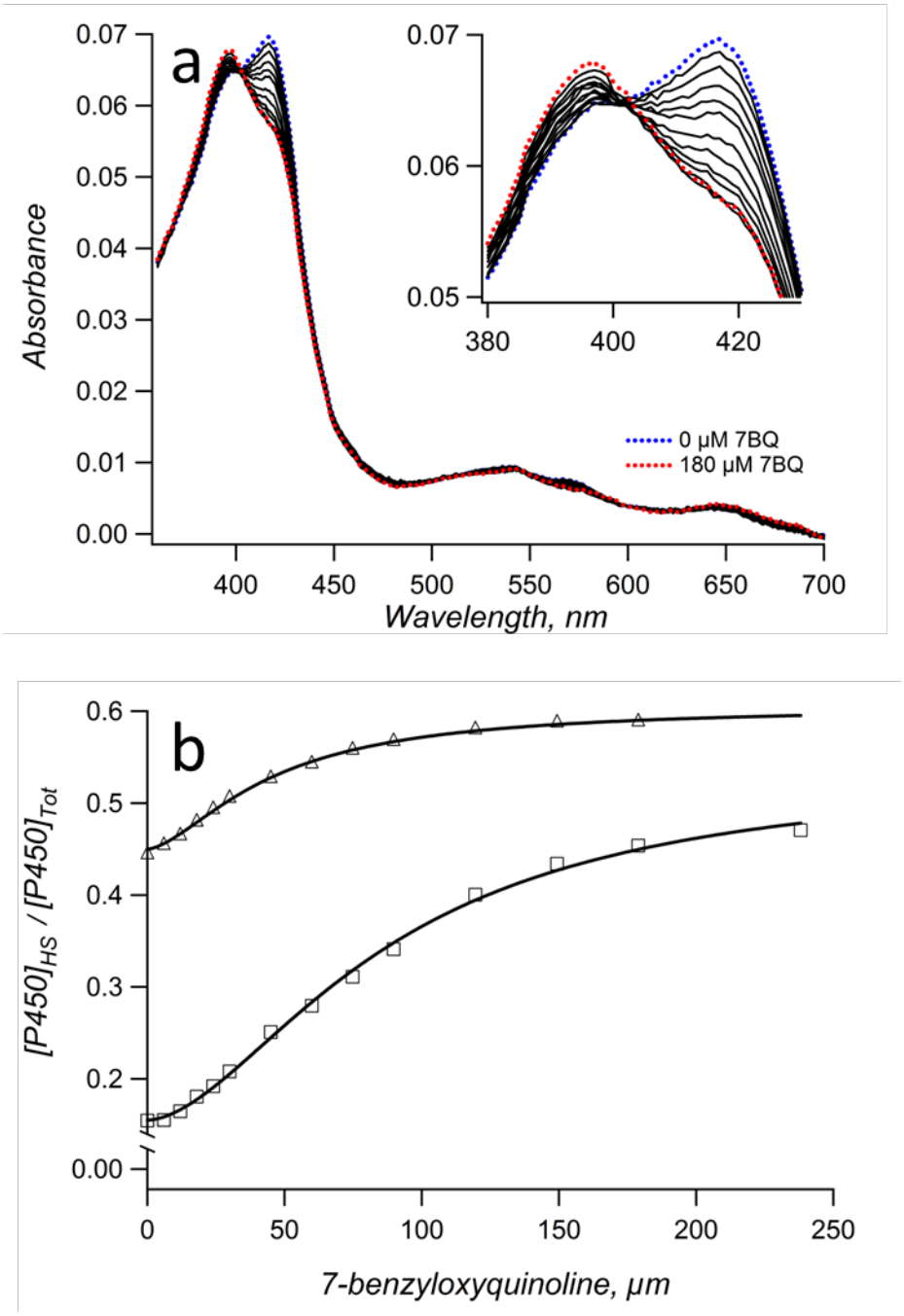

Figure 58: Titration of the CYP3A4 I369F mutant with 7-benzyloxyquinoline (7BQ). Panel (a) shows the spectral series of the titration with the substrate and a zoom into the peak of the Soret band in the inset. Panel (b) represents a comparison between the titrations of the I369F mutant (triangles) and of the CYP3A4 wild type (squares). The parameters from the fitting of the Hill equation are shown in Table 18.

Cytochrome P450-based biosensors measure redox cycling, more precisely the consumption of electrons by the P450 enzymes that are directly "plugged" into the electrodes. The enzymatic activity in solution may therefore give more direct information about the sensitivity of a corresponding biosensor. For instance, in a recent report, Taurino and coworkers compared the

enzyme kinetics of L-lactate oxidases to electrochemical studies. They reported similar substrate-dependencies from the spectrophotometric detection of product formation and the amperometric signal of the electrode (*185*). We therefore studied the activity of all expressed mutants and the wild-type enzyme in a kinetic assay that detects the turnover of a fluorogenic substrate. The conditions for these assays are described in the methods section on p. 51. Specifically, we measured the turnover of the CYP3A4 substrates 7BQ and the resorufin derivative Vivid® BOMR. The turnover measurements of the two substrates monitored on a multi-well plate reader were specified in absorbance units min^{-1} and normalized with respect to the turnover of the wild type. The activities towards the substrates 7BQ and BOMR of the individual CYP3A4 mutants were determined at concentrations of 5 μM and 3 μM, respectively, and are compared in Figure 59. These concentrations represent the typical conditions employed for the screening of enzymatic activity, e.g. in inhibition assays.

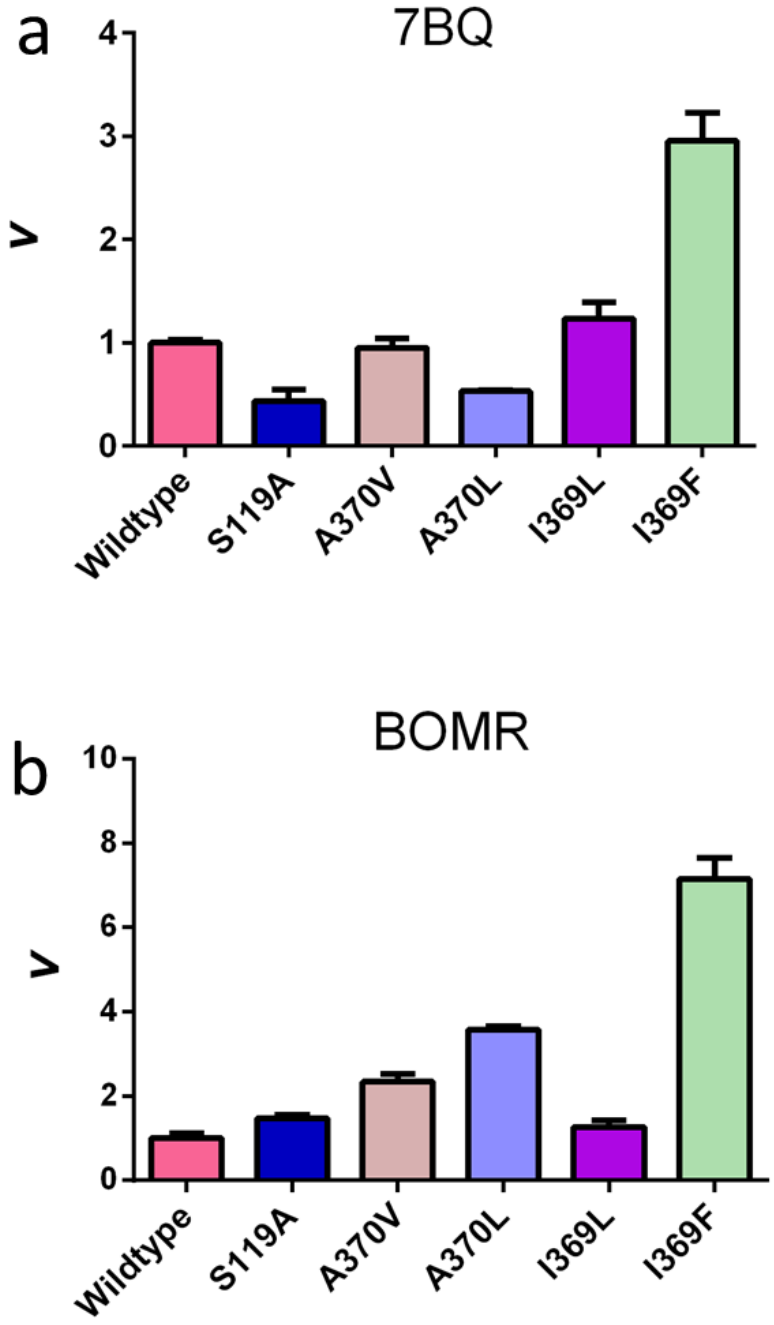

Figure 59: Turnover of the fluorogenic marker substrates (a) 7BQ and (b) BOMR by the generated mutants. The obtained activities in ΔAbs min^{-1} were normalized and expressed in units of wild-type turnover. The bars represent show the mean values of the measurements that were performed in triplicates, error bars represent the standard deviations.

The most interesting result from these assays are the markedly increased activities for the I369F mutant, which amounted to ca. 3-fold and 7-fold wild-type activity for 7BQ and BOMR, respectively.

7.1.3 DISCUSSION

In order to compare the relative affinities of CYP3A4 wild type and the I369F mutant, we recorded series of spectra for the titration of the two enzymes with ligands that show either sigmoidal or regular non-cooperative binding behavior. In our analysis of the series of absorbance spectra recorded upon titration with the ligands BCT, 7BQ, and TST, the substrates show on average double the affinity for the CYP3A4 I369F mutant with respect to the wild-type enzyme. In some cases, no reproducible values for the affinity constant for both enzymes could be determined and the affinities could thus not be compared. This was the case with the substrates ERY and EST, which did not induce a type-I spin shift in the wild-type enzyme and the I369F mutant, respectively. The 2-fold increase in affinity is yet to be explained. However, the simulations presented in chapter 4 suggest that the phenylalanine introduced by the I369F mutation in the vicinity of the active site projects further towards the Phe304 residue of the opposite I-helix (Figure 40 on p. 106). The phenylalanine substitute may block the free space adjacent to the active site that is available to non-productive substrate binding in the wild-type enzyme. It is plausible that this confinement causes a channeling of the substrates towards the heme iron (or the oxidizing species of the active site), and a displacement of the distal water ligand.

It is of interest to discuss the structural basis that allows the I-helix to adopt a strong kink as seen in MD simulations of the I369F mutant shown in chapter 4 (Figure 39, p. 105). This astonishing feature was only found in one of five MD simulations of the CYP3A4 I369F-$(CBZ)_2$ complex and therefore may be purely coincidental. However, it can be assumed as a possible structural constraint on this helix induced by the I369F mutation. In some X-ray structures of cytochromes P450, a functionally important water molecule is located between the highly conserved residues of the I-helix Ala305 and Thr309 that line the active site (*38*). The two conserved residues are located near the distal face of the heme ring. Indeed, in most bacterial structures of cytochromes P450, a water molecule has been identified inside the I-helix in this region. In some of the structures, the water molecule interacts with the side chain of a threonine of the I-helix. Most importantly, this causes an expansion of the helical groove and induces a kink that is characteristic for this helix in cytochromes P450. (*38, 186*). Although no water molecule was resolved in the first published CYP3A4 structure, a moderate kink in the I-helix is still present (*38*). In a CYP3A4 crystal structure published in the same year (2004), a water molecule that is in hydrogen bonding distance both to the backbone carbonyl oxygen of Phe304 and Glu308 (Figure 60) is resolved (*187*). Glu308 is another highly conserved residue that is (together with Thr309)

thought to position a water molecule for proton transfer to the reduced oxygen intermediates bound to the heme (*187*).

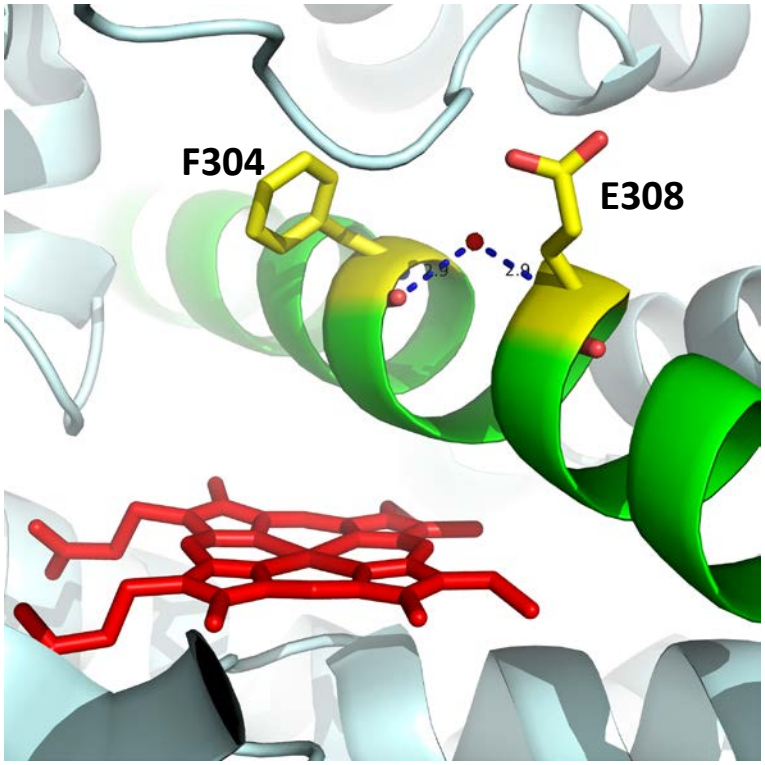

Figure 60: Structurally important water molecule in CYP3A4 X-ray structure 1TQN (*187*). The oxygen atom of water is equidistant (2.9 Å) from each carbonyl oxygen atom of Phe304 and the amide nitrogen atom of Glu308 of the I-helix (green). The heme is shown in red (structure reproduced in PyMol).

Interestingly, the pronounced kink that is found in one of the simulations of the I369F mutant with two carbamazepine molecules (chapter 4, Figure 39, p. 105) is accompanied by the disruption of the hydrogen bond between the side chain of Thr309 and the carbonyl oxygen of Ala305, which is present in the X-ray structure of the metyrapone-CYP3A4 complex (Figure 61a) (*38*). In the simulation of the I369F mutant, the β-hydroxyl group of Thr309 is shifted away from Ala305, but is in close distance to the carbonyl oxygen of the backbone of Phe304. This altered hydrogen bonding pattern likely permits the intrinsically destabilized conformation with the pronounced kink in the helix (Figure 61b).

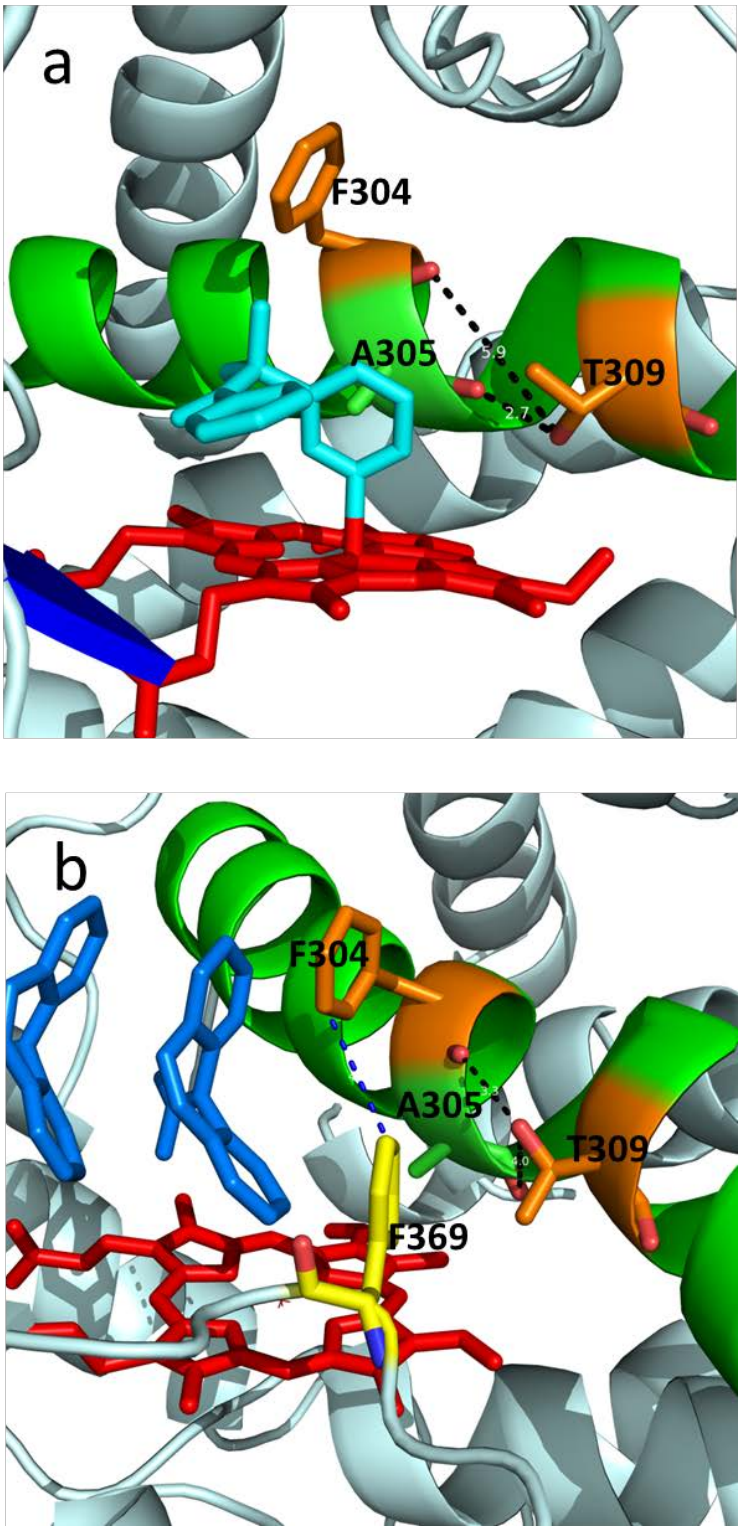

Figure 61: Structure of the CYP3A4-metyrapone (light blue) complex (a) compared to the largest cluster representative of the MD simulation of CYP3A4 with two carbamazepine molecules (marine) bound (b). In panel (a), Thr309 is hydrogen-bonded to the backbone of Ala305, whereas the interaction is disrupted and Ala305 replaced by Phe304 for side chain-backbone interactions in panel (b). Thr309 and Phe304 of the I-helix (green) are shown in orange, Phe369 and Ala370 in the I369F mutant are shown in yellow. The figure in (b) is based on the coordinates obtained from the simulations by T.K. (Chapter 4).

The 7-fold increase in the turnover kinetics of CBZ, BOMR, and 7BQ in the I369F mutant at low substrate concentrations is unlikely to be explained solely based on the moderate 2-fold increase in affinity. It may however result from a combination of the mutually reinforcing effects of increased substrate affinity and eased reduction of the iron (III) heme due to the high proportion of high-spin P450 in the I369F mutant in the absence of substrate. In conclusion, we have generated a CYP3A4 mutant that exhibits increased affinity and/or higher turnover to a broad spectrum of structurally different substrates and ligands. The I369F variant may be coupled ("plugged" (*188*)) as a recognition element to the electrodes of cytochrome P450-based sensors for drug monitoring. This mutant is expected to contribute to the development of cytochrome P450 biosensors with improved sensitivity to and detection capability of a broad spectrum of drugs that are substrates of the highly promiscuous CYP3A4. Yet, the actual relationships between the faradaic current to the electrodes and the enzymatic turnover are barely known. Therefore, further assessment of the utility of CYP3A4 for the use in drug detection requires investigations with the enzyme immobilized and coupled on an electrode surface.

7.2 KINETICS OF DITHIONITE-DEPENDENT REDUCTION OF CYP3A4 POINT MUTANTS

7.2.1 INTRODUCTION

In the last two decades, cooperativity in cytochromes P450 and its implications for drug-drug interactions have attracted increasing interest. Studies of the mechanistic basis of cooperativity focused to a large part on cytochrome P450 3A4 (CYP3A4) that metabolizes a broad range pharmaceutical drugs. Evidence for the presence of persistent conformational heterogeneity in the total CYP3A4 enzyme pool has accumulated, such that this divergence into functionally diverse, stable populations was assumed to be key to the complete understanding of the mechanisms of cooperativity (*67, 81, 189*). The divergence of the enzyme into several stable subpopulations with different functional properties is required to be considered for understanding the mechanism of cooperativity. Due to very slow transitions between the populations of distinct conformers, the distribution of the enzyme between these conformers stays constant within the time-frame of most experiments. The formation of cytochrome P450 oligomers in the microsomal membrane is believed to be a most probable explanation for persistent conformational heterogeneity (*105*). Even though the formation of oligomers is primarily a determinant for the competition of individual P450

molecules for NADPH-P450 reductase (CPR), it is known to affect other functional properties of the microsomal monooxygenases.

Some evidence for oligomerization in solution is given by the fact that CYP3A4 (57 kDa) can be concentrated above membranes of a molecular weight cut-off of 100 kDa without passing through the membrane. Moreover, while substrates induce an almost complete spin-shift of > 90% in monomerized CYP3A4, for instance in enzyme incorporated as monomers into nanodiscs (a protein scaffold for co-integration of membrane proteins with lipids)(*56, 86, 190*), the total high-spin shift induced in CYP3A4 in solution is limited and usually does not increase to fractions >70% of total cytochrome P450 (see chapters 5-7). In studies of pressure-induced transitions of CYP2B4, only 65 – 70% of the enzyme was susceptible to a pressure-induced P450 → P420 transition (*70, 131*). Such non-uniform behaviour disappears upon monomerization of cytochrome P450 upon treatment with detergent. Oligomerization may lead to differences between the oligomer subunits in their interaction with substrates or sensitivity for pressure-induced inactivation (P450 → P420 transition) (*105*).

In their work, Davydov and coworkers demonstrated important differences in the kinetics of reduction of CYP3A4 by $Na_2S_2O_4$. Reduction by dithionite is used in routine quantification of cytochrome P450 (see chapters 3 and 5) (*31*).

Here we apply our generated CYP3A4 site-directed mutants to studies involving rapid mixing of the enzymes with a dithionite-containing solution to monitor the reduction kinetics in solution. The overall stoichiometry of the reaction that takes place upon mixing in the chamber of the stopped-flow is:

$$Fe^{3+} + SO_2^{\square -} + CO \rightarrow Fe^{2+} \cdots CO + SO_2 \qquad (7.1)$$

Since the accessibility of water to the heme iron appears to be restricted in some of the mutants (predominantly I369F and S119A), we assumed that the investigations may add some important insight into the relevance of the active site amino acids to the native function of CYP3A4.

7.2.2 RESULTS

The kinetics of the reaction were determined via the appearance of the Soret peak of the iron (II) cytochrome P450 3A4 that was centred at 448 nm. The absorbance at 448 nm of the dithionite-dependent reduction reaction is shown as a function of time in Figure 62. Figure 62a shows the evolution of the absorbance in the reactions with the individual mutants, while Figure 62 compares

the normalised relative changes. The results of the fits to a sum of three exponentials are shown in Table 19. The results for wild-type CYP3A4 are in good agreement with previously published data (*105*). We obtained an equal distribution between the species that react with the slow, intermediate, and fast exponential phase of the reduction. Mutants I369F and A370L showed the slowest overall reduction kinetics and we obtained the highest proportion of slow phase in the two mutants I369F and S119A. These mutants both exhibit ca. equivalent proportions of low- and high-spin cytochrome P450 in absence of substrate.

To the naked eye, it appears that S119A is the most peculiar case due to the very fast partial reduction of the enzyme pool that is followed by comparably slow reduction of the rest of the enzymes. This leads to a crossing of the curves in Figure 62b, in which the total changes in absorbance are normalized. Apparently, the difference between the rates of reduction of high-spin and low-spin P450 is particularly strong in this mutant.

Table 19: Kinetic parameters of dithionite-dependent reduction of CYP3A4 wild type and mutants.*

Mutant	k_1	k_2	k_3	F_1	F_2	F_3
w/t	3.6 ± 0.3	0.56 ± 0.02	0.095 ± 0.005	0.36 ± 0.03	0.31 ± 0.01	0.34 ± 0.02
S119A	4.7 ± 0.5	0.43 ± 0.02	0.048 ± 0.002	0.24 ± 0.02	0.173 ± 0.005	0.59 ± 0.01
I369F	1.5 ± 0.4	0.30 ± 0.04	0.058 ± 0.06	0.11 ± 0.02	0.32 ± 0.03	0.57 ± 0.05
I369L	3.7 ± 0.2	0.59 ± 0.04	0.099 ± 0.05	0.433 ± 0.008	0.291 ± 0.005	0.28 ± 0.01
A370L	1.8 ± 0.3	0.36 ± 0.02	0.066 ± 0.02	0.11 ± 0.01	0.39 ± 0.01	0.50 ± 0.01
A370V	2.9 ± 0.9	0.47 ± 0.06	0.086 ± 0.08	0.19 ± 0.02	0.40 ± 0.01	0.41 ± 0.02

*The values given in the table represent the mean values at least three experiments, and the "±" values show the respective confidence interval calculated for $p = 0.05$.

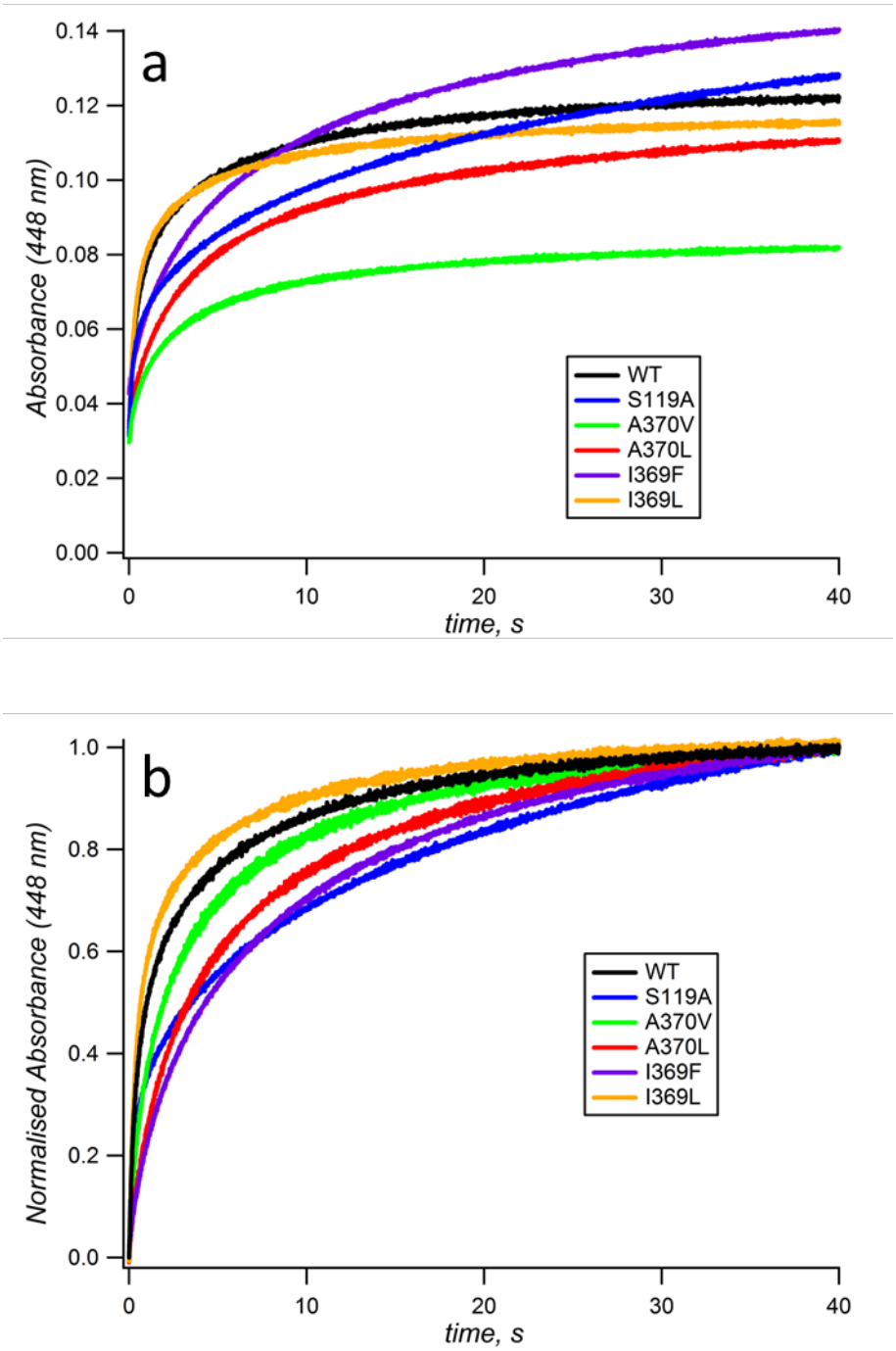

Figure 62: Kinetics of dithionite-dependent reduction of CYP3A4 wild type and mutants. In panel (a), the absorbance at λ = 448 nm is plotted against time. In panel (b), the total Δ absorbance is normalised and plotted against time.

7.2.3 DISCUSSION

It was demonstrated by Hintz and Peterson that the kinetics of reduction of substrate-free cytochrome P450 101 ($P450_{cam}$) by dithionite obeys pseudo-first order kinetics. (*191*). Our data presented could be fit to the sum of three exponential functions which are thought to correspond to

the pseudo-first order reaction of three different species present in the enzyme pool. The fitting to the sum of two exponential functions lead to systematic deviations between the spectroscopy data and the fits. A model based on the existence of the enzyme in only two species such as the high-spin and low-spin iron (III) cytochrome P450 is therefore not sufficient to explain the data. Hence, at least two functionally diverse populations with different functional properties are assumed to be present in solution, which are formed in the natural environment in the lipid bilayer (*78*).

In the work reported on CYP101, binding of the substrate camphor strongly decreased the rate constant of reduction. This finding was attributed to the restriction of the access of the charged reducing species $SO_2^{\bullet-}$ to the P450 heme iron upon ligand binding (*191*). Later, it was shown by Davydov and co-workers that the binding of type-I ligands perturbs the distribution between the species F_1 and F_3 that correspond to the fractions of the total enzyme which are reduced with reaction rates k_1 and k_3 (fast and slow phases), respectively. Type-I transition led to a shift towards the species F_3, and the content of high-spin cytochrome P450 CYP3A4 correlated with the fractions of the slow reduction rate of the iron (III) heme (*105*). In our work, the mutations S119A and I369F show similarly high proportions of the F_3 species that reacts at the slow rate k_3 ((59 ± 1)% and (57 ± 5)%, respectively), whereas the proportion of the fast rate is strongly decreased with respect to the wild-type enzyme.

Figure 63 shows that there some correlation between the high-spin proportion in the total cytochrome P450 pool and the slow reaction rate. There are however other factors adding to the complexity of this system, such as the unknown influence of the amino acid substitutions on the iron (III) → iron (II) reduction rates of the different (spin) species in the sample. For quantitative statements, it may be tested whether global fitting of a joint set of rate constants to all of the data elucidates better correlations between the spin proportions and the fractions F_i in the model. Due to the fact that this mutant exhibits inverse spin shift upon ligand binding (see chapter 5), the S119A mutant offers the possibility for an interesting experiment to explore whether the presence of a ligand in the active site or rather the spin state of the heme iron in cytochrome P450 is critical for the redistribution between the fast and slow kinetic phases of the reduction. If the main effect is assumed to stem from the change in spin equilibrium, an increase in the fast phase of the reaction is expected. This is however not true if the presence of a ligand is assumed to be decisive for the reduction of the rate constant.

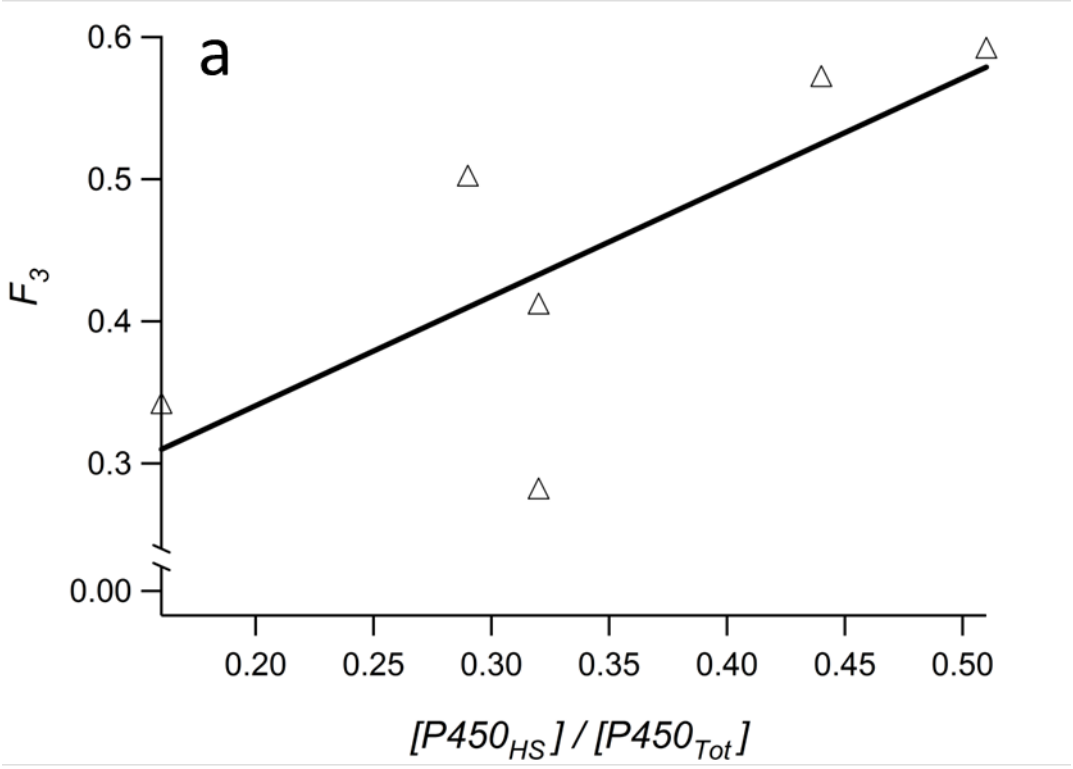

b

Mutant	F_3	HS
Wildtype	0.34	0.16
S119A	0.59	0.51
I369F	0.57	0.44
I369L	0.28	0.32
A370L	0.50	0.29
A370V	0.41	0.32

Figure 63: The fraction of the slow phase of dithionite-dependent reduction (F_3) is plotted against the high spin content in the substrate-free enzyme mutants. A correlation coefficient of $\rho^2 = 0.56$ was obtained. The values for the fraction of the slow phase of the reduction and the HS content are shown in panel (b).

8 CONCLUSION

Cytochrome P450 3A4 is the most abundant cytochrome P450 in the microsomes of human liver and metabolizes > 50% of all pharmaceutical drugs. It exhibits numerous forms of atypical kinetics that can lead to drug-drug interactions and adverse drug reactions in drug therapy, which is an issue of high importance for the pharmaceutical industry. More than 2000 papers that list the keyword CYP3A4 have been published in 2013, with a tendency to rise each year. Some functional features of this enzyme remain unresolved. Complex functional aspects of CYP3A4 were investigated in this thesis. In our study, we combined molecular dynamics simulations, performed within a scientific collaboration, to generate CYP3A4 mutants *via* site-directed mutagenesis, with biophysical and biochemical techniques for the analysis of the generated mutants. This strategy proved to be useful for the production of enzyme variants with altered functional properties, the study of which was presented in this thesis.

CYP3A4 S119A differs from the wild type by a hydroxyl group. The removal of this functional group produces an enzyme that exhibits spin transitions that occur in the opposite direction of the most frequent transition in cytochromes P450 upon substrate binding (type-I transition). The mutant I369F exhibits higher affinity for several structurally different ligands than the wild type and shows higher turnover rates of some substrates at low concentrations. One of the key findings in this work is that the five generated enzyme mutants differ in cooperative kinetics and substrate inhibition in the epoxidation reaction of CBZ. Whereas low affinity to CBZ goes together with cooperative CBZ epoxidation kinetics, an increased affinity results in a more pronounced substrate inhibition than in the wild-type enzyme.

Most of the numerous substrates of CYP3A4 bind weakly to the enzyme and give rise to low turnover numbers. Some determinants for improved binding of certain ligands are known from cases where X-ray structures of CYP3A4-ligand complexes have been determined. The preference of CYP3A4 for certain substrates over others is, however, poorly predictable, particularly due to the large flexibility in some parts of the enzyme. We expected based on structural data and MD simulations that substitutions of the amino acid residues Ser119, Ile369, and Ala370 affect the binding of carbamazepine and most likely many other substrates. However, two of the mutations, S119A and I369F, revealed entirely unforeseen changes in the enzyme.

The largest reduction in the affinity for bromocriptine ensues from the S119A mutation. For this mutant, it was reported that the association of a class of peptidomimetic analogues of the drug ritonavir does not lead to a rise in thermal stability of the enzyme, and that the kinetics of ligand association with these drugs are perturbed (*174*). The water network in the active site of this mutant must be disrupted, which follows from its inverse spin shift seen upon titration with a type-I substrate and its existence to high proportions in the high-spin state in the absence of substrate. The

findings of inverse and bidirectional spin shifts are unique to this mutant and hopefully will provide an incentive for other researchers to explore the challenging question about the exact mechanism of this transition.

Since the appearance of the first crystal structures of CYP3A4 in the year 2004 (*38, 187*), few mutants of CYP3A4 have been explored. This is also a result of the fact that the identified single nucleotide polymorphisms in CYP3A4 studied to date do not translate into very important inter-individual variability in metabolism *in vivo.* Even though 28 polymorphisms of CYP3A4 exist, their implications for human metabolism are less important when compared to the polymorphisms of the major polymorphic microsomal cytochromes P450, examples of which are CYP2D6 and 2C19 (*192*). Induction of expression and drug-drug interactions are however factors that strongly affect CYP3A4-based metabolism. The many types of atypical kinetics exhibited by CYP3A4 contribute to the variability in the metabolism *in vivo*.

Further progress in the development of cytochrome P450-based biosensors is desirable for drug detection and for therapeutic monitoring similar to the one with glucose sensors that have revolutionized diabetes care. CYP3A4 exhibits a large flexible binding pocket suitable to accommodate large molecules (e.g. the 734 kDa erythromycin or the 1200 kDa cyclosporine). The development of a mutant that is specific for a small molecule like carbamazepine for the incorporation into CYP3A4 biosensors requires a substantial reduction in the volume of the active site. Most likely, this implicates several rounds of mutagenesis combined with the verification of the activity of the generated mutants, and finally a design of the active site to specifically accommodate the desired drug. Retention of normal function in a CYP3A4 variant that has been extensively mutagenized is unlikely in the light of the drastic changes that are exerted already by minor modifications of single amino acids, as demonstrated in this thesis. Minor substitutions (such as the exchange of serine for an alanine in the S119A mutant) and possibly even conservative substitutions may strongly affect enzyme function. The generation of a substrate-specific enzyme variant from a very promiscuous wild-type enzyme that metabolizes hundreds of substrates would be extremely challenging. Therefore, the design of a specific mutant based on a bacterial cytochrome P450 with a narrow native substrate range and a smaller binding pocket, e.g. cytochrome $P450_{cam}$, appears to constitute a more promising approach.

With the mutant I369F we were able to show that it is possible to modulate the affinities of CYP3A4 for substrates. I369F shows a ~3-fold higher turnover of carbamazepine to the epoxide product than the wild type at a concentration of 50 μM substrate. The mutant metabolizes the resorufin derivative BOMR ca. 7 times faster than the wild type at 3 μM substrate. The turnover of 7-benzyloxyquinoline is about 3 times that of wild type CYP3A4 at [7BQ] = 5 μM. In addition to

the results from turnover studies, I369F binds all tested substrates with higher affinity than the wild type. More data could be gathered, but a tendency is already clear: I369F appears to be a mutant that exhibits a higher affinity to several structurally different classes of small molecule CYP3A4 substrates and shows increased rates of turnover at low (sub-K_M) substrate concentration. Rationalization of this affinity shift based only on the paradigm of enzyme-substrate interaction (‘*induced fit*’) appears problematic, since the I369F mutant exhibits a lower affinity constant to structurally diverse substrate classes. In CYP3A4, also other determinants are key to ligand association, for instance flexible domains that allow the proper arrangement of ligands in the binding pocket (*45*), or an efficient direction of the ligand through the substrate access channel to the deeply buried active site. It remains unclear whether a putative switch in the hydrogen bonding pattern and the resulting predicted kinked I-helix of CYP3A4 are actually relevant to the structure of CYP3A4 I369F. Such a conformational change was obtained in only a fraction (20%) of all snapshots of the performed MD simulations of a I369F-$(CBZ)_2$ complex. However, it may constitute a possible conformational switch. The kinked I-helix along with the extended side chain of the phenylalanine introduced at position 369 could entail a decrease in the volume of the active site and thus offer a tighter fit for small ligand molecules.

The development of cytochrome P450-dependent biosensors for drug detection based on the CYP3A4 I369F mutant may seem problematic due to substrate inhibition. A direct consequence from substrate inhibition is that one value for the response of the sensor corresponds to two substrate concentrations. This problem could be solved by the implementation of several compartments on the sensor, which would each contain a different CYP3A4 mutant as the substrate recognition element. Each of the selected mutants should exhibit a different range of linear response to substrate that would optimally mutually overlap. With such an approach based on a combination of building blocks into a single sensor, unambiguous allocation between signal and substrate concentrations would be possible. It remains in the hands of both engineers and biochemists to build new biosensors that are sufficiently sensitive to detect drugs at therapeutic levels. The development of such biosensors would pave the way for an application of this enabling technology in biomedicine and eventually in wearable devices for therapeutic drug monitoring in personalized medicine.

REFERENCES

1. Lewis, D. F. V. (2001) *Guide to cytochromes p450: Structure and function*, Taylor & Francis, London and New York.
2. Garfinkel, D. (1958) Studies on pig liver microsomes. I. Enzymic and pigment composition of different microsomal fractions, *Arch. Biochem. Biophys. 77*, 493-509.
3. Klingenberg, M. (1958) Pigments of rat liver microsomes, *Arch. Biochem. Biophys. 75*, 376-386.
4. Omura, T., and Sato, R. (1964) Carbon monoxide-binding pigment of liver microsomes. 2. Solubilization, purification, and properties *J. Biol. Chem. 239*, 2379-&.
5. Omura, T. (1999) Forty years of cytochrome p450, *Biochem. Biophys. Res. Commun. 266*, 690-698.
6. Mardis, E. R. (2008) The impact of next-generation sequencing technology on genetics, *Trends Genet. 24*, 133-141.
7. Schuster, S. C. (2008) Next-generation sequencing transforms today's biology, *Nat Meth 5*, 16-18.
8. Shendure, J., and Ji, H. (2008) Next-generation DNA sequencing, *Nat Biotech 26*, 1135-1145.
9. Mardis, E. R. (2008) Next-generation DNA sequencing methods, In *Annual review of genomics and human genetics*, pp 387-402.
10. Metzker, M. L. (2010) Sequencing technologies - the next generation, *Nat Rev Genet 11*, 31-46.
11. Sevrioukova, I. F., and Poulos, T. L. (2013) Understanding the mechanism of cytochrome p450 3a4: Recent advances and remaining problems, *Dalton Trans. 42*, 3116-3126.
12. Dus, K., Katagiri, M., Yu, C. A., Erbes, D. L., and Gunsalus, I. C. (1970) Chemical characterization of cytochrome p-450cam, *Biochem. Biophys. Res. Commun. 40*, 1423-1430.
13. Poulos, T. L., Finzel, B. C., and Howard, A. J. (1987) High-resolution crystal structure of cytochrome p450cam, *J. Mol. Biol. 195*, 687-700.
14. Ichikawa, Y., and Yamano, T. (1967) Reconversion of detergent- and sulfhydryl reagent-produced p-420 to p-450 by polyols and glutathione, *Biochim. Biophys. Acta - Bioenergetics 131*, 490-497.
15. Hanukoglu, I. (1996) Electron transfer proteins of cytochrome p450 systems, In *Advances in molecular and cell biology* (Bittar, E. E., Ed.), pp 29-56, Elsevier.
16. Reed, J. R., and Backes, W. L. (2012) Formation of p450-p450 complexes and their effect on p450 function, *Pharmacol. Ther. 133*, 299-310.
17. Jin, S., Makris, T. M., Bryson, T. A., Sligar, S. G., and Dawson, J. H. (2003) Epoxidation of olefins by hydroperoxo−ferric cytochrome p450, *J. Am. Chem. Soc. 125*, 3406-3407.
18. Davydov, R., Macdonald, I. D. G., Makris, T. M., Sligar, S. G., and Hoffman, B. M. (1999) Epr and endor of catalytic intermediates in cryoreduced native and mutant oxy-cytochromes p450cam: Mutation-induced changes in the proton delivery system, *J. Am. Chem. Soc. 121*, 10654-10655.
19. Denisov, I. G., Makris, T. M., and Sligar, S. G. (2001) Cryotrapped reaction intermediates of cytochrome p450 studied by radiolytic reduction with phosphorus-32, *J. Biol. Chem. 276*, 11648-11652.
20. Denisov, I. G., Makris, T. M., Sligar, S. G., and Schlichting, I. (2005) Structure and chemistry of cytochrome p450, *Chem. Rev. 105*, 2253-2278.

21. Rittle, J., and Green, M. T. (2010) Cytochrome p450 compound i: Capture, characterization, and c-h bond activation kinetics, *Science 330*, 933-937.
22. Schlichting, I., Berendzen, J., Chu, K., Stock, A. M., Maves, S. A., Benson, D. E., Sweet, B. M., Ringe, D., Petsko, G. A., and Sligar, S. G. (2000) The catalytic pathway of cytochrome p450cam at atomic resolution, *Science 287*, 1615-1622.
23. Vaz, A. D. N., McGinnity, D. F., and Coon, M. J. (1998) Epoxidation of olefins by cytochrome p450: Evidence from site-specific mutagenesis for hydroperoxo-iron as an electrophilic oxidant, *Proc. Natl. Acad. Sci. U.S.A. 95*, 3555-3560.
24. Chandrasena, R. E. P., Vatsis, K. P., Coon, M. J., Hollenberg, P. F., and Newcomb, M. (2003) Hydroxylation by the hydroperoxy-iron species in cytochrome p450 enzymes, *J. Am. Chem. Soc. 126*, 115-126.
25. Sheng, X., Zhang, H., Hollenberg, P. F., and Newcomb, M. (2009) Kinetic isotope effects in hydroxylation reactions effected by cytochrome p450 compounds i implicate multiple electrophilic oxidants for p450-catalyzed oxidations, *Biochemistry 48*, 1620-1627.
26. Newcomb, M., Zhang, R., Chandrasena, R. E. P., Halgrimson, J. A., Horner, J. H., Makris, T. M., and Sligar, S. G. (2006) Cytochrome p450 compound i, *J. Am. Chem. Soc. 128*, 4580-4581.
27. Sheng, X., Horner, J. H., and Newcomb, M. (2008) Spectra and kinetic studies of the compound i derivative of cytochrome p450 119, *J. Am. Chem. Soc. 130*, 13310-13320.
28. Sheng, X., Zhang, H., Im, S.-C., Horner, J. H., Waskell, L., Hollenberg, P. F., and Newcomb, M. (2009) Kinetics of oxidation of benzphetamine by compounds i of cytochrome p450 2b4 and its mutants, *J. Am. Chem. Soc. 131*, 2971-2976.
29. Ortiz de Montellano, P. R., (Ed.) (2005) *Cytochrome p450 - structure, mechanism, and biochemistry*, 3 ed., Kluwer Academic/Plenum Publishers, New York.
30. Wang, M., Roberts, D. L., Paschke, R., Shea, T. M., Masters, B. S. S., and Kim, J.-J. P. (1997) Three-dimensional structure of nadph–cytochrome p450 reductase: Prototype for fmn- and fad-containing enzymes, *Proc. Natl. Acad. Sci. U.S.A. 94*, 8411-8416.
31. Guengerich, F. P., Martin, M. V., Sohl, C. D., and Cheng, Q. (2009) Measurement of cytochrome p450 and nadph-cytochrome p450 reductase, *Nat. Protocols 4*, 1245-1251.
32. Kasper, C. B. (1971) Biochemical distinctions between the nuclear and microsomal membranes from rat hepatocytes: The effect of phenobarbital administration, *J. Biol. Chem. 246*, 577-581.
33. Xia, C., Hamdane, D., Shen, A. L., Choi, V., Kasper, C. B., Pearl, N. M., Zhang, H., Im, S.-C., Waskell, L., and Kim, J.-J. P. (2011) Conformational changes of nadph-cytochrome p450 oxidoreductase are essential for catalysis and cofactor binding, *J. Biol. Chem. 286*, 16246-16260.
34. Flück, C. E., Tajima, T., Pandey, A. V., Arlt, W., Okuhara, K., Verge, C. F., Jabs, E. W., Mendonca, B. B., Fujieda, K., and Miller, W. L. (2004) Mutant p450 oxidoreductase causes disordered steroidogenesis with and without antley-bixler syndrome, *Nat. Genet. 36*, 228-230.
35. Huang, N., Pandey, A. V., Agrawal, V., Reardon, W., Lapunzina, P. D., Mowat, D., Jabs, E. W., Vliet, G. V., Sack, J., Flück, C. E., and Miller, W. L. (2005) Diversity and function of mutations in p450 oxidoreductase in patients with antley-bixler syndrome and disordered steroidogenesis, *Am. J. Hum. Genet. 76*, 729-749.
36. Xia, C., Panda, S. P., Marohnic, C. C., Martásek, P., Masters, B. S., and Kim, J.-J. P. (2011) Structural basis for human nadph-cytochrome p450 oxidoreductase deficiency, *Proc. Natl. Acad. Sci. U.S.A. 108*, 13486-13491.
37. Guengerich, F. P. (1999) Cytochrome p-450 3a4: Regulation and role in drug metabolism, *Annu. Rev. Pharmacol. Toxicol. 39*, 1-17.

38. Williams, P. A., Cosme, J., Vinković, D. M., Ward, A., Angove, H. C., Day, P. J., Vonrhein, C., Tickle, I. J., and Jhoti, H. (2004) Crystal structures of human cytochrome p450 3a4 bound to metyrapone and progesterone, *Science 305*, 683-686.
39. Cupp-Vickery, J. R., and Poulos, T. L. (1995) Structure of cytochrome p450eryf involved in erythromycin biosynthesis, *Nat Struct Mol Biol 2*, 144-153.
40. Park, H., Lee, S., and Suh, J. (2005) Structural and dynamical basis of broad substrate specificity, catalytic mechanism, and inhibition of cytochrome p450 3a4, *J. Am. Chem. Soc. 127*, 13634-13642.
41. Khan, K. K., He, Y. Q., Domanski, T. L., and Halpert, J. R. (2002) Midazolam oxidation by cytochrome p450 3a4 and active-site mutants: An evaluation of multiple binding sites and of the metabolic pathway that leads to enzyme inactivation, *Mol. Pharmacol. 61*, 495-506.
42. Harlow, G. R., and Halpert, J. R. (1997) Alanine-scanning mutagenesis of a putative substrate recognition site in human cytochrome p450 3a4 - role of residues 210 and 211 in flavonoid activation and substrate specificity, *J. Biol. Chem. 272*, 5396-5402.
43. Wang, H., Dick, R., Yin, H., Licad-Coles, E., Kroetz, D. L., Szklarz, G., Harlow, G., Halpert, J. R., and Correia, M. A. (1998) Structure−function relationships of human liver cytochromes p450 3a: Aflatoxin b1 metabolism as a probe, *Biochemistry 37*, 12536-12545.
44. Harlow, G. R., and Halpert, J. R. (1998) Analysis of human cytochrome p450 3a4 cooperativity: Construction and characterization of a site-directed mutant that displays hyperbolic steroid hydroxylation kinetics, *Proc. Natl. Acad. Sci. U. S. A. 95*, 6636-6641.
45. Ekroos, M., and Sjögren, T. (2006) Structural basis for ligand promiscuity in cytochrome p450 3a4, *Proc. Natl. Acad. Sci. U.S.A. 103*, 13682-13687.
46. Denisov, I. G., Shih, A. Y., and Sligar, S. G. (2012) Structural differences between soluble and membrane bound cytochrome p450s, *J. Inorg. Biochem. 108*, 150-158.
47. Zhao, Y., White, M. A., Muralidhara, B. K., Sun, L., Halpert, J. R., and Stout, C. D. (2006) Structure of microsomal cytochrome p450 2b4 complexed with the antifungal drug bifonazole: Insight into p450 conformational plasticity and membrane interaction, *J. Biol. Chem. 281*, 5973-5981.
48. Sineva, E. V., Rumfeldt, J. A. O., Halpert, J. R., and Davydov, D. R. (2013) A large-scale allosteric transition in cytochrome p450 3a4 revealed by luminescence resonance energy transfer (lret), *PLoS ONE 8*, e83898.
49. Davydov, D. R., Rumfeldt, J. A. O., Sineva, E. V., Fernando, H., Davydova, N. Y., and Halpert, J. R. (2012) Peripheral ligand-binding site in cytochrome p450 3a4 located with fluorescence resonance energy transfer (fret), *J. Biol. Chem. 287*, 6797-6809.
50. Dabrowski, M. J., Schrag, M. L., Wienkers, L. C., and Atkins, W. M. (2002) Pyrene·pyrene complexes at the active site of cytochrome p450 3a4: Evidence for a multiple substrate binding site, *J. Am. Chem. Soc. 124*, 11866-11867.
51. Egnell, A.-C., Houston, B., and Boyer, S. (2003) In vivo cyp3a4 heteroactivation is a possible mechanism for the drug interaction between felbamate and carbamazepine, *J. Pharmacol. Exp. Ther. 305*, 1251-1262.
52. Yun, C.-H., Miller, G. P., and Guengerich, F. P. (2000) Rate-determining steps in phenacetin oxidations by human cytochrome p450 1a2 and selected mutants, *Biochemistry 39*, 11319-11329.
53. Fisher, M. T., and Sligar, S. G. (1985) Control of heme protein redox potential and reduction rate: Linear free energy relation between potential and ferric spin state equilibrium, *J. Am. Chem. Soc. 107*, 5018-5019.
54. Sligar, S. G., Cinti, D. L., Gibson, G. G., and Schenkman, J. B. (1979) Spin state control of the hepatic cytochrome p450 redox potential, *Biochem. Biophys. Res. Commun. 90*, 925-932.

55. Sligar, S. G. (1976) Coupling of spin, substrate, and redox equilibriums in cytochrome p450, *Biochemistry 15*, 5399-5406.
56. Nath, A., Atkins, W. M., and Sligar, S. G. (2007) Applications of phospholipid bilayer nanodiscs in the study of membranes and membrane proteins, *Biochemistry 46*, 2059-2069.
57. Das, A., Grinkova, Y. V., and Sligar, S. G. (2007) Redox potential control by drug binding to cytochrome p450 3a4, In *J. Am. Chem. Soc.*, pp 13778-13779.
58. Denisov, I. G., and Sligar, S. G. (2012) A novel type of allosteric regulation: Functional cooperativity in monomeric proteins, *Arch. Biochem. Biophys. 519*, 91-102.
59. Zhou, S.-F. (2008) Drugs behave as substrates, inhibitors and inducers of human cytochrome p450 3a4, *Curr. Drug Metab. 9*, 310-322.
60. Kempf, D. J., Marsh, K. C., Kumar, G., Rodrigues, A. D., Denissen, J. F., McDonald, E., Kukulka, M. J., Hsu, A., Granneman, G. R., Baroldi, P. A., Sun, E., Pizzuti, D., Plattner, J. J., Norbeck, D. W., and Leonard, J. M. (1997) Pharmacokinetic enhancement of inhibitors of the human immunodeficiency virus protease by coadministration with ritonavir, *Antimicrob. Agents Chemother. 41*, 654-660.
61. Koudriakova, T., Iatsimirskaia, E., Utkin, I., Gangl, E., Vouros, P., Storozhuk, E., Orza, D., Marinina, J., and Gerber, N. (1998) Metabolism of the human immunodeficiency virus protease inhibitors indinavir and ritonavir by human intestinal microsomes and expressed cytochrome p4503a4/3a5: Mechanism-based inactivation of cytochrome p4503a by ritonavir, *Drug Metab. Disposition 26*, 552-561.
62. Sevrioukova, I. F., and Poulos, T. L. (2010) Structure and mechanism of the complex between cytochrome p4503a4 and ritonavir, *Proc. Natl. Acad. Sci. U.S.A. 107*, 18422-18427.
63. Wells, A. V., Li, P., Champion, P. M., Martinis, S. A., and Sligar, S. G. (1992) Resonance raman investigations of *escherichia coli*-expressed *pseudomonas putida* cytochrome p450 and p420, *Biochemistry 31*, 4384-4393.
64. Martinis, S. A., Blanke, S. R., Hager, L. P., Sligar, S. G., Hui Bon Hoa, G., Rux, J. J., and Dawson, J. H. (1996) Probing the heme iron coordination structure of pressure-induced cytochrome p420cam, *Biochemistry 35*, 14530-14536.
65. Davydov, D. R., Hui Bon Hoa, G., and Peterson, J. A. (1999) Dynamics of protein-bound water in the heme domain of p450bm3 studied by high-pressure spectroscopy: Comparison with p450cam and p450 2b4, *Biochemistry 38*, 751-761.
66. Davydov, D. R., Petushkova, N. A., Archakov, A. I., and Hui Bon Hoa, G. (2000) Stabilization of p450 2b4 by its association with p450 1a2 revealed by high-pressure spectroscopy, *Biochem. Biophys. Res. Commun. 276*, 1005-1012.
67. Davydov, D. R., Halpert, J. R., Renaud, J. P., and Hui Bon Hoa, G. (2003) Conformational heterogeneity of cytochrome p450 3a4 revealed by high pressure spectroscopy, *Biochem. Biophys. Res. Commun. 312*, 121-130.
68. Perera, R., Sono, M., Sigman, J. A., Pfister, T. D., Lu, Y., and Dawson, J. H. (2003) Neutral thiol as a proximal ligand to ferrous heme iron: Implications for heme proteins that lose cysteine thiolate ligation on reduction, *Proc. Natl. Acad. Sci. U.S.A. 100*, 3641-3646.
69. Sun, Y., Zeng, W., Benabbas, A., Ye, X., Denisov, I., Sligar, S. G., Du, J., Dawson, J. H., and Champion, P. M. (2013) Investigations of heme ligation and ligand switching in cytochromes p450 and p420, *Biochemistry 52*, 5941-5951.
70. Davydov, D. R., Knyushko, T. V., and Hoa, G. H. (1992) High pressure induced inactivation of ferrous cytochrome p-450 lm2 (iib4) co complex: Evidence for the presence of two conformers in the oligomer, *Biochem. Biophys. Res. Commun. 188*, 216-221.
71. Atkins, W. M., Wang, R. W., and Lu, A. Y. H. (2001) Allosteric behavior in cytochrome p450-dependent in vitro drug−drug interactions: A prospective based on conformational dynamics, *Chem. Res. Toxicol. 14*, 338-347.

72. Denisov, I. G., Baas, B. J., Grinkova, Y. V., and Sligar, S. G. (2007) Cooperativity in cytochrome p450 3a4, *J. Biol. Chem. 282*, 7066-7076.
73. Davydov, D. R. (2011) Microsomal monooxygenase as a multienzyme system: The role of p450-p450 interactions, *Expert Opinion on Drug Metabolism & Toxicology 7*, 543-558.
74. Davydov, D. R., and Halpert, J. R. (2008) Allosteric p450 mechanisms: Multiple binding sites, multiple conformers or both?, *Expert Opin Drug Metab Toxicol 4*, 1523-1535.
75. Atkins, W. M. (2006) Current views on the fundamental mechanisms of cytochrome p450 allosterism, *Expert Opinion on Drug Metabolism & Toxicology 2*, 573-579.
76. Whitty, A. (2008) Cooperativity and biological complexity, *Nat Chem Biol 4*, 435-439.
77. Korzekwa, K. R., Krishnamachary, N., Shou, M., Ogai, A., Parise, R. A., Rettie, A. E., Gonzalez, F. J., and Tracy, T. S. (1998) Evaluation of atypical cytochrome p450 kinetics with two-substrate models: Evidence that multiple substrates can simultaneously bind to cytochrome p450 active sites, *Biochemistry 37*, 4137-4147.
78. Davydov, D. R., Davydova, N. Y., Sineva, E. V., Kufareva, I., and Halpert, J. R. (2013) Pivotal role of p450–p450 interactions in cyp3a4 allostery: The case of α-naphthoflavone, *Biochem. J. 453*, 219-230.
79. Frank, D. J., Denisov, I. G., and Sligar, S. G. (2011) Analysis of heterotropic cooperativity in cytochrome p450 3a4 using α-naphthoflavone and testosterone, *J. Biol. Chem. 286*, 5540-5545.
80. Tsalkova, T. N., Davydova, N. Y., Halpert, J. R., and Davydov, D. R. (2007) Mechanism of interactions of alpha-naphthoflavone with cytochrome p450 3a4 explored with an engineered enzyme bearing a fluorescent probe, *Biochemistry 46*, 106-119.
81. Koley, A. P., Buters, J. T. M., Robinson, R. C., Markowitz, A., and Friedman, F. K. (1997) Differential mechanisms of cytochrome p450 inhibition and activation by α-naphthoflavone, *J. Biol. Chem. 272*, 3149-3152.
82. Davydov, D. R., Baas, B. J., Sligar, S. G., and Halpert, J. R. (2007) Allosteric mechanisms in cytochrome p450 3a4 studied by high-pressure spectroscopy: Pivotal role of substrate-induced changes in the accessibility and degree of hydration of the heme pocket, *Biochemistry 46*, 7852-7864.
83. Egnell, A.-C., Houston, J. B., and Boyer, C. S. (2005) Predictive models of cyp3a4 heteroactivation: In vitro-in vivo scaling and pharmacophore modeling, *J. Pharmacol. Exp. Ther. 312*, 926-937.
84. Davydov, D. R., Davydova, N. Y., Tsalkova, T. N., and Halpert, J. R. (2008) Effect of glutathione on homo- and heterotropic cooperativity in cytochrome p450 3a4, *Arch. Biochem. Biophys. 471*, 134-145.
85. Yamazaki, H., Ueng, Y.-F., Shimada, T., and Guengerich, F. P. (1995) Roles of divalent metal ions in oxidations catalyzed by recombinant cytochrome p450 3a4 and replacement of nadph-cytochrome p450 reductase with other flavoproteins, ferredoxin, and oxygen surrogates, *Biochemistry 34*, 8380-8389.
86. Baas, B. J., Denisov, I. G., and Sligar, S. G. (2004) Homotropic cooperativity of monomeric cytochrome p450 3a4 in a nanoscale native bilayer environment, *Arch. Biochem. Biophys. 430*, 218-228.
87. Yamazaki, H., Johnson, W. W., Ueng, Y.-F., Shimada, T., and Guengerich, F. P. (1996) Lack of electron transfer from cytochrome b_5 in stimulation of catalytic activities of cytochrome p450 3a4, *J. Biol. Chem. 271*, 27438-27444.
88. Shet, M. S., Faulkner, K. M., Holmans, P. L., Fisher, C. W., and Estabrook, R. W. (1995) The effects of cytochrome b_5, nadph-p450 reductase, and lipid on the rate of 6β-hydroxylation of testosterone as catalyzed by a human p450 3a4 fusion protein, *Arch. Biochem. Biophys. 318*, 314-321.

89. Shimada, T., Mernaugh, R. L., and Guengerich, F. P. (2005) Interactions of mammalian cytochrome p450, nadph-cytochrome p450 reductase, and cytochrome b5 enzymes, *Arch. Biochem. Biophys. 435*, 207-216.
90. Yamazaki, H., Nakano, M., Imai, Y., Ueng, Y.-F., Guengerich, F. P., and Shimada, T. (1996) Roles of cytochrome b_5 in the oxidation of testosterone and nifedipine by recombinant cytochrome p450 3a4 and by human liver microsomes, *Arch. Biochem. Biophys. 325*, 174-182.
91. Perret, A., and Pompon, D. (1998) Electron shuttle between membrane-bound cytochrome p450 3a4 and b5 rules uncoupling mechanisms, *Biochemistry 37*, 11412-11424.
92. Tsoulis, C. J., and Hobkirk, R. (1981) Factors affecting the 16α-hydroxylation of estrone 3-sulfate by guinea pig liver microsomes, *Can. J. Biochem. 59*, 454-460.
93. Ueng, Y.-F., Shimada, T., Yamazaki, H., and Guengerich, F. P. (1995) Oxidation of aflatoxin b1 by bacterial recombinant human cytochrome p450 enzymes, *Chem. Res. Toxicol. 8*, 218-225.
94. Denisov, I. G., Frank, D. J., and Sligar, S. G. (2009) Cooperative properties of cytochromes p450, *Pharmacol. Ther. 124*, 151-167.
95. Fernando, H., Halpert, J. R., and Davydov, D. R. (2006) Resolution of multiple substrate binding sites in cytochrome p450 3a4: The stoichiometry of the enzyme-substrate complexes probed by fret and job's titration, *Biochemistry 45*, 4199-4209.
96. Roberts, A. G., Campbell, A. P., and Atkins, W. M. (2005) The thermodynamic landscape of testosterone binding to cytochrome p450 3a4: Ligand binding and spin state equilibria, *Biochemistry 44*, 1353-1366.
97. Sligar, S. G., and Denisov, I. G. (2007) Understanding cooperativity in human p450 mediated drug-drug interactions, *Drug Metab. Rev. 39*, 567-579.
98. Denisov, I. G., Grinkova, Y. V., McLean, M. A., and Sligar, S. G. (2007) The one-electron autoxidation of human cytochrome p450 3a4, *J. Biol. Chem. 282*, 26865-26873.
99. Lampe, J. N., Fernández, C., Nath, A., and Atkins, W. M. (2007) Nile red is a fluorescent allosteric substrate of cytochrome p450 3a4, *Biochemistry 47*, 509-516.
100. Nath, A., Fernández, C., Lampe, J. N., and Atkins, W. M. (2008) Spectral resolution of a second binding site for nile red on cytochrome p4503a4, *Arch. Biochem. Biophys. 474*, 198-204.
101. Asciutto, E. K., Dang, M., Pochapsky, S. S., Madura, J. D., and Pochapsky, T. C. (2011) Experimentally restrained molecular dynamics simulations for characterizing the open states of cytochrome p450cam, *Biochemistry 50*, 1664-1671.
102. Lee, Y.-T., Glazer, E. C., Wilson, R. F., Stout, C. D., and Goodin, D. B. (2010) Three clusters of conformational states in p450cam reveal a multistep pathway for closing of the substrate access channel, *Biochemistry 50*, 693-703.
103. Markwick, P. R. L., Pierce, L. C. T., Goodin, D. B., and McCammon, J. A. (2011) Adaptive accelerated molecular dynamics (ad-amd) revealing the molecular plasticity of p450cam, *The Journal of Physical Chemistry Letters 2*, 158-164.
104. Davydov, D. R., Karyakin, A. V., Binas, B., Kurganov, B. I., and Archakov, A. I. (1985) Kinetic studies on reduction of cytochromes p-450 and b5 by dithionite, *Eur. J. Biochem. 150*, 155-159.
105. Davydov, D. R., Fernando, H., Baas, B. J., Sligar, S. G., and Halpert, J. R. (2005) Kinetics of dithionite-dependent reduction of cytochrome p450 3a4: Heterogeneity of the enzyme caused by its oligomerization, *Biochemistry 44*, 13902-13913.
106. Fernando, H., Halpert, J. R., and Davydov, D. R. (2008) Kinetics of electron transfer in the complex of cytochrome p450 3a4 with the flavin domain of cytochrome p450bm-3 as evidence of functional heterogeneity of the heme protein, *Arch. Biochem. Biophys. 471*, 20-31.

107. Koley, A. P., Buters, J. T. M., Robinson, R. C., Markowitz, A., and Friedman, F. K. (1995) Co binding kinetics of human cytochrome p450 3a4: Specific interaction of substrates with kinetically distinguishable conformers, *J. Biol. Chem. 270*, 5014-5018.
108. Davydov, D. R., Sineva, E. V., Sistla, S., Davydova, N. Y., Frank, D. J., Sligar, S. G., and Halpert, J. R. (2010) Electron transfer in the complex of membrane-bound human cytochrome p450 3a4 with the flavin domain of p450bm-3: The effect of oligomerization of the heme protein and intermittent modulation of the spin equilibrium, *Biochim. Biophys. Acta - Bioenergetics 1797*, 378-390.
109. Yamazaki, H., Gillam, E. M. J., Dong, M.-S., Johnson, W. W., Guengerich, F. P., and Shimada, T. (1997) Reconstitution of recombinant cytochrome p450 2c10(2c9) and comparison with cytochrome p450 3a4 and other forms: Effects of cytochrome p450–p450 and cytochrome p450–b_5 interactions, *Arch. Biochem. Biophys. 342*, 329-337.
110. Hill, A. V. (1913) The combinations of haemoglobin with oxygen and with carbon monoxide. I, *Biochem. J. 7*, 471-480.
111. Yoon, M. Y., Campbell, A. P., and Atkins, W. M. (2004) "Allosterism" in the elementary steps of the cytochrome p450 reaction cycle, *Drug Metab. Rev. 36*, 219-230.
112. Yamazaki, H., and Shimada, T. (2006) Cytochrome p450 reconstitution systems, In *Cytochrome p450 protocols* (Phillips, I., and Shephard, E., Eds.), pp 61-71, Humana Press, New York.
113. Shet, M. S., Fisher, C. W., Holmans, P. L., and Estabrook, R. W. (1993) Human cytochrome p450 3a4: Enzymatic properties of a purified recombinant fusion protein containing nadph-p450 reductase, *Proc. Natl. Acad. Sci. U.S.A. 90*, 11748-11752.
114. Brian, W. R., Sari, M. A., Iwasaki, M., Shimada, T., Kaminsky, L. S., and Guengerich, F. P. (1990) Catalytic activities of human liver cytochrome p-450 iiia4 expressed in *saccharomyces cerevisiae*, *Biochemistry 29*, 11280-11292.
115. Bistolas, N., Wollenberger, U., Jung, C., and Scheller, F. W. (2005) Cytochrome p450 biosensors--a review, *Biosensors Bioelectron. 20*, 2408-2423.
116. Fantuzzi, A., Fairhead, M., and Gilardi, G. (2004) Direct electrochemistry of immobilized human cytochrome p450 2e1, *J. Am. Chem. Soc. 126*, 5040-5041.
117. Sadeghi, S. J., Fantuzzi, A., and Gilardi, G. (2011) Breakthrough in p450 bioelectrochemistry and future perspectives, *Biochimica Et Biophysica Acta-Proteins and Proteomics 1814*, 237-248.
118. Krishnan, S., Wasalathanthri, D., Zhao, L., Schenkman, J. B., and Rusling, J. F. (2011) Efficient bioelectronic actuation of the natural catalytic pathway of human metabolic cytochrome p450s, *J. Am. Chem. Soc. 133*, 1459-1465.
119. Asturias-Arribas, L., Alonso-Lomillo, M., Dominguez-Renedo, O., and Julia Arcos-Martinez, M. (2013) Electrochemical determination of cocaine using screen-printed cytochrome p450 2b4 based biosensors, *Talanta 105*, 131-134.
120. Huang, M., Xu, X., Yang, H., and Liu, S. (2012) Electrochemically-driven and dynamic enhancement of drug metabolism via cytochrome p450 microsomes on colloidal gold/graphene nanocomposites, *RSC Advances 2*, 12844-12850.
121. Krishnan, S., Schenkman, J. B., and Rusling, J. F. (2011) Bioelectronic delivery of electrons to cytochrome p450 enzymes, *The Journal of Physical Chemistry B 115*, 8371-8380.
122. Dodhia, V. R., Sassone, C., Fantuzzi, A., Nardo, G. D., Sadeghi, S. J., and Gilardi, G. (2008) Modulating the coupling efficiency of human cytochrome p450 cyp3a4 at electrode surfaces through protein engineering, *Electrochem. Commun. 10*, 1744-1747.
123. Yacobi, A., Zlotnick, S., Colaizzi, J. L., Moros, D., Masson, E., Abolfathi, Z., LeBel, M., Mehta, R., Golander, Y., and Levitt, B. (1999) A multiple-dose safety and bioequivalence study of a narrow therapeutic index drug: A case for carbamazepine, *Clin. Pharmacol. Ther. 65*, 389-394.

124. Knowles, S. R., Dewhurst, N., and Shear, N. H. (2012) Anticonvulsant hypersensitivity syndrome: An update, *Expert Opin. Drug Saf. 11*, 767-778.
125. Shear, N. H. S., Stephen P. (1988) Anticonvulsant hypersensitivity syndrome: In vitro assessment of risk, *The American Society for Clinical Investigation 82*, 1826- 1832.
126. The UniProt Consortium. (2014) Activities at the universal protein resource (uniprot), *Nucleic Acids Res. 42*, D191-D198.
127. Myers, E. W., and Miller, W. (1988) Optimal alignments in linear space, *Computer applications in the biosciences : CABIOS 4*, 11-17.
128. Goujon, M., McWilliam, H., Li, W., Valentin, F., Squizzato, S., Paern, J., and Lopez, R. (2010) A new bioinformatics analysis tools framework at embl-ebi, *Nucleic Acids Res. 38*, W695-699.
129. McWilliam, H., Li, W., Uludag, M., Squizzato, S., Park, Y. M., Buso, N., Cowley, A. P., and Lopez, R. (2013) Analysis tool web services from the embl-ebi, *Nucleic Acids Res. 41*, W597-600.
130. Blanchard, J. S. (1984) Buffers for enzymes, In *Methods enzymol.* (William, B. J., Ed.), pp 404-414, Academic Press.
131. Davydov, D. R., Deprez, E., Hui Bon Hoa, G., Knyushko, T. V., Kuznetsova, G. P., Koen, Y. M., and Archakov, A. I. (1995) High-pressure-induced transitions in microsomal cytochrome p450 2b4 in solution: Evidence for conformational inhomogeneity in the oligomers, *Arch. Biochem. Biophys. 320*, 330-344.
132. Shen, A. L., Porter, T. D., Wilson, T. E., and Kasper, C. B. (1989) Structural analysis of the fmn binding domain of nadph-cytochrome p-450 oxidoreductase by site-directed mutagenesis, *J. Biol. Chem. 264*, 7584-7589.
133. Schollmeyer, P., and Klingenberg, M. (1962) On the cytochrome content of animal tissue, *Biochem Z. 335*, 426-439.
134. Masters, B. S. S., and Okita, R. T. (1980) The history, properties, and function of nadph-cytochrome p-450 reductase, *Pharmacol. Ther. 9*, 227-244.
135. Fernando, H., Davydov, D. R., Chin, C. C., and Halpert, J. R. (2007) Role of subunit interactions in p450 oligomers in the loss of homotropic cooperativity in the cytochrome p450 3a4 mutant l211f/d214e/f304w, *Arch. Biochem. Biophys. 460*, 129-140.
136. Cornish-Bowden, A. (1979) *Fundamentals of enzyme kinetics*, Butterworth London.
137. Segel, I. H. (1975) *Enzyme kinetics: Behavior and analysis of rapid equilibrium and steady-state enzyme systems*, Wiley-Interscience, New York.
138. Renaud, J. P., Davydov, D. R., Heirwegh, K. P., Mansuy, D., and Hui Bon Hoa, G. H. (1996) Thermodynamic studies of substrate binding and spin transitions in human cytochrome p-450 3a4 expressed in yeast microsomes, *Biochem. J. 319*, 675-681.
139. Brooks, B. R., Brooks, C. L., Mackerell, A. D., Nilsson, L., Petrella, R. J., Roux, B., Won, Y., Archontis, G., Bartels, C., Boresch, S., Caflisch, A., Caves, L., Cui, Q., Dinner, A. R., Feig, M., Fischer, S., Gao, J., Hodoscek, M., Im, W., Kuczera, K., Lazaridis, T., Ma, J., Ovchinnikov, V., Paci, E., Pastor, R. W., Post, C. B., Pu, J. Z., Schaefer, M., Tidor, B., Venable, R. M., Woodcock, H. L., Wu, X., Yang, W., York, D. M., and Karplus, M. (2009) Charmm: The biomolecular simulation program, *J. Comput. Chem. 30*, 1545-1614.
140. MacKerell, A. D., Feig, M., and Brooks, C. L. (2003) Improved treatment of the protein backbone in empirical force fields, *J. Am. Chem. Soc. 126*, 698-699.
141. Foloppe, N., Sagemark, J., Nordstrand, K., Berndt, K. D., and Nilsson, L. (2001) Structure, dynamics and electrostatics of the active site of glutaredoxin 3 from *escherichia coli*: Comparison with functionally related proteins, *J. Mol. Biol. 310*, 449-470.
142. Vanommeslaeghe, K., Hatcher, E., Acharya, C., Kundu, S., Zhong, S., Shim, J., Darian, E., Guvench, O., Lopes, P., Vorobyov, I., and Mackerell, A. D. (2010) Charmm general force

field: A force field for drug-like molecules compatible with the charmm all-atom additive biological force fields, *J. Comput. Chem. 31*, 671-690.
143. Vanommeslaeghe, K., and MacKerell, A. D. (2012) Automation of the charmm general force field (cgenff) i: Bond perception and atom typing, *J. Chem. Inf. Model 52*, 3144-3154.
144. Vanommeslaeghe, K., Raman, E. P., and MacKerell, A. D. (2012) Automation of the charmm general force field (cgenff) ii: Assignment of bonded parameters and partial atomic charges, *J. Chem. Inf. Model 52*, 3155-3168.
145. Van Der Spoel, D., Lindahl, E., Hess, B., Groenhof, G., Mark, A. E., and Berendsen, H. J. C. (2005) Gromacs: Fast, flexible, and free, *J. Comput. Chem. 26*, 1701-1718.
146. Jorgensen, W. L., Chandrasekhar, J., Madura, J. D., Impey, R. W., and Klein, M. L. (1983) Comparison of simple potential functions for simulating liquid water, *J. Chem. Phys. 79*, 926-935.
147. Darden, T., York, D., and Pedersen, L. (1993) Particle mesh ewald: An n·log(n) method for ewald sums in large systems, *J. Chem. Phys. 98*, 10089-10092.
148. Hess, B., Bekker, H., Berendsen, H. J. C., and Fraaije, J. G. E. M. (1997) Lincs: A linear constraint solver for molecular simulations, *J. Comput. Chem. 18*, 1463-1472.
149. Bussi, G., Donadio, D., and Parrinello, M. (2007) Canonical sampling through velocity rescaling, *J. Chem. Phys. 126*, 14101-14107.
150. Parrinello, M., and Rahman, A. (1981) Polymorphic transitions in single crystals: A new molecular dynamics method, *J. Appl. Phys. 52*, 7182-7190.
151. Nosé, S., and Klein, M. L. (1983) Constant pressure molecular dynamics for molecular systems, *Mol. Phys. 50*, 1055-1076.
152. The PyMOL molecular graphics system, v. S., LLC.
153. Seeber, M., Cecchini, M., Rao, F., Settanni, G., and Caflisch, A. (2007) Wordom: A program for efficient analysis of molecular dynamics simulations, *Bioinformatics 23*, 2625-2627.
154. Vitalis, A., and Caflisch, A. (2012) Efficient construction of mesostate networks from molecular dynamics trajectories, *J. Chem. Theory Comput. 8*, 1108-1120.
155. Vitalis, A., Steffen, A. T., Lyle, N., Mao, A. H., and Pappu, R. V. Campari, *http://sourceforge.net/projects/campari*.
156. Dutton, D. R., Reed, G. A., and Parkinson, A. (1989) Redox cycling of resorufin catalyzed by rat liver microsomal nadph-cytochrome p450 reductase, *Arch. Biochem. Biophys. 268*, 605-616.
157. Itoh, M., Adachi, T., and Tokumura, K. (1984) Time-resolved fluorescence and absorption spectra and two-step laser excitation fluorescence of the excited-state proton transfer in the methanol solution of 7-hydroxyquinoline, *J. Am. Chem. Soc. 106*, 850-855.
158. Lee, S.-I., and Jang, D.-J. (1995) Proton transfers of aqueous 7-hydroxyquinoline in the first excited singlet, lowest triplet, and ground states, *The Journal of Physical Chemistry 99*, 7537-7541.
159. Shimada, T., Yamazaki, H., Mimura, M., Inui, Y., and Guengerich, F. P. (1994) Interindividual variants in human liver cytochrome-p-450 enzymes involved in the oxidation of drugs, carcinogens and toxic chemicals - studies with liver-microsomes of 30 japanese and 30 caucasians, *J. Pharmacol. Exp. Ther. 270*, 414-423.
160. Pearce, R. E., Vakkalagadda, G. R., and Leeder, J. S. (2002) Pathways of carbamazepine bioactivation in vitro i. Characterization of human cytochromes p450 responsible for the formation of 2- and 3-hydroxylated metabolites, *Drug Metab. Disposition 30*, 1170-1179.
161. Kerr, B. M., Thummel, K. E., Wurden, C. J., Klein, S. M., Kroetz, D. L., Gonzalez, F. J., and Levy, R. (1994) Human liver carbamazepine metabolism: Role of cyp3a4 and cyp2c8 in 10,11-epoxide formation, *Biochem. Pharmacol. 47*, 1969-1979.

162. Nakamura, H., Nakasa, H., Ishii, I., Ariyoshi, N., Igarashi, T., Ohmori, S., and Kitada, M. (2002) Effects of endogenous steroids on cyp3a4-mediated drug metabolism by human liver microsomes, *Drug Metab. Disposition 30*, 534-540.
163. Nakamura, H., Torimoto, N., Ishii, I., Ariyoshi, N., Nakasa, H., Ohmori, S., and Kitada, M. (2003) Cyp3a4 and cyp3a7-mediated carbamazepine 10,11-epoxidation are activated by differential endogenous steroids, *Drug Metab. Disposition 31*, 432-438.
164. Maekawa, K., Yoshimura, T., Saito, Y., Fujimura, Y., Aohara, F., Emoto, C., Iwasaki, K., Hanioka, N., Narimatsu, S., Niwa, T., and Sawada, J. (2009) Functional characterization of cyp3a4.16: Catalytic activities toward midazolam and carbamazepine, *Xenobiotica 39*, 140-147.
165. Torimoto, N., Ishii, I., Hata, M., Nakamura, H., Imada, H., Ariyoshi, N., Ohmori, S., Igarashi, T., and Kitada, M. (2003) Direct interaction between substrates and endogenous steroids in the active site may change the activity of cytochrome p450 3a4, *Biochemistry 42*, 15068-15077.
166. Ueng, Y.-F., Kuwabara, T., Chun, Y.-J., and Guengerich, F. P. (1997) Cooperativity in oxidations catalyzed by cytochrome p450 3a4, *Biochemistry 36*, 370-381.
167. Houston, J. B., and Kenworthy, K. E. (2000) In vitro-in vivo scaling of cyp kinetic data not consistent with the classical michaelis-menten model, *Drug Metab. Disposition 28*, 246-254.
168. He, Y. A., He, Y. Q., Szklarz, G. D., and Halpert, J. R. (1997) Identification of three key residues in substrate recognition site 5 of human cytochrome p450 3a4 by cassette and site-directed mutagenesis, *Biochemistry 36*, 8831-8839.
169. Kumar, S., Davydov, D. R., and Halpert, J. R. (2005) Role of cytochrome b5 in modulating peroxide-supported cy3a4 activity: Evidence for a conformational transition and cytochrome p450 heterogeneity, *Drug Metab. Dispos. 33*, 1131-1136.
170. Sevrioukova, I. F., and Poulos, T. L. (2013) Dissecting cytochrome p450 3a4–ligand interactions using ritonavir analogues, *Biochemistry 52*, 4474-4481.
171. Sevrioukova, I. F., and Poulos, T. L. (2012) Structural and mechanistic insights into the interaction of cytochrome p4503a4 with bromoergocryptine, a type i ligand, *J. Biol. Chem. 287*, 3510-3517.
172. Isin, E. M., and Guengerich, F. P. (2006) Kinetics and thermodynamics of ligand binding by cytochrome p450 3a4, *J. Biol. Chem. 281*, 9127-9136.
173. Hosea, N. A., Miller, G. P., and Guengerich, F. P. (2000) Elucidation of distinct ligand binding sites for cytochrome p450 3a4, *Biochemistry 39*, 5929-5939.
174. Sevrioukova, I. F., and Poulos, T. L. (2013) Pyridine-substituted desoxyritonavir is a more potent inhibitor of cytochrome p450 3a4 than ritonavir, *J. Med. Chem. 56*, 3733-3741.
175. Davydov, D. R., Botchkareva, A. E., Kumar, S., He, Y. Q., and Halpert, J. R. (2004) An electrostatically driven conformational transition is involved in the mechanisms of substrate binding and cooperativity in cytochrome p450eryf, *Biochemistry 43*, 6475-6485.
176. Stresser, D. M., Blanchard, A. P., Turner, S. D., Erve, J. C. L., Dandeneau, A. A., Miller, V. P., and Crespi, C. L. (2000) Substrate-dependent modulation of cyp3a4 catalytic activity: Analysis of 27 test compounds with four fluorometric substrates, *Drug Metab. Disposition 28*, 1440-1448.
177. Lu, P., Lin, Y., Rodrigues, A. D., Rushmore, T. H., Baillie, T. A., and Shou, M. (2001) Testosterone, 7-benzyloxyquinoline, and 7-benzyloxy-4-trifluoromethyl-coumarin bind to different domains within the active site of cytochrome p450 3a4, *Drug Metab. Disposition 29*, 1473-1479.
178. Stresser, D. M., Turner, S. D., Blanchard, A. P., Miller, V. P., and Crespi, C. L. (2002) Cytochrome p450 fluorometric substrates: Identification of isoform-selective probes for rat cyp2d2 and human cyp3a4, *Drug Metab. Disposition 30*, 845-852.

179. Baririan, N., Desager, J.-P., Petit, M., and Horsmans, Y. (2006) Cyp3a4 activity in four different animal species liver microsomes using 7-benzyloxyquinoline and hplc/spectrofluorometric determination, *J. Pharm. Biomed. Anal. 40*, 211-214.
180. Yarman, A., Wollenberger, U., and Scheller, F. W. (2013) Sensors based on cytochrome p450 and cyp mimicking systems, *Electrochim. Acta 110*, 63-72.
181. Lazarou, J., Pomeranz, B. H., and Corey, P. N. (1998) Incidence of adverse drug reactions in hospitalized patients: A meta-analysis of prospective studies, *JAMA 279*, 1200-1205.
182. Evans, W. E., and Relling, M. V. (1999) Pharmacogenomics: Translating functional genomics into rational therapeutics, *Science 286*, 487-491.
183. Glucose, T. J. D. R. F. C., and Group, M. S. (2008) Continuous glucose monitoring and intensive treatment of type 1 diabetes, *New Engl. J. Med. 359*, 1464-1476.
184. Gough, D. A., Kumosa, L. S., Routh, T. L., Lin, J. T., and Lucisano, J. Y. (2010) Function of an implanted tissue glucose sensor for more than 1 year in animals, *Science Translational Medicine 2*, 42ra53.
185. Taurino, I., Reiss, R., Richter, M., Fairhead, M., Thöny-Meyer, L., De Micheli, G., and Carrara, S. (2013) Comparative study of three lactate oxidases from aerococcus viridans for biosensing applications, *Electrochim. Acta 93*, 72-79.
186. Haines, D. C., Tomchick, D. R., Machius, M., and Peterson, J. A. (2001) Pivotal role of water in the mechanism of p450bm-3, *Biochemistry 40*, 13456-13465.
187. Yano, J. K., Wester, M. R., Schoch, G. A., Griffin, K. J., Stout, C. D., and Johnson, E. F. (2004) The structure of human microsomal cytochrome p450 3a4 determined by x-ray crystallography to 2.05-å resolution, *J. Biol. Chem. 279*, 38091-38094.
188. Xiao, Y., Patolsky, F., Katz, E., Hainfeld, J. F., and Willner, I. (2003) "Plugging into enzymes": Nanowiring of redox enzymes by a gold nanoparticle, *Science 299*, 1877-1881.
189. Koley, A. P., Robinson, R. C., Markowitz, A., and Friedman, F. K. (1997) Drug-drug interactions: Effect of quinidine on nifedipine binding to human cytochrome p450 3a4, *Biochem. Pharmacol. 53*, 455-460.
190. Grinkova, Y. V., Denisov, I. G., and Sligar, S. G. (2010) Functional reconstitution of monomeric cyp3a4 with multiple cytochrome p450 reductase molecules in nanodiscs, *Biochem. Biophys. Res. Commun. 398*, 194-198.
191. Hintz, M. J., and Peterson, J. A. (1981) The kinetics of reduction of cytochrome p-450cam by reduced putidaredoxin, *J. Biol. Chem. 256*, 6721-6728.
192. Lamba, J. K., Lin, Y. S., Thummel, K., Daly, A., Watkins, P. B., Strom, S., Zhang, J., and Schuetz, E. G. (2002) Common allelic variants of cytochrome p450 3a4 and their prevalence in different populations, *Pharmacogenetics 12*, 121-132.